UNIVERSITY POLITEHNICA OF TIMISOARA

FACULTY OF ELECTRICAL ENGINEERING

CONTRIBUTIONS TO THE CONTROL OF VARIABLE SPEED GENERATORS FOR RENEWABLE ENERGY

Ph.D. Thesis

M.Sc.El.Eng. Ioan Serban

Supervisor: Prof. Dr.-Ing. Ion Boldea, IEEE Fellow

Timisoara

2005

ABSTRACT

The present thesis is dedicated to high performance control of the variable speed generators for renewable energy applications in general, and for wind power applications in special. Thus, the thesis is offering some modern solutions based on the control of doubly-fed induction generator with power electronics converters connected in the rotor circuit as the main solution for this kind of applications.

By the end of the 90s wind energy became the most important sustainable energy resource. In the last decade of the 20th century worldwide wind capacity doubled approximately every 3 years and the cost of electricity from wind power has fallen to about one sixth of the costs in the early 80s. And the cumulative capacity is growing worldwide by approximately 25% per year. Currently, 5 countries – Germany, USA, Denmark, India and Spain concentrate more than 83% of worldwide wind energy capacity in their countries, but the utilization of the wind power is fast spreading to other areas of the world and the technology has become very complex. It involves technical disciplines such as aerodynamics, structural dynamics, mechanics, electrical machinery, power electronics, signal electronics, automation and control.

The main goal of this thesis is to offer new high performance solutions in the area of control of the doubly-fed induction generator with a bidirectional power converter in the rotor circuit, solution which has actually more than 50% of the world market share of wind turbine concepts and the trend is growing.

A very important topic of the thesis is the sensorless control of the generator under power system faults, as in the latest years the penetration of the wind power in the power systems has grown tremendously and accordingly with the latest regulations, the generator should remain connected during the power grid shortcircuits. This implies a set of measures to be taken for control and protection of the power electronics.

Index terms / Keywords – renewable energy systems, variable speed generators, wind turbines, doubly-fed induction generator, bidirectional power electronics converters, active and reactive power control

PREFACE

The present thesis represents an approach, based on the doubly-fed induction generator with a bidirectional inverter in the rotor circuit, to high-performance technologies for control of the variable speed electric generators.

Study motivation

The wind energy was the fastest growing technology in the last century, and the utilization of the wind power is spreading continuously. The growing imposes higher and higher demands for the electric generator and its control. This prompted a lot of research and development engineers to look for advanced power electronics and control techniques, in order to improve the behaviour and the performances of the generating systems.

The motivation of the work for the present thesis is fully based on the above mentioned statement. The most of the considered solutions were subject of industrial research and development studies. The target of the thesis was to offer concrete solutions for advanced control of actual electric generator systems for wind power applications.

An important part of the thesis was the development of accurate simulation models for studying the behaviour of the system especially under power grid faults. This was done in Institute of Energy Technology, Aalborg University, Aalborg, Denmark.

The experimental work was carried out this year in the Intelligent Motion Control Laboratory at Faculty of Electrical Engineering, University "Politehnica" of Timisoara, Timisoara, Romania.

Objectives of the thesis

The major objectives of the thesis are to:

- offer an overview of the variable speed generators and their control for renewable power applications and systems, including the prime mover, gearbox, electric generator, power electronics and control;
- developing the accurate simulation models for the complete system with doubly-fed induction generator;
- analyse the requirements of the power systems for the generator systems, as the penetration of the wind power is higher and higher;
- analyze the behaviour of the doubly-fed induction generator system under power grid shortcircuit and search for a possible method to control and protect the power electronics without disconnected the system from the power system
- improve the quality of the active and reactive power control under different conditions;
- find a sensorless control strategy, robust and accurate in all circumstances: starting-up, under-synchronous operation, synchronous and over-synchronous operation;
- investigate the possibilities of the system for self-starting and motoring regime, mandatory for pumping in pump storage micro-hydropower applications or for 4-quadrant limited speed range operation in large power drives.

Outline (organization) of the thesis

The thesis is organized in 7 chapters following the above-presented objectives.

The *first chapter* presents a comprehensive overview of actual variable speed generators and their control. Detailed information are given for all actual and also for some prospective solutions.

In the *second chapter* the simulation models developed for analysis of the doubly-fed induction generator system with bidirectional inverter in the rotor circuit are described and discussed. The simulated behaviour of the system under power grid shortcircuit is presented. A possible solution to control and protect the power electronics circuits without disconnected the system from the power grid is introduced.

In the *third chapter*, the simulated sensorless active and reactive power control of the system is illustrated in detail. The power grid shortcircuit situation is again analyzed. Under possible power grid transients the necessity of taking into account of the saturation in the sensorless algorithm is demonstrated as mandatory.

In the *forth chapter* the experimental investigation of the system in motoring regime is presented and discussed. New state observers and a sensorless control strategy were introduced and good results are shown down to 5 rpm. Also very good dynamics are illustrated, as the set-up is regenerative.

In the *fifth chapter* the experimental investigation of the system in generating regime is presented. Two flux observers and a sensorless algorithm based on a model-reference adaptive system (MRAS) were developed and tested. The results are illustrated and discussed. Good performances of the speed and position estimation are proved in all situations and over the whole speed range.

In the *sixth chapter* the test rig used for the whole experimental work is presented and commented and in the *seventh chapter* the work is summarized and the conclusion, contributions and the future perspectives are stressed.

ACKNOWLEDGEMENTS

I wish to express my deep gratitude to my supervisor Prof. Ion Boldea. His guidance, support and encouragement made this work possible. I would like to thank also Prof. Frede Blaabjerg from the Institute of Energy Technology, Aalborg University, Denmark for his support and for the fruitful discussions during and after my researching period in Aalborg.

My special gratitude to my actual chief in ebm-papst St. Georgen GmbH & Co. KG, St. Georgen, Germany (formerly PAPST-MOTOREN GmbH & Co. KG), Dorin Iles-Klumpner for sharing his time and knowledge with me. His friendship and support are invaluable for me.

Many thanks to Prof. Gheorghe Daniel Andreescu from Faculty of Automation and Computers, Timisoara, Romania. His numerous inputs during the experimental work were very helpful.

I want to thank all of those who contributed to my engineering education and also to my collegues from Intelligent Motion Control Laboratory at Faculty of Electrical Engineering, Timisoara; Asoc. Prof. Lucian Tutelea and Assist. Prof. Cristian Lascu deserve my special gratitude.

Finally, and most of all, I want to thank my parents. They are a tireless source of love and support. This thesis is dedicated to them.

St. Georgen, July the 29th, 2005

Ioan Serban

TABLE OF CONTENTS

NOMENCLATURE

Roman letters

v_{sa}, v_{sb}, v_{sc}	- voltages of stator phases a, b, and c	[V]
$v_{s\alpha}$, $v_{s\beta}$	- voltages of stator α-, and β-axis phases	[V]
v_{sd}, v_{sq}	- voltages of stator d-, and q-axis phases	[V]
v_{ra}, v_{rb}, v_{rc}	- voltages of rotor phases a, b, and c	[V]
$v_{r\alpha}$, $v_{r\beta}$	- voltages of rotor α-, and β-axis phases	[V]
v_{rd}, v_{rq}	- voltages of rotor d-, and q-axis phases	[V]
v_{ga}, v_{gb}, v_{gc}	- voltages of grid phases a, b, and c	[V]
$v_{g\alpha}$, $v_{g\beta}$	- voltages of grid α-, and β-axis phases	[V]
v_{gd}, v_{gq}	- voltages of grid d-, and q-axis phases	[V]
v_{DC}	- DC voltage	[V]
i_{sa}, i_{sb}, i_{sc}	- currents of stator phases a, b, and c	[A]
$i_{s\alpha}$, $i_{s\beta}$	- currents of stator α-, and β-axis phases	[A]
i_{sd}, i_{sq}	- currents of stator d-, and q-axis phases	[A]
i_{ra}, i_{rb}, i_{rc}	- currents of rotor phases a, b, and c	[A]
$i_{r\alpha}$, $i_{r\beta}$	- currents of rotor α-, and β-axis phases	[A]
i_{rd}, i_{rq}	- currents of rotor d-, and q-axis phases	[A]
i_{ga}, i_{gb}, i_{gc}	- currents of grid phases a, b, and c	[A]
$i_{g\alpha}$, $i_{g\beta}$	- currents of grid α-, and β-axis phases	[A]
i_{gd}, i_{gq}	- currents of grid d-, and q-axis phases	[A]
i_{ms}	- stator magnetizing current	[A]
J	- rotor moment of inertia	$[kg \cdot m^2]$
L_s	- stator total inductance	[H]
$L_{s\sigma}$	- stator leakage inductance	[H]
L_m	- magnetizing inductance	[H]
L_r	- rotor total inductance	[H]

$L_{r\sigma}$	- rotor leakage inductance	[H]
R_s	- stator resistance	[Ω]
R_r	- rotor resistance	[Ω]
p	- number of pole pairs	–
T_{em}	- electromagnetic torque	[Nm]
T_m	- mechanical torque	[Nm]
P_s	- stator active power	[W]
Q_s	- stator reactive power	[VAr]
S_s	- stator apparent power	[VA]
P_m	- mechanical power	[W]

Greek letters

λ	- tip speed ratio	-
ω_m	- mechanical turbine speed	[rad/s]
ω_s	- mechanical turbine speed	[rad/s]
ω_r	- mechanical turbine speed	[rad/s]
ω_{slip}	- slip speed	[rad/s]
θ_s	- stator flux angle	[rad]
θ_r	- rotor angle (position)	[rad]
θ_{slip}	- angle between stator flux and rotor (slip)	[rad]
ρ_1	- angle between rotor current and stator	[rad]
ρ_2	- angle between rotor current and rotor	[rad]
ψ_s	- stator flux	[Wb]
ψ_r	- rotor flux	[Wb]
ψ_m	- magnetizing flux	[Wb]
σ	- leakage factor	-
σ_s	- stator leakage factor	-
σ_r	- stator leakage factor	-

Abbreviations

CSCF	- constant speed, constant frequency
VSCF	- variable speed, constant frequency
DFIG	- doubly-fed induction generator
DFIM	- doubly-fed induction motor
GSC	- grid-side converter
MSC	- machine-side converter
SVM	- space vector modulation
PWM	- pulse width modulation
AFC	- automatic frequency control
EMF	- electromotive force
AC	- alternating current
DC	- direct current

Chapter 1

Variable speed generators: a review

Abstract

In this chapter, an overview of the variable speed generators and their control is presented. The historical developments and the worldwide current status of the wind turbines are presented in the beginning. Then, the generators and power electronics concepts are detailed from the electrical point of view. Classical and new solutions are discussed based on technical aspects and market trends.

1.1 Introduction

The power from the wind is used since at least 3000 years ago, mainly for providing mechanical power to pump water or for grinding grains.

Even if the first wind turbines have been developed in the beginning of the 20^{th} century, only in the 1970s once with the "oil crisis" the interest in the power from the wind starts to increase, and this time the main focus was on providing electrical energy instead of mechanical energy [1]. From then on, the technology was improved step by step, and in 1990s wind energy has re-emerged as the most important sustainable "green" energy resource. From 1995 on, the worldwide installed wind capacity doubled every 3 years as the cost of electricity from wind power has fallen to about 1:7 from the cost in the early 1980s. And the things are far from a stop. According to estimations the cumulative capacity will grow annually with 25%.

This tremendously increasing of the installed capacity pushed the technology very fast in the new dimensions. 15 years ago a 300kW turbine with 30 m rotor diameter was usual. 5 years ago 2MW turbines with 80 m rotor diameter was already in production at many manufacturers and now 3.6 MW turbines are available, 5MW wind turbines (128 m diameter) have already tested and 6-7 MW turbines will be built very soon. In paragraph 1.2 a more detailed status of the wind turbines worldwide is

provided and in Paragraph 1.3 the actual solutions regarding the electrical generators and their power electronics and control are presented.

1.2 Wind turbines – current status worldwide / Historical developments

In 1891 Danish Poul la Cour started his work on an electrical wind turbine at Askov folk high school. This was the first electrical wind turbine and the start of Danish wind turbines. During both World Wars Denmark was cut off from its supply of oil and thus power from wind turbines was very important. The wind turbines produced by F.L. Smidth in 1941-42 can be considered forerunners of modern wind turbine generators. The Smidth turbines were the first turbines using modern airfoils. At the same time, the American Palmer Putnam built a 53m diameter wind turbine for the Morgan Smith Co. but with a different philosophy. The Danish turbine was based on an upwind rotor with stall regulation, operating at low speed. The American turbine was based on a downwind rotor with variable pitch regulation and it was not successful. Thus it was dismantled in 1945.

In 1957 J. Juul made his 200kW wind turbine in Denmark. It was installed in Gedser and it generated approx. 220 000 MWh during 1956-1967. At the same time, the German Hütter developed a new turbine with a new concept (the turbine comprised two slender fiberglass blades mounted downwind of the tower on a teetering hub). This turbine was very known for its efficiency.

During the oil crisis in the mid if the 1970s the Danish and German wind turbine industry was irreversibly started. During the 1980s, turbines increased in size, but the penetration in the electrical power systems was marginal. Thus, there were no major problems with the induction generators drawing reactive power from the grid. At the end of the 80s the larger Danish wind turbines were equipped with a 35m rotor and a 350-450 kW induction generator.

More advanced drive trains have been made since the beginning of the 90s, and more solutions were tested, as more and more attention is paid to produce more energy but environmental friendly, and the penetration of the wind turbines into the power systems became higher and higher.

The growth of wind energy was not evenly distributed around the world. About 75% of the capacity is installed in Europe, 18% in North America and 8% in Asia and Pacific (see Table 1.1).

Table 1.1 Operational wind power capacity worldwide [1]

Region	Installed capacity (MW) by end of the year						
	1995	**1997**	**1999**	**2000**	**2001**	**2002**	**2003**
Europe	2518	4766	9307	12972	17500	21319	28706
North America	1676	1611	2619	2695	4245	4708	6677
South and Central America	11	38	87	103	135	137	139
Asia and Pacific	626	1149	1403	1795	2330	2606	3034
Middle East and Africa	13	24	39	141	147	149	150

Also, between 1995-2003, about 76% of all new grid-connected wind turbines worldwide were installed in Europe. The trend is illustrated in Figure 1.1.

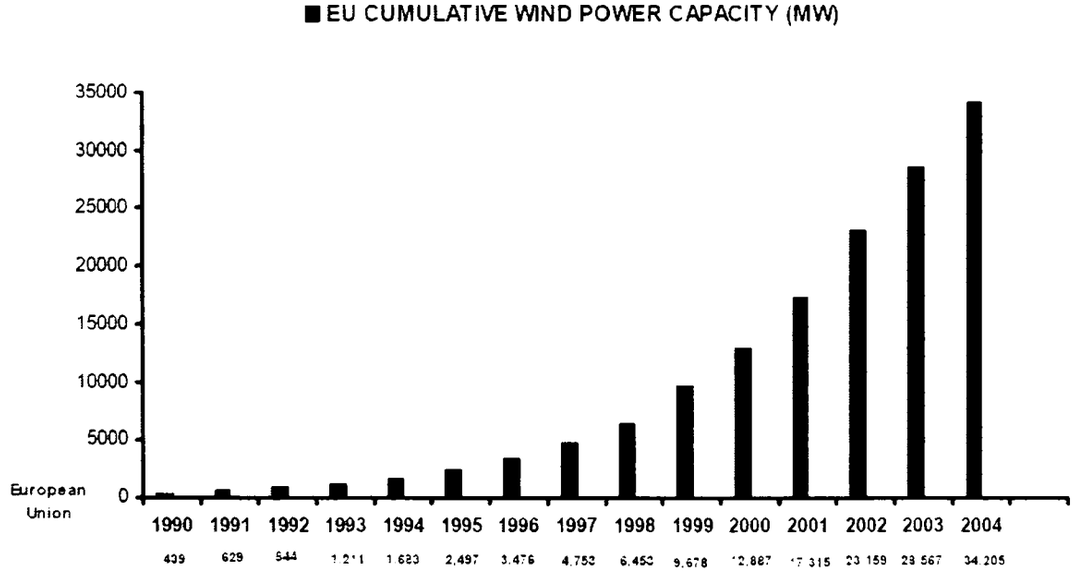

Figure 1.1 Cumulative wind power capacity between 1990 and 2004 in European Union. [2]

Today, five countries: Germany, USA, Denmark, India and Spain concentrate more than 83% of worldwide energy capacity in their countries (see Table 1.2).

Table 1.2 Operational wind power capacity in Europe [2]

Country	Installed capacity (MW) by end of the year	
	1995	**2003**
Germany	1136	14609
Denmark	619	3110
Spain	145	6202
Netherlands	236	912
UK	200	649
Sweden	67	399
Italy	25	904
Greece	28	375
Ireland	7	186
Portugal	13	299
Austria	3	415
Finland	7	51
France	7	239
Norway	4	101
Others	21	255
TOTAL	**2518**	**28706**

1.3 Generators and power electronics for wind turbines

Generally speaking, there are two constructive types of electric generators:

- Horizontal axis;
- Vertical axis;

Respectively, there are two operating modes in generating [3] :

- Constant Speed – Constant Frequency (CSCF) – this system always needs back to back inverters;
- Variable Speed – Constant Frequency (VSCF) – this system needs a speed controller to obtain the maximum from wind power and a converter to change Variable Frequency (VF) into Constant Frequency (CF);

The task of a wind turbine is to convert the energy stored in the wind into mechanical energy, which can be used directly or further converted into electrical energy. Figure 1.2 presents a road map on how to convert mechanical energy into

electrical energy applying the optional control concept of variable speed, i.e. conversion of a mechanical torque input at variable speed to an electrical power output at fixed frequency. Figure 1.2 includes both conventional asynchronous and synchronous generator concepts and conventional, multipolar and novel machine designs. The term "Novel Machines" in Figure 1.2, covers e.g. the reluctance machine, the Windformer [4], etc. In the case of the generator in [4], the "Large PE converter" is a simple diode bridge and the grid is a HVDC-grid. However, at a certain stage, the HVDC has to be converted into AC.

It should be noted that the doubly-fed induction generator has two possible implementations, where 1) the rotor is connected to the grid through a small frequency converter or 2) the rotor is connected to an external power conversion unit (small power converter or passive components), as it also can be observed in Figure 1.2. In the case of the OptiSlip concept of Vestas, the energy coming from the external power converter unit is dissipated as heat loss.

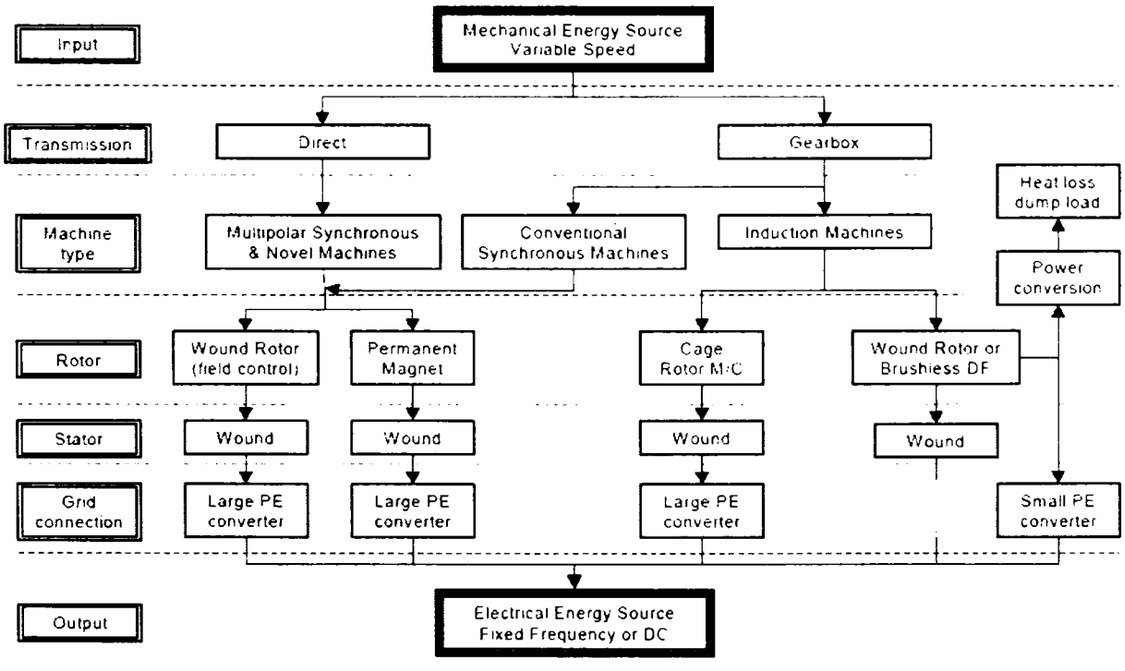

Figure 1.2 Road map: conversion process of Mechanical Energy to Electrical Energy in wind turbines [5].M/C: Multipole/Conventional and DF: Doubly Fed.

One way of describing the *state of the art* regarding wind turbines is to grasp the supplier rates of the manufacturers and then map the applied concept of each manufacturer with respect to the applied concept. Ref. [5] has ranked the top 10 suppliers with respect to sold MW in 1999. This ranking has in [6] been used to investigate the applied configuration and control concept of the large wind turbines. The result is shown in Table 1.3 and the particular configurations illustrated in Figure 1.3.

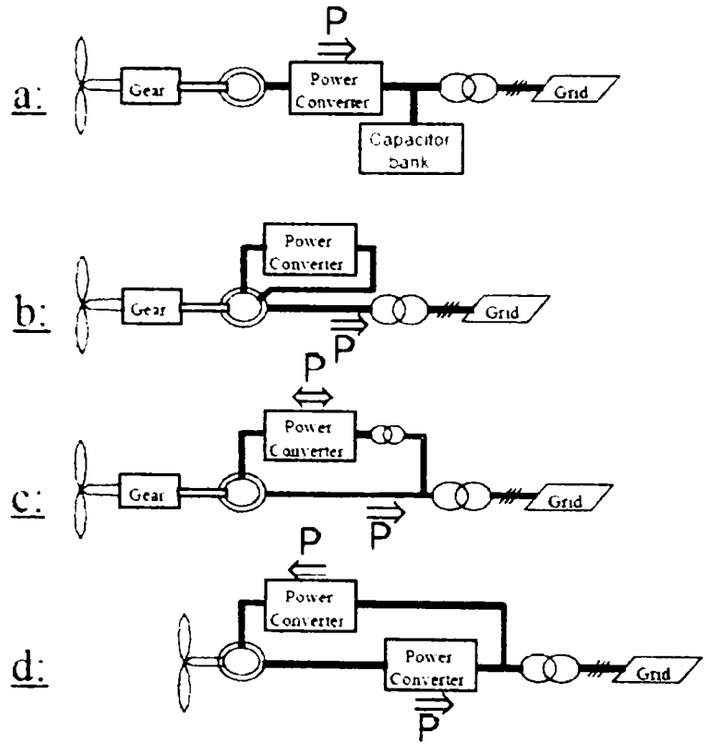

Figure 1.3 Applied topologies for large grid connected wind turbines with and without gearbox. The power flow is indicated by arrows. [7]

Depending on the particular topology in Figure 1.3, the term *Power Converter* covers different types of power electronic components such as: a soft starter (part a), an external variable rotor resistance (part b) , a rectifier (part d – rotor connected) and a frequency converter (part c and d). All the configurations presented in Table 1.3 are 3-bladed and upwind wind turbines with tubular tower. The manufacturers applying configuration "c" and "d" are all using IGBT-based converters.

Table 1.3 Applied concept of the two largest (alias newest) wind turbines from each manufacturer of the top 10 suppliers world wide [7]

Manufacture (top 10 supp.)	**Wind turbine**	**Conf.** Fig. 5.	**Power control features**	**Comments**
Vestas Wind System (Denmark)	V80 – 2 MW	c	Pitch and variable speed	Range: 905 rpm. to 1915 rpm.
	V66 – 1.65 MW	b	Pitch and OptiSlip	Range: 1500 rpm. to 1650 rpm.
Gamesa (Spain)	G52 – 850 kW	c	Pitch and variable speed	Range: 900 rpm. to 1650 rpm.
	G47 – 660 kW	c	Pitch and variable speed	Range: 1200 rpm. to 1626 rpm.
Enercon (Germany)	E-66 – 1.8 MW	d	Pitch and variable speed	Gearless. Range: 10 rpm. to 22 rpm.
	E-58 – 1 MW	d	Pitch and variable speed	Gearless. Range: 10 rpm. to 24 rpm.
NEG Micon (Denmark)	NM 2000/72	a	Active stall	Two speed
	NM 1500C/64	a	Stall	Two speed
Bonus (Denmark)	2 MW	a	Active stall	Two speed
	1.3 MW	a	Active stall	Two speed
Nordex (German-Danish)	N80/2500 kW	c	Pitch and variable speed	Range: 700 rpm. to 1303 rpm.
	N60/1300 kW	a	Stall	Two speed
Enron Wind (USA)	1.5s – 1.5 MW	c	Pitch and variable speed	Range: 989 rpm. to 1798 rpm.
	900s – 900 kW	c	Pitch and variable speed	Range: 1000 rpm. to 2000 rpm.
Ecotecnia (Spain)	1250 kW	No technical informations were available on the internet		
	750 kW			
Suzlon (India)	No technical informations were available on the internet			
Dewind (Germany)	D4 – 600 kW	c	Pitch and variable speed	Range: 680 rpm. to 1327 rpm.
	D6 – 1.25 MW	c	Pitch and variable speed	Range: 700 rpm. to 1350 rpm.

Thus, the present state-of-art of large wind turbines is including:

- **pitch control** combined with variable speed. Moreover, the variable speed concept is mainly realised using configuration "c", i.e. the doubly-fed induction generator with a rotor connected IGBT-based frequency converter. The blades can be turned out or into the wind as the power output becomes too high or too low respectively. This type of control has certain advantages like good power control (at high wind speeds the mean value of the power output is kept close to the rated power of the generator), assisted start-up and emergency stop. The disadvantages are technical complexity of the pitch mechanism and the higher power fluctuations at high wind speeds. Also, the instantaneous power will, because of wind gusts and the limited speed of the pitch mechanism, fluctuate around the rated mean value of the power [8].
- **active stall** with a two speed induction generator. At low wind speeds the blades are pitched similarly with the pitch control in order to achieve maximum efficiency. At high wind speeds the blades go into a deeper stall by being pitched into the direction opposite to that of pitch control. Thus, the turbine achieves a smoother limited power, without higher power fluctuations like in the case of pitch-controlled turbines. The active stall control has the advantage of being able to compensate variations in air density. The combination with the pitch mechanism helps in case of emergency stops and for starting-up.
- only one of the top-10 manufacturers is building a **gearless** (variable speed) wind turbine.

Table 1.4 presents an overview of the market share of each wind turbine concept from 1998 to 2002. Is evident that the market share of the fixed-speed wind turbine concept (type A) decreased during this period, while the DFIG concept (type C) became the dominant concept. The full variable-speed concept (type D) slightly

increased its market share, thus becoming the third most important concept in 2001 and 2002.

Table 1.4 World market share of wind turbine concepts between 1998 and 2002. [8]

Concept*					
	1998	1999	2000	2001	2002
Type A	39.6	40.8	39	31.1	27.8
Type B	17.8	17.1	17.2	15.4	5.1
Type C	26.5	28.1	28.2	36.3	46.8
Type D	16.1	14.0	15.6	17.2	20.3
Total installed power (MW)**	2349	3788	4381	7058	7248
Percentage share of the world market (supply)**	92.4	90.1	94.7	97.6	97.5

* - for the concepts see Figure 1.3.

** - for the 13 suppliers studied: Vestas, Gamesa, Enercon, NEG Micon, Bonus, Nordex, GE Wind/Enron, Ecotechnia, Suzlon, Dewind, Repower, Mitsubishi, Made.

The market position of the type B (Vestas – Optislip) was almost constant during this period of time, but in the last 2 years decreased seriously, its share being occupied by the type C concept.

Table 1.4 presents also the total capacity installed annually by the 13 suppliers studied. Thus, the total capacity in 2002 was three times that in 1998, especially because the increased rated power of the wind turbines.

The most significant reason for the popularity of the doubly fed induction generator concept is the relatively small size of power converter – approximately 10-25 % of nominal turbine power – which is a cost efficient solution in order to obtain variable speed. Meanwhile, one drawback is the inevitable application of slip-rings. However, they have been significantly improved the last years.

When a stand-alone generator has to be conceived and designed, a basic structure followed by models, analysis and digital simulations for each part of the system and for the entire system must be done.

For this, before comparing different stand-alone generator solutions already available, some topologies together with advantages and drawbacks for electrical

generators, power converters, control strategies already in use and already presented in the specialized literature, will be shown in what follows.

1.3.1 The electrical generators

Today, before including an electrical generator in any operating system, studies and analysis, especially using the finite element method of analysis, are expected and easy to implement.

The generator has to work with a power source (the turbine rotor) which supplies very fluctuating mechanical power (shaft torque).

In what follows, some advantages and drawbacks for different electrical generators will be presented, in this way possible candidates for a stand-alone generator can be noticed.

1.3.1.1 The induction generator

Mainly used in power generating systems, the induction generator has two different topologies:

A. Induction generator with squirrel cage rotor, very popular due its rotor mechanical simplicity, high efficiency and low maintenance requirements (type A). During normal operation and direct connection to a stiff AC grid, this generator is very robust and stable. The slip varies and increases with increasing load. The major problem is the full load power factor is relatively low due to the magnetizing current extracted from the grid by the stator winding. At high wind speeds the generator can produce more active power with the price of the more reactive power drawn from the grid. And the amount of the reactive power is uncontrollable because it is varying with the wind conditions. Also, in case of a fault, the generator without any reactive power compensation can produce voltage instability of the grid. During a fault the rotor speed increases and, after the fault is cleared, the stator winding draws a lot of reactive power from the grid which leads to a serious decreasing in voltage [9,10,11]. The squirrel-cage induction generator can be used both in fixed-speed wind turbines and in full variable-speed wind turbines (with bidirectional full-load back-to-back power converter).

B. Induction generator with wounded rotor. The output power of the generator can be controlled and optimized, solutions in this sense were already made. Here, the

disadvantage is represented by the wounded rotor, which implies more production costs and can affect the machine lifetime, depending on the operating conditions [12 – 23]. The wind power applications use most commonly two DFIG configurations:

- **OptiSlip® induction generator** introduced by the Danish manufacturer Vestas. It has a variable external resistance connected in the rotor circuit in order to change the slip of the generator by modifying the total rotor resistance. This could be done with a converter mounted on the rotor shaft, thus no slip rings are necessary. The other advantage is the extended speed range compared with the squirrel-cage induction generator. The disadvantages are the configuration still needs a reactive power compensation system, the control of active and reactive power is poor and the slip power is dissipated into the rotor resistance as losses.

- **Doubly-fed induction generator** which as already stated is one of the most interesting solutions with a growing market. It has a bidirectional power converter connected between the rotor circuit and the power grid and the stator is directly connected to the power grid. If the rotor winding is properly dimensioned, no transformer is necessary for adapting the system to the power grid and the power of the converter could be reduced to only 20-30% from the total power of the generator, accordingly to the desired speed range. The fast and decoupled control of the active and reactive power could be implemented.

Induction machines are well suited for operating at variable speed. They have a relatively high power density, are durable and require little maintenance (especially for squirrel cage induction generator). The induction generator remains a solid solution for wind turbine generators applications [24-40].

1.3.1.2 The synchronous generator

In contrast to the asynchronous machine, the synchronous generator is much more expensive and mechanically much more complicated than an induction generator with the same power. However, the big advantage is that it does not need a reactive magnetizing current.

Anyway, for high power (from hundred of kW to several MW) wind turbine generators applications, the synchronous generator in non-salient construction are properly used. Two classical types of SG are used in the wind turbine industry:

- **wound rotor synchronous generator**; Enercon and Lagerwey use this wind turbine concept (type D). The stator winding is connected to the grid through a full-scale power converter and the multipole (low speed) rotor winding is excited with direct current. Alternatively, an exciter in combination with a rotating rectifier could be used. It has the advantage that it does not need a gearbox, but the disadvantage is the large and heavy generator. The manufacturer Made also applied this concept, but with a 4-pole (high speed) generator and a gearbox.

- **permanent-magnets synchronous generator**; the efficiency is higher than in the induction machine, as the excitation is provided without any supplementary energy supply. This allows an operation at high power factor, but the permanent magnets are rather expensive and the manufacturing costs of the generator especially at high power are also not negligible. Moreover, a full-power converter should be use for adapting the voltage and frequency from the generator to the parameters of the power grid.

In what it follows other variable speed generators will be briefly discussed. They are not in series production, but could become in the future possible candidates for generating applications in general and for the wind turbines industry in special.

1.3.1.3 The axial-flux generator/torus generator

This new solution is a synchronous generator with field winding and PM, having a disc rotor (see Figure 1.4).

The main disadvantages of the axial flux generator are its manufacture difficulty and its high inertia, for this it is not so used in turbine applications only in those where a gearbox is not needed and so a design for low speed drive is required.

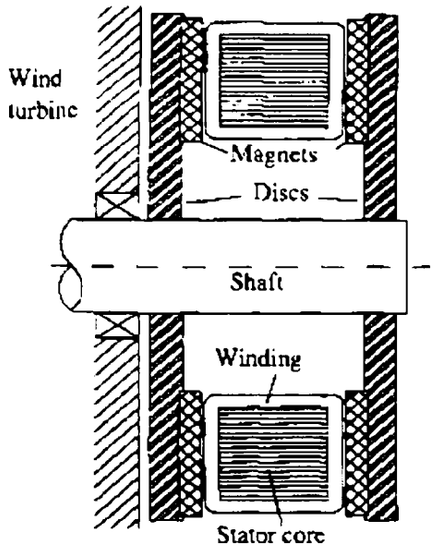

Figure 1.4 The torus generator

With a wounded toroidal stator, without slots but with PMs, this type of generator was already proposed as a solution for wind turbine generator systems.

An axial-flux PM generator for a 5kW gearless wind energy system integrated with a photovoltaic energy converter as a hybrid stand-alone system already exists [41]. In order to eliminate the use of gearbox, subject of vibrations, noise and with appreciable maintenance costs, a direct-coupled variable-speed wind turbine is proposed to verify the viability of the scheme and the feasibility of integrating wind and photovoltaic energy converters to generate electricity and to achieve optimum exploitation of these two energy sources. Despite a number of practical difficulties, mainly of mechanical nature, the performances measured for a prototype were good.

1.3.1.4 The switched reluctance generator

Proposed for generating applications, the switched reluctance machine proof it's simplicity, low cost, rugged configuration and most of all its fault tolerance but also its dependency on power electronics (for control).

The wide speed constant power and voltage recovery under sudden load variation are still to be demonstrated.

1.3.1.5 The hybrid and synchronous reluctance generators

Double salient generators with stator PMs and pulsating (homopolar) flux linkage have been proposed long ago. With the same rotor topology like switched reluctance machine but having stator PMs for excitation purpose, the cogging torque for these machines is an important factor which has to be consider in the designing process.

One PM generator of 5.5 kW was already analysed, using the finite element method, for wind turbine generator purpose [42]. Still rather large electrical time constant leads to slow load rejection while homopolar flux variation in the coils makes only partial use of stator coils and the power/volume is slighty lower than for PM rotor generators. Mechanical and thermal difficulties with PMs on the rotor seems to be the main liability of such configurations, besides added costs and relatively low speed operation (because of the presence of PMs in the rotor).

The synchronous reluctance generator (axially laminated, with flux barriers) is a single salient machine in which the rotor is constructed so to employ the the principle of reluctance torque to produce electromechanical energy conversion (see Figure 1.5). In this case, only the rotor has salient poles while the stator inner surface is the same as for the induction machine.

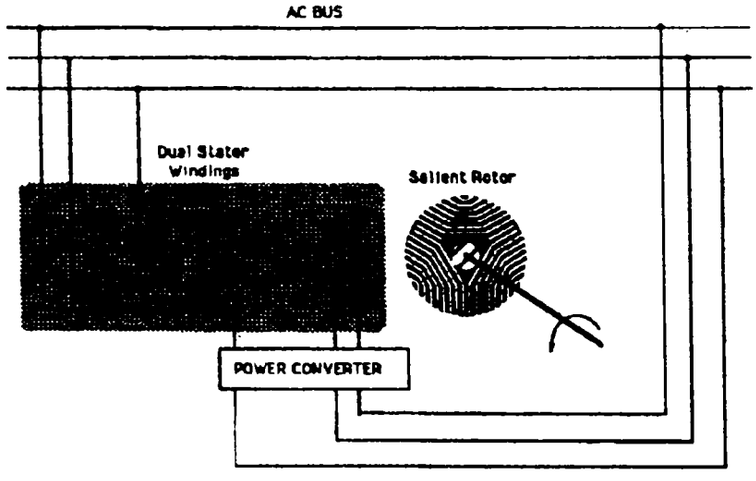

Figure 1.5 The reluctance synchronous generator in a wind turbine generator application [43]

With the development of high-energy PM materials, it is possible to make PM generators more reliable and compact. Recent investigations shows us a growing

demand for wind generators with larger output power used as hybrid energy systems in remote areas.

A prototype machine, PM outer rotor type (see Figure 1.6), was built and tested for wind turbine application. [44]

The results indicate a good efficiency (86%) and operating availability for different work conditions but still the presence of the PMs on the rotor surface constitutes a real drawback.

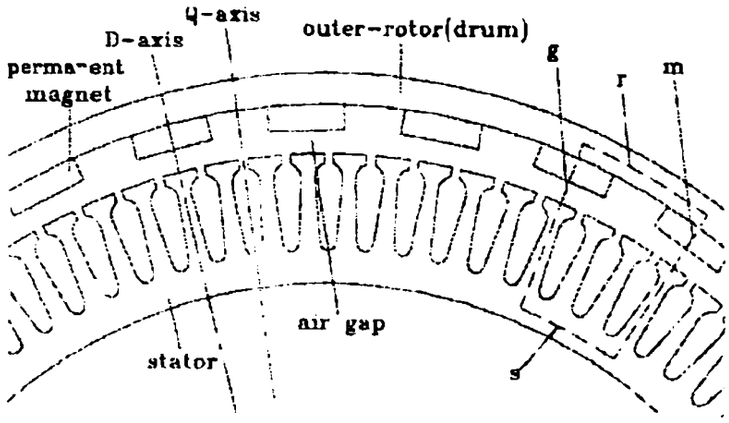

Figure 1.6 The outer rotor generator

Of course, many other types of electrical generators like transverse flux machine, double salient PM machine are presented in the specialized literature. Choosing the right solution for a specific application remains a problem which has to be carefully handled.

1.3.2 The power electronics

In this part, different power converter topologies which can be approach for wind turbine generator applications will be presented.

It can by easily observed that many different power converter topologies can be used, depending on the electrical generator type, the turbine model (CSCF or VSCF) and of course, on the grid type.

1.3.2.1 The rectifier

The common topology is the six diode rectifier, useful only for one quadrant operation, when no control before the DC bus is needed. This is the main drawback of the diode rectifier.

The diode bridges with downstream direct-current regulators can fulfil many demands. As well as rapid influence of the current path, harmonic waves in the generator can be largely suppressed, the need for storage elements in the intermediate circuit is reduced.

The controlled rectifier, as part of a back to back converter, is useful when full control of grid current and/or good power quality factor are required.

One of the methods to assure a good power quality factor, is to increase the voltage on the DC link when is necesary, from the rectifier and DC link side:

- use of high voltage rectifiers;
- use of boost choppers;

or from the inverter side:

- use of a boost transformer;
- use of a combination of boost transformers;

1.3.2.2 The back to back power converter

This power converter topology is used when the power flow of the grid side converter is controlled to keep the DC link voltage constant while the control of generator side is set to assure the field and the reference speed demands so, as results, for stand-alone applications too.

Figure 1.7 shows us one of the back to back topologies in which the grid is in single phase configuration.

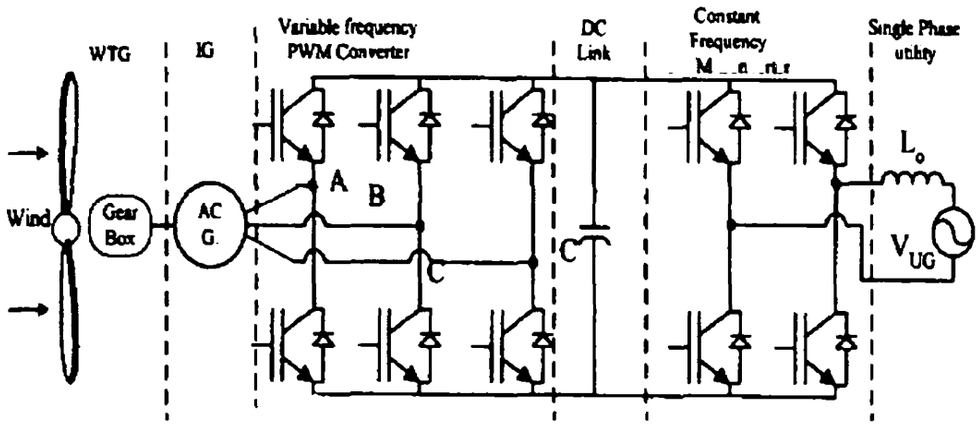

Figure 1.7 The back to back power converter for a wind turbine generator system with single phase grid

1.3.2.3 Matrix, tandem and multilevel converters

Due to the fast development, more complex and efficient power converters were introduced.

Some of those new power converters are:

- the matrix converter; [45]
- the tandem converter;
- the multilevel converter.

Their control complexity, the increased number of switches and transducers, the absence of DC link and the output voltage limitation (both for matrix converter), filters complexity, still keeping them away from small stand-alone applications but near future researches might give them a real chance on this market.

Anyway, new methods to evaluate and compare different converter topologies efficiency are already presented for variable speed application. One of them presents the advantage of using back to back converter instead of three level converter for a doubly-fed induction generator power system.[46]

Using complex power converter structures in case of isolated grid, where stand alone generating systems are used must be avoided because of economical cost reasons – a complex solution implies high costs – and also because of losses – an increased number of power switches working in the same time will increase the losses. Anyway, the power converter topology mostly depends on generator type and of course on stand-alone energy conversion system configuration.

1.3.3 Control strategies

Reliable operation must be guaranteed for stand-alone turbine generating systems in all operating states. It is necessary to develop a local plant/grid specific profile of requirements, to expand this into a strategy that takes into account the desires of operators, manufacturers, power supply companies, standards.

A variety of control methods are already developed, depending on the generator type, the grid and the power electronics converters [47 – 59].

For small wind power plants, stand-alone wind turbine generators sensing the blade pitch is relatively costly. Anyway, the output power can be adjusted faster by electric regulators of the turbine output, this has to be considered for VSCF type of stand-alone wind turbine generators.

Simple variable speed system using a standard V/Hz control and squirrel cage induction generator (see Figure 1.8) was already presented. [60]

This control essentially adjusts the applied frequency in relation to the mechanical speed of the turbine in order to keep the turbine operating at its maximum power coefficient.

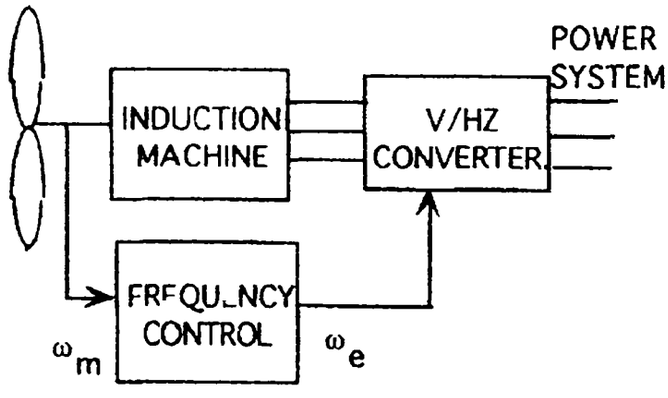

Figure 1.8 A simple control scheme for variable speed wind turbines

The simulation results, made for a 20kW system, show us that at low speeds the system followed the maximum power characteristic and at high speeds the speed and power were limited.

To make power generation truly cost effective and reliable, advance control techniques are imperative.

Based on both mechanical and electrical dynamics, nonlinear and adaptive control algorithms are derived. Such a technique was verified on a two-bladed horizontal-axis wind turbine with good results. [61]

Closed-loop control system can assure maximum power transfer (look-up table relates the electrical power output of the system to the shaft speed).

A control strategy for power smoothing in wind energy application, especially for stand-alone wind turbine generator using linearised or fuzzy controller augmented by a feed-forward compensation scheme (see Figure 1.9) was developed and presented in [62].

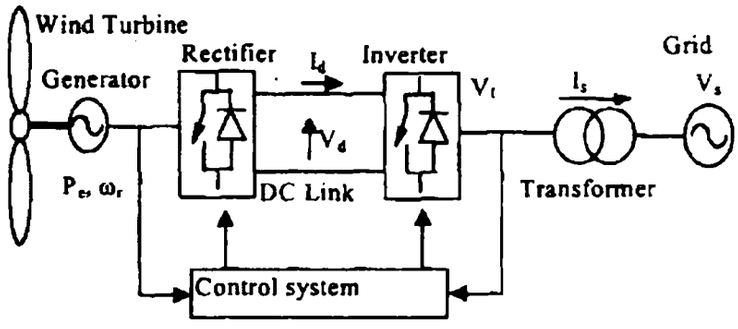

Figure 1.9 A variable speed wind turbine with fuzzy logic control system

1.3.4 Stand-alone systems, different topologies

The solution shown in Figure 1.10, can be used for stand-alone variable speed operation of the system for both squirrel cage and doubly fed induction generators. [63]

The control complexity lies in the fact that stable grid voltages are not available and that power flow balance assumes a central importance. It is for interest to compare the complexity and converter rating of the two systems (one with squirrel cage and the other one with wounded rotor).

The system for wounded rotor is more complex (see Figure 1.10), as expected but both strategies are promising as long as more research has to be done.

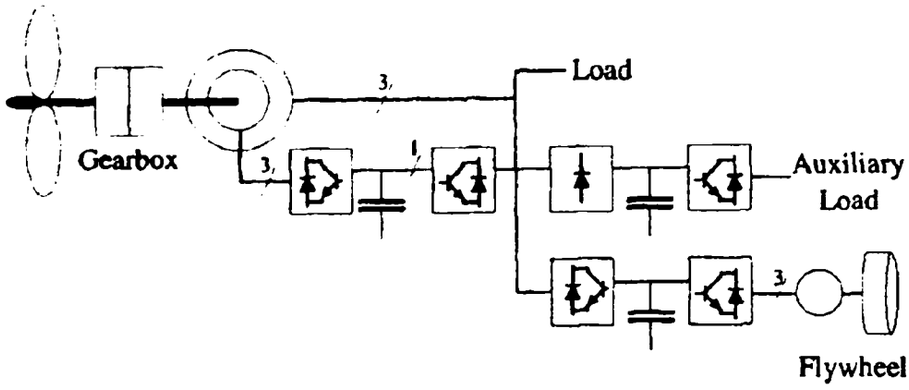

Figure 1.10 Stand-alone wind turbine generator with doubly-fed induction generator [63]

Other control strategies, like: sliding mode, field oriented, neural networks, were detailed presented in a lot of papers. [64], [65]

Sliding mode and fuzzy logic control seems to be a preferred solution for stand-alone applications. Many papers form last years are presenting such control strategies as an alternative to the classic ones. [66], [67], [68]

Like power converters, the control strategy strongly depends on generating system structure, for stand-alone applications, fast response on load changes and permanent provide of maximum output power are essential. For this, it is recommended to be tested many control strategies (at least two of them) and choosing the right one after comparing simulation results. A good example in this way is that shown in [69] where the influence of control strategies on the turbine energy systems depending on some important site conditions and design parameters is presented.

Small stand-alone WTG with a simple closed-loop control system to assure maximum power transfer by the aid of a look-up table which relates the electrical power output of the system to the shaft speed, is developed in [70].

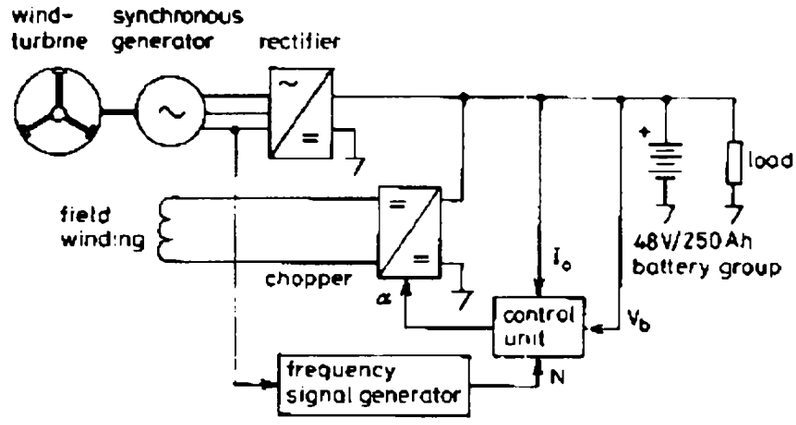

Figure 1.11 Schematic diagram of a stand-alone wind turbine generator

A new criterion for determining optimum dimensions of a generator for wind energy conversion system applications is than introduced. This criterion envisages a maximisation of the energy output for the chosen wind regime while keeping the generator costs at a minimum value.

The power extraction for a turbine depends on three factors:

- the available power;
- the generator external characteristics;
- the capability of the generator to fast response;

The power quality factor refers to the voltage stability, frequency stability and the absence of various forms of electrical noise (flicker or harmonic distortion) on the electrical grid side.

One of the methods to assure a good power quality factor is to increase the voltage on the DC link, when is necessary, from the electrical generator by:

- use of separate two coils in the stator;
- shunt capacitors (to provide reactive compensation for synchronous generators and to improve the field for induction generators);
- use of the second inverter to assure a capacitive current for the field;
- use of one or three ventils after the rectifier;

Steady state and dynamic operation of a novel stand-alone, single-phase induction generator scheme are presented in [71]. The load voltage and frequency are controlled by a single-phase, full-bridge, bipolar pulse-width modulated DC/AC

inverter. A battery feeding the inverter supplies real power to the generator when the load demand is greater than the power supplied by the prime mover (see Figure 1.12).

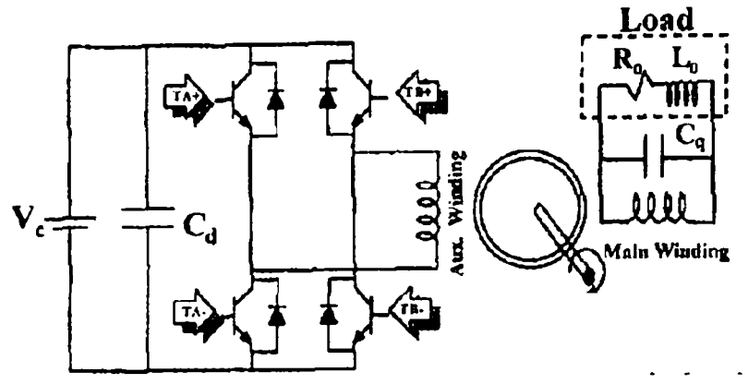

Figure 1.12 Schematic diagram of the single-phase induction generator with a battery-PWM inverter system

Simulation results showed that the output voltage varies almost linearly with the modulation index. Furthermore, the generator can operate with a lower rotor speed with the battery-inverter system supplying the apparent power to meet the load requirements and generator losses.

The system perturbation factors for a stand-alone generator are:

- the unstable speed;
- load variation (weak grids);

Results of a theoretical and laboratory experimental investigation for variable speed generating wind turbine system using a 5.5 kW squirrel cage induction generator which is controlled using a PWM voltage source inverter and a simple speed controller to maintain optimum power transfer for the wind turbine in varying wind speed conditions. is presented. [72]

Instead of significant power extraction from wind energy, comparing to a constant speed operation. the additional losses incurred in frequency conversion demonstrates the availability of this method only for WTG erected in places with frequent wind gusts.

A new DC link voltage boost scheme for adequate voltage coordination in grid connected wind energy conversion system (see Figure 1.13) is presented in [73].

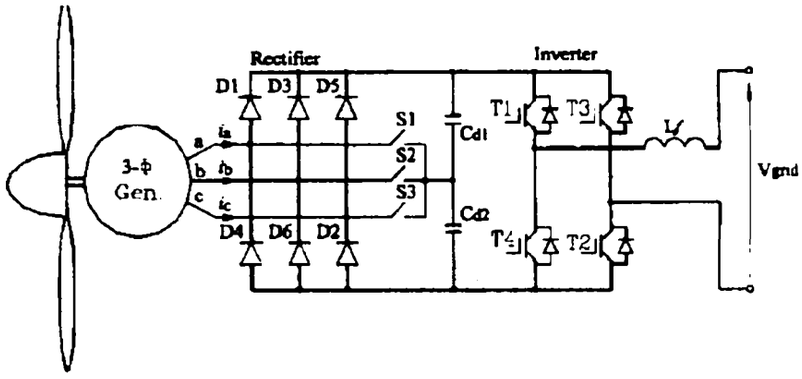

Figure 1.13 Proposed DC link boost scheme

The method provides a simple structure to solve d.c. link voltage shortage problem at low winds by adding one or three switches between the input legs of the rectifier and the middle point of the d.c. link reservoir capacitor.

Using a multiplex control function, the symmetrical double voltage method can change to not-symmetrical and unbalanced generator output to a symmetrical and a balanced one [74].

1.3.5 Converter-fed variable speed pumped-storage system

Experience with the first converter-fed variable speed pumped-storage system, which begun operation at the Yagisawa scheme in Japan 1990, has led to the adoption of this concept for further schemes in the country. Let's look at the advantages and characteristics of the system and outlines its prospects for application at future hydro schemes [75].

In Japan, power companies have, for some time, been investigating new technology to keep the frequency of the grid constant. As high quality energy is increasingly required, it is necessary to adjust the power generated very precisely in accordance with load variations, to achieve a balance whereby load matches generated power precisely.

The system frequency during off-peak times (night time and holidays) is mainly controlled by thermal powerplants in Japan. However, as the proportion of nuclear power generation increases, the use of thermal units for off-peak supply is tending to decrease. There is now concern that the automatic frequency control (AFC) capacity required for the system will become inadequate. If AFC can be achieved by

the pumping unit of a pumped-storage unit, rather than a thermal plant, the AFC capacity can be maintained.

In conventional pumping units, however, the generator-motor rotates at synchronous speed constantly. In conditions of constant speed, a conventional pump-turbine cannot vary the input because of its inherent characteristics. However, a variable speed system can do this [76].

This is the main incentive for the development of the variable speed pumped-storage system.

1.3.5.1 System configuration

The system configuration of a converter-fed variable speed pumped-storage system is shown in Figure 1.14 as a single line diagram.

The system essentially consists of a pump-turbine, a generator-motor, a frequency converter (cycloconverter in Figure 1.14) and a control system.

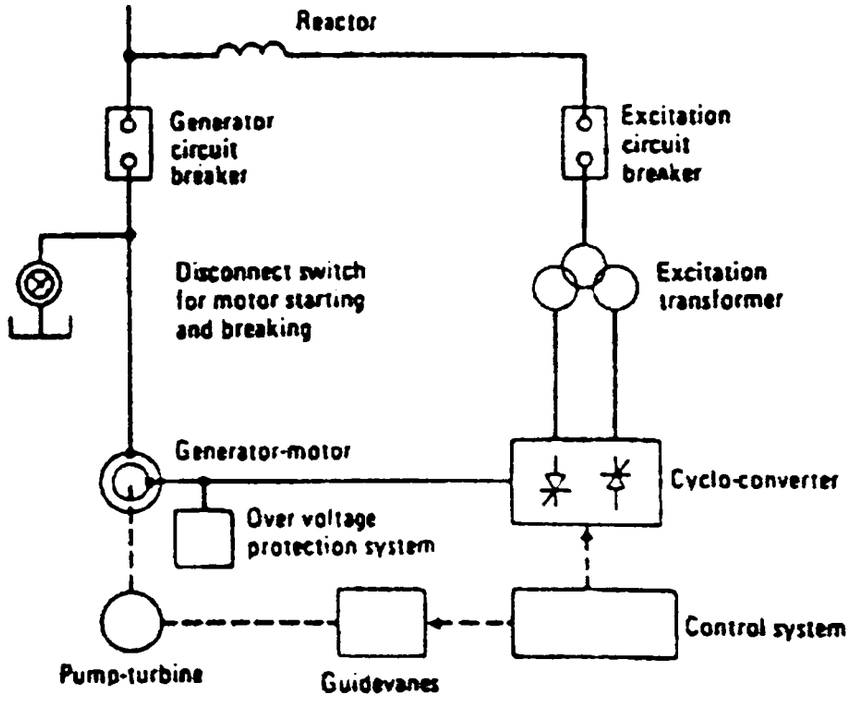

Figure 1.14 Configuration of the converter-fed variable speed pumped-storage system developed in Japan.

The generator-motor and frequency converter in particular are different from those in a conventional synchronous machine. The generator-motor has a cylindrical rotor with three-phase distributed field windings. When these windings are excited by

three phase field current, a rotating magnetic field is generated at the rotor, even if the rotor is at standstill mechanically speed controlled. The mechanical speed plus the electrical speed equals synchronous speed. This is one of the basic principles of the variable speed pumped storage system.

The frequency converter is an excitation system which supplies three-phase excitation current to the field windings of the generator-motor.

The control system not only controls the active and reactive power but also the speed of the unit. They are controlled to optimum values by a digital microprocessor in each of the operating conditions.

1.3.5.2 Advantages

Some of the main advantages of the variable speed system are as follows.

- **Adjustable power for AFC operation in the pumping mode**

The relationship between the pumping head and the pump input is shown in Figure 1.15. In the case of a conventional machine, the pump input is fixed according to the available pumping head. On the other hand, a variable speed machine can vary the pump input by its speed being varied within a specified range.

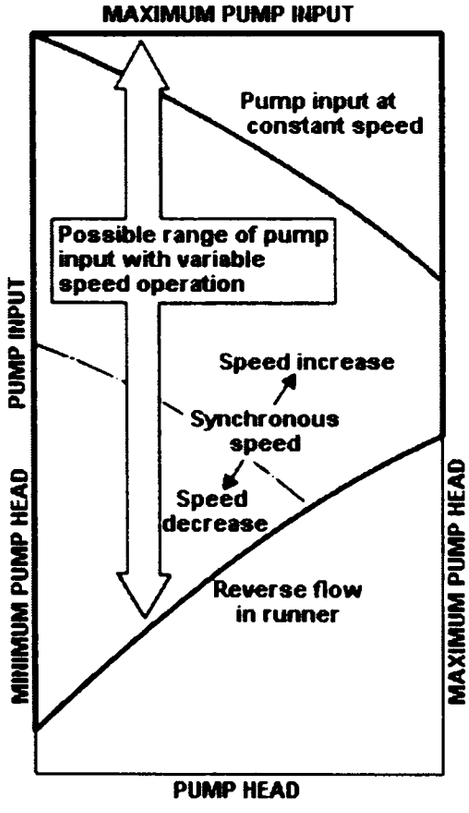

Figure 1.15 AFC operating in pumping mode varies the pump input.

At a certain pumping head, for example, when the machine increases speed, the pump input becomes larger. Because of this characteristics, it is possible to supply power for AFC using a pumped-storage plant.

- **High pump-turbine efficiency**

In the case of a conventional pump-turbine, the unit must rotate at synchronous speed even if there is an optimum speed at which maximum efficiency can be obtained. However, a variable speed machine can be operated at the optimum speed for each available head. The efficiency of the pump-turbine can thus be improved by approximately 10%. These features are shown in Figure 1.16.

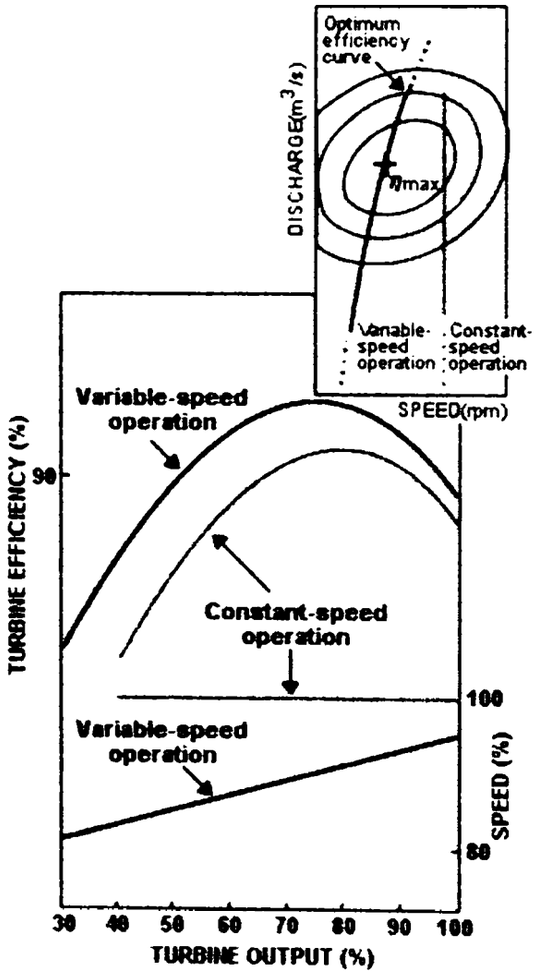

Figure 1.16 10% increase gained in efficiency because turbine operating.

- **Suppression of power system fluctuation**

In the case of a conventional machine, it is impossible to control the internal phase angle instantly because the rotor poles are mechanically fixed to the rotor. A variable

speed machine has no fixed poles, and can therefore control the internal phase angle directly using the frequency converter. This characteristic not only allows for stable operation of the machine itself, but also contributes to the stability of the grid, in the event of power fluctuations occuring. Examples of cases of this suppression are shown in Figure 1.17.

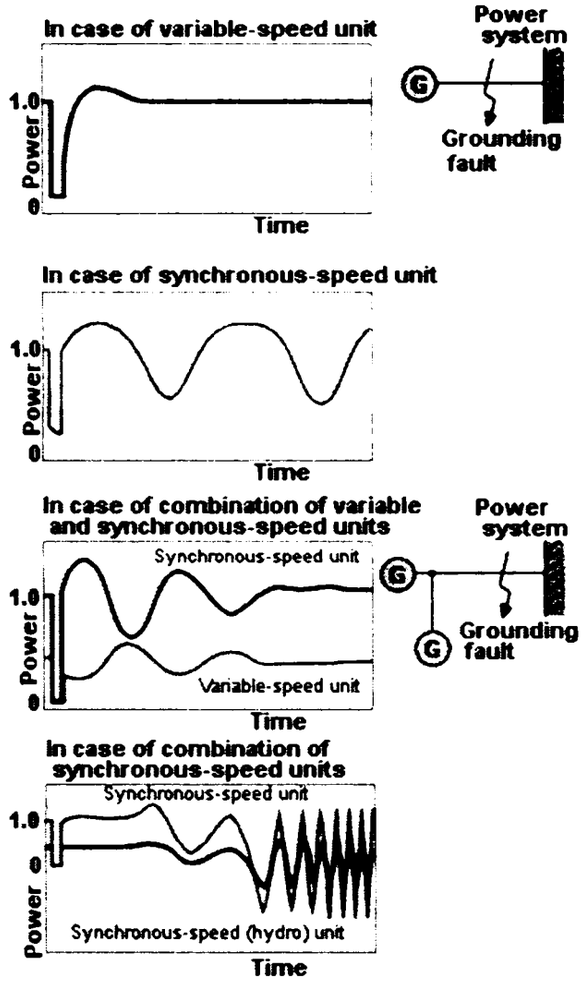

Figure 1.17 Suppression of power system fluctuation.

- **Smooth pump startup**

A conventional machine requires additional equipment to start in the pumping mode. The frequency converter starts the machine without any extra equipment. The frequency converter starts the machine with the primary stator winding being short-circuited and then synchronizes it with the grid, as shown in Figure 1.18.

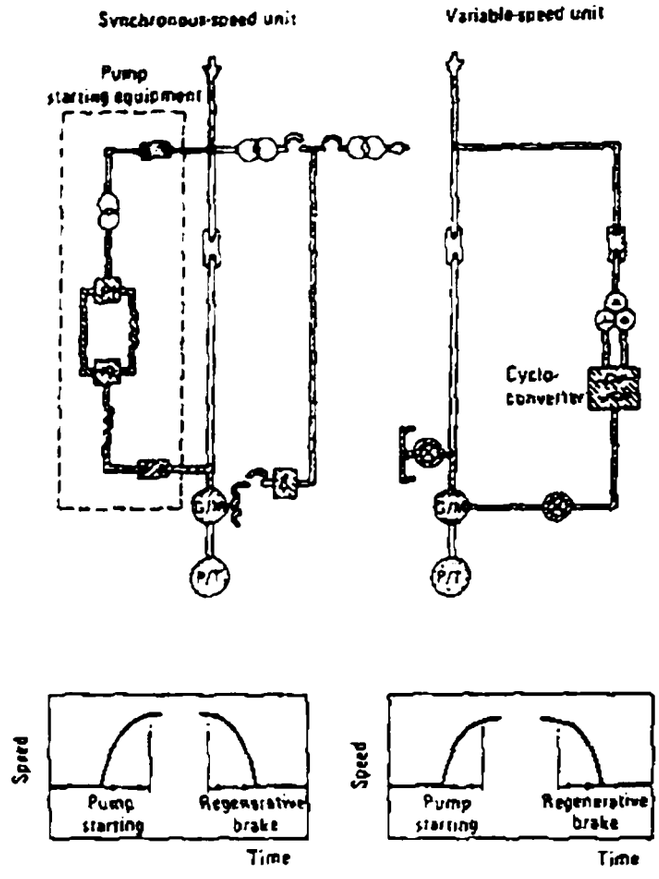

Figure 1.18 Pump startup.

The variable speed system has various additional advantages, as follows: extension of the pump-turbine operating head range in the generating mode, better use of stored water and no air pollution because the AFC is adjusted by the variable speed system rather than thermal plants.

1.3.5.3 Development and characteristics of the system

The recent development of large-scale generator-motors, large capacity electronic systems, elaborate micro-processors, and digital control have made it possible to move ahead with the variable speed pumped-storage concept.

Generator – motor

To solve one of the most important problems of supporting the rotor coil end, a special U-bolt support was developed, consists of a high-strength, high-rigidity retaining ring, and a large number of non-magnetic steel U-bolts to link the coil ends and the retaining ring.

The ventilation was enhanced by choosing a system in which ventilation is provided in the in the radial direction from the inner bore of the rotor core by the centrifugal action of the radial ducts of the rotor core and spokes.

The collector ring for the variable speed generator-motor is a three-phase structure, and has to withstand a high voltage and large current. To check the reliability and ease of maintenance, an actual six collector ring model for a 300 MW class generator-motor was manufactured and tested

Frequency converter

There are two types of frequency converter for the variable speed pumped-storage system. One is a cycloconverter, and the other is an GTO inverter-converter. The cycloconverter consists of thyristors, and has been used in conventional motors, so no special development or tests were required.

Control system

As shown in Figure 1.19, the control system comprises: a sequence control section, which also interfaces with other control systems, protection relaying systems, and operator(s); a plant control section, to control active and reactive power; a guidevane control section; a speed control section; and, a frequency converter and current control section.

The plant control section consists of active power (P) control, and reactive power (Q). Signals from the q-axis component and the d-axis component of the secondary current of the generator-motor control P and Q, respectively and independently.

In the generating mode, the active power is controlled by guidevane opening, and the speed is controlled to obtain high efficiency of the pump-turbine. In the pumping mode, on the other hand, both the speed and active power are controlled by the q-axis component of the secondary current of the generator-motor (Iq^*), see Figure 1.19.

The effective control is achieved by elaborate microprocessor and digital control.This unit begun operation in 1990 as the world's first application of the converter-fed variable speed system. The ratings of the main components are shown in Table 1.5. The various advantages of the system have been verified by field tests

and commercial operation, as the unit has been operating successfully. Till now many other units was developed. (see the ratings of other 2 units in Japan in Table 1.6)

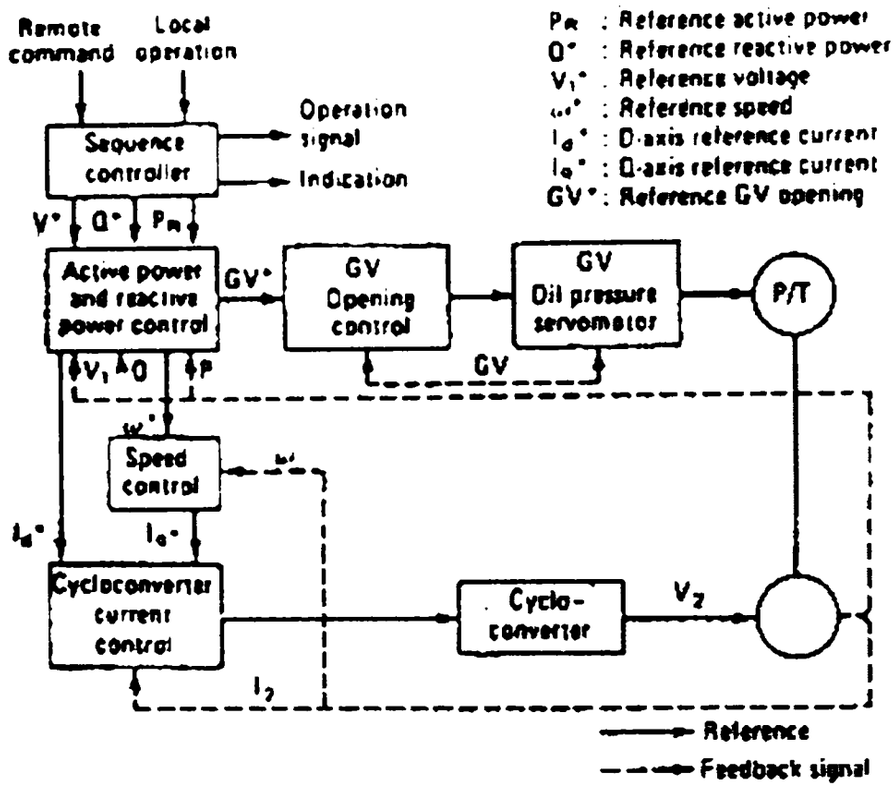

Figure 1.19 Block diagram of the control system

Table 1.5 Ratings of the main components for Yagisawa (unit 2)

Component	Characteristic	Rating
Pump-turbine	Max. output (MW)	87.4
	Head (m)	53 to 111
	Pump input (MW)	53 to 82
	Pumping head (m)	63 to 112.5
Generator-motor	Rated output (MVA)	85
	Rated voltage (kV)	13.8
	Rotating speed (rpm)	130 to 156
Frequency-converter	Type	Cycloconverter
	Rated output (MVA)	25.8
	Rated voltage (kV)	4.8
	Rated current (kA)	3.1
	Output frequency (Hz)	0.25 to 4.6

Table 1.6 Ratings of main components for Sabigawa (unit 3) and Okukiyotsu II (unit 2)

Component	Characteristic	Sabigawa unit 3	Okukiyotsu II unit 2
Pump-turbine	Max. output (MW)	309	310
	Head (m)	304 to 372	432 to 494
	Pump input (MW)	200 to 330	230 to 340
	Pumping head (m)	330 to 387	460 to 514
Generator-motor	Rated output (MVA)	360	345
	Rated voltage (kV)	16.5	16.5
	Rotating speed (rpm)	375±8%	429±5%
Frequency-converter	Type	Cycloconverter	GTO inverter-converter
	Rated output (MVA)	51.1	31.5
	Rated voltage (kV)	5.90	3.04
	Rated current (kA)	5.00	5.98
	Output frequency (Hz)	0.25 to 4	0.25 to 2.5

1.3.6 Dual Stator Winding Induction Generator

The dual stator winding synchronous machine was introduced at the beginning of this century as a means of increasing the power capability of large synchronous generators. In the recent past, it was used as a source of both regulated dc and ac output voltages. Dual stator winding reluctance machines have also been investigated for both drive and autonomous generator operations. The angular speed of the generated voltage is equal to the electrical rotor angular speed in the dual stator winding synchronous generator. In the dual stator winding reluctance generator, the sum of the angular electrical frequencies of the currents in the two stator windings equals the electrical frequency of the shaft (in the steady state) – rigidly tying the frequency of the generated voltage to the shaft speed. In applications with variable turbine (rotor) speeds, load frequency control is slightly complicated by dual synchronous and reluctance generators. Although it is realized that dual stator winding induction machines may be used as generators in view of the additional degree of freedom given by the uncoupled relationship between the rotor speed and frequency of generated voltage, it has not been fully explored until now.

Two types of dual stator winding induction machines with standard squirrel-cage rotor structure have been proposed. In the first design, there are two identical three-phase windings (control and power winding sets) which are wound for the same number of poles. However, these two windings are electrically displaced from each

other. In the most recently proposed design. the control and power windings are wound for different pole numbers with no displacement between the power and control windings using the regular squirrel-cage rotor structure – ideally decoupling the torque production of the two windings when individually excited. Of course, there are the doubly fed induction machines with specially designed rotor cage structures.

The generator scheme presented is based on the dual stator winding induction machine with displaced power and control winding sets [77]. The power and control windings have the same number of poles. In Figure 1.20 (a), a three-phase pulse width modulation (PWM) dc-ac inverter under sine-triangle control and fed with a battery source is connected to the control windings.

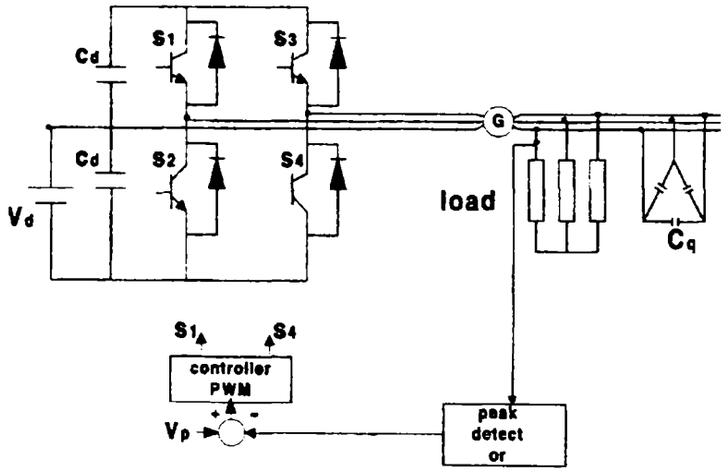

a)

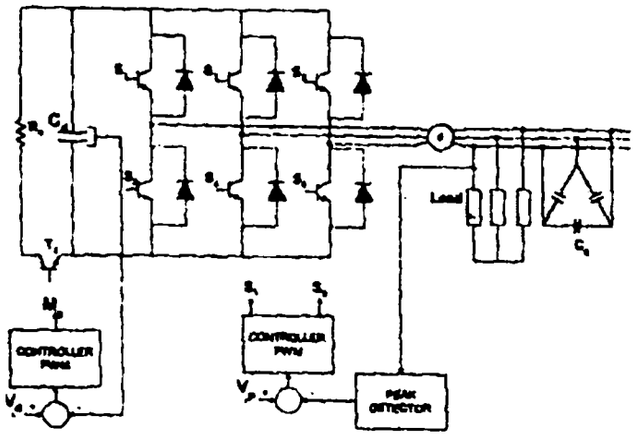

b)

Figure 1.20 Schematic diagram of the dual stator winding induction generator with dc-ac inverter. (a) With a battery source. (b) With a charged dc capacitor

The DC-AC PWM inverter, augmenting the compensating three-phase delta-connected capacitors Cq, provides reactive power to the generator system, fixes the load frequency, and influences the magnitude of the load voltage by regulating the modulation index magnitude. Indeed, the frequency of the reference signal of the PWM becomes the frequency of the generated load voltage.. The battery source acts as a real power buffer. When the real power provided by the rotor shaft exceeds the load real power demand and system losses, the excess power is stored in the battery through the bidirectional inverter.

If, on the other hand, the real power demand of the load and losses exceeds the input real power from the shaft, the balance is supplied by the battery. Another advantage of this scheme is the possibility of maintaining a load voltage magnitude with the desired load frequency, even when the rotor slip is positive for a relatively short period. While the machine motors, the battery provides the needed real power through the inverter to the load.

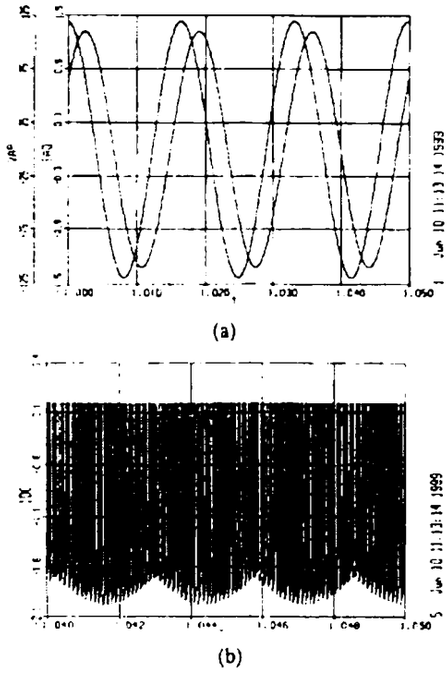

Figure 1.21 Generator waveforms: a) load voltage (V) and current (A); time in seconds requiring the decrease of the duty ratio (increasing the effective discharge resistance value) so as to maintain the reference capacitor voltage

The scheme in Figure 1.20 (b) has a charged dc capacitor connected to the inverter input. If the load is light, the dc capacitor may overcharge and the system becomes instable. If the load is heavy, the capacitor discharges, and the load voltage collapses. To ensure stable operation, a discharge resistor is connected across the charged capacitor through a transistor or MOSFET under PWM duty ratio control. The duty ratio control, which seeks to regulate the capacitor voltage , presents a variable resistance (which dissipates the excess real power) to the charged capacitor. The inverter PWM modulation index magnitude control regulates the load voltage. A feedback control scheme is required to operate the system stably. Since there is no source of active power on the inverter side if the rotor slip is positive the load voltage decays and may ultimately collapse.

The generator waveforms (load voltage and current) are illustrated in Figure 1.21 a) and b). The change of the load impedance was performed and the results are shown in Figure 1.22. In Figure 1.22 a) the reference and the measured load voltage are illustrated and in Figure 1.22 b) the inverter input currents are shown.

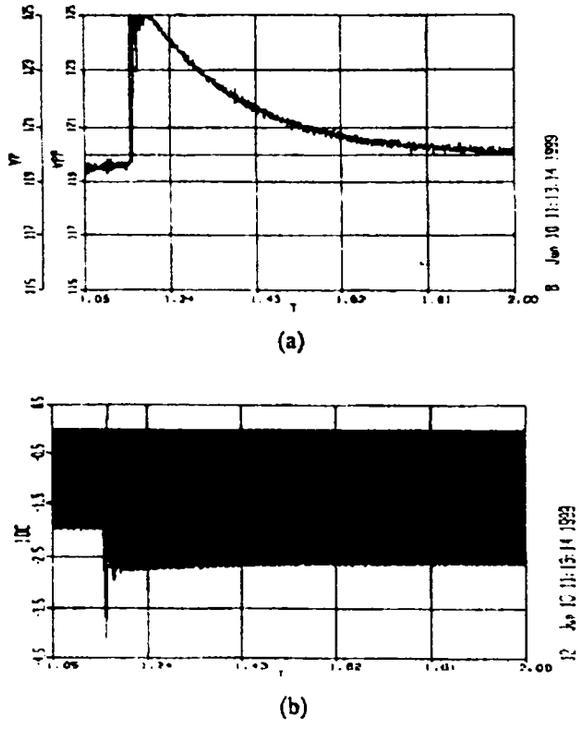

Figure 1.22 Dynamics of generator to change in load impedance from 20 to 200 Ω, voltage reference = 120V a) Reference and peak load voltage (V), b) Inverter input current (A), time in seconds

1.3.7 Direct Power Control of DFIG

Conventionally, grid-connected cage rotor induction machines are used as wind generators at medium power level. When connected to the constant frequency network, the induction generator runs at near synchronous speed drawing the magnetizing current from the mains, thereby resulting in constant speed constant frequency (CSCF) operation. However, the power capture due to fluctuating wind speed can be substantially improved if there is flexibility in varying the shaft speed.

In such variable speed constant frequency (VSCF) application rotor side control of grid-connected doubly-fed induction machine is an attractive solution. In the system under consideration, the stator is directly connected to the three phase grid and the rotor is supplied by two back-to-back PWM converters (see Figure 1.23).

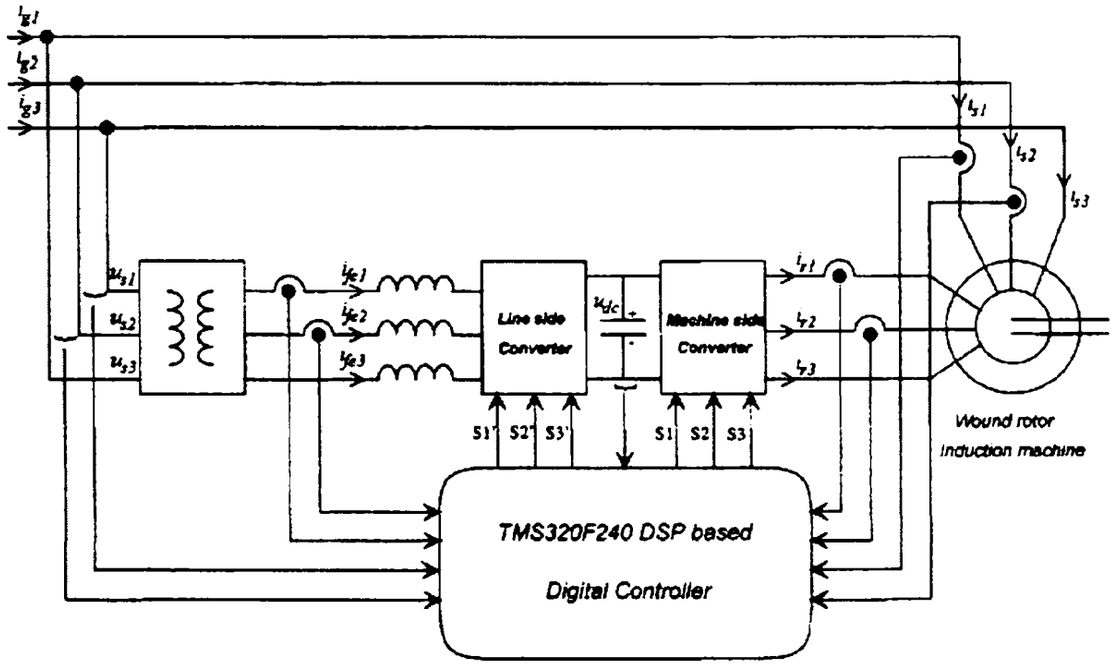

Figure 1.23 Schematic block diagram of the DFIG system. [59]

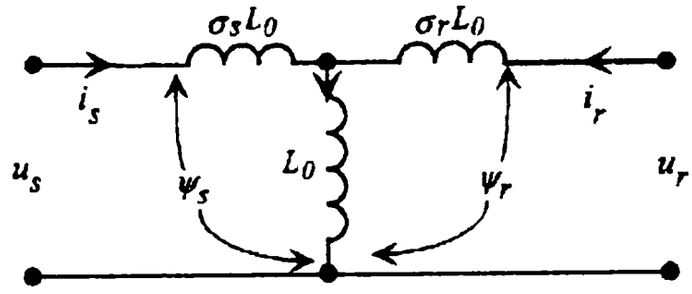

Figure 1.24 Approximate equivalent circuit

The equivalent circuit is shown in Figure 1.24. Such an arrangement provides flexibility of operation in subsynchronous and supersynchronous speeds both in the generating and motoring modes. The rating of the power converters used in the rotor circuit is substantially lower than the machine rating and is decided by the range of operating speed. Of the two converters, the function of the line side converter is to regulate the dc bus voltage and act as unity power factor interface to the grid for either direction of power flow. The machine side converter has to control the torque and flux of the machine or alternatively the active and reactive powers. The conventional approach for independent control of active and reactive powers handled by the machine is stator flux oriented vector control with rotor position sensors. The performance of the system in this case depends on the accuracy of computation of the stator flux and the accuracy of the rotor position information derived from the position encoder. Alignment of the position sensor is moreover difficult in a doubly-fed wound rotor machine. Position sensorless vector control methods have been proposed by several research groups in the recent past. A dynamic torque angle controller was proposed. This method uses integration of the PWM rotor voltage to compute the rotor flux; hence satisfactory performance cannot be achieved at or near synchronous speed. Most of the other methods proposed make use of the measured rotor current and use coordinate transformations for estimating the rotor position. Varying degree of dependence on machine parameters is observed in all these strategies.

Alternative approaches to field oriented control such as direct self control (DSC) and direct torque control (DTC) have been proposed for cage rotor induction machines. In these strategies, two hysteresis controllers, namely a torque controller and a flux controller, are used to determine the instantaneous switching state for the

inverter. These methods of control are computationally very simple and do not require rotor position information.

In what follows, a recently developed algorithm [59], for independent control of active and reactive powers with high dynamic response in case of a doubly-fed induction machine is described. The instantaneous switching state of the rotor side converter is determined based on the active and reactive powers measured in the stator circuit. Thus, unlike existing DTC techniques, measurements are carried out at one terminal of the machine whereas the switching action is carried out at another terminal. Here the directly-controlled quantities are the stator active and reactive powers; hence, the algorithm is referred to as *direct power control (DPC)* in the text.

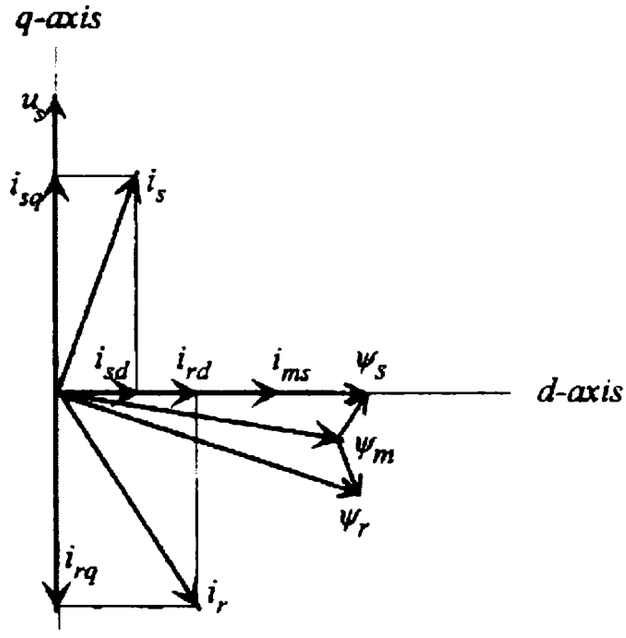

Figure 1.25 Phasor diagram

The proposed algorithm also differs from conventional DTC in that it does not use integration of PWM voltages. Hence, it can work stably even at zero rotor frequency. The method is inherently position sensorless and does not depend on machine parameters like stator/rotor resistance. It can be applied to VSCF applications like wind power generation as well as high power drives. The concept of direct power control is first introduced and details of the control strategy are discussed.

1.3.7.1 The concept of DPC

The basic concept of direct control of active and reactive powers can be appreciated from the phasor diagrams based on the equivalent circuit of the doubly-fed machine as shown in Figure 1.24. From the phasor diagram in Figure 1.25 it is noted that the component of the stator current i_{sq} has to be controlled to control the stator active power P_s and i_{sd} has to be controlled to control the stator reactive power Q_s. This is achieved in turn by controlling the rotor currents i_{rq} and i_{rd}, respectively, in conventional field oriented control strategy. The effect of injection of these rotor currents on the air-gap and rotor fluxes can be derived by subtracting and adding the respective leakage fluxes. The variation of the rotor flux with variations in the active and reactive power demand is shown in Figure 1.26 a) and b).

In Figure 1.26 a) $i_{rd} = 0$ i.e., the reactive power is fed completely from the stator side. Under this condition if i_{rq} is varied from 0 to full load, the locus of $\underline{\psi}_r$ varies along A–B which indicates a predominant change in angle δ between $\underline{\psi}_s$ and $\underline{\psi}_r$, whereas the magnitude of $\underline{\psi}_r$ does not change appreciably. In other words, a change in the angle δ would definitely result in a change in the active power handled by the stator in a predictable fashion.

In Figure 1.26 b) the stator active power demand is maintained constant so that i_{rq} is constant and i_{rd} is varied from 0 to the rated value of i . Here the locus of varies along C–D, resulting in a predominant change in magnitude of $\underline{\psi}_r$, whereas the variation of δ is small. Therefore, the reactive power drawn from the grid by the stator can be reduced by increasing the magnitude of the rotor flux and vice-versa.

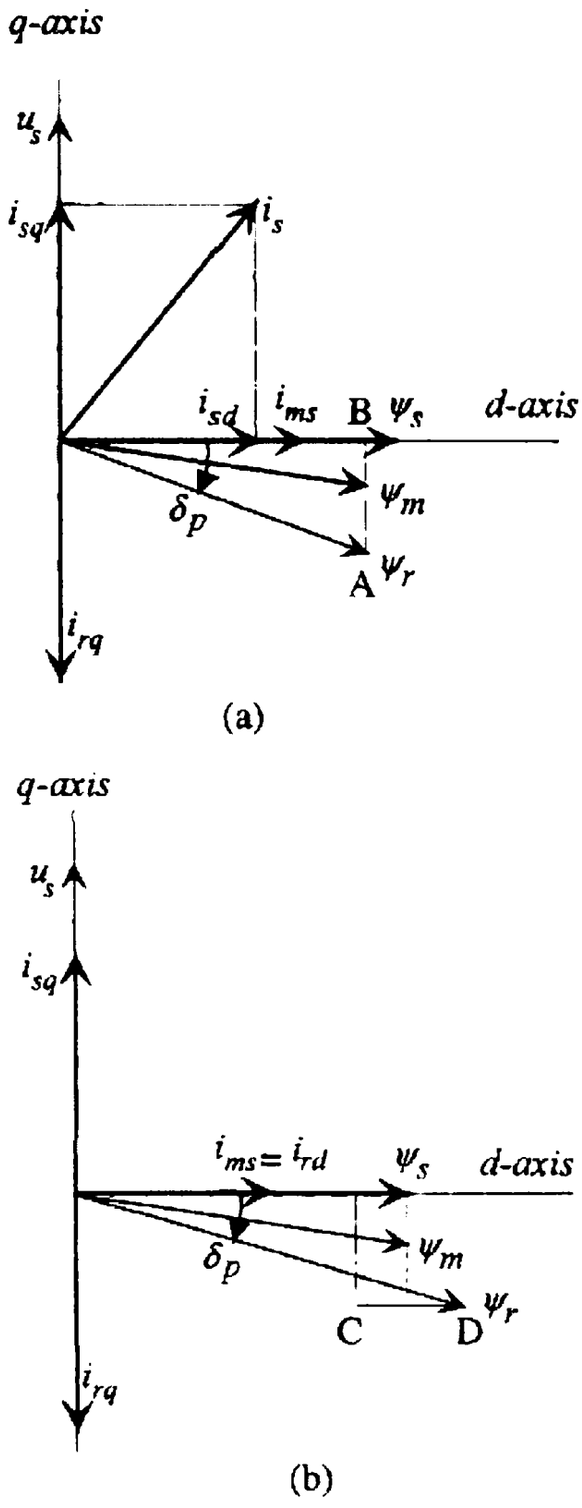

Figure 1.26 Phasor diagram showing variations in rotor flux with change in active and reactive power.

It may be noted that the phasor diagrams as indicated in Figure 1.26 a) and 1.26 b) remain the same irrespective of the reference frame; the frequency of the phasors merely changes from one reference frame to the other. It can be concluded from the above discussion that:

i) The stator active power can be controlled by controlling the angular position of the rotor flux vector.

ii) The stator reactive power can be controlled by controlling the magnitude of the rotor flux vector.

These two basic notions are used to determine the instantaneous switching state of the rotor side converter to control the active and reactive power as discussed in the following section.

1.3.7.2 Voltage Vectors and Their Effects

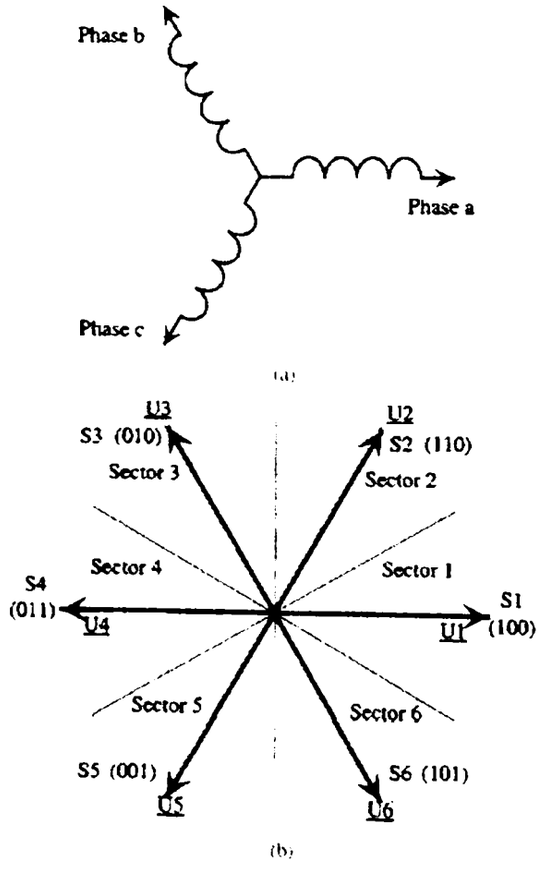

Figure 1.27 (a) Orientation of the rotor winding in space with respect to which the voltage space phasors are drawn and (b) voltage space phasors.

Assuming that the orientation of the three phase rotor winding in space at any instant of time is as given in Figure 1.27 a), the six active switching states S1, S2...S6 would result in the voltage space vectors U1, U2, ..., U6 (see Figure 1.27 b) at that instant.

In order to make an appropriate selection of the voltage vector the space phasor plane is first subdivided into six 60^0 sectors 1,2...6. The instantaneous magnitude and angular velocity of the rotor flux can now be controlled by selecting a particular voltage vector depending on its present location. The effect of the different vectors as reflected on the stator side active and reactive powers, when the rotor flux is positioned in Sector 1 is illustrated in the following subsections.

1.3.7.3 Effect of Active Vectors on Active Power.

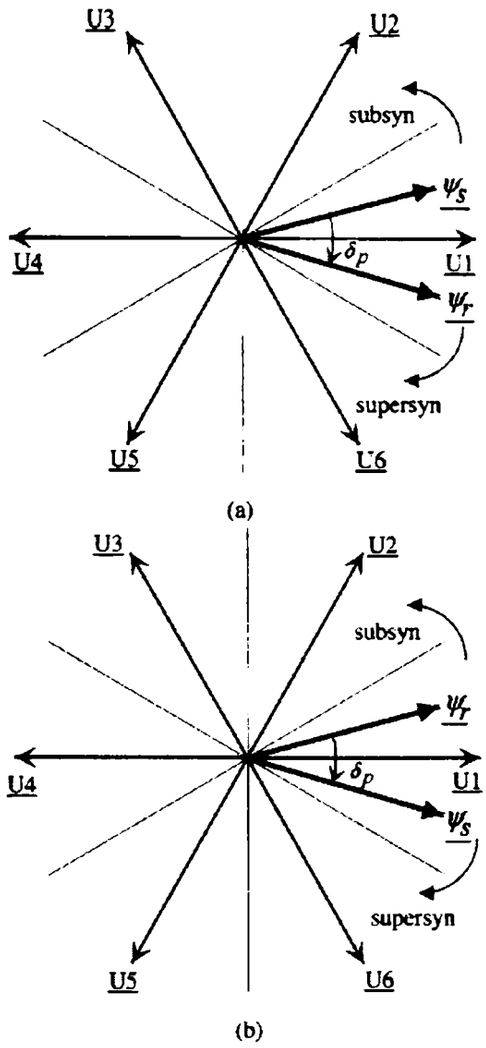

Figure 1.28 Flux vectors in (a) motoring mode and (b) generating mode.

Considering anti clockwise direction of rotation of the flux vectors in the rotor reference frame to be positive, it may be noted that $\underline{\psi}_s$ is ahead of $\underline{\psi}_r$ in motoring mode of operation and $\underline{\psi}_s$ is behind $\underline{\psi}_r$ in generating mode. This is illustrated in Figure 1.28 a) and b) respectively.

In the rotor reference frame the flux vectors rotate in the positive direction at subsynchronous speeds, remain stationary at synchronous speed and start rotating in the negative direction at supersynchronous speeds.

Assuming that the rotor flux is positioned in Sector 1, application of voltage vectors U2 and U3 accelerates $\underline{\psi}_r$ in the positive direction. In the motoring mode of operation, this reduces the angular separation between the two fluxes resulting in a reduction of active power drawn by the stator. In the generating mode of operation, application of vectors U2 and U3 results in an increase in angular separation between the two and thereby an increase in the active power generated by the stator. (P_s being negative for generation, application of U2 and U3 still results in a reduction of positive active power.) Similarly it can be seen that the effect of U5 and U6 on the active power would be exactly opposite to that of U2 and U3 in both the motoring and generating modes.

Power drawn by the stator being taken as positive and power generated being taken as negative, it may therefore, be concluded that, if the rotor flux is in the k-th sector, where k = 1, 2, 3....6 application of vectors U (k+1) and U (k+2) would result in a reduction in the stator active power and application of vectors U (k-1) and U (k-2) would result in an increase in the stator active power.

1.3.7.4 Effect of Active Vectors on Reactive Power.

From the phasor diagrams Figure 1.26 a) and b) it can be seen that the reactive power drawn by the stator depends upon the component of $\underline{\psi}_r$ along $\underline{\psi}_s$ i.e. $\underline{\psi}_{rd}$. The angle between $\underline{\psi}_s$ and $\underline{\psi}_r$ i.e. δ being small, the magnitude of $\underline{\psi}_r$ is approximately equal to $\underline{\psi}_{rd}$. Therefore, when the rotor flux vector is located in Sector 1, voltage vectors U1, U2, and U6 and increase the magnitude of $\underline{\psi}_r$ whereas, U3, U4, and U5 reduce it. This holds good irrespective of whether the machine is operating in motoring or generating mode. An increase in magnitude of $\underline{\psi}_r$ indicates an increased amount of reactive power being fed from the rotor side and hence, a reduction in the reactive power

drawn by the stator resulting in an improved stator power factor. A decrease in magnitude of $\underline{\psi}_r$ amounts to lowering of the stator power factor. As a generalization it can therefore, be said that if the rotor flux resides in the sector, switching vectors U(k), U(k+1), and U(k-1) reduce the reactive power drawn from the stator side and U(k+2), U(k-2), U(k+3) increase the reactive power drawn from the stator side.

1.3.7.5 Effect of Zero Vector on Active Power.

The effect of the zero vectors is to stall the rotor flux without affecting its magnitude. This results in an opposite effect on the stator active power in subsynchronous and supersynchronous modes of operation.

In subsynchronous motoring, application of a zero vector increases δ as $\underline{\psi}_s$ keeps rotating in the positive direction at slip speed. Above the synchronous speed, $\underline{\psi}_s$ rotates in the counter clockwise direction thereby reducing δ. Hence active power drawn by the stator increases for subsynchronous operation and decreases for supersynchronous operation. Active power generated being negative, the same conclusion holds true for the generating modes as well.

1.3.7.6 Effect of Zero Vector on Reactive Power.

Since a zero vector does not change the magnitude of the rotor flux its effect on the reactive power is rather small. Nevertheless, there is some small change in Q_s; its effect being dependent on whether the angle between the stator and rotor fluxes increases or decreases due to the application of a zero vector.

Table 1.7 Effect of zero vector on reactive power

Speed	Motoring	Generating
Subsynchronous	$\delta_p \uparrow \Rightarrow \psi_{rd} \downarrow \Rightarrow Q_s \uparrow$	$\delta_p \downarrow \Rightarrow \psi_{rd} \uparrow \Rightarrow Q_s \downarrow$
Supersynchronous	$\delta_p \downarrow \Rightarrow \psi_{rd} \uparrow \Rightarrow Q_s \downarrow$	$\delta_p \uparrow \Rightarrow \psi_{rd} \downarrow \Rightarrow Q_s \uparrow$

Note: $\uparrow$ denotes increase, $\downarrow$ denotes decrease

An increase in angular separation between the two fluxes reduces $\underline{\psi}_{rd}$ resulting in an increment of Q_s drawn from the stator side. The converse is true when δ reduces.

It is observed that the change in Q_s due to the application of the zero vector is different in all the 4 modes of operation. This is summarized in Table 1.7.

1.3.7.7 Control Algorithm

With the inferences drawn in the previous section it is possible to switch an appropriate voltage vector in the rotor side at any given instant of time to increase or decrease the active or reactive power in the stator side. Therefore, any given references for stator active and reactive powers can be tracked within a narrow band by selecting proper switching vectors for the rotor side converter. This is the basis of the direct power control strategy. The details of the control algorithm are discussed in the following subsections. It should be noted that the torque reference for the machine is decided by an outer loop for either motoring or generating application. The reference for the stator power can. therefore, be calculated as:

$$P_s^* = m_d^* \cdot \omega_s \tag{1.1}$$

Q_s^* is set according to the desired power factor at the stator terminals.

1.3.7.8 Measurement of Stator Active and Reactive Power

The active and reactive powers on the stator side can be directly computed from the stator currents and voltages. Assuming a balanced three phase three wire system, only two currents and two voltages need to be measured. The active and reactive powers can be expressed as:

$$P_s = \frac{2}{3}\left(v_{s\alpha} i_{s\alpha} + v_{s\beta} i_{s\beta}\right) \tag{1.2}$$

$$Q_s = \frac{2}{3}\left(v_{s\beta} i_{s\alpha} - v_{s\alpha} i_{s\beta}\right) \tag{1.3}$$

where:

$$v_{s\alpha} = \frac{3}{2} v_{s1} \tag{1.4}$$

$$v_{s\beta} = \frac{\sqrt{3}}{2}\left(v_{s1} + 2v_{s2}\right) \tag{1.5}$$

and.

$$i_{s\alpha} = \frac{3}{2} i_{s1} \tag{1.6}$$

$$i_{s\beta} = \frac{\sqrt{3}}{2}(i_{s1} + 2i_{s2}) \tag{1.7}$$

1.3.7.9 Defining References and Errors

As shown in Figure 1.29. P_s^* is the reference for stator active power.

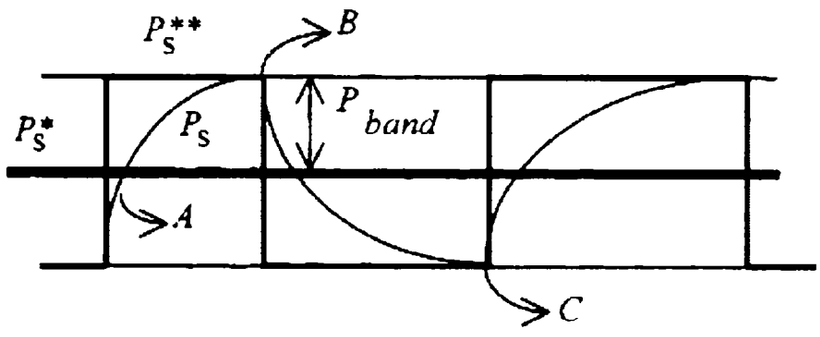

Figure 1.29 Hysteresis control of active power

The actual power P_s is to be controlled to stay within a band of width P_{band} about P_s^*. This is achieved by defining an auxiliary reference P_s^{**} and switching as per the following logic.

$$\begin{aligned} &P_{err} = P_s^{**} - P_s \\ &if\ (P_{err} > 0)\ P_s^{**} = P_s^{*} + P_{band} \\ &else\ P_s^{**} = P_s^{*} - P_{band} \end{aligned} \tag{1.8}$$

In a similar manner the error and reference for the reactive power can be written as:

$$\begin{aligned} &Q_{err} = Q_s^{**} - Q_s \\ &if\ (Q_{err} > 0)\ Q_s^{**} = Q_s^{*} + Q_{band} \\ &else\ Q_s^{**} = Q_s^{*} - Q_{band} \end{aligned} \tag{1.9}$$

1.3.7.10 Switching Vector Selection

In order to determine the appropriate switching vector at any instant of time, the errors in P_s and Q_s, and the sector in which the rotor flux vector is presently residing are taken into consideration. Thus the following two switching tables for active vector selection can be generated. Tables 1.8 and 1.9 correspond to negative P_{err} and positive P_{err}, respectively.

Table 1.8 Selection of active switching states when (P_{err} <= 0)

	Sector 1	Sector 2	Sector 3	Sector 4	Sector 5	Sector 6
Qerr > 0	S5	S6	S1	S2	S3	S4
Qerr <= 0	S6	S1	S2	S3	S4	S5

Table 1.9 Selection of active switching states when (P_{err} >0)

	Sector 1	Sector 2	Sector 3	Sector 4	Sector 5	Sector 6
Qerr > 0	S3	S4	S5	S6	S1	S2
Qerr <= 0	S2	S3	S4	S5	S6	S1

If the rotor side converter is switched in accordance to these tables it is possible to control the active and reactive powers in the stator side within the desired error bands. But the use of active vectors alone would result in nonoptimal switching of the converter and also a higher switching frequency.

By considering the effect of the zero vector on active and reactive powers, the logic for selecting the zero vector can be summarized as in Table 1.10.

Table 1.10 Condition for selection of zero vector

Speed	Motoring	Generating
Subsynchronous	$Q_{err} \geq 0$ && $P_{err} \geq 0$	$Q_{err} < 0$ && $P_{err} \geq 0$
Supersynchronous	$Q_{err} < 0$ && $P_{err} < 0$	$Q_{err} \geq 0$ && $P_{err} < 0$

During subsynchronous motoring mode of operation, the application of a zero vector will increase Q_s as seen from Table 1.7. As δ_p increases under this condition, P_s also increases. Hence, when the errors in Q_s and P_s are positive, a zero vector is

applied to effect an increment in both the stator active and reactive powers and thereby bring down the errors. The other entries in the table can be worked out in a similar manner. Whenever a zero vector has to be applied, the one nearest to the present active vector is selected to minimize the number of switchings.

Also, it is observed that the effect of the zero state on P_s is opposite in the subsynchronous and supersynchronous modes of operation. This criterion is used in detecting the transition from subsynchronous to supersynchronous operation and *vice-versa*.

1.3.7.11 Sector identification of Rotor Flux

In order to implement the switching algorithm the present sector of the rotor flux has to be identified. The exact position of the rotor flux space phasor within the sector is not of importance as far as the selection of the switching vectors is concerned. The proposed method of sector identification is based on the direction of change in Q_s when a particular switching vector is applied. The concept is illustrated by the following example. Suppose that the present position of the rotor flux is in Sector 1 and it is moving in the positive direction (corresponding to subsynchronous operation). Therefore, application of switching states S2 and S6 results in a reduction of Q_s and application of S3 and S5 results in an increase of Q_s. When the rotor flux vector crosses over to Sector 2, the effect of states S3 and S6 on Q_s would reverse. Vector $\underline{U3}$ would now act to reduce Q_s instead of increasing it. Similarly the effect of vector $\underline{U6}$ on Q_s would also be opposite. These reversals in the direction of change of Q_s, when a particular vector is applied, can be detected and a decision for sector change may be taken on this basis. Similarly, if the flux vector is rotating in the negative direction (supersynchronous operation) the effect of states S2 and S5 on Q_s would change in direction when $\underline{\psi}_r$ changes over from Sector 1 to Sector 6. Thus in any particular direction of rotation there are two vectors which can provide the information for a change in sector. Since the rotor flux vector cannot jump through sectors the change will always be by one sector, either preceding or succeeding. In this method, even though the exact position of the flux is unknown, the sector information can be updated just by observing the changes in Q_s due to the applied

vectors. It may be noted that the effect of the vectors on would not provide a conclusive inference about the change in sector.

The expected direction of change in Q_s due to the application of any switching state in the different sectors can be summed up as shown in Table 1.11.

Table 1.11 Expected direction of change Q_s

	S0	S1	S2	S3	S4	S5	S6	S7
Sector 1	0	-	-	+	+	+	-	0
Sector 2	0	-	-	-	+	+	+	0
Sector 3	0	+	-	-	-	+	+	0
Sector 4	0	+	+	-	-	-	+	0
Sector 5	0	+	+	+	-	-	-	0
Sector 6	0	-	+	+	+	-	-	0

It may however. be noted that in a particular sector not all vectors will be applied. For example, in sector k, vectors U(k) and U(k+3) will never be applied. These vectors would have predominant effect on the reactive power, but their effect on the active power would depend on the actual position of the rotor flux vector in the sector. In most applications there is hardly any requirement for fast transient changes in reactive power; so it is not necessary to apply the strongest vector to effect any change in Q_s. In the switching logic, therefore, only those vectors are selected which have uniform effects on P_s and Q_s in terms of their direction of change irrespective of the position of the rotor flux in a particular sector.

For any given vector applied in a particular sector the expected direction of change in Q_s can be read off from Table 1.11 The actual direction of change can be computed from the present value of Q_s and its previous value.

Table 1.12 Direction of change of sector

	S0	S1	S2	S3	S4	S5	S6	S7
Sector 1	0	0	-1	+1	0	-1	+1	0
Sector 2	0	+1	0	-1	+1	0	-1	0
Sector 3	0	-1	+1	0	-1	+1	0	0
Sector 4	0	0	-1	+1	0	-1	+1	0
Sector 5	0	+1	0	-1	+1	0	-1	0
Sector 6	0	-1	+1	0	-1	+1	0	0

If the actual direction of change is opposite to the expected direction of change then a decision on change of sector is taken. Whether the sector change has to be

effected in the clockwise or anti clockwise direction depends on the applied vector and the observed change in. This information is stored in another lookup table (Table 1.12).

The method of sector identification is therefore, independent of any machine parameter but relies on directly measurable fixed frequency quantities. It is also independent of the rotor frequency and can work stably at or near synchronous speed.

1.3.8 Vector Control of DFIG

In the following sections the principle of vector control of doubly-fed induction generator with two inverters connected back-to-back in the rotor circuit will be presented (see also Figure 1.23 for a general schematic of the system).

1.3.8.1 Control of supply (line) – side PWM converter [12]

The objective of the supply-side converter is to keep the DC-link voltage constant regardless of the magnitude and direction of the rotor power. A vector-control approach is used with a reference frame oriented along the stator voltage vector, enabling independent control of the active and reactive power flowing between the supply and the supply-side converter. The PWM converter is current regulated, with the direct axis current used to regulate the DC-link voltage and the quadrature axis current component used to regulate the reactive power. A standard regular asymmetric sampling PWM scheme [12] is used. Figure 1.30 shows the schematic of the supply-side converter.

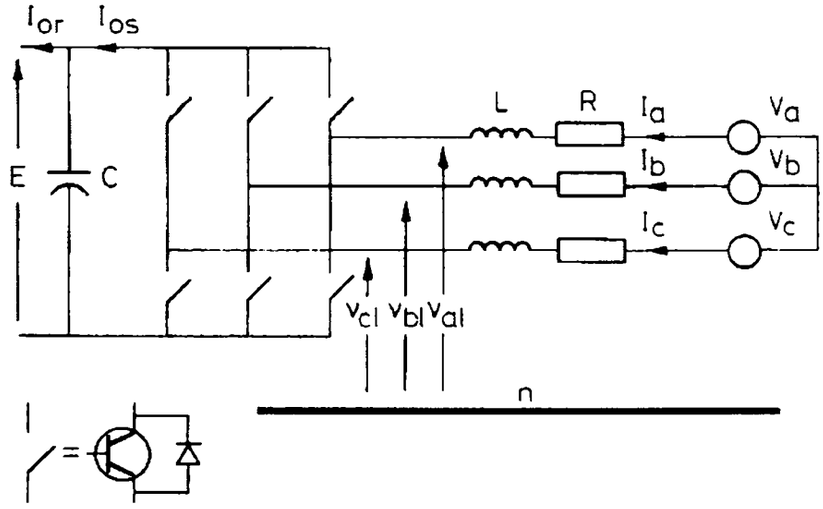

Figure 1.30 Supply-side converter arrangement

The voltage balance across the inductors is:

$$\begin{bmatrix} v_a \\ v_b \\ v_c \end{bmatrix} = R\begin{bmatrix} i_a \\ i_b \\ i_c \end{bmatrix} + L\frac{d}{dt}\begin{bmatrix} i_a \\ i_b \\ i_c \end{bmatrix} + \begin{bmatrix} v_{a1} \\ v_{b1} \\ v_{c1} \end{bmatrix} \tag{1.10}$$

where L and R are the line inductance and resistance, respectively. using the transformations Equation 1.10 is transformed into a dq reference frame rotating at ω_e:

$$\begin{aligned} v_d &= Ri_d + L\frac{di_d}{dt} - \omega_e L i_q + v_{d1} \\ v_q &= Ri_q + L\frac{di_q}{dt} + \omega_e L i_d + v_{q1} \end{aligned} \tag{1.11}$$

With the scaling factors used in the transformations, the active and reactive power flow is:

$$\begin{aligned} P &= 3(v_d i_d + v_q i_q) \\ Q &= 3(v_d i_q + v_q i_d) \end{aligned} \tag{1.12}$$

The angular position of the supply voltage is calculated as:

$$\theta_e = \int \omega_e dt = \tan^{-1}\frac{v_\beta}{v_\alpha} \tag{1.13}$$

where v_α and v_β are the α, β (stationary 2-axis) stator-voltage components.

Aligning the d-axis of the reference frame along the stator-voltage position given by Equation 1.13, v_q is zero, and, since the amplitude of the supply voltage is constant v_d is constant. The active and reactive power will be proportional to i_d and i_q respectively.

Neglecting harmonics due to switching and the losses in the inductor resistance and converter, we have:

$$
\begin{aligned}
Ei_{ox} &= 3v_d i_d \\
v_d &= \frac{m_1}{2\sqrt{2}} E \\
i_{ox} &= \frac{3}{2\sqrt{2}} m_1 i_d \\
C\frac{dE}{dt} &= i_{ox} - i_{or}
\end{aligned}
\tag{1.14}
$$

From Equation 1.14, it is seen that the DC-link voltage can be controlled via i_d. The control scheme thus utilizes current control loops for i_d and i_q, with the i_d demand being derived from the DC link voltage error through a standard PI controller. The i_q demand determines the displacement factor on the supply-side of the inductors. The strategy is shown in Figure 1.31.

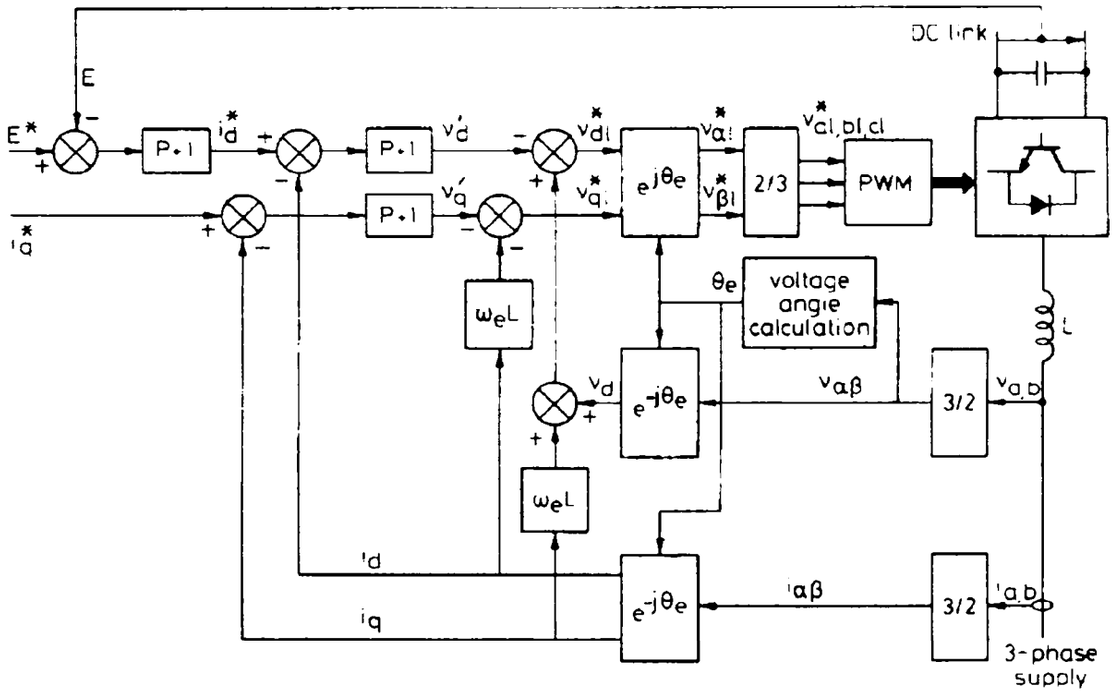

Figure 1.31 Vector control structure for the supply-side converter [12]

From Equation 1.11 the plant for the current control loops is given by:

$$
F(s) = \frac{i_d(s)}{v_d(s)} = \frac{i_q(s)}{v_q(s)} = \frac{1}{Ls + R}
\tag{1.15}
$$

where

$$v_{d1}^{*} = -v_d + \left(\omega_e L i_q + v_d\right)$$
$$v_{q1}^{*} = -v_q - \left(\omega_e L i_d\right) \tag{1.16}$$

In Equation 1.16, v^{*}_{d1} and v^{*}_{q1} are the references values for the supply-side converter, and the terms in brackets constitute voltage-compensation terms.

1.3.8.2 Control loop designs

The design of the current controllers follows directly from Equation 1.15, which can be written in the z domain as:

$$F(z) = \frac{(1-A)/R}{(z-A)};\ A = e^{-(R/L)T_s} \tag{1.17}$$

where T_s is the sample time (0.5 ms). The converter may be modeled by a pure delay of two sample periods yielding the control schematic of Figure 1.32 for which standard design techniques may be applied. For the inductors used, R=0.1 Ω, L = 12 mH, a design for a nominal closed-loop natural frequency of 125 Hz and ζ=0.8 can be obtained using the PI controller:

$$G(z) = 4.72(z-0.96)/(z-1) \tag{1.18}$$

The design of the DC-link voltage controller may be carried out in the continuous domain, and it is assumed that the inner i_d loop is ideal. From Equation 1.14 the effective transfer function of the plant is:

$$\frac{E(s)}{i_d(s)} = \frac{3m_1}{2\sqrt{2}C_s} \tag{1.19}$$

and the closed-loop block diagram is shown in Figure 1.32 , in which i_{or} is represented as a disturbance. Again, standard classical design is appropriate. Inserting values of E^{*} = 550 V, m_1 = 0.75 (for V_s = 250V), C = 2.4 mF and T_s = 5 ms, a controller of 0.12(z-0.9248)/(z-1) can be shown to give a nominal closed-loop natural frequency of 25 $rads^{-1}$, with ζ = 0.7. This is 50 times slower than th loop sampling frequency, and justifies the continuous design.

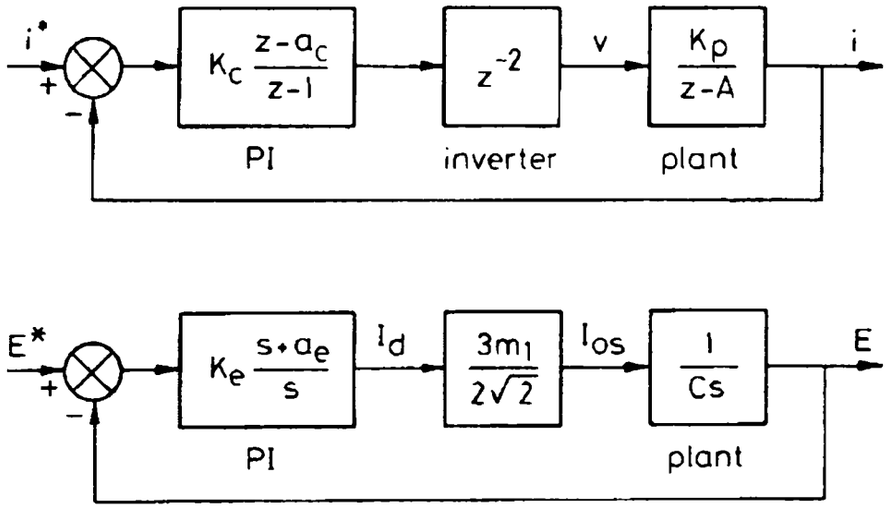

Figure 1.32 Supply-side converter current control loop and DC-link voltage control loop.

1.3.8.3 Machine control

The induction machine is controlled in a synchronously rotating dq frame with the d-axis oriented along the stator-flux vector position. In this way, a decoupled control between the electrical torque and the rotor excitation is obtained. The rotor-side PWM converter provides the actuation, and the control requires the measurement of the stator and rotor currents, stator voltage and the rotor position. There is no need to know the rotor-induced EMF, as is the case for the implementation with naturally commutated converters.

Since the stator is connected to the grid, and the influence of the stator resistance is small, the stator magnetizing current i_{ms} can be considered constant. Under stator-flux orientation, the relationship between the torque and the dq axis voltages, currents and fluxes (all scaled to be numerically equal to the AC per-phase values) may be written as:

$$\psi_s = \psi_{ds} = L_0 i_{ms} = L_s i_{ds} + L_0 i_{dr}$$

$$\psi_{dr} = \frac{L_0^2}{L_s} i_{ms} + \sigma L_r i_{dr}$$

$$\psi_{qr} = \sigma L_r i_{qr}$$

$$i_{qs} = -\frac{L_0}{L_s} i_{qr}$$

$$v_{dr} = R_r i_{dr} + \sigma L_r \frac{di_{dr}}{dt} - \omega_{slip} \sigma L_r i_{qr}$$

$$v_{qr} = R_r i_{qr} + \sigma L_r \frac{di_{qr}}{dt} + \omega_{slip} (L_m i_{ms} + \sigma L_r i_{dr})$$

$$T_e = -3 \frac{P}{2} L_m i_{ms} i_{qr}$$

$$\omega_{slip} = \omega_e - \omega_r$$

$$\sigma = 1 - \frac{L_0^2}{L_s L_r}$$

$$L_m = \frac{L_0^2}{L_s} \tag{1.20}$$

The stator flux angle is calculated from:

$$\psi_{\alpha s} = \int (v_{\alpha s} - R_s i_{\alpha s}) dt$$

$$\psi_{\beta s} = \int (v_{\beta s} - R_s i_{\beta s}) dt \tag{1.21}$$

$$\theta_s = \tan^{-1} \frac{\psi_{\beta s}}{\psi_{\alpha s}}$$

where θ_s is the stator-flux vector position. The integral in Equation 1.21 is solved using the digital passband filter, with cutoff frequencies of 0.5 Hz and 1 Hz to eliminate DC offsets. From Equation 1.19, the torque is proportional to i_{qr} and can be regulated using v_{qr}. The rotor excitation current i_{dr} is controlled using v_{dr}. Assuming that all reactive power to the machine is supplied by the stator, i^*_{dr} may be set to zero.

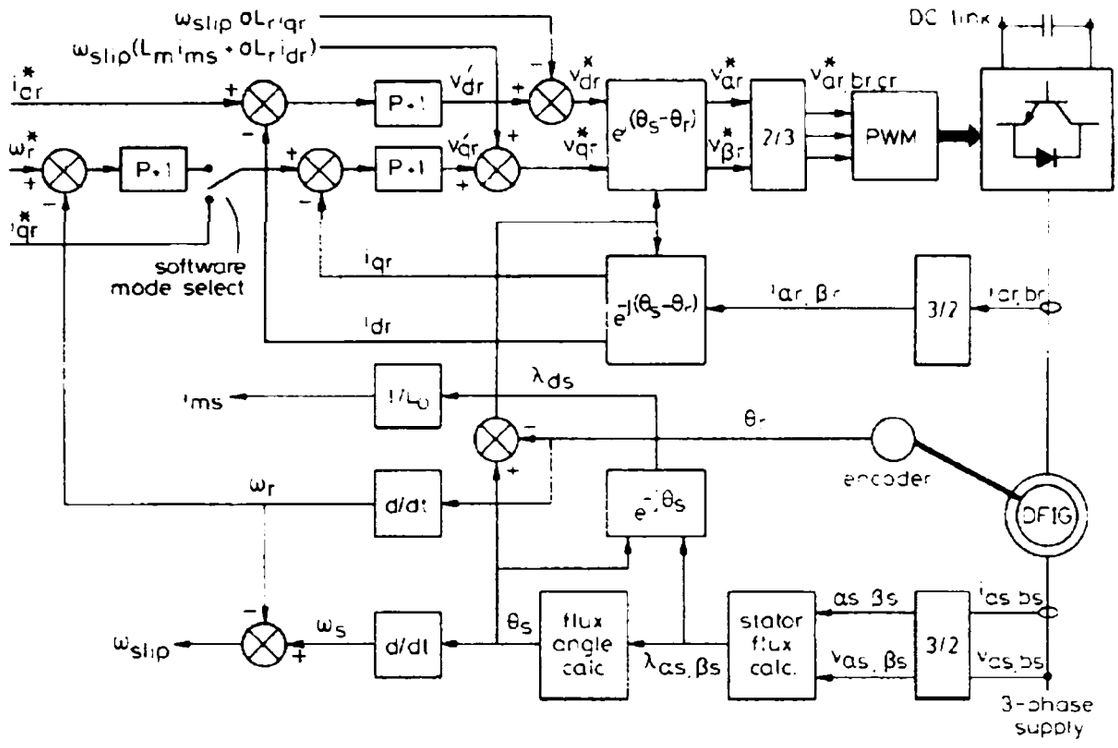

Figure 1.33 Vector-control structure for DFIG

Figure 1.33 shows a schematic block diagram for the machine control. The reference q axis rotor current can be obtained either from a outer speed-control loop or from a reference torque imposed on the machine. These two options may be termed a speed-control mode or torque-control mode for the generator.

A similar analysis for the control of the dq current can be carried out for the supply-side converter can likewise be done for the control of the dq rotor machine currents. From the rotor voltage equation in Equation 1.20 we have:

$$v'_{dr} = R_r i_{dr} + \sigma L_r \frac{di_{dr}}{dt}$$
$$v'_{qr} = R_r i_{qr} + \sigma L_r \frac{di_{qr}}{dt} \qquad (1.22)$$

The i_{dr} and i_{qr} errors are processed by the PI controller to give v'_{dr} and v'_{qr}, respectively. To ensure good tracking of these currents, compensation terms are added to v'_{dr} and v'_{qr} to obtain the reference voltages v^*_{dr} and v^*_{qr} according to:

$$v_{dr}^{*} = v'_{dr} - \omega_{slip}\sigma L_r i_{qr}$$
$$v_{qr}^{*} = v'_{qr} + \omega_{slip}(L_m i_{ms} + \sigma L_r i_{dr}) \quad (1.23)$$

which is analogous with Equation 1.16.

1.3.8.4 Control loop designs

The plant for the current-control design is similar to the case of the supply-side converter current controller (see Figure 1.32) with the following variable substitutions:

$$i_d, i_q \Rightarrow i_{dr}, i_{qr}$$

$$v'_d, v'_q \Rightarrow v'_{dr}, v'_{qr}$$

$$R \Rightarrow R_r$$

$$L \Rightarrow \sigma L_r$$

$$K_c \Rightarrow K_i$$

$$a_c \Rightarrow a_i$$

With T_s = 0.5 ms, a nominal closed-loop natural frequency of 130 Hz with ζ = 0.8 is obtained, with the controller 20 (z-0.985)(z-1).

A speed controller is needed when the machine operates in the speed controller is carried out in the continous domain, in a similar way to that of the voltage controller for the supply-side converter, assuming also that the current controllers are much faster than the speed loop and are thus considered ideal. The second order system of Figure 1.32 is obtained (without the i_{or} disturbance) with the following variable substitutions:

$$E \Rightarrow \omega_r$$

$$i_d \Rightarrow i_{qr}$$

$$\frac{3m_1}{2\sqrt{2}} \Rightarrow \frac{-3p}{2} L_m i_{ms} \quad (1.24)$$

$$i_{os} \Rightarrow T_e$$

$$\frac{1}{Cs} \Rightarrow \frac{1}{Js + B}$$

$$K_e \Rightarrow K_\omega$$

$$a_e \Rightarrow a_\omega$$

The rotor speed is obtained from a rotor-position measurement, which provides 720 pulses per revolution. With a sample time of 0.1 s a resolution of 0.833rpm is obtained. The magnetizing current can be obtained as $i_{ms} = V_s/\omega_e L_0$. With T_s = 0.1s and with the appropriate parameters, a nominal closed-loop natural frequency of 0.05Hz with ζ = 0.9 is obtained, with the controller 0.49 (z-0.988)/(z-1). Although a faster speed controller can be designed for the speed-control mode, in practice it is found the noise considerations limit the closed-loop natural frequency. This derives from the fact that the speed demand is obtained from a mechanical torque observer, which effectively estimates the shaft acceleration from a limited-resolution speed encoder.[78]

Conclusion

In this first chapter a review of the existent systems with variable speed generators is presented. The historical developments and the present status of the variable speed generators especially for wind power applications (which, through their nature, introduce the concept of variable speed generators) are presented in detail. The market trends and solutions applied by several wind turbines manufacturers are discussed.

Then an overview of the generators, power electronics and of the control systems is presented. There are both, solutions being in series production and also non-commercial solutions, but possible candidates in the future for renewable energy generating systems.

Finally, three systems, considered by the author as "key applications" are analyzed in this chapter:

- the doubly-fed induction generator with a cycloconverter connected in the rotor circuit for variable speed pump-storage hydropower plant. This solution was implemented in Japan for a several stations, including the big hydropower group in the world (400 MVA). Also, 2 similar groups are operational in Germany, at

Goldisthal on Schwarza river in the south of Thüringen (2x331 MVA, 18 kW, 66 MVA cycloconverters + 30 MVA starting converter)

- the induction generator with dual stator winding
- the doubly fed induction generator, with two inverters connected back-to-back in the rotor circuit. Here two control solutions are presented and discussed: direct power control and vector control. The following chapters will deal only with the vector control of the doubly fed induction generator.

References

[1] T. Ackermann (Editor), "Wind Power in Power Systems", book, *John Wiley & Sons 2005*, Chapter 1: Thomas Ackermann – Introduction.

[2] EWEA Website: www.ewea.org, News Release: Wind Power Continues to Grow in EU but faces constraints of Grid and Administrative Barriers.

[3] S. Scridon, "Different Topologies for Stand-Alone Wind Turbines", *Preliminary Report, Institute of Energy Technology, Aalborg University 2001.*

[4] M.Dahlgren, H.Frank, M.Leijon, F.Owman, L.Walfridsson, "Wind power goes large scale", *ABB Review, vol. 3/2000, pp. 31-37,* http://www.abb.com/abbreview.

[5] BTM Consults Aps, "International Wind Energy Development- World Market Update 2000", *ISBN 87-987788-0-3, 2001, BTM Consults Aps. Ringkobing, Denmark.*

[6] L.H.Hansen, L.Helle, F.Blaabjerg, E.Ritchie, S.Munk-Nielsen, H.W.Bindner, P.Sørensen, B.Bak-Jensen, "Conceptual survey of Generators and Power Electronics for Wind Turbines", *Riso-R-1205(EN), 2001. Risø National* Laboratory, Denmark.

[7] L. H Hansen, F. Blaabjerg, H. C. Christensen, U. Lindhard, K. Eskildsen, "Generators and Power Electronics Technology for Wind Turbines", *Proceedings of IECON 2001.*

[8] T. Ackermann (Editor), "Wind Power in Power Systems", book, *John Wiley & Sons 2005*, Chapter 4: Anca. D. Hansen – Generators and Power Electronics for Wind Turbines.

[9] O Ojo, O. Omozusi, A. Jimoh, "Expanding the Operating Range of a Single-Phase Induction Generator with a PWM Inverter" , *Proceedings of IEEE-IAS, 1998.*

[10] A. M. Garcia, T A. Lipo, "Dual Stator Winding Induction Machine Drive", *Proceedings of IEEE-IAS 1998.*

[11] O. Ojo, I. E. Davidson, "PWM-VSI Inverter-Assisted Stand Alone Dual Stator Winding Induction Generator", *IEEE Transactions on Industry Applications, vol. 36, no.6, November/December 2000.*

[12] R. Pena, J. C. Clare, G. M. Asher, "Doubly fed induction generator using back-to-back PWM converters and its application to variable speed wind-

energy generation", *IEE Proc. Electr. Power Appl, Vol. 143, No.3, May 1996.*

[13] L. Morel, H. Godfroid, A. Mirzain, J. M. Kauffmann, "Double fed induction machine: converter optimisation and field oriented control without position sensor", *IEE Proc.-Electr. Power Appl. Vol. 145, No. 4, July 1998.*

[14] L. Schreier, M. Chomat, J. Bendl, "Working Regions of Adjustable-Speed Units with Doubly Fed Machines", *IEEE 1999.*

[15] V. Bartos, A. Kotlanova, "Transient phenomena in the system with the double fed asynchronous machine", *ICEM 2000, Espoo-Finland.*

[16] VA TECH ELIN GMBH, "Variable Speed Motor/Generator"

[17] V. De Oliveira, E. Monmasson, R. Meuret, J. P. Louis, "Steady State Analysis of a Double Fed Induction Generator for Aircraft Application", *Proceedings of Electromotion 2001, Bologna.*

[18] A. M. Mostafa, A. L. Mohamadein, E. M. Rashad, "Analysis of Series-Connected Wound-Rotor Self-Excited Induction Generator"

[19] C. Brune, R. Spee, A. K. Wallace, "Experimental Evaluation of a Variable-Speed, Doubly-Fed Wind-Power Generation System", *IEEE 1993.*

[20] L. Schreier, M. Chomat, J. Bendl, "Operation of System Double Fed Machine-Turbine in Power Network, Power Electronics and Variable Speed Drives", *Proceedings of Power Electronics and Variable Speed Drives, 18-19 September 2000 Conference Publication No. 475 © IEE 2000.*

[21] B. Hopfensperger, D. J. Atkinson, R. A. Lakin, "The Application of Field Oriented Control to a Cascaded Doubly-Fed Induction Machine", *Proceedings of Power Electronics and Variable Speed Drives, 18-19 September 2000, Conference Publication No. 475 © IEE 2000.*

[22] S. Bhowmik, R. Spee, J. H. R. Enslin, "Performance Optimization for Doubly Fed Wind Power Generation Systems", *IEEE 1999.*

[23] I. F. Soran, "The Steady State and Transient Performances of a Double Fed Asynchronous Machine (DFAM)", *Proceedings of EPE 1991, Firenze.*

[24] M. T. El-Hagry, M. N. Eskander, "Estimation of Rotor Voltage Vector on the Double Excited Induction Machine Used in WECS", *Electric Machines and Power Systems Journal, No. 8, 1997.*

[25] M. N. Eskander, M. T.El-Hagry, "Optimal Performance of Double Output Induction Generator Used in WECS", *Electric Machines and Power Systems Journal, No. 10, 1997.*

[26] R. M. Hilloowala, A. M. Sharaf, "Modelling, Simulation and Analysis of Variable Speed Constant Frequency Wind Energy Conversion Scheme Using Self-Excited Induction Generator", *IEEE 1991.*

[27] E. Muljadi, J. Sallan, M. Sanz, C. P. Butterfield, "Investigation of Self-Excited Induction Generators for Wind Turbine Applications", *IEEE 1999.*

[28] F. Castelli Dezza, A. Di Gerlando, R. Perrini, "Performance Comparison Among Different Converters Fed by Self Excited Wind Driven Induction Generators, Electrical Machines and Drives", *Proceedings of Power Electronics and Variable Speed Drives, 11-13 September 1995, Conference Publication No. 412, © IEE, 1995.*

[29] A.A.Shaltout, M.A.Abdel-Halim, "Solid-State Control of a Wind-Driven Self-Excited Induction Generator", *Electric Machines and Power Systems Journal, No. 5, 1995.*

[30] A. K. Tiwari, S. S. Murthy, B. Singh, "Design Based Analysis of Two Winding Capacitor Self Excited Single Phase Induction Generator", *Proceedings of ICEM 2000.*

[31] M. Boger, A. Wallace, "Performance Capability Analysis of the Brushless Doubly-Fed Machine as a Wind Generator", *Proceedings of Electrical Machines and Drives, 11-13 September 1995, Conference Publication No. 412, © IEE, 1995.*

[32] M. A. Abdel-Halim, "Solid-State Control of a Grid Connected Induction Generator", *EPCS 29, pp. 163-178, 2001.*

[33] *** , "A Novel Control Strategy for the Rotor Side Control of a Doubly-Fed Induction Machine"

[34] ***, "Sensorless Control Strategies for Power Smoothing in Wind Energy Applications Using a Flywheel Driven by a Vector Controlled Induction Machine"

[35] L. Refoufi, B. A. T. Al Zahavi, A. G. Jack, "Analysis and Modelling of the Steady State Behaviour of the Static Kramer Induction Generator", *IEEE Transactions on Energy Conversion, vol. 14, No.3, Sept. 1999.*

[36] I. Tamrakar, O. P. Malik, "Power Factor Correction of Induction Motors Using PWM Inverter Fed Auxiliary Stator Winding", *IEEE Transactions on Energy Conversion, vol. 14, No.3, Sept. 1999.*

[37] L. H. Hansen, P. Sorensen, U. S. Paulsen, "Variable Speed Wind Turbine using full Conversion", *Proceedings of NORPIE 2000.*

[38] I. Cadirci, M. Ermis, E. Nalcaci, B. Ertan, M. Rahman, "A Solid State Direct On Line Starter for Medium Voltage Induction Motors with Minimized Current and Torque Pulsation", *IEEE Transactions on Energy Conversion, vol. 14, No.3, Sept. 1999.*

[39] F. Giraud, Z. M. Salameh, "Wind-Driven Variable-Frequency, Double-Output, Induction Generator", *EMPS Journal, no. 26, pp 287-297, 1998.*

[40] I. Cadirci, M. Ermis, "Performance Evaluation of a Wind Driven DOIG Using a Hybrid Model", *IEEE 1997.*

[41] B. J. Chalmers, W. Wu, E. Spooner, "An Axial-Flux Permanent Magnet Generator for a Gearless Wind Energy System", *IEEE 1998.*

[42] J. Rizk, M. Nagrial, "Design of Permanent Magnet Generators for Wind Turbines", *Proceedings of AUPEC 1999.*

[43] Y. Tang, L. Xu A. Novel, "Wind Power Generating System Using Field Orientation Controlled Doubly-Excited Brushless Reluctance Machine", *IEEE 1992.*

[44] J. Y. Chen, C. V. Nayar, "A Direct-Coupled, Wind-Driven Permanent Magnet Generator", *IEEE 1998.*

[45] L. Zhang, C. Watthanasarn, W. Sheperd, "Application of a Matrix Converter for the Power Control of a Variable-Speed Wind-Turbine Driving a Doubly-Fed Induction Generator", *IEEE Library.*

[46] L. Helle, S. M. Nielsen, "Comparison of Converter Efficiency in Large Variable Speed Wind Turbines", *IEEE 2001.*

[47] B. Robyns, M. Nasser, F. Berthereau, F. Labrique, "Equivalent Continuous Dynamic Model of a Variable Speed Wind Generator", *Proceedings of Electromotion 2001, Bologna.*

[48] E. C. Tsimplostephanakis, A. N. Safacas, "Optimisation of the Voltage and Frequency Controller for a Week Grid Including a Wind Energy Conversion System", *Proceedings of Electromotion 2001, Bologna.*

[49] B. K. Lee, M. Ehsani, "A Simplified Functional Simulation Model for Three-Phase Voltage-Source Inverter Using Switching Function Concept", *IEEE Transactions on Industrial Electronics, vol. 48, no. 2, April 2001.*

[50] V. Akhmatov, H. Knudsen, A. H. Nielsen, "Advanced Simulation of Windmills in the Electric Power Supply", *EPES 22 (2000), pp 421-434.*

[51] B. Borowy, Z. M. Salameh, "Dynamic Response of a Stand Alone Wind Energy Conversion System with Battery Energy Storage to a Wind Gust", *IEEE 1996.*

[52] Z. Chen, E. Spooner, "A Modular, Permanent-Magnet Generator for Variable Speed Wind Turbines", *Proceedings of Electrical Machines and Drives, 11-13 September 1995, Conference Publication No. 412, ©IEE 1995.*

[53] A. J. G. Westlake, J. R. Bumby, "Design Interactions of a Flexible Stator Mounting for a Permanent magnet Synchronous Generator"

[54] R. M. Hilloowala, A. M. Sharaf, "A Utility Interactive Wind Energy Conversion Scheme with an Asynchronous DC Link Using A Supplementary Control Loop, *IEEE Transactions on Energy Conversion", Vol. 9, No. 3, September 1994.*

[55] M. R. Mohan, S. R. Paranjothi, S. P. Israel, "Use of Pumped-Hydro as Peak Load Management Plant in Optimal Scheduling of Power Systems", *Electric Machines and Power Systems Journal, no. 25, pp 1047-1061, 1997.*

[56] S. Arnalte, J. C. Burgos, J. L. Rodriguez-Amenedo, "Direct Torque Control of a Doubly Fed Induction Generator for Variable Speed Wind Turbines"

[57] M. A. Al-Gilani, S. P. Gupta, "Cycloconverter-Excited Squirell-Cage Machine as a Wind-Power Converter", *Proceedings of EMPS 2000.*

[58] *** - "Implementation of a Cycloconverter Based Induction Motor Controller"

[59] R. Datta, V. T. Ranganathan, "Direct Power Control of Grid-Connected Wound Rotor Induction Machine Without Rotor Position Sensor", *IEEE Transactions on Power Electronics, vol. 16, no.3, May. 2001.*

[60] D. S. Zinger, E. Muljadi, A. Miller, "A Simple Control Scheme for Variable Speed Wind Turbines", IEEE 1996,

[61] Y. D. Song, B. Dhinakaran, X. Bao, "Control of Wind Turbines Using Nonlinear Adaptive Field Excitation Algorithms", *Proceedings of AACC 2000.*

[62] R. Cardenas, R. Pena, G. Asher, J. Clare, "Control Strategies for Energy Recovery from a Flywheel Using a Vector Controlled Induction Machine", *IEEE 2000.*

[63] R. Cardenas, R. Pena, G. Asher, J. Clare, "Vector Controlled Induction Machine for Stand-Alone Wind Energy Applications", *IEEE 2000.*

[64] R. B. Chedid, S. H. Karaki, C. El-Chamali, "Adaptive Fuzzy Control for Wind-Diesel Weak Power Systems", *IEEE 2000*

[65] R. Cardenas, R. Pena, G. Asher, J. Clare, "Control Strategies for Enhanced Power Smoothing in Wind Energy Systems Using a Flywheel Driven by a Vector-Controlled Induction Machine", *IEEE 2001.*

[66] M. G. Simoes, Bimal K. Bose, R. J. Spiegel, "Design and Performance Evaluation of a Fuzzy Logic Based Variable Speed Wind Generation System", *IEEE 1996.*

[67] F. Valenciaga, P. F. Puleston, R. J. Mantz, "Passivity/Sliding Mode Control of a Stand-Alone Hybrid Generation System", *IEE Proc.-Control Theory Appl., Vol.147, no. 6, November 2000.*

[68] Z. Chen, S. Gomez, M. McCormick, "A Fuzzy Logic Controlled Power Electronic System for Variable Speed Wind Energy Conversion Systems", *IEE 2000*

[69] R. Hoffmann, P. Mutschler, "The Influence of Control Strategies on the Energy Capture of Wind Turbines", *IEEE 2000*

[70] M. Ermis, H. B. Ertan, E. Akpinar, F. Ulgut, "Autonomous Wind Energy Conversion System with a Simple Controller for Maximum Power Transfer", *IEE Proceedings – B, vol. 139, no.5, September 1992.*

[71] O. Ojo, O. Omozusi, A. Ginart, B. Gonoh, "The Operation of a Stand-Alone, Single-Phase Induction Generator Using a Single-Phase, Pulse-Width Modulated Inverter With a Battery Supply", *IEEE 1998.*

[72] A. McIver, D.G. Holmes, P.Freere Optimal Control of a Variable Speed Wind Turbine under Dynamic Wind Conditions. *IEEE 1996.*

[73] H. Huang, L. Chang, "A New DC Link Voltage Boost Scheme of IGBT Inverters for Wind Energy Extraction", *IEEE 2000.*

[74] S. Muller, M. Deicke, R. W. De Doncker, "Adjustable Speed Generators for Wind Turbines based on Doubly-fed Induction Machines and 4-Quadrant IGBT Converters Linked to the Rotor", *IEEE 2000.*

[75] K. Kudo, "Japanese experience with a converter-fed variable speed pumped-storage system", *Hydropower & Dams, March 1994.*

[76] S. Furuya, F. Wada, K. Hachiya, K. Kudo, "Large Capacity GTO Inverter-Converter for Double-Fed Adjustable Speed System", *Symposium Tokyo 1995 © CIGRE.*

[77] O. Ojo, I. E. Davidson, "A dual stator winding induction generator with a four switch inverter-battery scheme for control", *Proceedings of PESC 2000.*

[78] R. Cardenas, "Control of wind turbines using switched reluctance generators", Ph. D Thesis, 1996, University of Nottingham, UK.

Chapter 2

DFIG modeling for power grid operation

Abstract

This chapter deals with the simulation of the complete DFIG system for power grid operation. The behavior of the system is deeply analyzed under normal conditions and under fault conditions of the power grid. The operation under fault conditions, especially under shortcircuits of the power grid is very important, due to the last power system requirements that clearly specifies that the high power wind generators should "ride through faults" coming from the power grid. This means that during the shortcircuits of the network, the generator should not be disconnected, in order to be able, after the shortcircuit is cleared, to provide immediately the power necessary to recover the voltage of the grid, and to prevent oscillations of the power system (penetrated higher and higher by the power coming from the wind generators). Thus, special measured should be taken into account in order to prevent serious damages of the power electronics or of the generator, especially in the case of off-shore turbines, where the equipments are installed on the sea, at 20 km or more from the land and any intervention requires additional important financial support.

The simulated system includes the turbine, the gearbox, the DFIG itself, the two power converters (grid-side converter and machine side converter, both vector controlled), the DC link, the line-filter and the power grid. First, the models of all mentioned components are described and commented. Then, the operation of the system under the normal conditions of the power grid is presented and discussed.

In the second part of the chapter, the operation of the system under shortcircuit of the power grid is analyzed. Possible measured to protect the converters and to improve the behavior of the system under these conditions are discussed

2.1 Introduction

When a short-circuit fault occurs in the network, then the voltage dip and the current transients in the generator windings and in the converter occur. Although, due to the lack of power transfer from the generator to the network, the turbine severely accelerates. In this situations, there are two risks:

- damage of the converter due to the over-currents
- mechanical damage of the turbine due to the overspeeding

A lot of attention must be paid in order to avoid these problems. The actions that may be taken are different, and are dependent of the type of the turbine: small on-land or large off-shore.

In the case of small on-land wind turbines farms, no technical specifications are made, and the turbines could be automatically tripped and stopped when the settings of the monitored values are exceeded. The converter could be blocked, the rotor could be opened or short-circuited and a "safety stop" procedure could be initiated. This can be realized by aerodynamic breaking which means pitching the blades at the maximum reference and locking the shaft at the zero speed. Extended discussion of these methods is made in [1].

The technical requirements for the wind turbines in large off-shore wind farms are defined in standards. Those wind farms are treated as large power supply units and their disconnection will not be accepted as the turbine should contribute with power after the fault.

In those cases, other methods for improving the performance under such conditions, and protection should be taken into account.

In the following paragraphs the extended presentation of the studied system (2 MW, 4-pole generator) and how it was modeled will be made, its control will be discussed and various simulation results (in normal operation and under a power grid short-circuit) will be presented.

2.2 Simulation models of the DFIG system

A schematic diagram of the overall studied system is shown in Figure 2.1. Two voltage-fed PWM converters are inserted in the rotor circuit, with the supply-side PWM converter connected to the grid via a RL filter, which limits the high-frequency ripple due to switching harmonics.[2].

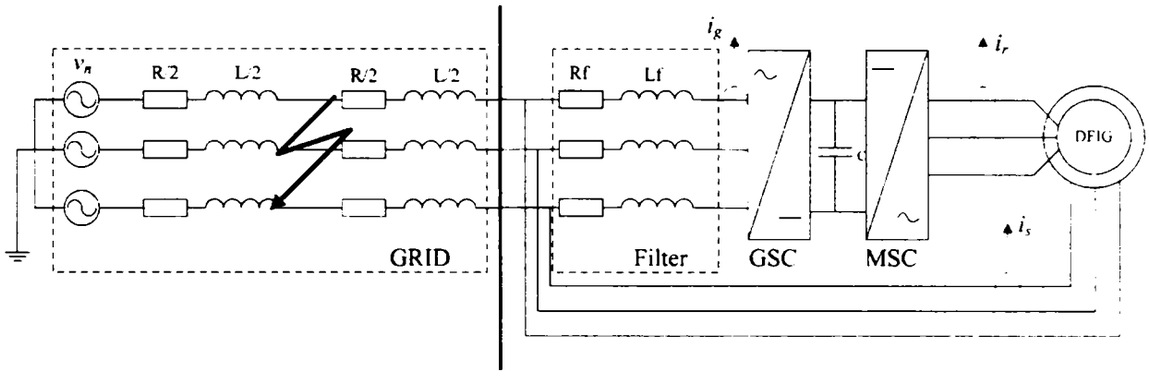

Figure 2.1 The doubly-fed induction generator connected to the power grid.

The complete simulation model of the system was implemented in Matlab-Simulink (see Figure 2.2), and the parts are explained in what it follows.

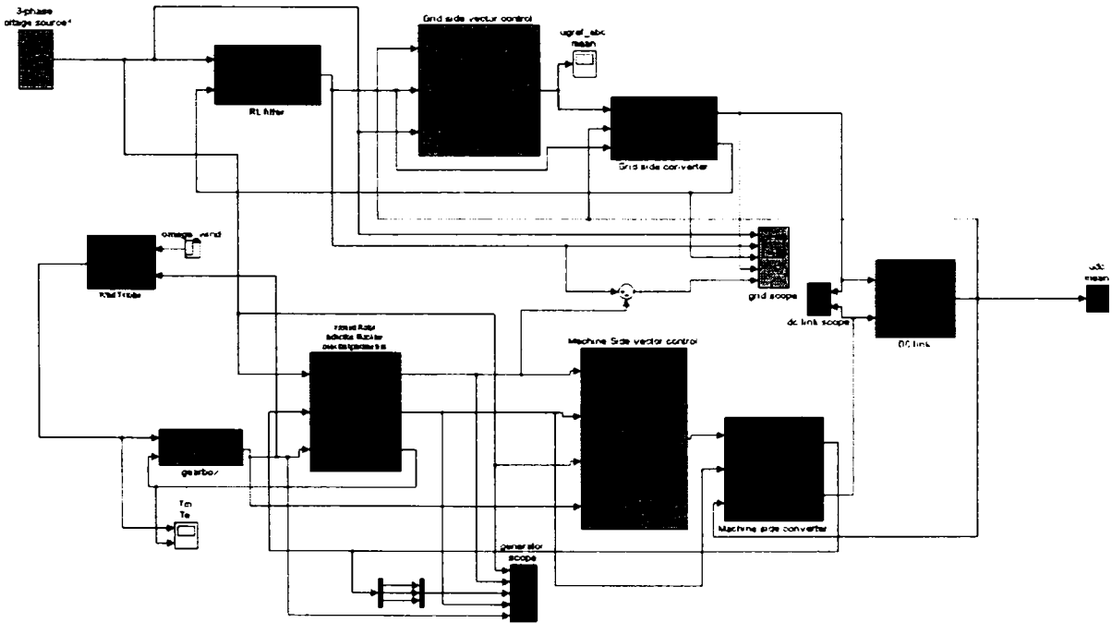

Figure 2.2 The overview of the simulation system

2.2.1 The wind turbine model

The wind turbine is modeled in terms of optimal tracking, to provide maximum energy capture from the wind. The implemented characteristics are presented in Figure 2.3.

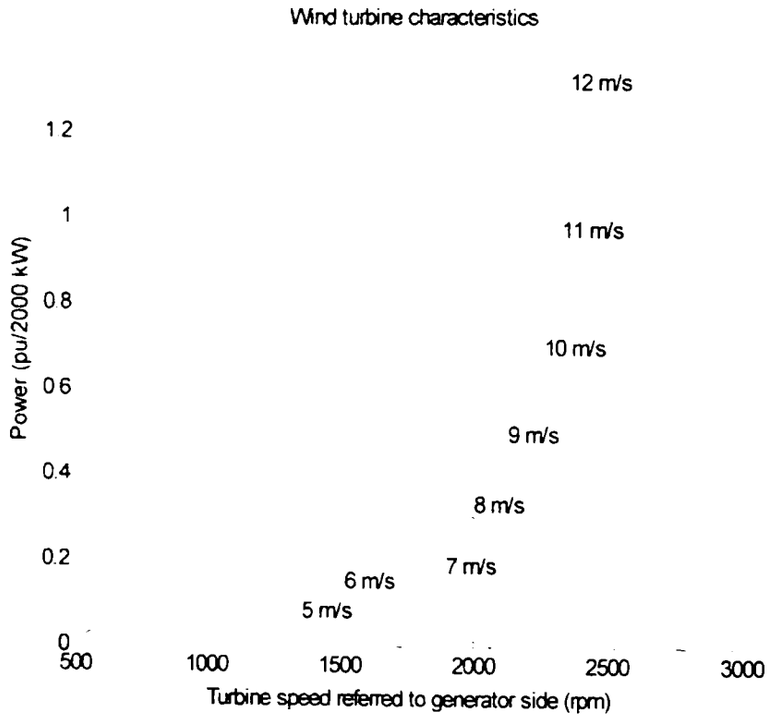

a)

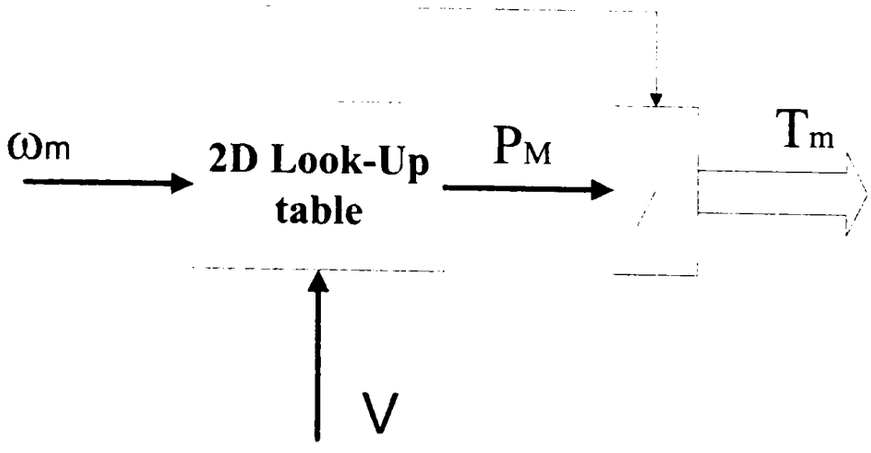

b)

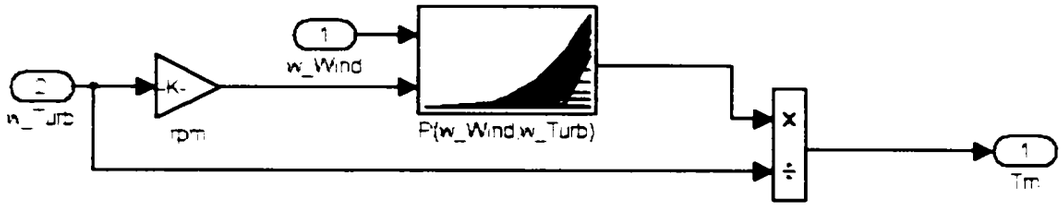

c)

Figure 2.3 Implemented wind turbine characteristics: a) aerodynamic characteristics. b) the turbine torque model. c) the simulation model

These characteristics are based on:

$$P_M = \frac{1}{2} \cdot \rho_{air} \cdot C_p(\lambda, \beta) \cdot \pi \cdot R^2 \cdot V^3 \tag{2.1}$$

where C_p - power efficiency coefficient; V – wind velocity; β - pitch angle; R – blade radius; P_M – mechanical power produced by the wind turbine; ρ_{air} – air density (usually 1.225 kg/m^3)

Applying the tip speed ratio λ :

$$\lambda = \frac{\omega_m \cdot R}{V} \tag{2.2}$$

where ω_m is the mechanical speed of the turbine, equation (2.1) may be rewritten as:

$$P_M^{opt} = \frac{1}{2} \cdot \rho_{air} \cdot \pi \cdot R^5 \cdot \frac{C_p^{opt}}{\lambda_{opt}^3} \cdot \omega_m^3 = K_w \cdot \omega_m^3 \tag{2.3}$$

where K_w is the wind turbine dependent coefficient.

Equation (2.3) holds the key of the optimization of the variable-speed wind turbine by tracking the optimal turbine speed at a given wind speed. The result of the optimization is reaching in fact the optimal power efficiency at the given speed. In the simulation the optimum power is returned by the model through a 2D look-up table having the wind speed and the speed of the generator as inputs, with interpolation of the turbine characteristics, with the action of the governor considered as

instantaneous. These data can be obtain from the manufacturer, for a specific type of the turbine.

2.2.2 The DFIG model

Stator and rotor voltages expressed in terms of d and q axes quantities rotating in an arbitrary reference frame with the speed ω_k are given by [3]:

$$v_{sd} = R_s \cdot i_{sd} + \frac{d\psi_{sd}}{dt} - \omega_k \cdot \psi_{sq} \tag{2.4}$$

$$v_{sq} = R_s \cdot i_{sq} + \frac{d\psi_{sq}}{dt} + \omega_k \cdot \psi_{sd} \tag{2.5}$$

$$v_{rd} = R_r \cdot i_{rd} + \frac{d\psi_{rd}}{dt} - (\omega_k - \omega_r) \cdot \psi_{rq} \tag{2.6}$$

$$v_{rq} = R_r \cdot i_{rq} + \frac{d\psi_{rq}}{dt} + (\omega_k - \omega_r) \cdot \psi_{rd} \tag{2.7}$$

Stator and rotor fluxes are expressed in function of the current by:

$$\psi_{sd} = L_s \cdot i_{sd} + L_m \cdot i_{rd} \tag{2.8}$$

$$\psi_{sq} = L_s \cdot i_{sq} + L_m \cdot i_{rq} \tag{2.9}$$

$$\psi_{rd} = L_r \cdot i_{rd} + L_m \cdot i_{sd} \tag{2.10}$$

$$\psi_{rq} = L_r \cdot i_{rq} + L_m \cdot i_{sq} \tag{2.11}$$

Also, the electromagnetic torque:

$$T_e = \frac{3}{2} \cdot p \cdot (\psi_{sd} \cdot i_{sq} - \psi_{sq} \cdot i_{sd}) \tag{2.12}$$

The implementation of the above equations, the structure of the whole DFIG model and the corresponding mask of the system are illustrated in Figure 2.4 [4].

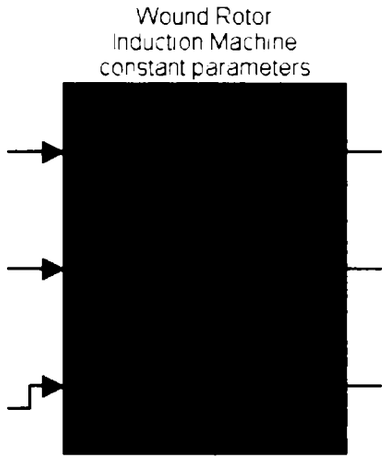

a)

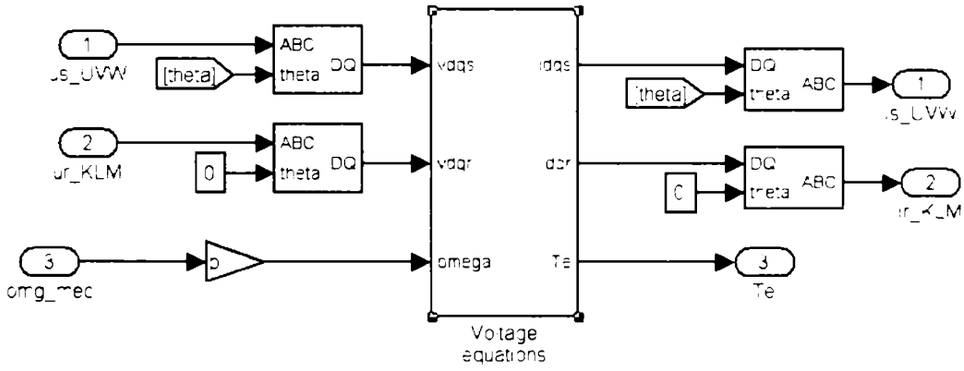

b)

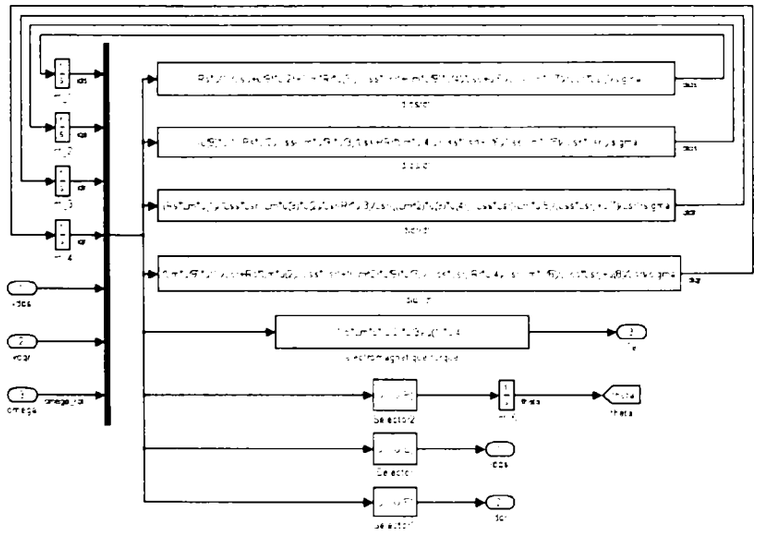

c)

Figure 2.4 The model of the DFIG: a) mask of the model. b) implementation of the model, c) implementation of the equations

Usually a speed range of ± 25% is chosen around the synchronous speed [5]. To have a lower current at the rotor-side of the machine equivalent with a lower converter sizing, and the same voltage at the rotor-side and the stator-side at the limits of the speed range (the voltage adapting transformer between the converter and the power system is avoided), a transformer ratio K of the generator windings of 4 is chosen:

$$v_{r\max} = K \cdot |s_{\max}| \cdot (v_s)_{rated} \tag{2.13}$$

2.2.3 The grid-side converter (GSC) model

The supply side converter is used to control the DC link voltage regardless of the level and the direction of the rotor power (Figure 2.5). A vector-control strategy is used, with the reference frame oriented along the stator voltage [6]. The converter is current regulated with the direct axis current used to control the DC-link voltage, meanwhile the transverse axis current is used to regulate the displacement between the voltage and the current (and thus the power factor) [7]. In fact, the reference of I_{gq} should be imposed as zero, if no circulation of reactive power is desired through the rotor circuit, and this is the present case.

The voltage equations (see Figure 2.1) are:

$$\begin{bmatrix} v_{ga} \\ v_{gb} \\ v_{gc} \end{bmatrix} = R_f \begin{bmatrix} i_{ga} \\ i_{gb} \\ i_{gc} \end{bmatrix} + L_f \frac{d}{dt} \begin{bmatrix} i_{ga} \\ i_{gb} \\ i_{gc} \end{bmatrix} + \begin{bmatrix} v_a^* \\ v_b^* \\ v_c^* \end{bmatrix} \tag{2.14}$$

where L_f and R_f are the line inductance and resistance of the filter, i_{ga}, i_{gb}, i_{gc} are the phase currents, and v^*_a, v^*_b, v^*_c are the phase voltages should be produced by the converter.

Respectively, using the transformations into a dq reference frame rotating at ω_e the equations yield:

$$v_{gd} = R_f i_{gd} + L_f \frac{di_{gd}}{dt} - \omega_e L_f i_{gq} + v'_{gd} \tag{2.15}$$

$$v_{gq} = R_f i_{gq} + L_f \frac{di_{gq}}{dt} + \omega_e L_f i_{gd} + v'_{gq} \tag{2.15'}$$

The voltage being aligned with the grid d-axis, v_{gq} = 0, and the terms v_{gd}+$\omega_e L_f i_{gq}$ and $\omega_e L_f i_{gq}$ are added respectively subtracted as compensation terms.

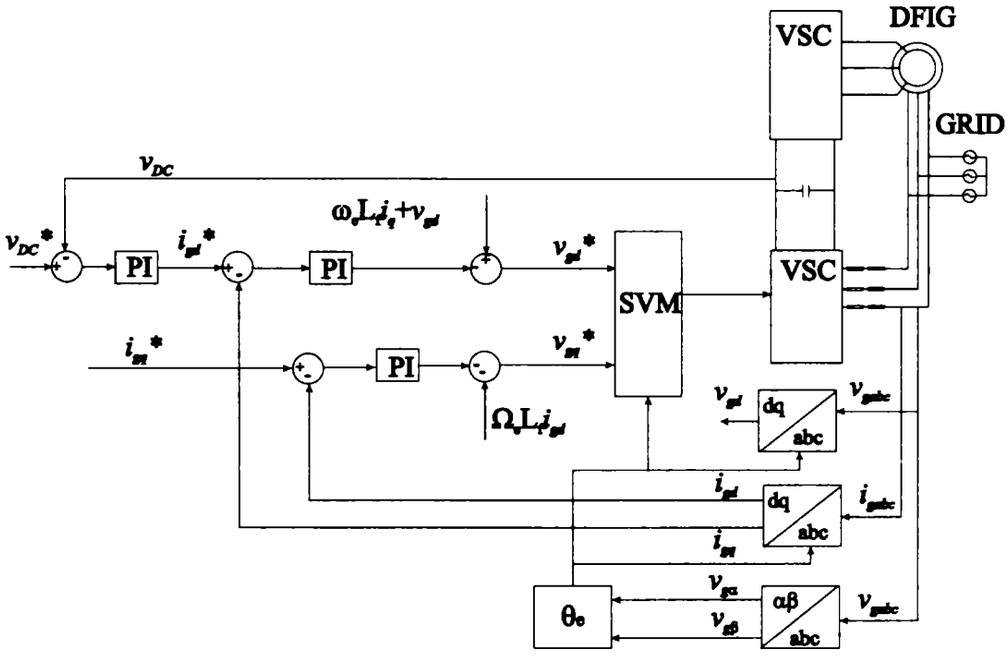

Figure 2.5 The block diagram of the supply-side converter control.

The angular position of the supply voltage θ_e is calculated as:

$$\theta_e = \tan^{-1} \frac{v_{g\beta}}{v_{g\alpha}} \tag{2.16}$$

where $v_{g\alpha}$ and $v_{g\beta}$ are the grid voltages expressed in terms of α and β axes (stationary).

The design of the current controllers follows from the transfer function of the plant in the z-domain, the sampling time being 0.45 ms. For a nominal closed-loop natural frequency of 125 Hz and a damping factor of 0.8 the transfer function of the PI controller is:

$$G_{IG}(z) = 18.69(z-1335.4)/(z-1) \tag{2.17}$$

The current loop is designed much faster than the DC voltage loop and thus considered ideal. The transfer function of the DC voltage controller results in:

$$G_{UDC}(z) = 17.95(z-2640)/(z-1) \tag{2.18}$$

2.2.4 The machine-side converter (MSC) model

The generator is controlled in a synchronously rotating dq-frame, with the d-axis aligned with the stator-flux vector position, which ensures a decoupled control between the electromagnetic torque and the rotor excitation contribution (see Figure 2.6). In fact decoupled active and reactive power control [8,9] of the generator is obtained (Figure 2.6).

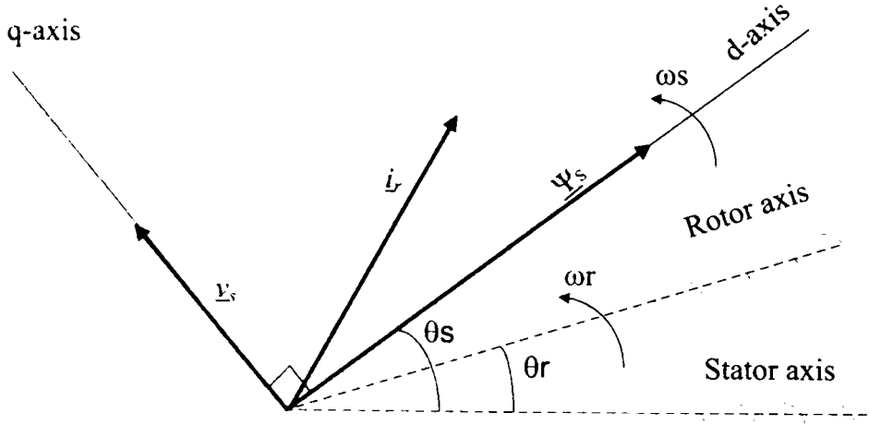

Figure 2.6 Location of different vectors in stationary coordinates.

Under stator-flux orientation ($\omega_k = \omega_e$), the rotor equations (2.6 – 2.7) could be re-written as:

$$v_{rd} = R_r i_{rd} + \sigma L_r \frac{di_{rd}}{dt} - \omega_{slip}\sigma L_r i_{rq} \tag{2.19}$$

$$v_{rq} = R_r i_{rq} + \sigma L_r \frac{di_{rq}}{dt} + \omega_{slip}(L_m i_{ms} + \sigma L_r i_{rd}) \tag{2.20}$$

where:

$$\omega_{slip} = \omega_s - \omega_r \tag{2.21}$$

σ – leakage factor:

$$\sigma = 1 - \frac{L_0^2}{L_s L_r} \tag{2.22}$$

L_0 is the cyclic magnetization inductance:

$$L_0 = \sqrt{L_m \times L_s} \tag{2.23}$$

And i_{ms} is the stator magnetization current:

$$i_{ms} = \frac{\psi_{sd}}{L_0} \tag{2.24}$$

Figure 2.7. presents a schematic block diagram of the machine-side converter vector control.

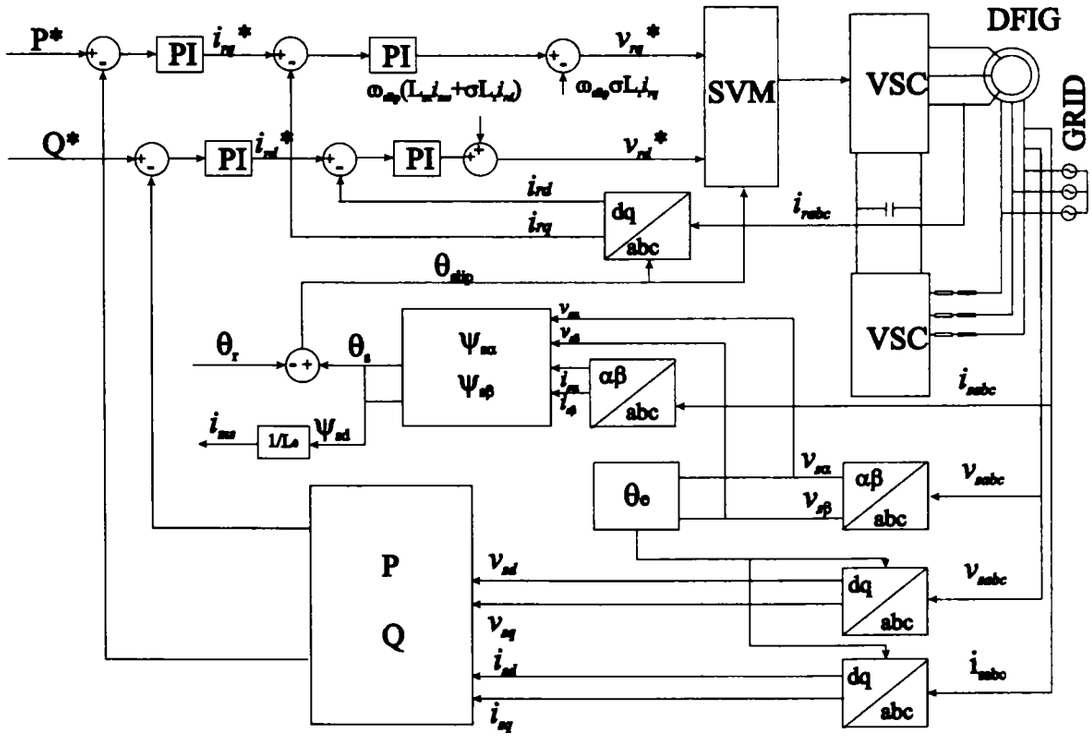

Figure 2.7 The block diagram of the machine-side converter control in a doubly-fed wind turbine.

Again knowing the transfer function of the plant and imposing the natural closed-loop frequency and the damping factor, the transfer function of the current controllers results in

$$G_{IR}(z) = 12\,(z-0.995)/(z-1) \tag{2.25}$$

The power loops are designed much slower than the current loops and the transfer function for the power controllers are thus obtained:

$$G_{PQ}(z) = 0.00009(z-0.9)/(z-1) \tag{2.26}$$

The reference voltages generated by the current control loops with back-EMF compensated are transformed back to the rotor reference frame and space vector modulated to generate the pulses for the inverter (VSC).

2.2.5 The active and reactive power calculator

Knowing the stator currents and voltages (measured), the stator active power is calculated as:

$$P = v_{sd} i_{sd} + v_{sq} i_{sq} \tag{2.27}$$

Also, the stator reactive power could be calculated as:

$$Q = -v_{sd} i_{sq} + v_{sq} i_{sd} \tag{2.28}$$

2.3 Operation of the DFIG system under normal conditions of the power grid

Extended simulations were performed on the model thus implemented, in order to deeply analyze the behavior of the system under different conditions.

First some control situations are presented, as the accuracy of the active and reactive power control is checked. In Figure 2.8 the active power reference (see also control block diagram in Figure 2.7) is modified from -1.2 MW to -1.4 MW (generating). The reference and the response in terms of active power is shown in Figure 2.8 a.

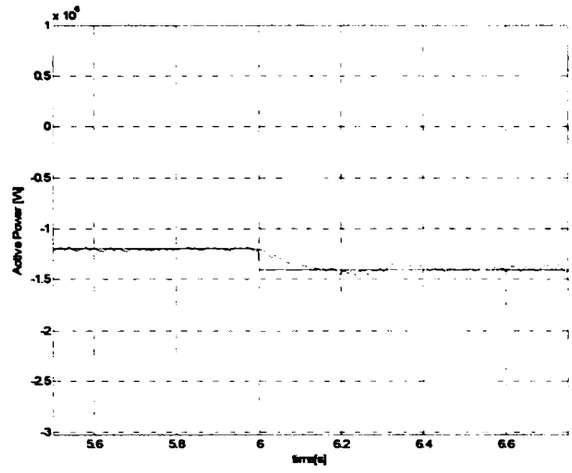

a)

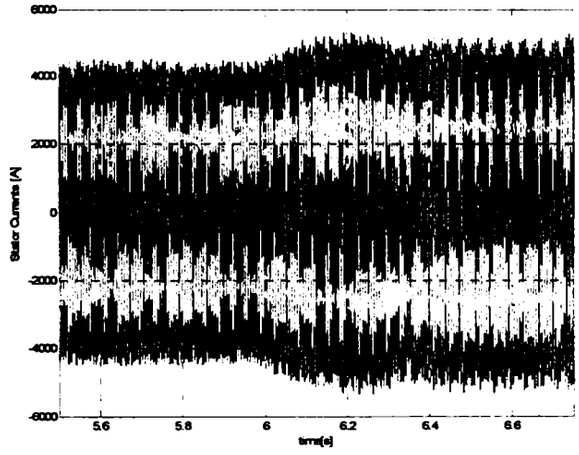

b)

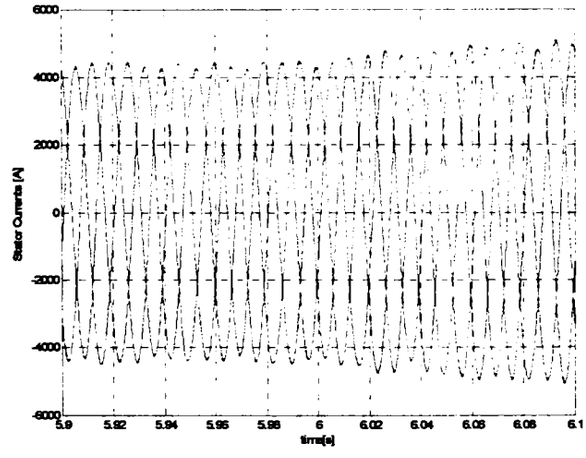

c)

Figure 2.8 Simulated step in reference of the active power: a) the reference and the response of the system, b) the stator currents, c) zoom in stator currents around the time of the step.

The stator currents for the step in active power reference are shown in Figure 2.8 b. For more clarity a zoom in time scale around the time of the step (6 sec) is performed in Figure 2.8 c.

Similarly with the active power, the response in terms of reactive power is analyzed. As already discussed, this is even more important than the response of active power, when the grid is weak and a very quick control of the voltage is desired. For this purposes the reference of the reactive power is modified from 300 kVAr (absorbing) to –300kVAr (producing). The response is shown in Figure 2.9.

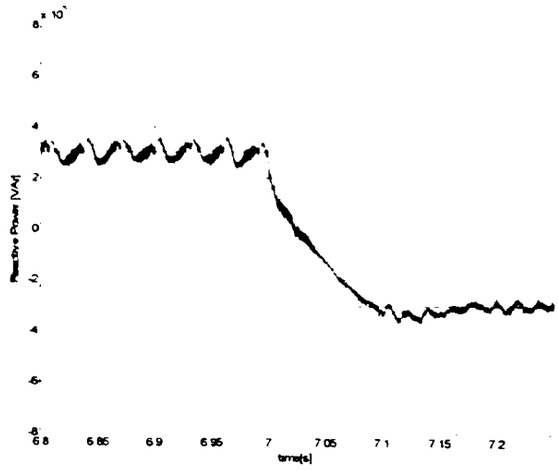

Figure 2.9 Simulated step in reference of the reactive power

Then, another more complex situation was analyzed: at 1.5 sec the wind speed is increased from 7 to 11m/s, then at 6 sec the reference of active power is increased from -1.2 MW at -1.4 MW while the reference of the reactive power is kept at 300 kVAR.

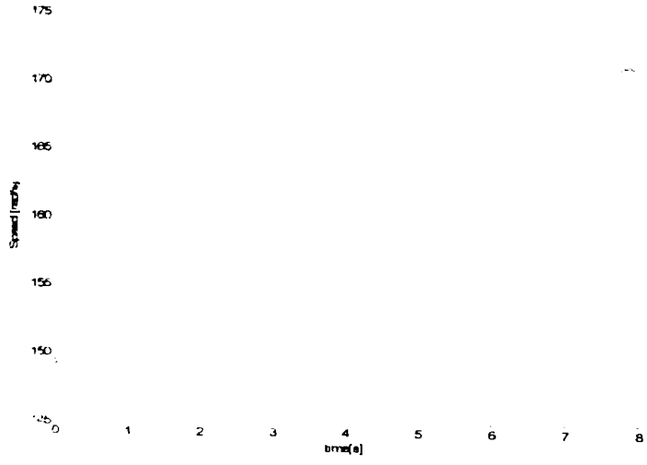

Figure 2.10 Speed of the generator

The speed of the generator is illustrated in Figure 2.10. The response at step in wind speed can be observed, as acceleration. Also, at 6 sec. due to the limited power of the system, the modification of the generated active power (loading) leads to a reduction of the speed.

The rotor currents are shown in Figure 2.11. During the acceleration of the generator, produced by the increasing of the wind speed, a passing through the synchronous speed is recorded. This could be observed at 2.2 sec.

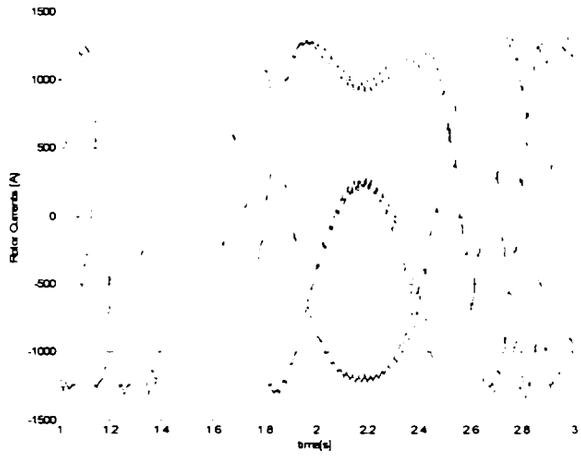

Figure 2.11 Rotor currents during transient in wind speed (the passing through synchronism can be observed)

In Figure 2.12 are presented the turbine torque and the electromagnetic torque, respectively, and in Figure 2.13 the DC bus voltage is illustrated.

From the grid-side point of view, the voltages from the grid are shown in Figure 2.14 a and the currents in the grid-side (through RL filter) are shown in Figure 2.14 b. A phase angle of 180^0 could be observed between the voltages and the currents, as a sign of no reactive power is circulated through the grid side but the active power is generated (corresponding to over-synchronism operation).

Also the total grid currents are illustrated in Figure 2.14 c. The phase angle corresponding to the level (and the direction) of "ordered" active and reactive powers could be observed there, between these currents ("seen" from the power system) and the grid voltages.

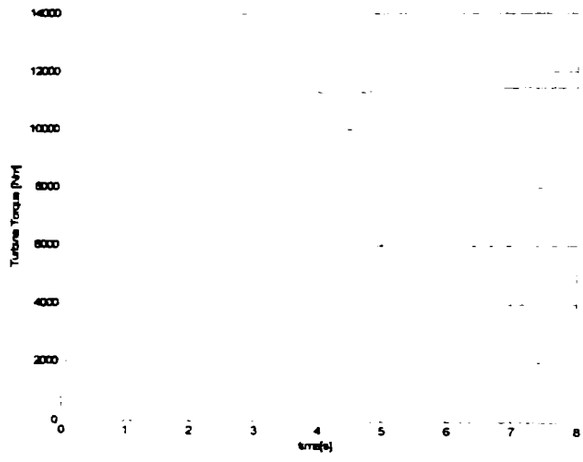

a)

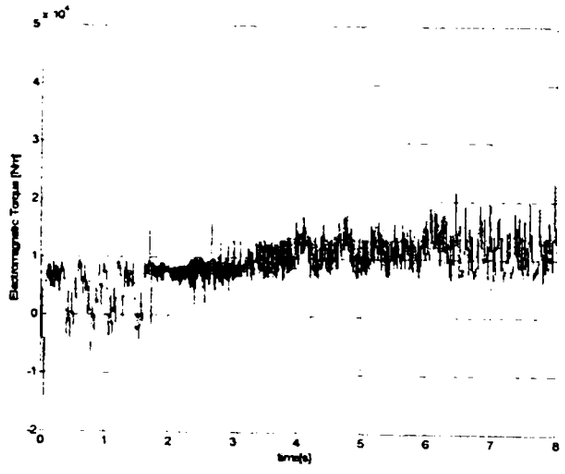

b)

Figure 2.12 a) The torque from the turbine, b) the electromagnetic torque

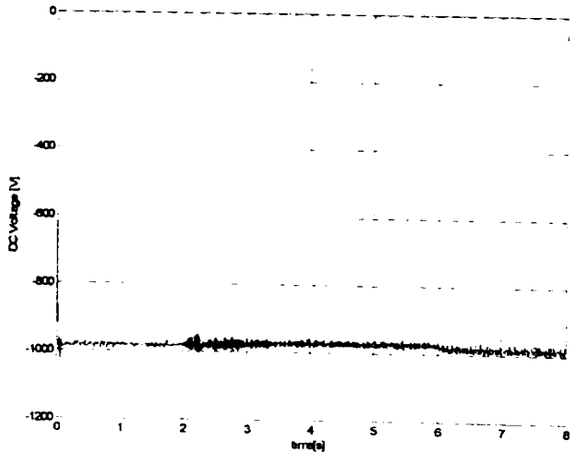

Figure 2.13 DC voltage.

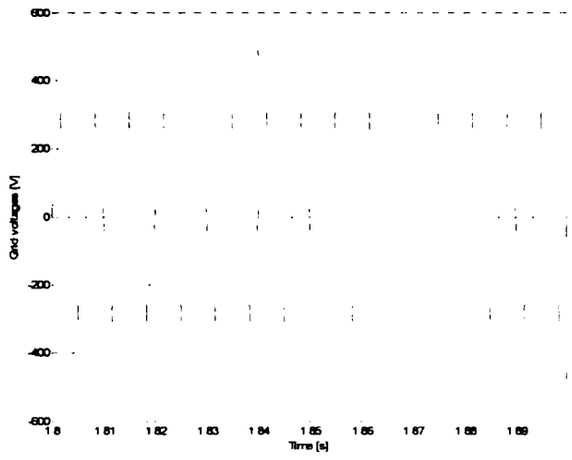

a)

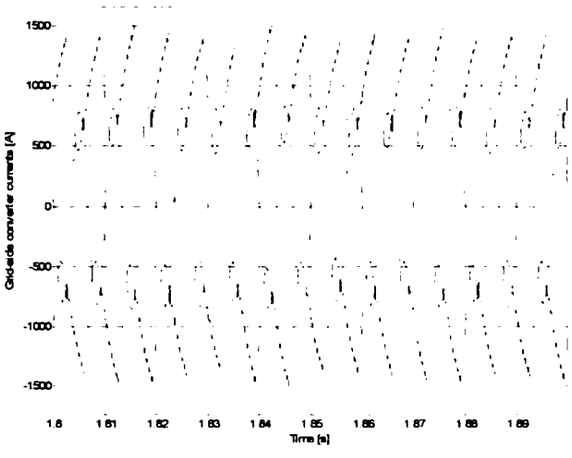

b)

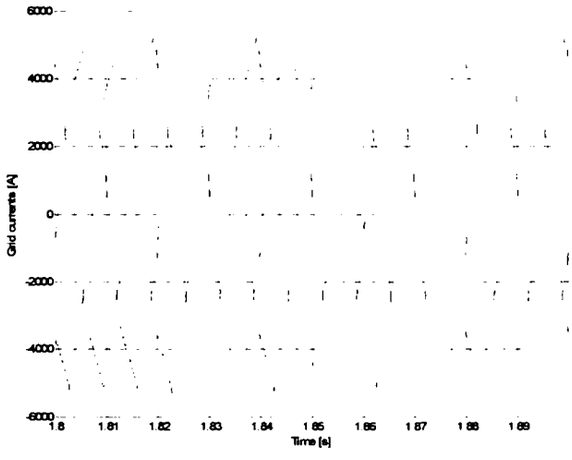

c)

Figure 2.14 a) The grid voltages, b) grid-side converter currents, c) grid total currents.

The reference and the response of the system in terms of active power are illustrated in Figure 2.15 a. The loading is quick and stable. The reactive power control is shown in Figure 2.15 b. The reference is kept at a constant value, and the control is also stable.

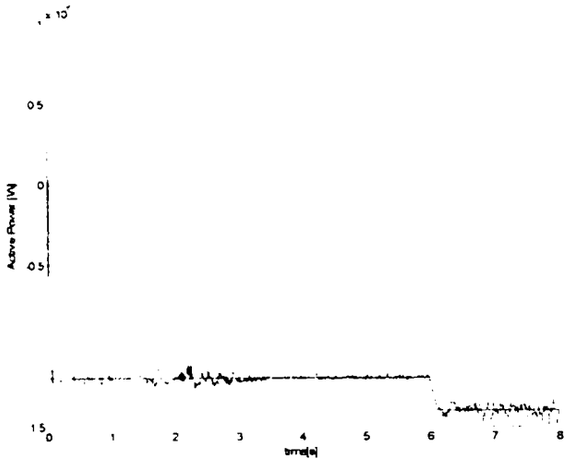

a)

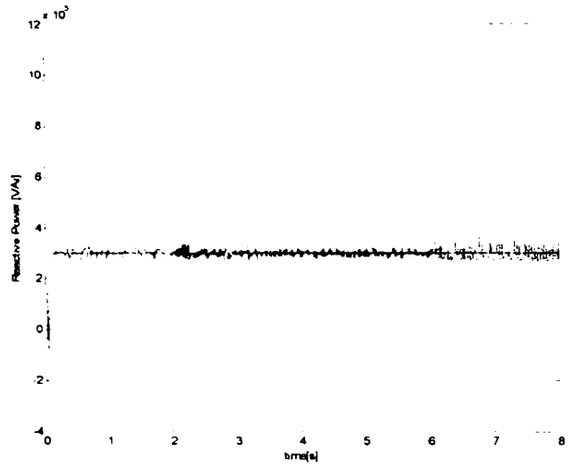

b)

Figure 2.15 The control of powers: a) active power, b) reactive power

For the same step in the active power reference, a few further waveforms are shown in what it follows. In Figure 2.16 a, the stator voltages are shown, quite constant in terms of amplitudes and frequency, as the grid is strong. The stator currents are shown in Figure 2.16 b, where the step in active power could be seen, and the pulse width modulated rotor voltages (from the output of the machine-side converter) are illustrated in Figure 2.16 c.

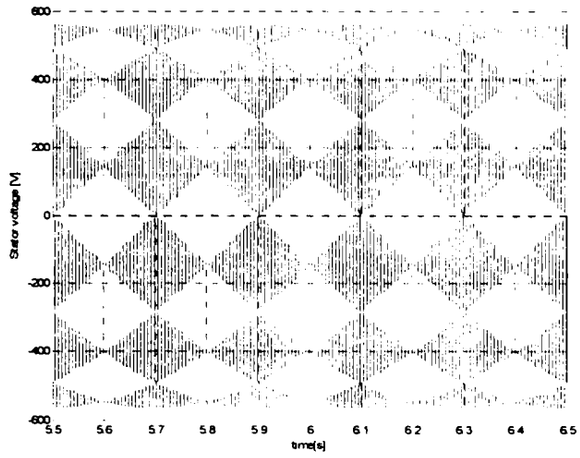

a)

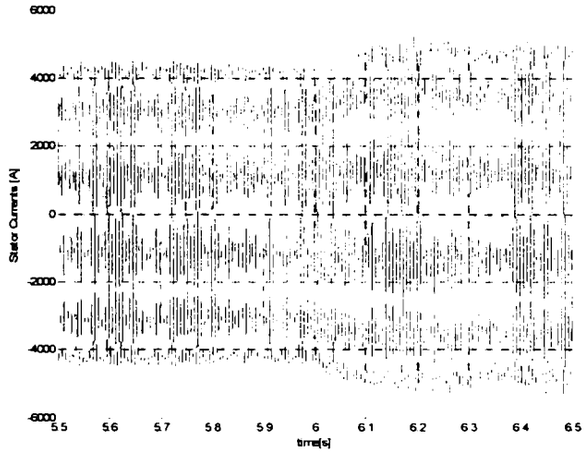

b)

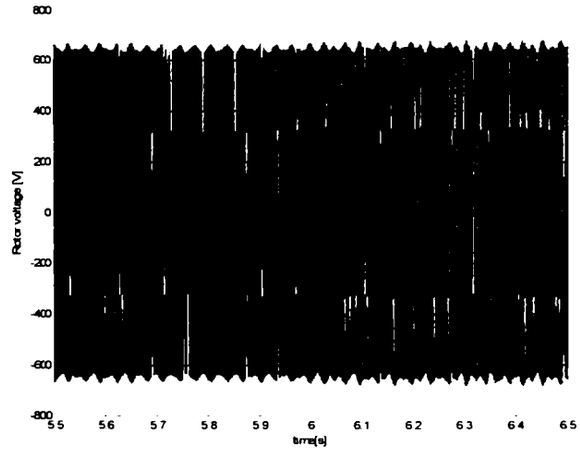

c)

Figure 2.16 Generator waveforms during the active power reference step: a) stator voltages, b) stator currents, c) rotor voltages.

2.4 Case study: three-phase shortcircuit of the power grid

In order to study the behavior of the whole system under a three-phase short-circuit on the power grid, without taking any protective measure, the grid is modeled as in Figure 2.1 and divided in two parts [10]. The short-circuit is applied at the middle of the line (see Figure 2.1) at 3.1 sec. and is cleared at 3.6 sec.

First, the stator voltages and currents are shown in Figure 2.17 a and b, respectively.

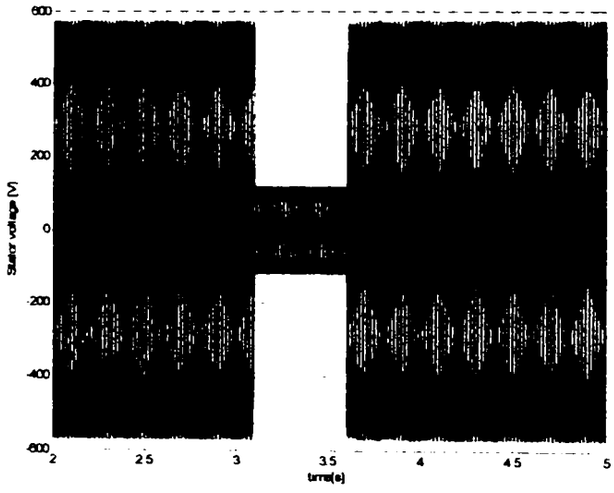

a)

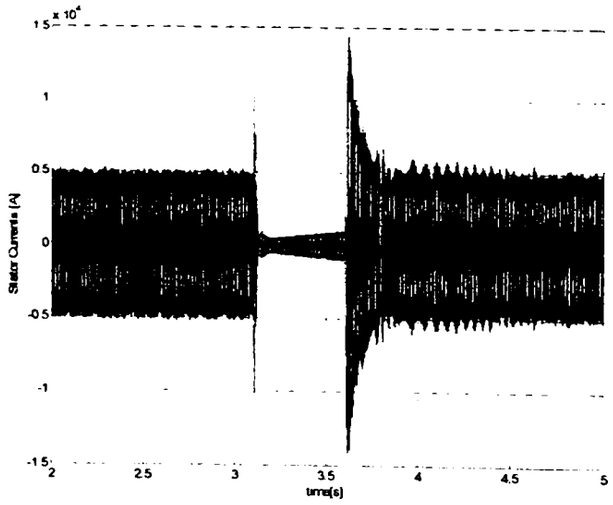

b)

Figure 2.17 Three-phase short-circuit on the power grid: a) stator voltage, b) stator currents

Then, the rotor quantities are illustrated, the voltages in Figure 2.18a and the currents in Figure 2.18 b.

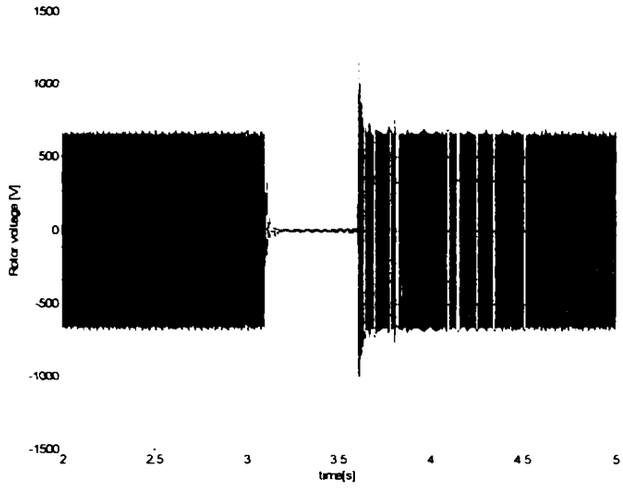

a)

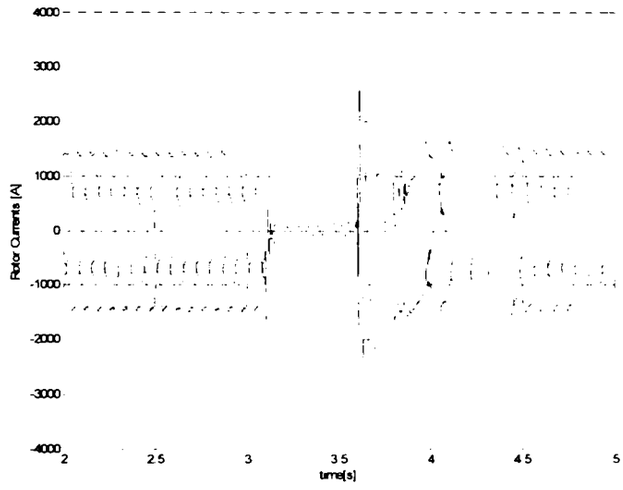

b)

Figure 2.18 Three-phase short-circuit on the power grid (cont.): a) rotor voltage, b) rotor currents

It can be seen there are two dominant current peaks, one at the start of the short-circuit, and one even more severe when the short-circuit is cleared.

The speed of the generator is shown in Figure 2.19 a and the turbine torque and the electromagnetic torque are shown in Figure 2.19 b and c, respectively.

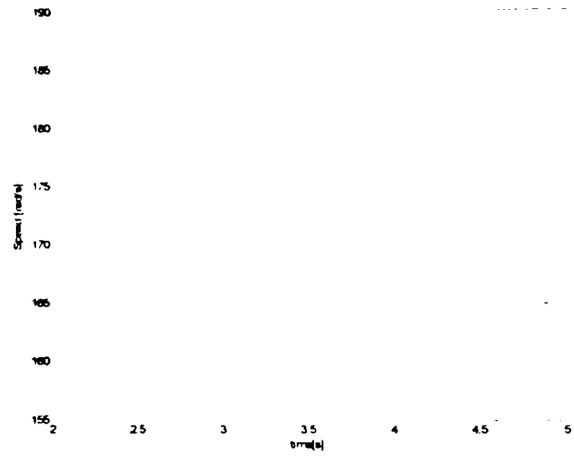

a)

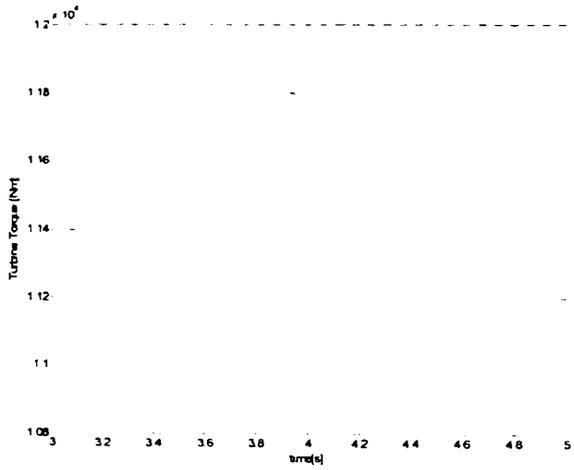

b)

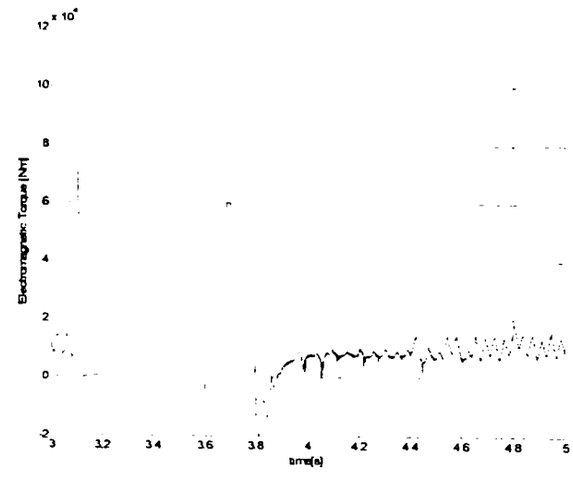

c)

Figure 2.19 Three-phase short-circuit on the power grid (cont.): a) speed, b) turbine torque, c) electromagnetic torque.

Two severe transients in torque also occur, and a transient in speed, which means that during the fault the electromagnetic torque is very small and thus the generator accelerates. The torque of the turbine is naturally decreased during the fault as the generator speed is increasing and the wind speed remains constant (see the characteristics in Figure 2.3)

Finally, the active and reactive power responses are illustrated in Figure 2.20.

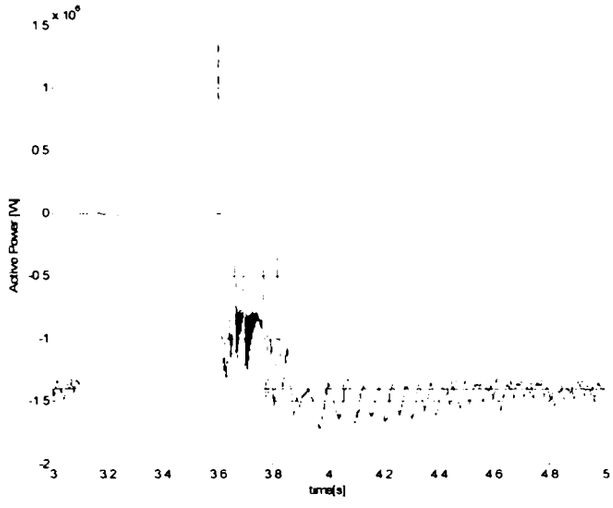

a)

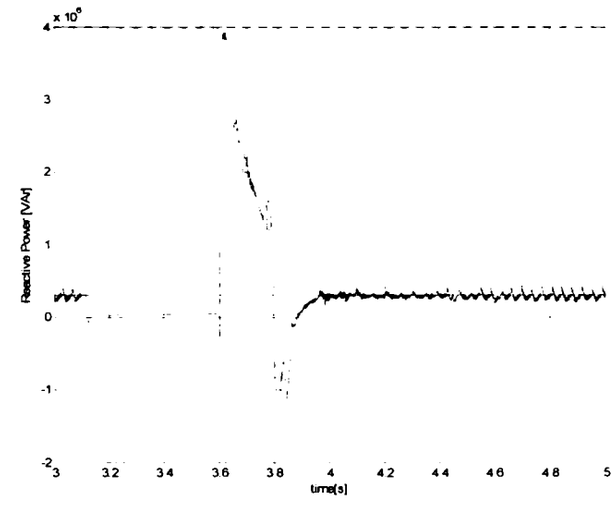

b)

Figure 2.20 Three-phase short-circuit on the power grid (cont.): a) active power, b) reactive power.

2.5 Mechanism to improve the performance of the system during fault

To reduce the transients due to short-circuit a few methods were investigated. The first was to reduce the active and reactive power references immediately after the fault occurs. But this did not produce any improvement.

The most efficient method according to this study was to limit the rotor currents. This was done by limiting the reference of the rotor currents, in fact the output of the active and reactive power PI controllers at the $\pm 1.5\ I_m$ in q-axis and at $\pm 0.5\ I_m$ in d-axis. The results are presented in what follows.

First the stator and rotor currents and the rotor and DC voltage are shown in Figure 2.21.

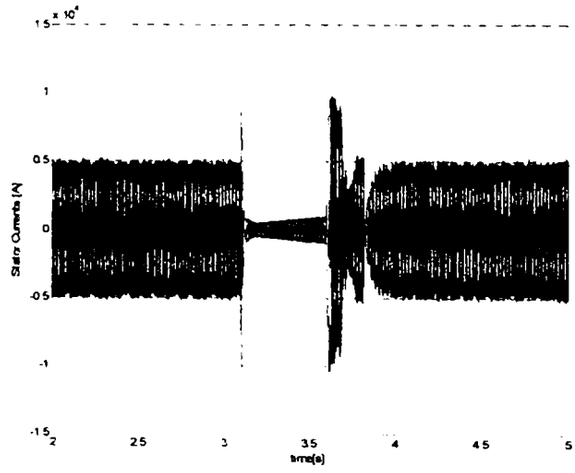

a)

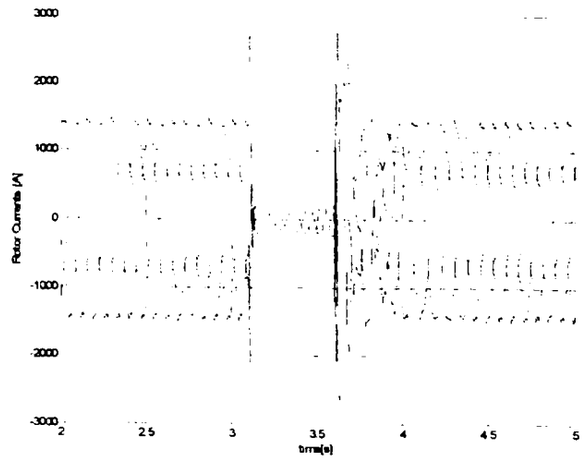

b)

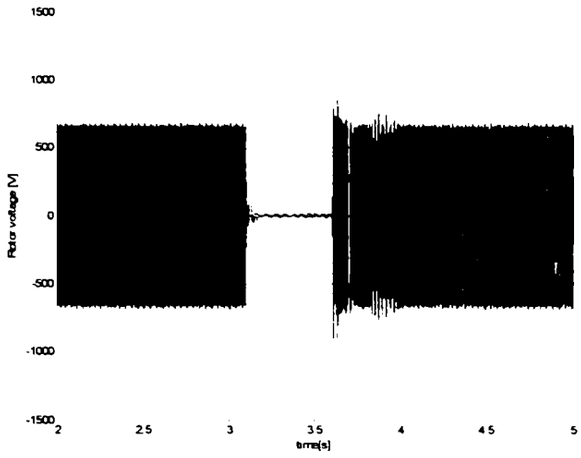

c)

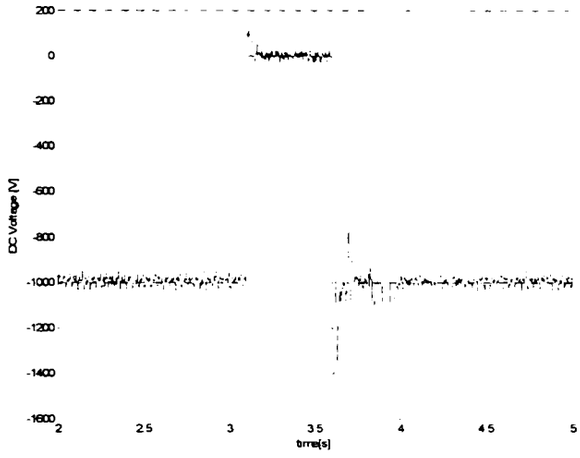

d)

Figure 2.21 Three phase short-circuit on the power grid, with limited rotor currents in the generator: a) stator currents, b) rotor currents, c) rotor voltages, d) DC voltage

Notable improvements can be easily noticed. First and the most important is the reduction of the second rotor current peak (when the short-circuit is cleared) with 50%. The stator current second peak is also reduced with the same amount.

The speed of the generator, the turbine torque and the electromagnetic torque are shown in Figure 2.22.

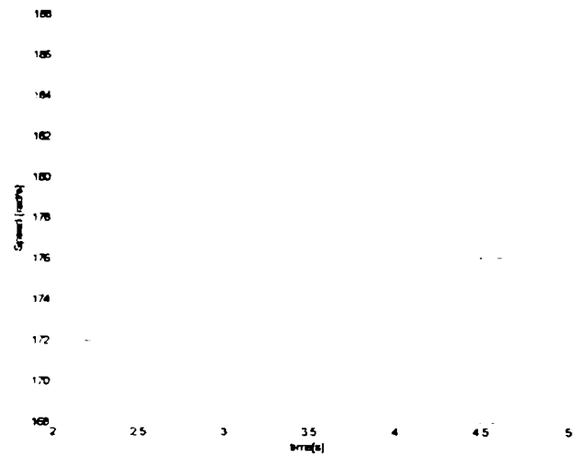

a)

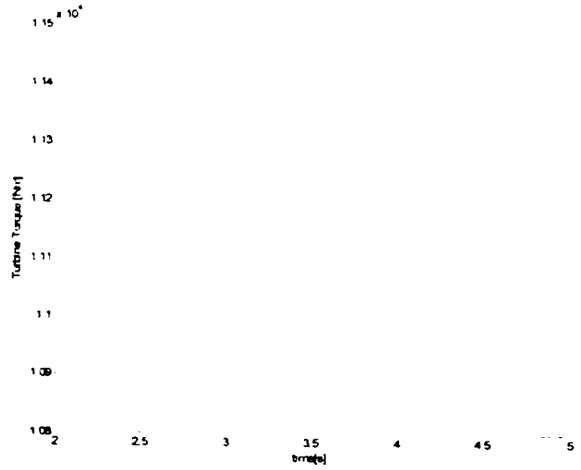

b)

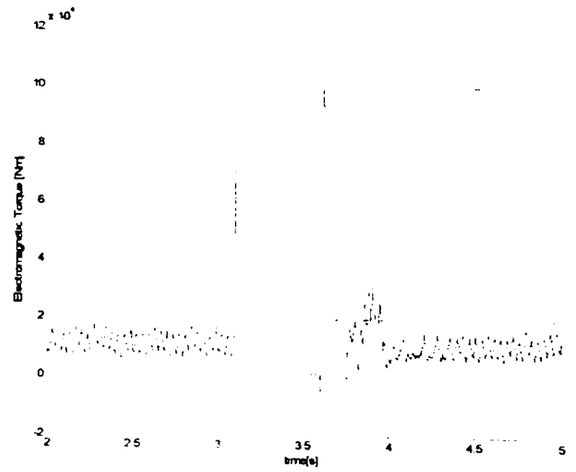

c)

Figure 2.22 Three phase short-circuit on the power grid, with limited rotor currents in the generator (cont): a) speed, b) turbine torque, c) electromagnetic torque

The acceleration of the generator is not avoided but, when the system is restoring, the deceleration is not so pronounced and the speed of the generator is stabilizing earlier (practically the system is recovering something more quickly than in the case with no limitations in the rotor currents).

Conclusion

For large power wind farms continuous operation during short-circuit faults is required. This mode becomes more and more important as the wind turbine should be able to contribute with power just after a short circuit. A detailed investigation on the control and behavior on the doubly-fed induction generator under power grid short-circuit was done in this chapter. The good dynamic performances and accuracy of the active and reactive power control were demonstrated.

Also the waveforms of the generator in a three-phase short-circuit are presented. For better continuous operation during short-circuit faults different methods were investigated. The modification of the power references during the fault in order to prevent the rotor overcurrents and generator overspeeding was performed but it did not produce the expected results. The best situation was obtained with the limitation of the rotor currents references (through the output limitation of the active and reactive power controllers).

References

[1] V. Akhmatov, "Modelling of variable speed wind turbines with doubly-fed induction generators in short term stability investigations," *3rd Int. Workshop on Transmission Networks for Offshore Wind Farms*, April 11-12, 2002, Stockholm, Sweden.

[2] R. Pena, J. C. Clare, G. M. Asher, "Doubly-fed induction generator using back-to-back PWM converters and its application to variable-speed wind-energy generation," *Proc. Inst. Elect. Eng.*, pt. B, vol. 143, pp. 231-241, May 1996.

[3] Ion Boldea, "Electric Drives", Chapter 14: Large Power Drives, 14.8 Sub and Hypersynchronous IM cascade drives, CRC Press Florida, ISBN: 0849325218, 1998.

[4] Florin Iov and all, "Wind Turbine Blockset", A flexible platform for simulation and optimizing of the wind turbines, Project, Institute of Energy Technology, Aalborg, Denmark, Risø National Laboratory, Denmark.

[5] U. Rädel, D. Navarro, G. Berger, S. Berg, "Sensorless Field-Oriented Control of a Slipring Induction Generator for a 2.5 MW Wind Power Plant from Nordex Energy GmbH", EPE 2001 Conference Proceedings, Graz.

[6] R. Datta, V.T. Ranganathan, "Direct Power Control of Grid-Connected Wound Rotor Induction Machine Without Rotor Position Sensors," IEEE Transactions On Power Electronics, vol. 16, no. 3, May 2001, pp. 390-399.

[7] L. Morel, H. Godfroid, A. Mirzaian, J. M. Kauffmann, "Double-fed induction machine: converter optimization and field oriented control without position sensor," *Proc. Inst. Elect. Eng.*, pt.B, vol. 145, pp. 360-368, July 1998.

[8] S. Müller, M. Deicke, R. W. De Doncker, "Adjustable speed generators for wind turbines based on double-fed induction machines and 4-quadrant IGBT converters linked to the rotor," *IEEE-IAS Annual Meeting*, 2000

[9] T. Senjyu, N. Sueyoshi, K. Uezato, H. Fujita, "Stability analysis of wind power generating system" Power Conversion Conference, 2002. PCC Osaka 2002 Proceedings, vol. 3: 2002 pp. 1441 –1446.

[10] P. Ledesma, J. Usaola, "Minimum Voltage Protections in Variable Speed Wind Farms", 2001 Porto Power Tech Conference, 10th – 13th September, Porto, Portugal

Chapter 3

Sensorless control of DFIG at power grid with faults

Abstract

The previous chapter dealt with the behavior of the 2 MW DFIG system during power grid shortcircuit, and with the mechanism to improve the performance of the system during faults, without disconnecting the generator from the power system.

In this chapter another problem is bring into discussion, regarding also the behavior of the system during faults. But, this time, the sensorless algorithm is introduced and deeply analyzed, especially during power grid shortcircuit.

The investigation is done especially in order to find the influence of magnetic saturation on the rotor position and speed estimators, and, in general, the system behavior in a sensorless vector control scheme during transients and shortcircuit faults (sensorless DFIG system "riding through fault")

The DFIG is driven by a wind turbine whose torque vs. generator speed at different wind speeds is optimized by the pitch control system.

A sudden three-phase shortcircuit at the middle of a typical local power grid is investigated.

A complete simulation under Simulink® environment for the whole system has been developed and applied to simulate transients as described above with and without considering the magnetic saturation in the machine.

It is shown by digital simulations that during shortcircuit the sensorless control fails without considering the magnetic saturation and, even during the sudden connection to the grid, the errors in position and speed estimation are notable.

3.1 Introduction

The electrical schematic of the whole system is shown in Figure 3.1. The system includes the wind turbine (not represented here), the generator itself, the vector controlled grid-side inverter, the vector controlled machine side inverter, the RL filter and the power grid.

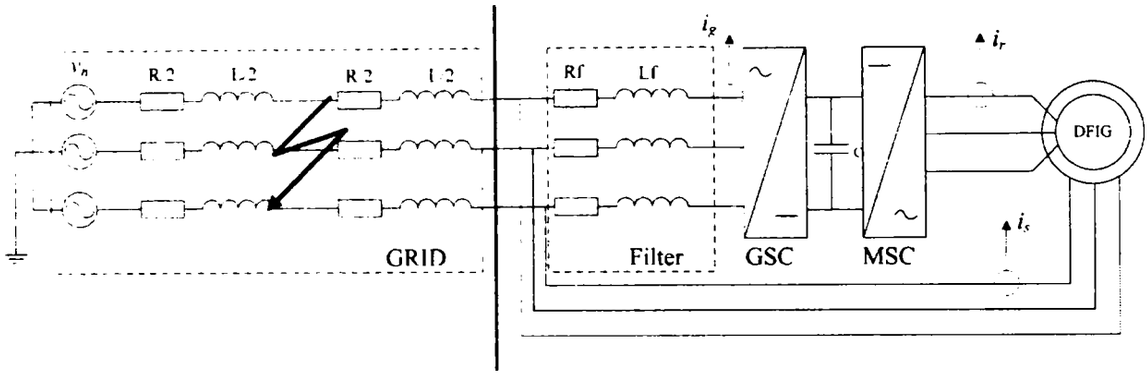

Figure 3.1 The doubly-fed induction generator connected to the power grid

The grid is modeled as divided in two equal parts in order to apply the shortcircuit at the middle.

As all the models were "in extenso" described in the previous chapter, in what it follows only the generator model will be again discussed, as the magnetic saturation was included in the model.

3.2 The DFIG model with magnetic saturation included

Stator and rotor voltages expressed in terms of d and q axes quantities rotating in an arbitrary reference frame with the speed ω_k are given by [1]:

$$v_{sd} = R_s \cdot i_{sd} + \frac{d\psi_{sd}}{dt} - \omega_k \cdot \psi_{sq} \tag{3.1}$$

$$v_{sq} = R_s \cdot i_{sq} + \frac{d\psi_{sq}}{dt} + \omega_k \cdot \psi_{sd} \tag{3.2}$$

$$v_{rd} = R_r \cdot i_{rd} + \frac{d\psi_{rd}}{dt} - (\omega_k - \omega_r) \cdot \psi_{rq} \tag{3.3}$$

$$v_{rq} = R_r \cdot i_{rq} + \frac{d\psi_{rq}}{dt} + (\omega_k - \omega_r) \cdot \psi_{rd} \tag{3.4}$$

Stator and rotor fluxes are expressed in function of the current by:

$$\psi_{sd} = L_s \cdot i_{sd} + L_m \cdot i_{rd} \tag{3.5}$$

$$\psi_{sq} = L_s \cdot i_{sq} + L_m \cdot i_{rq} \tag{3.6}$$

$$\psi_{rd} = L_r \cdot i_{rd} + L_m \cdot i_{sd} \tag{3.7}$$

$$\psi_{rq} = L_r \cdot i_{rq} + L_m \cdot i_{sq} \tag{3.8}$$

where variation of L_m is implemented as in Figure 3.2.

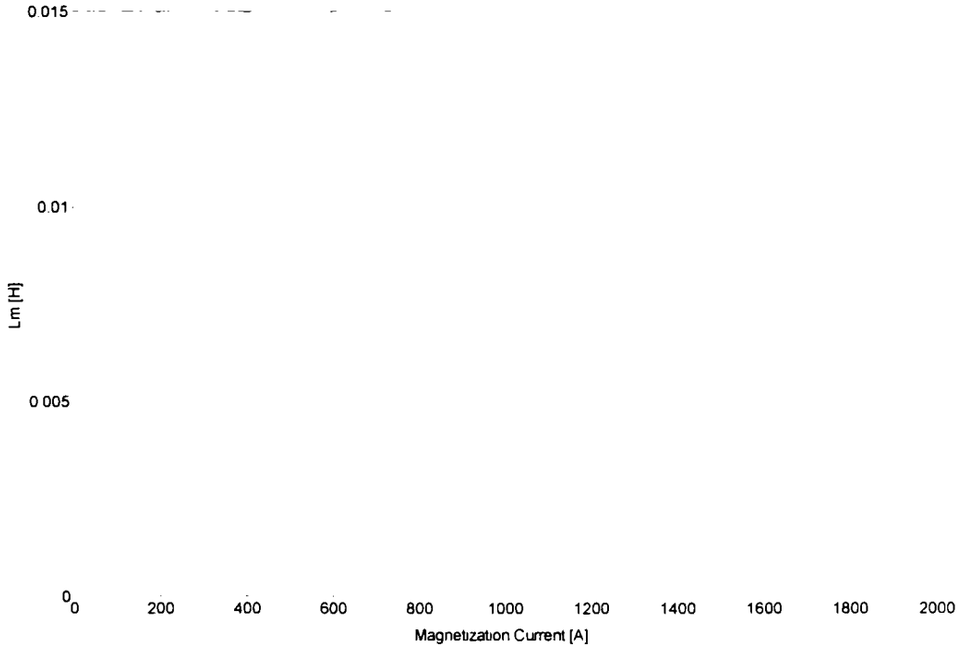

Figure 3.2 The magnetic saturation: variation of L_m versus magnetization current

Also, the electromagnetic torque:

$$T_e = \frac{3}{2} \cdot p \cdot \left(\psi_{sd} \cdot i_{sq} - \psi_{sq} \cdot i_{sd} \right) \tag{3.9}$$

The implementation of the above equations, the structure of the whole DFIG model and the corresponding mask of the system are illustrated in Figure 3.4 [2].

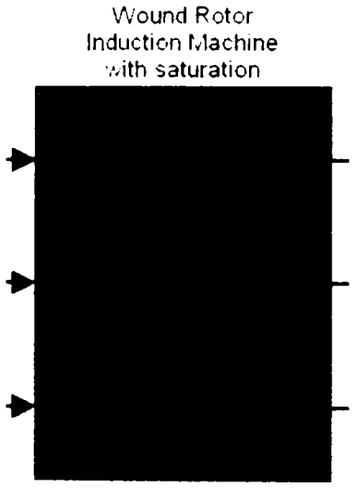

a)

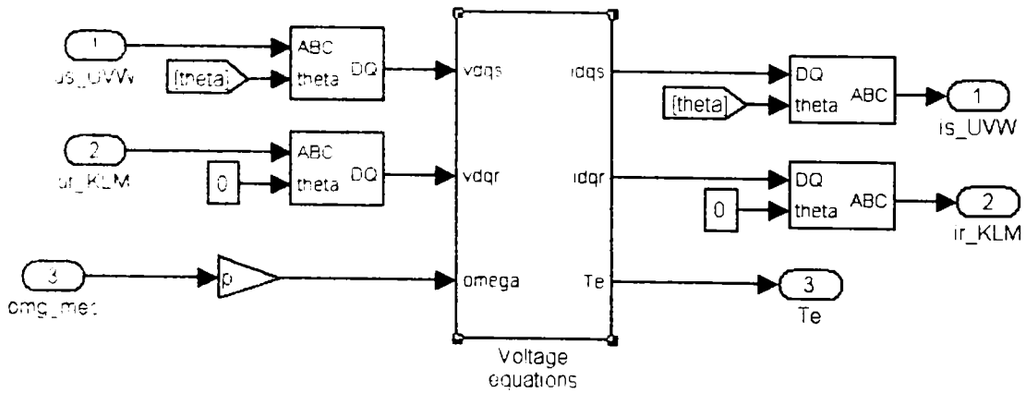

b)

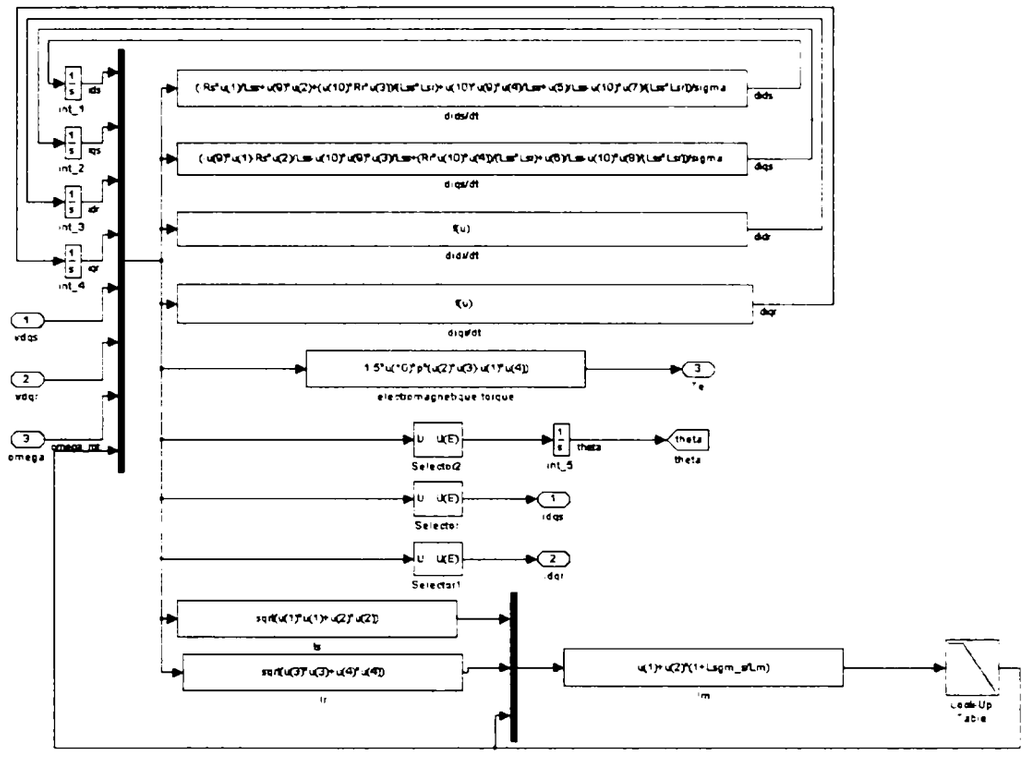

c)

Figure 3.3 The model of the DFIG: a) mask of the model, b) implementation of the model, c) implementation of the equations

Usually a speed range of ± 25% is chosen around the synchronous speed [3]. To have a lower current at the rotor-side of the machine equivalent with a lower converter sizing, and the same voltage at the rotor-side and the stator-side at the limits of the speed range (the voltage adapting transformer between the converter and the power system is avoided), a transformer ratio K of the generator windings of 4 is chosen:

$$v_{r\max} = K \cdot |s_{\max}| \cdot (v_s)_{rated} \tag{3.10}$$

3.3 Position and speed estimation

The generator is controlled in a synchronously rotating dq-frame, with the d-axis aligned with the stator-flux vector position, which ensures a decoupled control

between the electromagnetic torque and the rotor excitation contribution (see Figure 3.4).

In fact decoupled active and reactive power control [4,5] of the generator is obtained

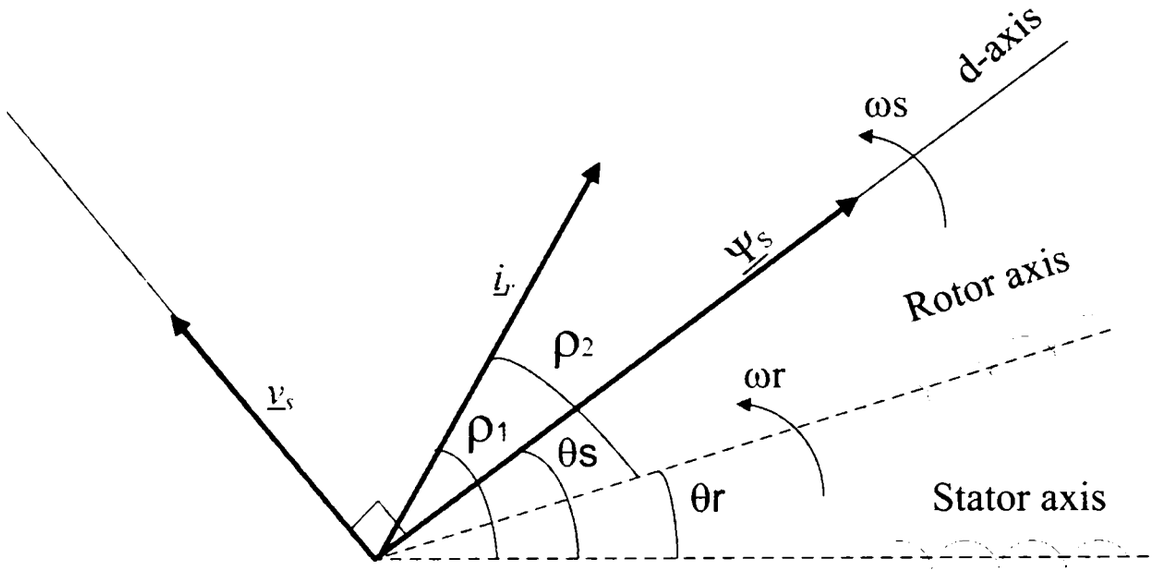

Figure 3.4 Location of different vectors in stationary coordinates.

3.3.1 Position and speed estimation without saturation included

In order to avoid using an encoder the position should be estimated for the vector control. Also speed information for the back-EMF compensation is needed.

The sensorless algorithm is based on the vector diagram in Figure 3.4 and is adapted from [6]. The rotor current (which can be measured in rotor coordinates) makes an angle ρ_1 with the stator axis and an angle ρ_2 with the rotor axis. The difference between ρ_1 and ρ_2 is the rotor position θ_r which must be determined. In Figure 3.6 the block diagram of the sensorless algorithm is presented and in what it follows it will be explained in detail.

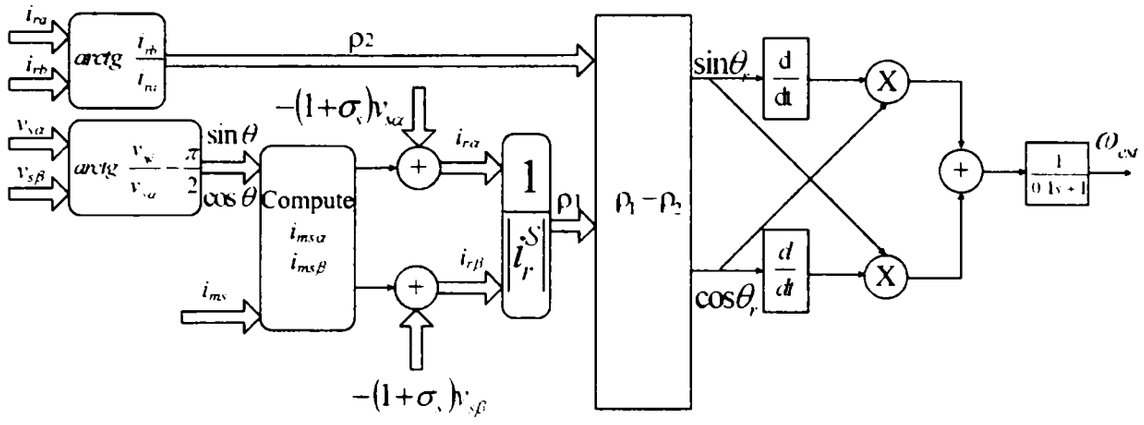

Figure 3.5 Block diagram of the position/speed sensorless algorithm.

The position of the stator flux magnetizing current is calculated assuming the stator resistance is very small and, hence, the stator flux is in quadrature with the stator voltage.

The magnitude of the stator magnetizing current is:

$$i_{ms} = \frac{v_s}{\omega_s L_0} \tag{3.11}$$

The i_{ms} components in stator coordinates can be calculated as:

$$i_{ms\alpha} = i_{ms} \cdot \sin\theta_e \tag{3.12}$$

$$i_{ms\beta} = -i_{ms} \cdot \cos\theta_e \tag{3.13}$$

The rotor currents in stator coordinates are:

$$i_{r\alpha} = i_{ms\alpha} - (1+\sigma_s) i_{s\alpha} \tag{3.14}$$

$$i_{r\beta} = i_{ms\beta} - (1+\sigma_s) i_{s\beta} \tag{3.15}$$

where:

$$\sigma_s = \frac{L_{sl}}{L_m}$$. L_{sl} – stator leakage inductance

Hence, the angle ρ_1 results:

$$\rho_1 = \frac{i_{r\beta}}{i_{r\alpha}} \tag{3.16}$$

As the rotor currents are directly measured in the rotor circuit, the angle ρ_2 can be immediately computed as:

$$\rho_2 = \frac{i_{rb}}{i_{ra}} \tag{3.17}$$

With angles ρ_1 and ρ_2 thus calculated, the rotor position can be now easily calculated:

$$\theta_r = \rho_1 - \rho_2 \tag{3.18}$$

The speed is estimated with the following equation:

$$\omega_{esl} = -\sin\theta_r \frac{d}{dt} \cdot \cos\theta_r + \cos\theta_r \cdot \frac{d}{dt} \cdot \sin\theta_r \tag{3.19}$$

The differential terms introduces some noise which has to be eliminated using a first order low-pass filter with a transfer function:

$$H_{filter}(s) = \frac{1}{0.1 \cdot s + 1} \tag{3.20}$$

3.3.2 Position and speed estimation with saturation included

The accuracy of computation of the rotor position depends on the value of i_{ms}. To estimate the magnetization current the magnetizing inductance L_m is required. If there is a serious variation in the grid voltage or in the supply frequency L_m will most likely saturate. In this condition the estimation of the rotor position is seriously affected.

However, any change in the magnitude of the stator flux can be correctly estimated using the following adaptive algorithm [7].

First, the algorithm is started with the value of i_{ms} in equation 3.11. After that, i_{ms} is computed by transforming the present rotor current sample to the stator coordinates using the unit vectors computed in the previous interval.

This is based on the following equations:

$$i'_{r\alpha}[k] = i_{ra}[k] \cdot \cos\theta_r[k-1] - i_{rb}[k] \cdot \sin\theta_r[k-1] \tag{3.21}$$

$$i'_{r\beta}[k] = i_{rb}[k] \cdot \cos\theta_r[k-1] + i_{ra}[k] \cdot \sin\theta_r[k-1] \tag{3.22}$$

$$i'_{ms\alpha}[k] = (1+\sigma_s) \cdot i_{s\alpha}[k] + i'_{r\alpha}[k] \tag{3.23}$$

$$i'_{ms\beta}[k] = (1+\sigma_s) \cdot i_{s\beta}[k] + i'_{r\beta}[k] \tag{3.24}$$

$$i'_{ms} = \sqrt{\left(i'^2_{ms\alpha} + i'^2_{ms\beta}\right)} \tag{3.25}$$

The block diagram with the adaptive computation of the i_{ms} is presented in Figure 3.6.

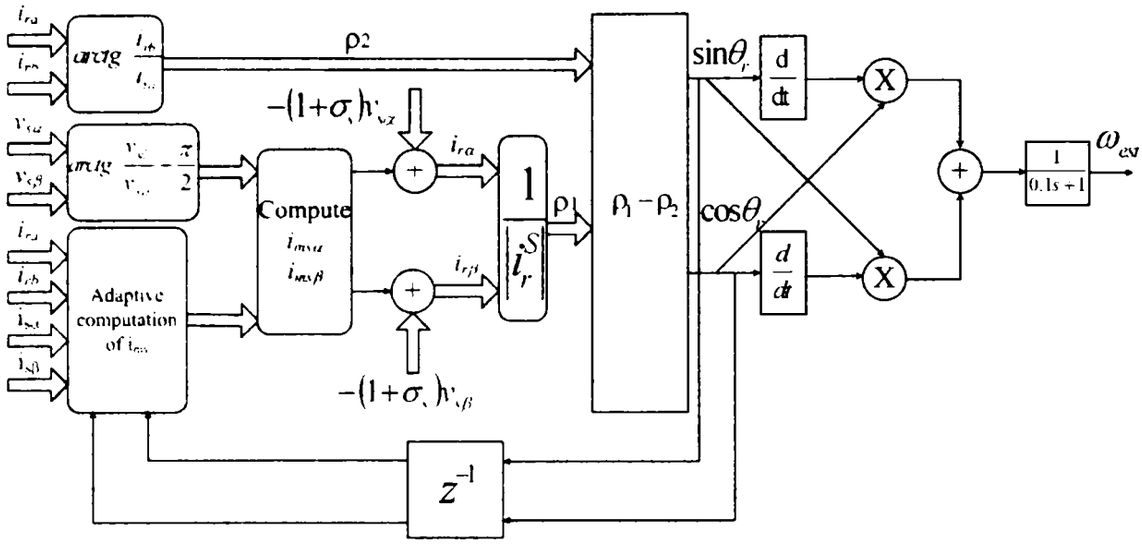

Figure 3.6 The block diagram of the position/speed sensorless algorithm with the adaptive computation of i_{ms}.

The algorithm is implemented on the simulation and the results are presented in what it follows.

3.4 Simulation results

All the control strategies, parameters etc. are as presented in the previous chapter.

In figure 3.7a) the comparison between the measured and the estimated rotor position is presented and in 3.7b) the comparison between the estimated and the measured speed is shown.

The results are satisfactory even during (3.1-3.6s) and after the shortcircuit (after 3.6s). The active power reference is maintained at 1.4MW. The reactive power reference is set at 0.4 MVAr. The control in terms of active and reactive power and also in rotor currents is rather accurate as it is shown in Figure 3.8 and 3.9 respectively.

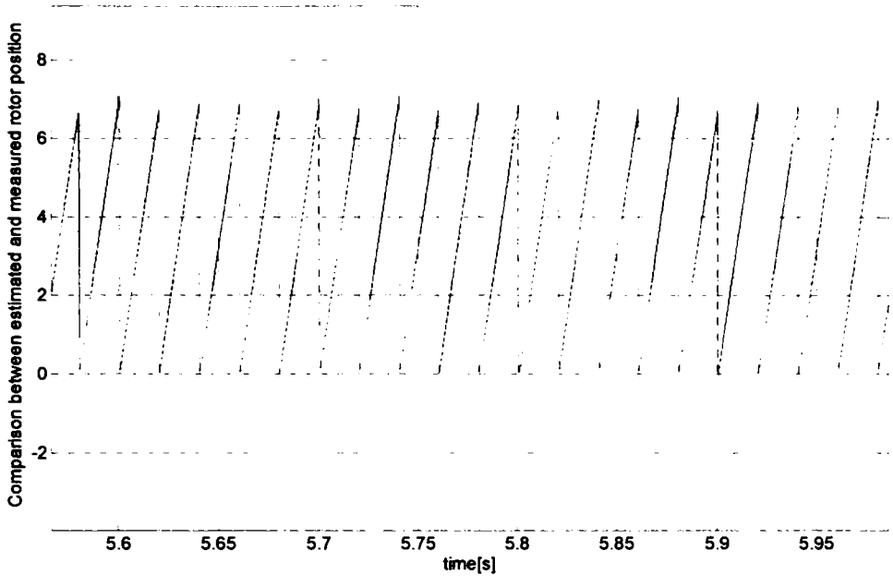
Comparison between estimated and measured rotor position
8
6
4
2
0
-2
5.6
5.65
5.7
5.75
5.8
5.85
5.9
5.95
time[s]

a)

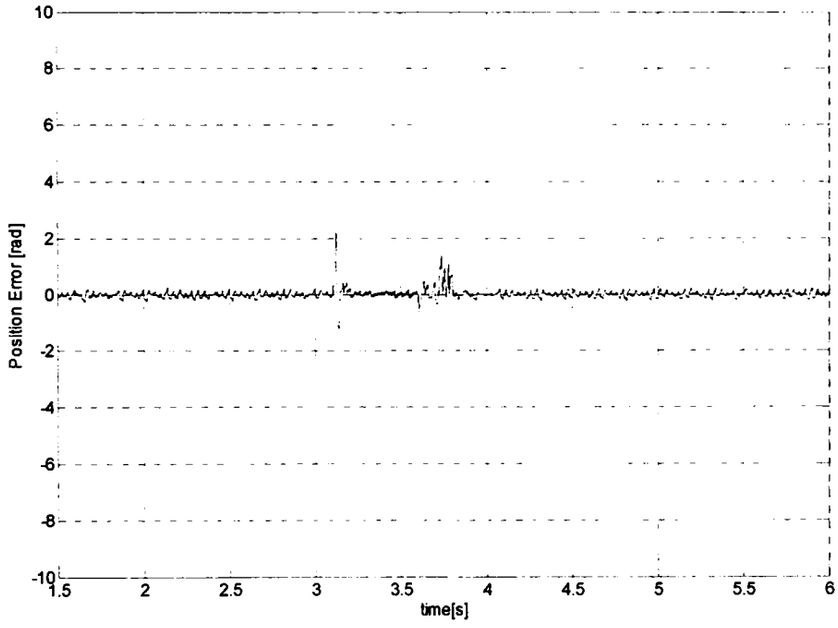
Position Error [rad]
10
8
6
4
2
0
-2
-4
-6
-8
-10
1.5
2
2.5
3
3.5
4
4.5
5
5.5
6
time[s]

b)

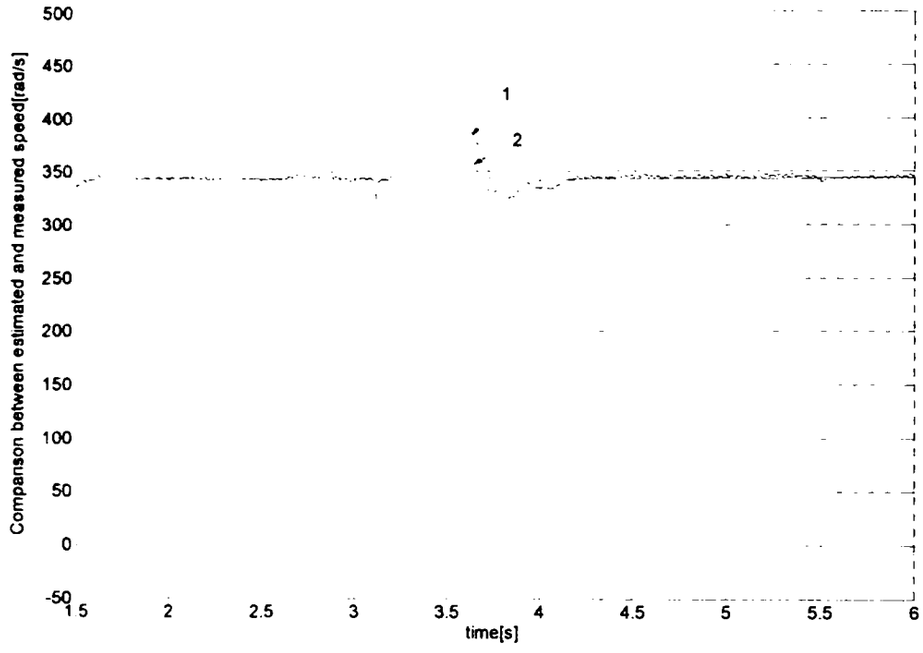

c)

Figure 3.7 The estimated and measured rotor position a), the error in position estimation b) and the estimated (1) and measured (2) speed c).

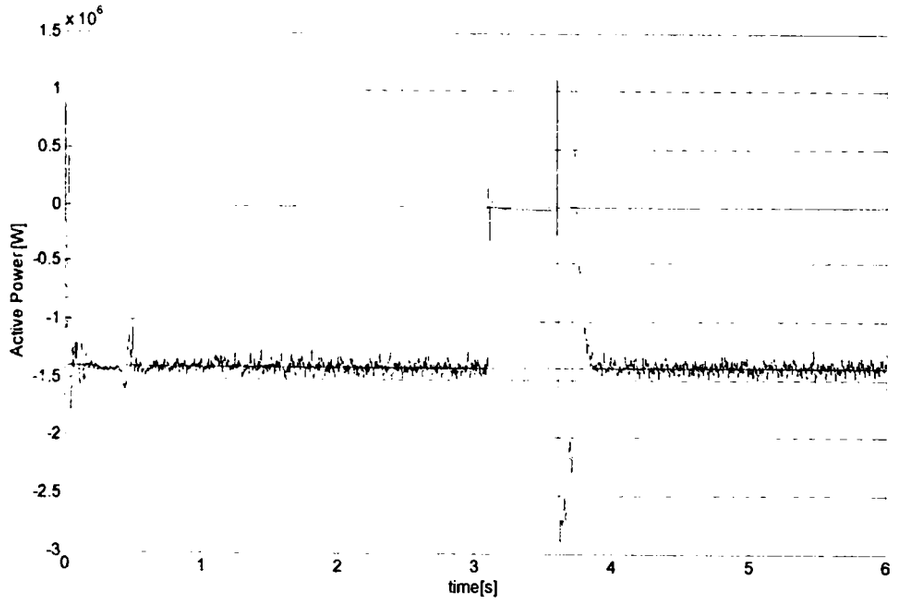

a)

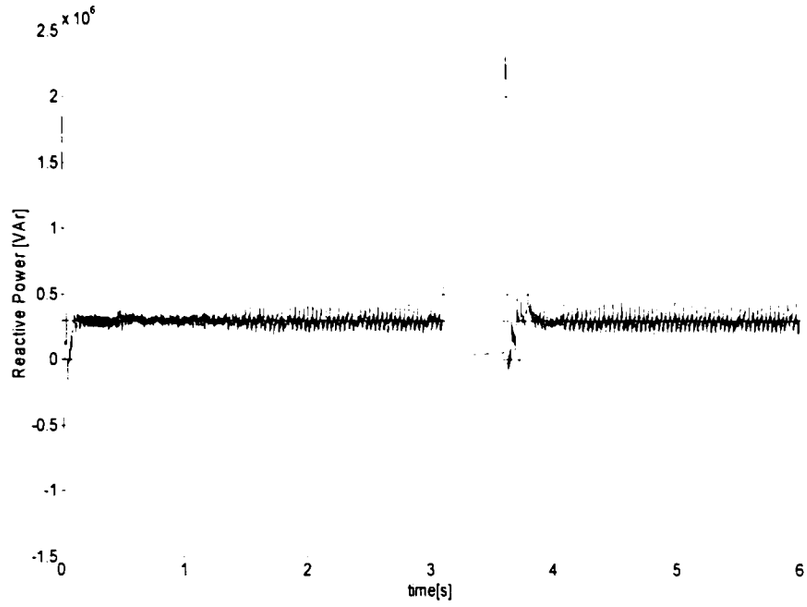

b)

Figure 3.8 The active (a) and reactive (b) powers.

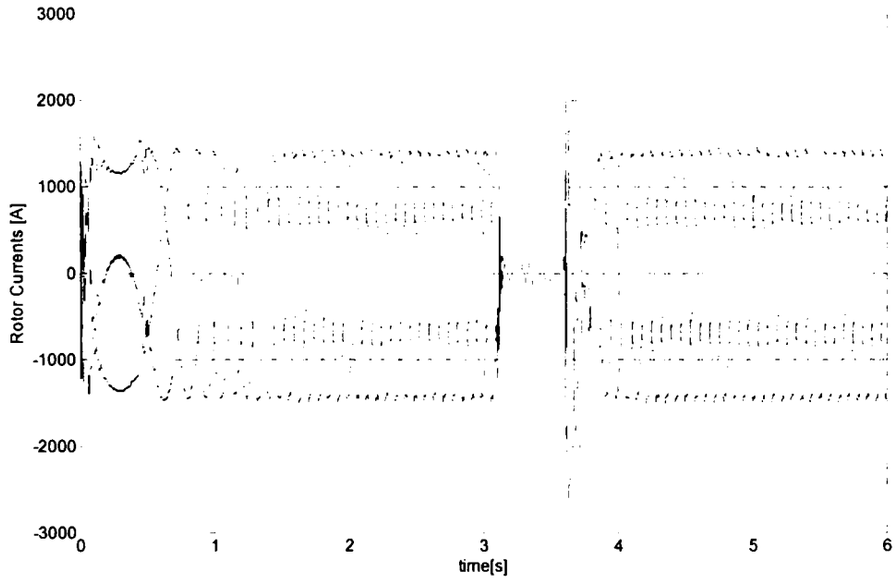

Figure 3.9 The rotor currents

In order to study the influence of taking into account the magnetic saturation in the estimator, the adaptive algorithm for calculation of i_{ms} is neglected, and the value of i_{ms} is considered constant along the simulation (see Paragraph 3.3.1). In this

new circumstance Figure 3.10 shows the comparison between the measured and estimated angle and between the estimated and measured speed.

It could be easily observed that immediately after the shortcircuit occurs the estimation is totally compromised due to imprecision in calculations with constant L_m. but the system works with the motion observer with variable L_m as it was discussed above.

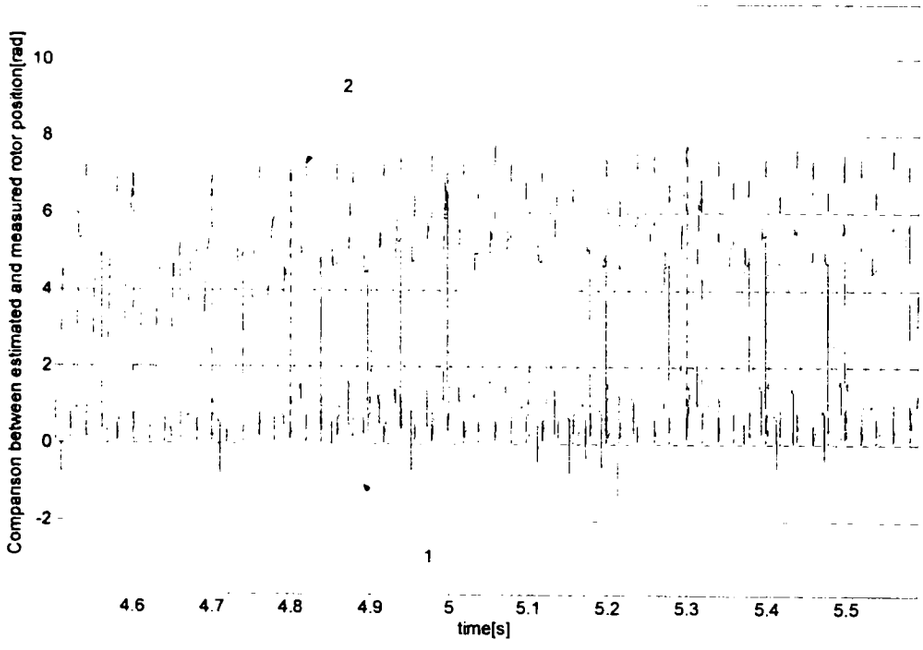

a)

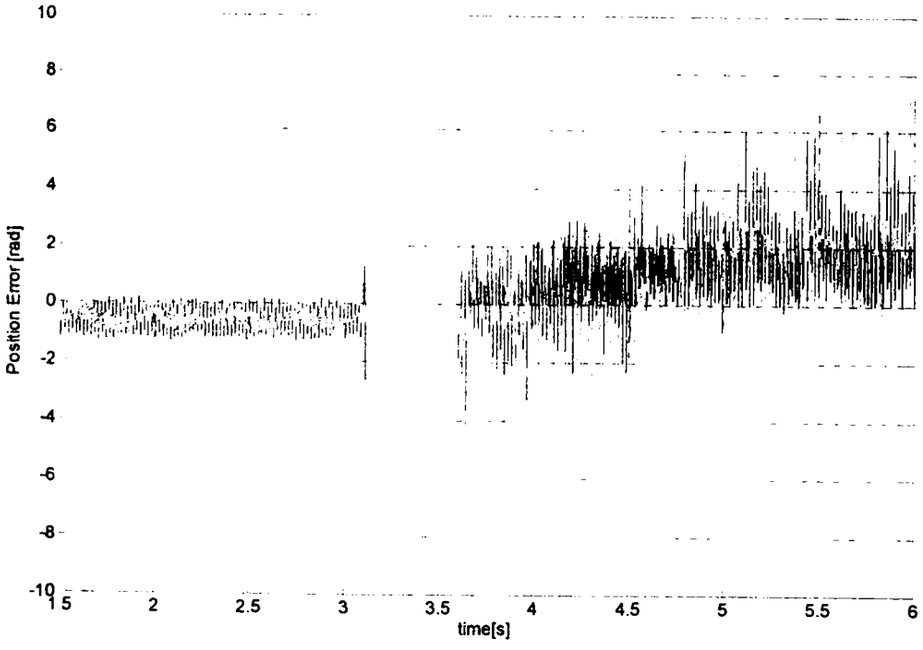

b)

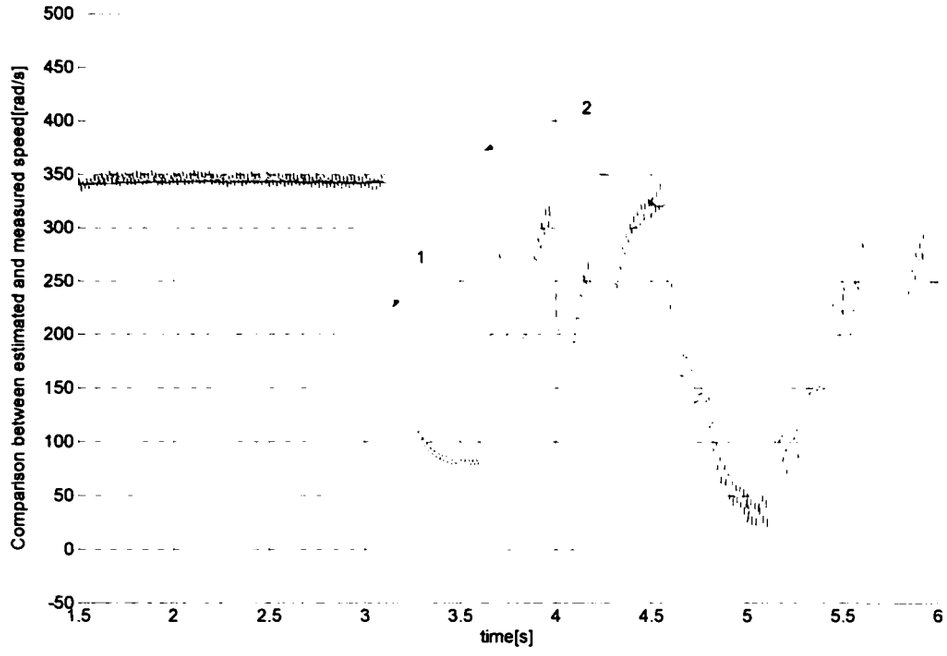

c)

Figure 3.10 The estimated (1) and measured (2) rotor position a), the error in rotor position estimation b) and the estimated (1) and measured (2) speed c) without considering the saturation in the estimators.

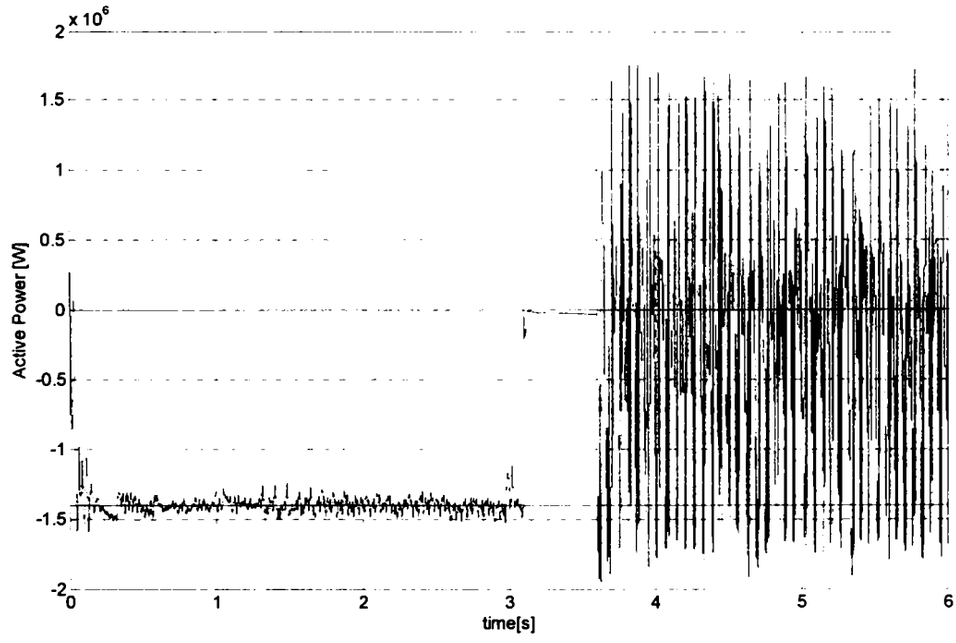

Figure 3.11 The active power without considering the saturation in the estimators.

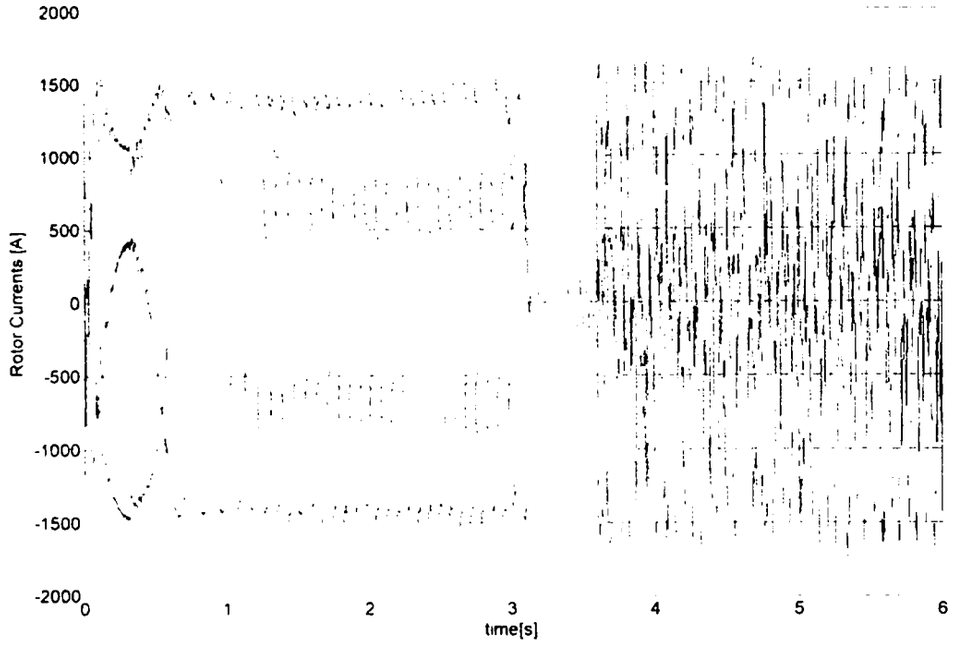

Figure 3.12 The rotor currents without considering the saturation in the estimators.

Also the control is irreversibly lost. For the same transient the control failure in power and rotor current (with constant L_m) is further illustrated in Figures 3.11 and 3.12.

This is a conclusive evidence that magnetic saturation is a must in the motion observer for successful robust control even during grid faults.

Conclusion

Position sensorless control is a very desirable feature for the DFIG for wind or hydro-power applications.

A motion state estimator was implemented, and it was described and discussed along this chapter. The taking into account of the magnetic saturation (or knowing the accurate value of the magnetizing inductance L_m) is shown mandatory, especially during the transients.

References

[1] Ion Boldea, "Electric Drives", Chapter 14: Large Power Drives, 14.8 Sub and Hypersynchronous IM cascade drives, CRC Press Florida, ISBN: 0849325218, 1998.

[2] Florin Iov and all, "Wind Turbine Blockset", A flexible platform for simulation and optimizing of the wind turbines, Project, Institute of Energy Technology, Aalborg, Denmark, Risø National Laboratory, Denmark.

[3] U. Rädel, D. Navarro, G. Berger, S. Berg, "Sensorless Field-Oriented Control of a Slipring Induction Generator for a 2.5 MW Wind Power Plant from Nordex Energy GmbH", EPE 2001 Conference Proceedings, Graz.

[4] S. Müller, M. Deicke, R. W. De Doncker, "Adjustable speed generators for wind turbines based on double-fed induction machines and 4-quadrant IGBT converters linked to the rotor," *IEEE-IAS Annual Meeting, 2000*

[5] T. Senjyu, N. Sueyoshi, K. Uezato, H. Fujita, "Stability analysis of wind power generating system," *Power Conversion Conference, 2002. PCC Osaka 2002 Proceedings, vol. 3: 2002 pp. 1441 –1446.*

[6] R. Datta, V.T. Ranganathan, "A simple position-sensorless algorithm for rotor-side field-oriented control of wound-rotor induction machine," *IEEE Transactions on Industrial Electronics, vol. 48, no.4, August 2001.*

[7] I. Serban, I. Boldea, F. Blaabjerg, "Sensorless doubly-fed induction control under power system transients and faults: the influence of magnetic saturation", *Proceedings of OPTIM 2004, Poiana Brasov, Romania*

Chapter 4

Sensorless DFIM drive control and performance

Abstract

The present chapter deals with the wound rotor induction machine (DFIM) drive. The machine is fed in the rotor by 2 inverters connected back to back, both of them vector controlled. This is similar with the doubly-fed induction generator setup discussed in the previous chapters, but with the difference the stator is short-circuited instead of being connected to the power grid. This operation mode is required for self (or assist) starting in pump storage and wind generator applications.

The inverters used are commercial. They share the same DC bus and one is connected with the output on the power grid (through an inductance), and the other with the output on the rotor of the DFIM.

Different kinds of tests were performed. Two combined flux observers were investigated and compared, one with the voltage model in parallel with the current model and one with both models connected in series.

A sensorless strategy based on a MRAS (model reference adaptive system) was implemented and tested at low speeds.

The control strategies, the flux observers and the MRAS were developed in Matlab-Simulink® and implemented using a dSpace® DS1103 single-board control and acquisition interface. The schemes used are illustrated in the chapter, and the experimental results are shown and discussed.

4.1 Introduction

The setup presented is similar with the DFIG setup discussed in the previous papers. But, the machine will be most of the time here in motoring regime, and the stator is short-circuited. The rotor side is kept the same as in the wind generator cases. This way, a dual inverter regenerative drive is in discussion. Its usage for self or assist starting in pump-storage or wind generators is of main interest here.

The main components models in the DFIM system are described in what it follows. The electrical schematic of the whole system is shown in Figure 4.1.

For pre-charging the DC link capacitors, a 3×100Ω resistor was used (not illustrated here) between the grid and the L filter; the resistors were short-circuited after the voltage in the DC link did reach approx 500V.

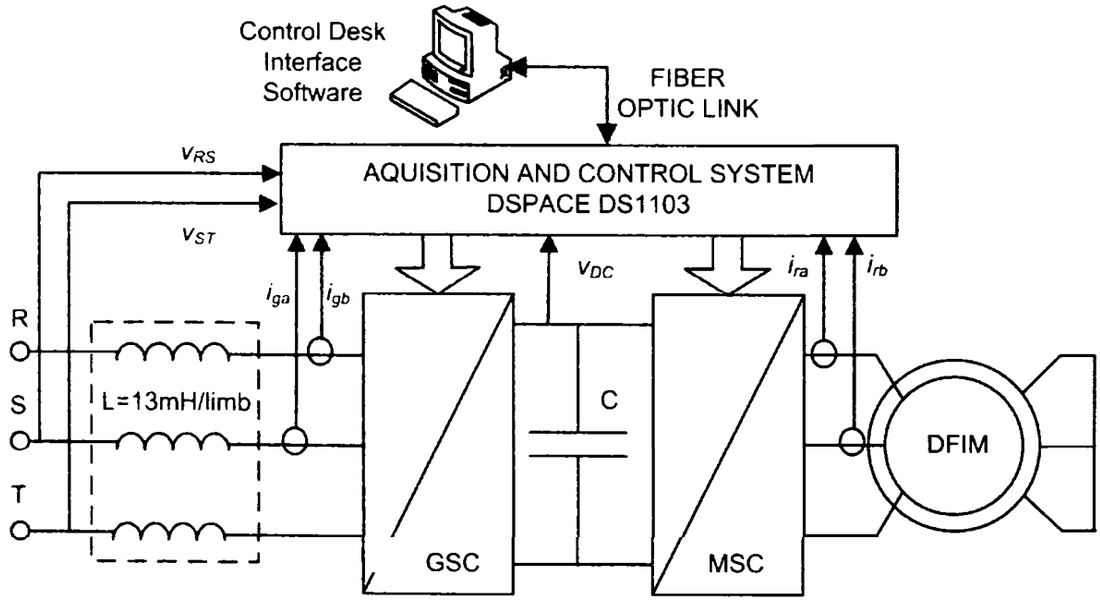

Figure 4.1 The DFIM drive system.

4.2 The DFIM drive system and its control

4.2.1 The motor

Stator and rotor voltages expressed in terms of d and q axes quantities rotating in an arbitrary reference frame with the speed ω_k are given by [1]:

$$\underline{v}_s = R_s \underline{i}_s + \frac{d\underline{\psi}_s}{dt} + j\omega_k \underline{\psi}_s \tag{4.1}$$

$$\underline{v}_r = R_r \underline{i}_r + \frac{d\underline{\psi}_r}{dt} + j(\omega_k - \omega_r)\underline{\psi}_r \tag{4.2}$$

where $\underline{v}_s$, $\underline{i}_s$, $\underline{\Psi}_s$ are the stator voltage, stator current and stator flux space vectors, $\underline{v}_r$, $\underline{i}_r$, $\underline{\Psi}_r$ are the rotor voltage, rotor current and rotor flux space vectors, R_s and R_r are the stator and rotor resistances, ω_k is the chosen coordinate system speed and ω_r is the rotor electrical speed.

Stator and rotor flux vectors, $\underline{\psi}_s$ and $\underline{\psi}_r$, expressed in terms of stator and rotor currents, $\underline{i}_s$ and $\underline{i}_r$, are:

$$\underline{\psi}_s = L_s \underline{i}_s + L_m \underline{i}_r \tag{4.3}$$

$$\underline{\psi}_r = L_r \underline{i}_r + L_m \underline{i}_s \tag{4.4}$$

The electromagnetic torque T_e is:

$$T_e = 1.5p(\psi_{sd} i_{sq} - \psi_{sq} i_{sd}) \tag{4.5}$$

The parameters for the motor are given in Chapter 6, which is fully dedicated to the experimental test rig.

As the original motor had a rated rotor voltage of 78V and a rated current of 23 A, a re-wounding of the rotor was made, in order to fit the converters ratings without inserting a transformer in the rotor circuit. The number of turns per coil was increased 5 times and the cross section of the conductor was decreased 5 times. Thus a rated stator voltage of 380 V was obtained together with a 5 times lower rated rotor current.

4.2.2 The grid-side converter and its control

The grid-side converter is used to control the DC link voltage regardless of the level and the direction of the rotor power (Figure 4.2). A vector-control strategy is used, with the reference frame oriented along the stator voltage [2]. The converter is current regulated with the direct axis current used to control the DC-link voltage; meanwhile the transverse axis current is used to regulate the displacement between the voltage and the current (and thus the power factor) [3].

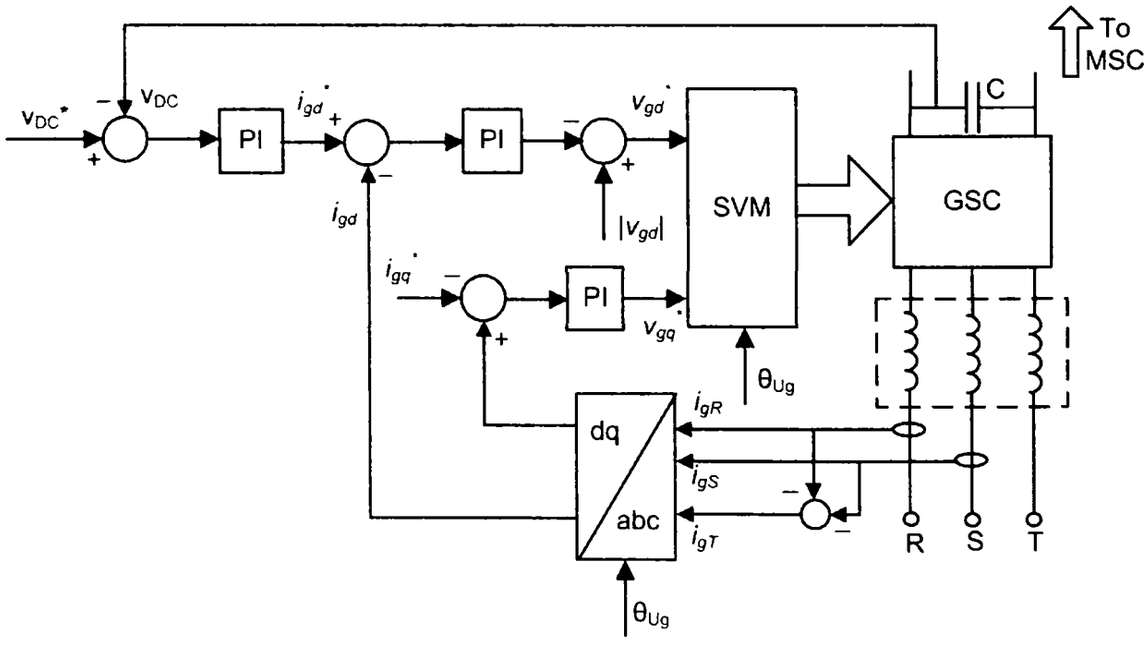

Figure 4.2 The grid-side converter control (GSC).

One of the most important tasks when connecting a power converter to the electrical grid is to make a fast and accurate measurement of the grid voltage phase angle in order to be able to control properly the power flow in or out of the power converter [4]. There are some methods well described in the literature. One of the simplest is zero crossing detection and in most cases this is sufficient, but will cause problems due to the switching noise and it is not precise when the grid is unbalanced [5]. Another method is to use a synchronous *dq*-reference PLL [6], synchronized with the input voltage frequency, but it still has problems when the grid is distorted. The angle produced will have harmonics, in that case. Filtering of the high-order harmonics is possible, but the low-order harmonics cannot be filtered, otherwise the bandwidth of the PLL will be too low.

Finally, one of the best methods is to split the three-phase system into positive, negative and zero sequence and to use only the positive sequence part of the signal for PLL [7]. But these methods will not be covered here. In the present case, a simplest method to get information on the grid voltage phase angle is used, due to its simplicity and due to the grid, which was without disturbances. This is briefly described in what it follows.

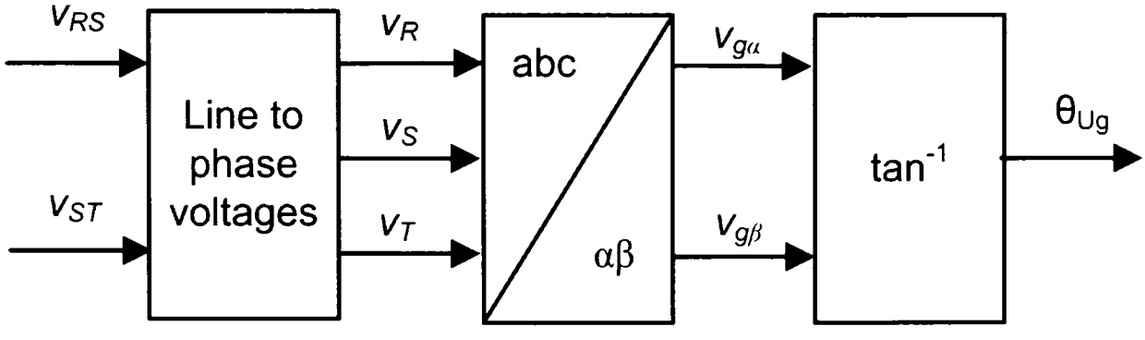

Figure 4.3 The computation of the grid voltage angle used for the coordinate transformations and for the SVM on the grid side converter control.

The line voltages are measured using two LEM LV 25-P voltage transducers with appropriate signal condition, thus at 500 V the output is 10 V, required for the A/D channels. The phase voltages are calculated from the line voltages (see Figure 4.3) and the $\alpha\beta$ components of the grid voltage are calculated from the phase voltages. Finally, the angle of the grid voltage is extracted [7]:

$$\theta_c = \tan^{-1}\frac{v_{s\beta}}{v_{s\alpha}} \tag{4.6}$$

A third LEM LV 25-P is used to measure the DC voltage with the same signal-conditioning interface. The grid currents are measured using two LA 55-P current transducers interfaced such that at 10A output will be 10V. The third grid current is calculated from the two measured, taking into account that the sum of all three currents is always zero.

Between grid converter and the grid itself a line filter was introduced to protect the inverter and to reduce the higher harmonic content in the line current, produced by the switching. This is in fact a simple *L*-filter. An *LC* or an *LCL* filter could be used, but the *L*-filter was chosen for simplicity. The frequency response of the *LCL* filter has a resonance peak, so the latter has to be designed such that the resonance peak not to interfere with the frequency response of the inverter output voltage; alternatively, a series resistor must be inserted to damp the resonance peak. The value for the inductance per limb was chosen 13 mH, but a rather good design value for the inductance in the filter is [4]:

$$L = \max\left(\frac{V_\vartheta}{\vartheta\omega_1 I_\vartheta}\right) \tag{4.7}$$

where ϑ is the order of the harmonic and V_ϑ the phase RMS value of the output phase voltage harmonic.

The design of the PI current controllers follows from the transfer function of the plant (in this case the line filter itself). The controllers produce the reference grid voltage vector $v_g^* = v_{gd}^* + jv_{gq}^*$:

$$v_{gd}^* = -\left(K_{Pig} + \frac{K_{Iig}}{s}\right)e_{igd} + |v_{gd}| \tag{4.8}$$

$$v_{gq}^{*} = -\left(K_{Pig} + \frac{K_{Iig}}{s} \right) e_{igq} \tag{4.9}$$

where K_{Pig} and K_{Iig} are the PI controllers gains and e_{igd} and e_{igq} are the errors of the grid currents i_{gd} and i_{gq} respectively.

Applying as design constraints a damping ratio of 0.7 and a closed-loop natural frequency of 125 Hz, the gains of the controllers results:

$$K_{Pig} = 30$$

$$K_{Iig} = 1000$$

The design for the DC-link voltage controller may be carried out assuming the inner current loop is ideal and knowing the value of the DC link capacitor (in our case 470 μF).

The controller produces the reference d-axis grid current i_{gd}^{*}:

$$i_{gd}^{*} = \left(K_{PVDC} + \frac{K_{IVDC}}{s} \right) e_{VDC} \tag{4.10}$$

where K_{PVDC} and K_{IVDC} are the PI controller gains and e_{VDC} is the error of the DC voltage v_{DC}.

Thus the controller gains yields:

$$K_{PVDC} = 0.1$$

$$K_{IVDC} = 0.3.$$

This is 10 times slower than the inner current loop.

4.2.3 The machine side converter and its control

The generator is controlled in a synchronously rotating *dq*-frame, with the d-axis aligned with the stator-flux vector position, which ensures a decoupled control between the electromagnetic torque and the rotor excitation contribution [8] (see Figure 4).

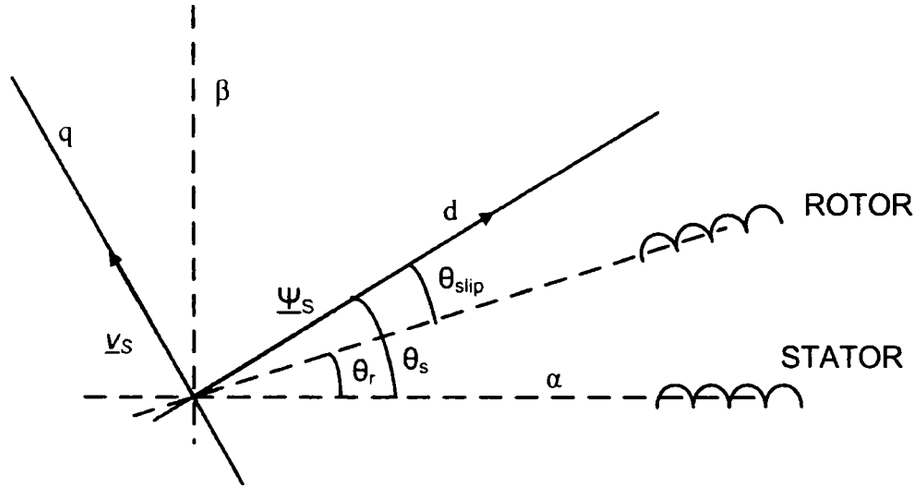

Figure 4.4 Location of vectors in stationary coordinates.

The control strategy is shown in Figure 4.5.

As it can be seen, two rotor currents and two stator currents are measured, and the third current in each case is calculated taking into account that always the sum of the currents is zero. The sensors are also type LEM LA 55-P.

The rotor currents are measured in their coordinates (rotor coordinates) and transformed into synchronous coordinates using the angle:

$$\hat{\theta}_{slip} = \hat{\theta}_s - \hat{\theta}_r \tag{4.11}$$

where $\hat{\theta}_s$ is the stator flux angle, and $\hat{\theta}_r$ the rotor position [9, 10].

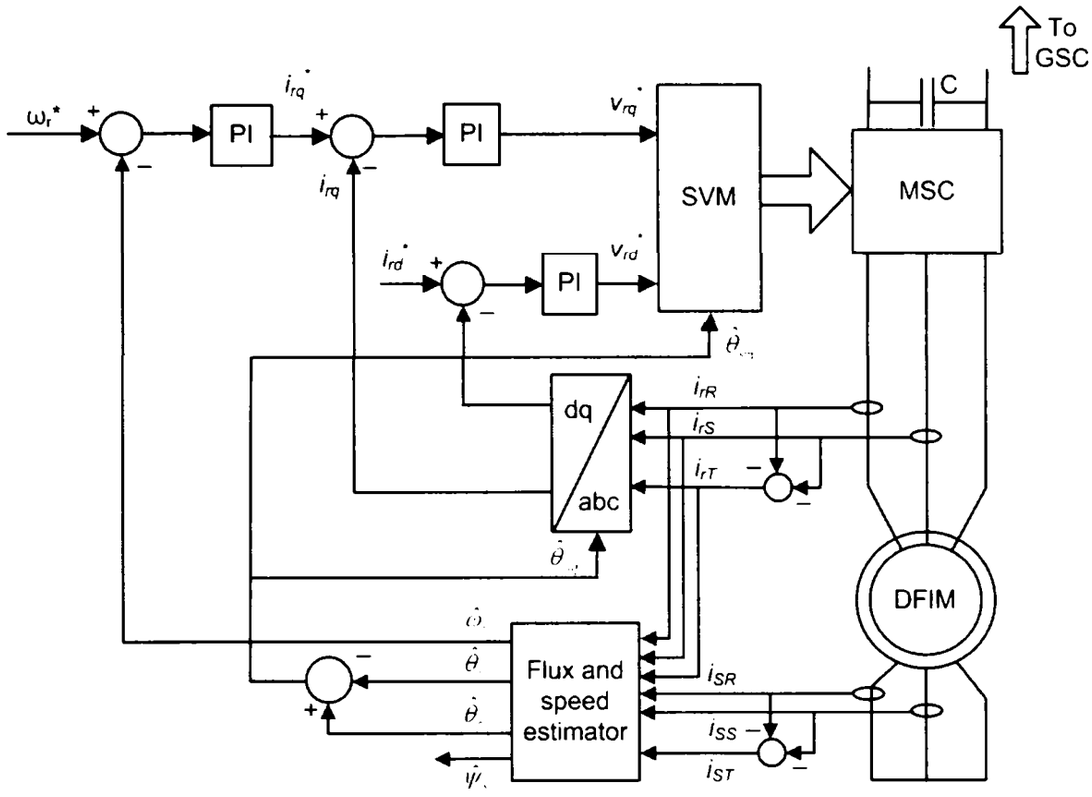

Figure 4.5 The machine-side converter control (MSC).

Reference voltages generated by the current control loops are transformed back to the rotor reference frame, using the same angle $\hat{\theta}_{slip}$. Standard space vector modulation is employed to generate the pulses for the inverter.

The current controllers are designed using the same strategy as in the case of the current controllers for the grid-side inverter. The controllers produce the reference rotor voltage vector $v_r^* = v_{rd}^* + jv_{rq}^*$:

$$v_{rd}^* = \left(K_{Pir} + \frac{K_{Iir}}{s} \right) e_{ird} \tag{4.12}$$

$$v_{rq}^* = \left(K_{Pir} + \frac{K_{Iir}}{s} \right) e_{irq} \tag{4.13}$$

where K_{Pir} and K_{Iir} are the PI controllers gains and e_{ird} and e_{irq} are the errors of the rotor currents i_{rd} and i_{rq} respectively.

The gains of the rotor current controllers thus results:

$$K_{Pir} = 40$$

$$K_{Iir} = 1500$$

The design for the speed controller may be carried out assuming again that the inner current loop is ideal. The controller produces the reference q-axis grid current i_{gd}^{*}:

$$i_{rq}^{*} = \left(K_{P\omega} + \frac{K_{I\omega}}{s} \right) e_{\omega} \tag{4.14}$$

where $K_{P\omega}$ and $K_{I\omega}$ are the PI controller gains and e_{ω} is the error of therotor speed.

Thus the controller gains yields:

$$K_{P\omega} = 0.1$$

$$K_{I\omega} = 0.3$$

This is almost 30 times slower than the inner current loop.

4.3 Flux and rotor speed position estimation

4.3.1 The stator flux estimation

As it was already stated two flux estimators were developed and used during the tests. Both of them are based on the voltage and the current stator flux models.

The estimator using the voltage and current models connected in parallel is illustrated in Figure 4.6. Estimated stator flux, as produced by the voltage model, is:

$$\hat{\psi}_{s\alpha\beta} = \int (v_{s\alpha\beta} - R_s i_{s\alpha\beta} + v_{comp\alpha\beta})dt \tag{4.15}$$

where $v_{s\alpha\beta} = 0$ in this case (the stator is short-circuited). Thus this model is supposed to be inaccurate, as any error in R_s is causing errors in the estimated stator flux.

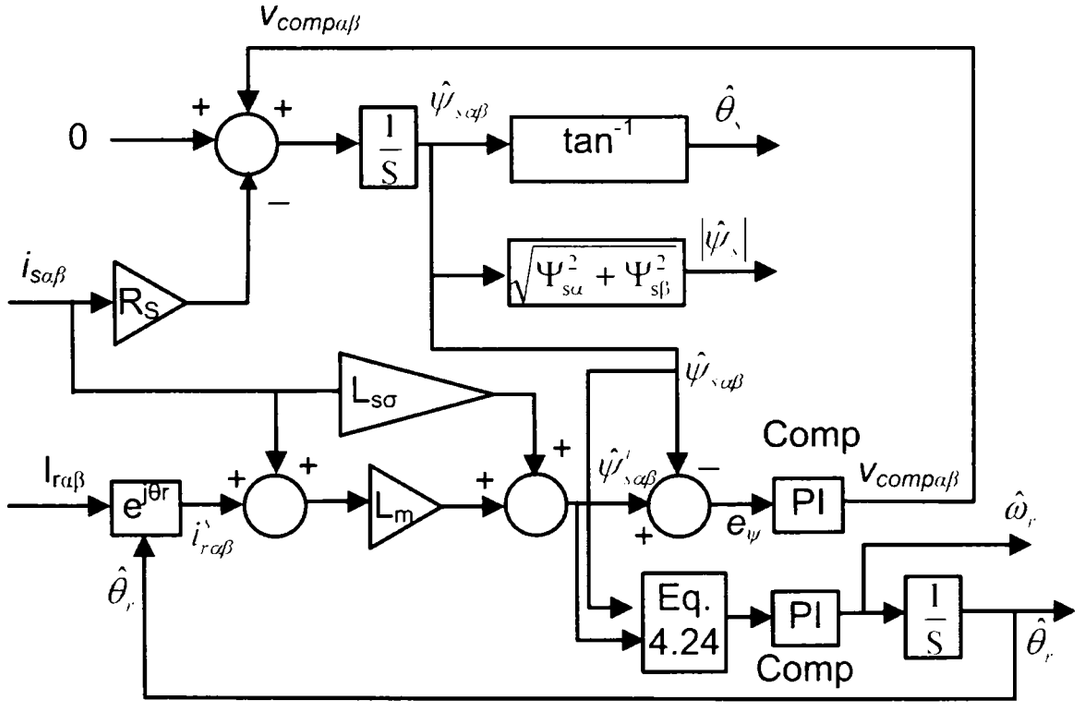

Figure 4.6 The flux estimator with parallel voltage and current models, and the rotor speed-position estimator MRAS.

The current model is based on (4.3):

$$\hat{\psi}'_{s\alpha\beta} = L_{s\sigma} i_{s\alpha\beta} + L_m (i_{s\alpha\beta} + i'_{r\alpha\beta}) \tag{4.16}$$

The rotor current is measured, but a transformation to stator coordinates is needed, using the estimated rotor position $\hat{\theta}_r$.

The flux error between the voltage model (4.15) and the current model (4.16) is passed through a PI controller, with K_{pcomp} = 10 and K_{icomp} = 10, which outputs a correction signal used to compensate the voltage model (see Figure 4.6):

$$v_{comp\alpha\beta} = \left(K_{Pcomp} + \frac{K_{Icomp}}{s} \right) e_{\psi} \tag{4.17}$$

where:

$$e_{\psi} = \hat{\psi}'_{s\alpha\beta} - \hat{\psi}_{s\alpha\beta} \tag{4.18}$$

This way the dc-offset drift of the ideal integrator (15) is eliminated. The PI compensator selects the current model at low speeds, while the voltage model prevails at medium and high speeds. Thus, the corrected stator flux vector is $\hat{\psi}_{s\alpha\beta}$ as given by (4.15). For comparison purposes only the stator flux obtained only from the current model, $\hat{\psi}'_{s\alpha\beta}$, was also considered.

The angle θ_s is obtained from the resultant stator flux components [11]:

$$\hat{\theta}_s = \tan^{-1} \frac{\hat{\psi}_{s\beta}}{\hat{\psi}_{s\alpha}} \tag{4.19}$$

Differences were noticed between the stator flux $\hat{\psi}_{s\alpha\beta}$ obtained from the compensated voltage model (4.15) and the stator flux $\hat{\psi}'_{s\alpha\beta}$ obtained from the current

model only (4.16). This was mainly due to parameter mismatch between the model and the real machine. To have one more view of this problem, another flux estimator was developed. This is an estimator that employs the voltage and the current models connected in series, as shown in Figure 4.7.

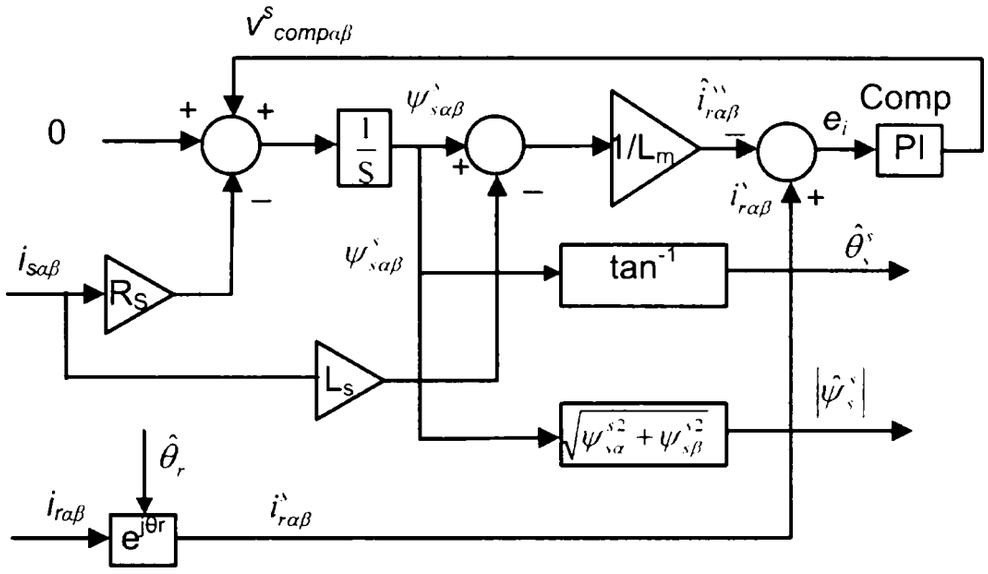

Figure 4.7 The alternative flux estimator with the voltage and current models connected in series.

It is basically relying on the same equations, but the current model is written such that the stator flux obtained from the voltage model is now used to estimate the rotor current in stator coordinates:

$$\hat{i}^s_{r\alpha\beta} = \frac{1}{L_m}\left(\hat{\psi}^s_{s\alpha\beta} - L_s i_{s\alpha\beta}\right) \tag{4.20}$$

where estimated stator flux is now:

$$\hat{\psi}^s_{s\alpha\beta} = \int\left(v_{s\alpha\beta} - R_s i_{s\alpha\beta} + v^s_{comp\alpha\beta}\right) \tag{4.21}$$

The rotor current is measured and transformed into stator coordinates using the estimated rotor position θ_r. The rotor-current error between the measured and estimated (4.20) rotor current is passed through a PI controller, with the same parameters as for the one in Figure 4.6, and its output is used to compensate the voltage model (Figure 4.7):

$$v'_{comp\alpha\beta} = \left(K_{Pcomp} + \frac{K_{Icomp}}{s} \right) e_i \tag{4.22}$$

where:

$$e_i = i'_{r\alpha\beta} - \hat{i}'^{ss}_{r\alpha\beta} \tag{4.23}$$

4.3.2 The rotor speed-position estimation

A speed-position estimator is developed based on MRAS (model reference adaptive system) algorithm. It is chosen for this purpose, due to its relative simplicity and proven efficiency over an extended speed range. There is quite simple to develop such a method because the flux estimator with parallel voltage and current models (Figure 4.6) offer $\alpha\beta$ components of the flux vectors obtained from both models [12].

The MRAS flux position error ε was calculated from the phases of the two flux estimations (4.24). The voltage model $\hat{\psi}_{s\alpha\beta}$ is the reference model, while the current model $\hat{\psi}'_{s\alpha\beta}$ is the adaptive model with the rotor position $\hat{\theta}_r$ as adaptive parameter.

$$\varepsilon = -\psi_{s\alpha}\psi'_{s\beta} + \psi'_{s\alpha}\psi_{s\beta} \tag{4.24}$$

This error is used to extract the rotor speed and position using a phase-locked loop (PLL) technique (Figure 4.6). The output of the PI compensator gives the estimated rotor speed ω_r, and after the integration, the estimated rotor position θ_r is obtained:

$$\hat{\omega}_r = \left(K'_{Pcomp} + \frac{K'_{Icomp}}{s} \right) \varepsilon \; ; \; \hat{\theta}_r = \int \hat{\omega}_r dt \tag{4.25}$$

Optimum parameters of the PI compensator were searched as a compromise between the speed of the PLL, especially during transients, and the level of oscillations in speed estimation, especially at low speeds.

The best parameters, seem to be: $K'_{Pcomp} = 100$, and $T_I = 5$ms (time constant of the compensator, $T_I = K'_{Pcomp} / K'_{Icomp}$).

Overall, this scheme has shown good accuracy over the whole speed range.

4.4 The test rig and experimental results

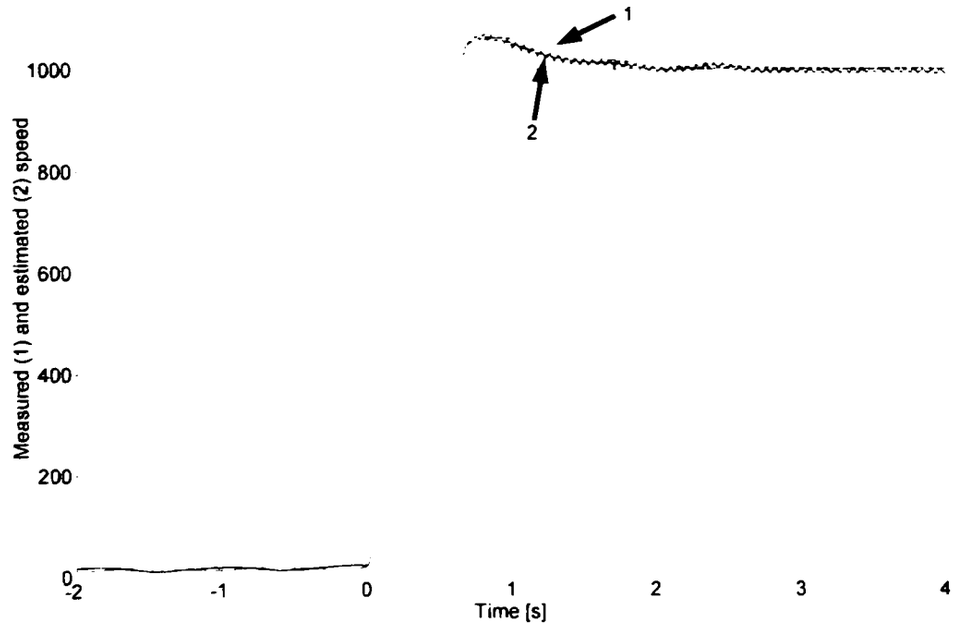

Figure 4.8 1) Estimated speed, and 2) measured speed at step speed from 15 rpm to 1000 rpm.

First, a speed response is shown at a step in reference speed from 15 to 1000 rpm. In Figure 4.8, the estimated speed 1), and the measured speed 2) are illustrated. The speed was measured for comparison using a Telemecanique - 5000 pulses encoder.

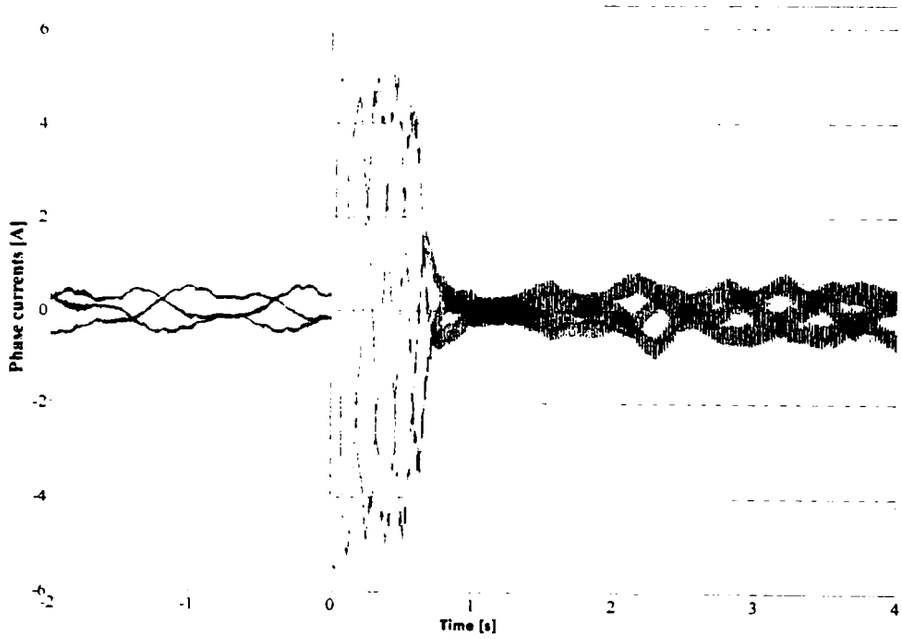

Figure 4.9 Phase stator currents at step speed from 15 rpm to 1000 rpm.

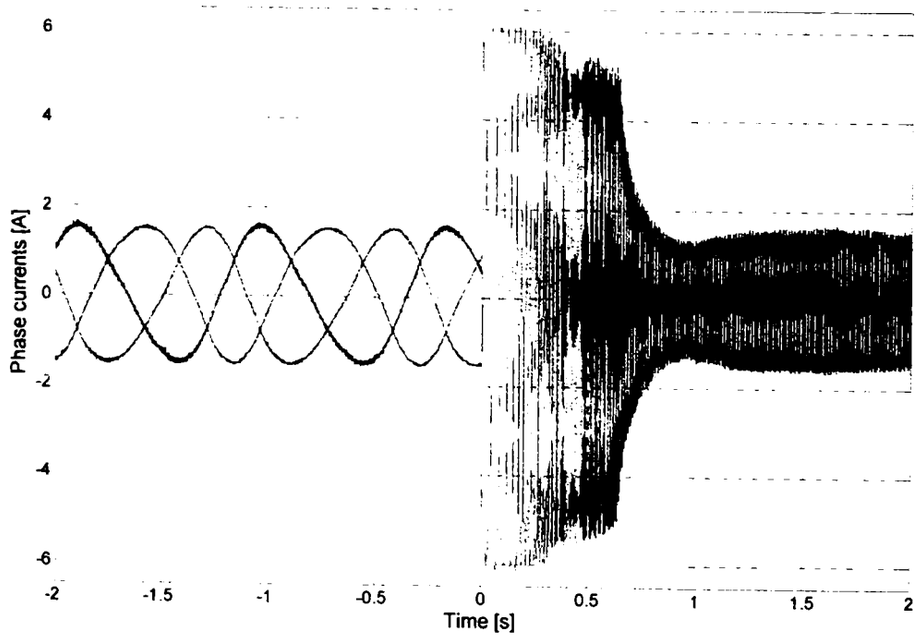

Figure 4.10 Phase rotor currents at step speed from 15 rpm to 1000 rpm.

For the same experiment, the stator phase currents are shown in Figure 4.9, and the rotor phase currents are shown in Figure 4.10

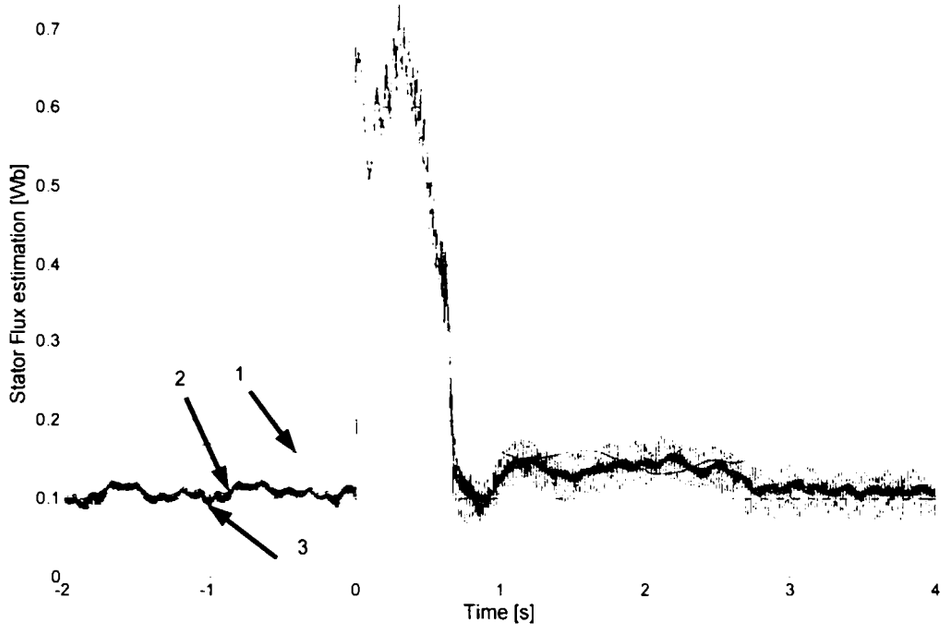

Figure 4.11 Stator flux estimation at step speed from 15 rpm to 1000 rpm: 1) parallel estimator, 2) series estimator, 3) parallel estimator, current model.

The estimated stator flux is illustrated in Figure 4.11 for the same step in reference speed from 15 to 1000 rpm.

Both estimations from the parallel estimator are shown: voltage compensated model 1), and current model 3); also, the estimation from the series estimator 2). It seems that the current model from the parallel estimator is quite the same with the series model, but the parallel estimator (voltage compensated model) has unrecoverable errors.

In Figure 4.12, also speed transients are shown, but from 500 to -500 rpm (reversal). The estimated rotor speed 1), and measured rotor speed 2) with the encoder are illustrated.

In Figure 4.13, the reference DC link voltage 1), and the measured DC link voltage 2) at the speed reversal from 500 to -500 rpm are shown.

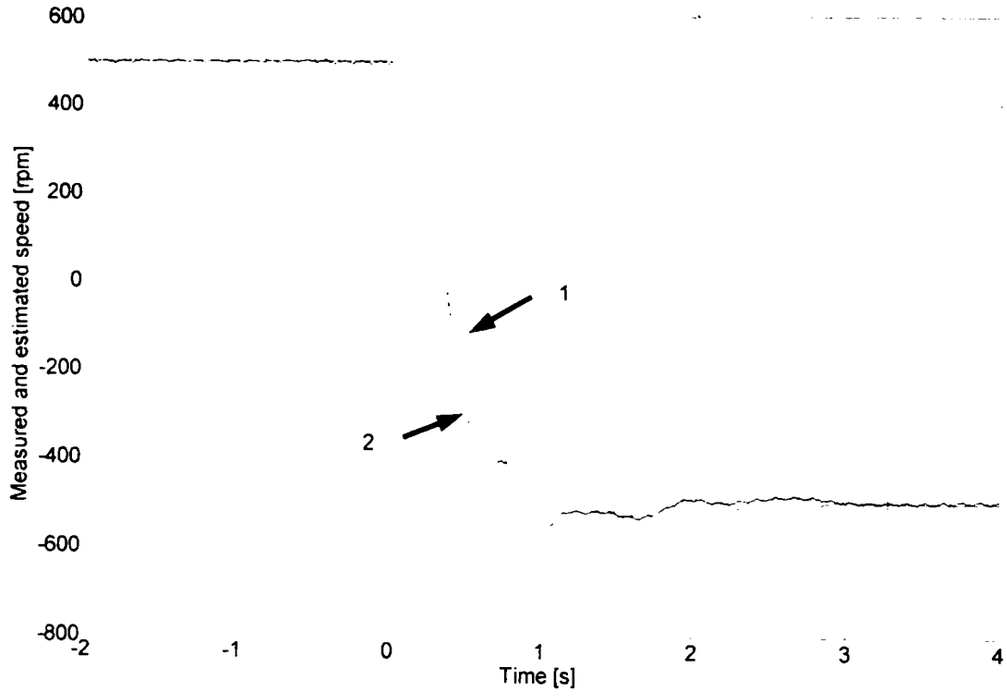

Figure 4.12 1) Estimated speed, and 2) measured speed at step speed from 500 rpm to -500 rpm.

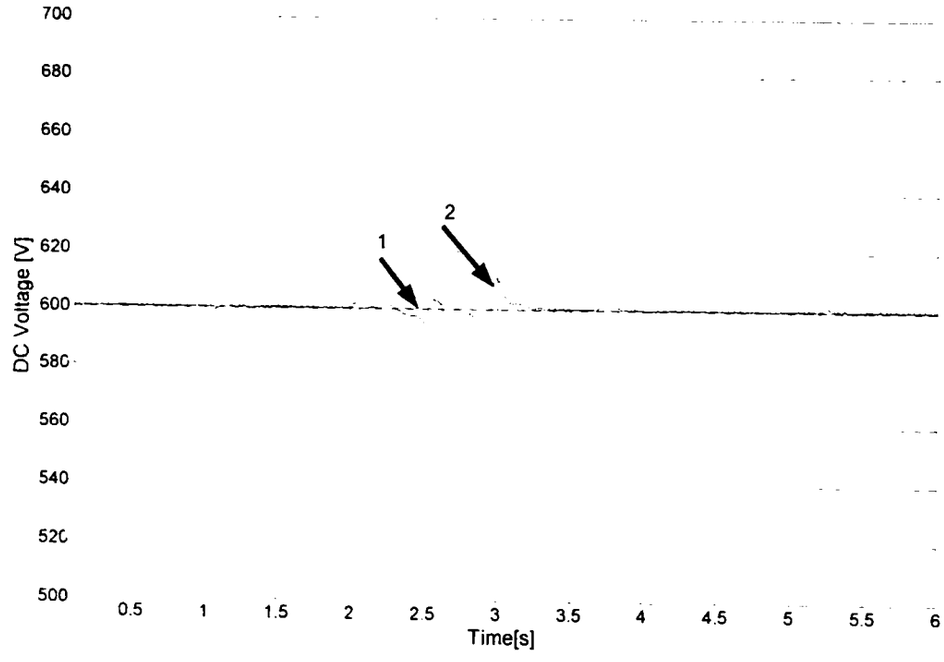

Figure 4.13 1) Reference DC voltage, and 2) measured DC voltage at step speed from 500 rpm to -500 rpm.

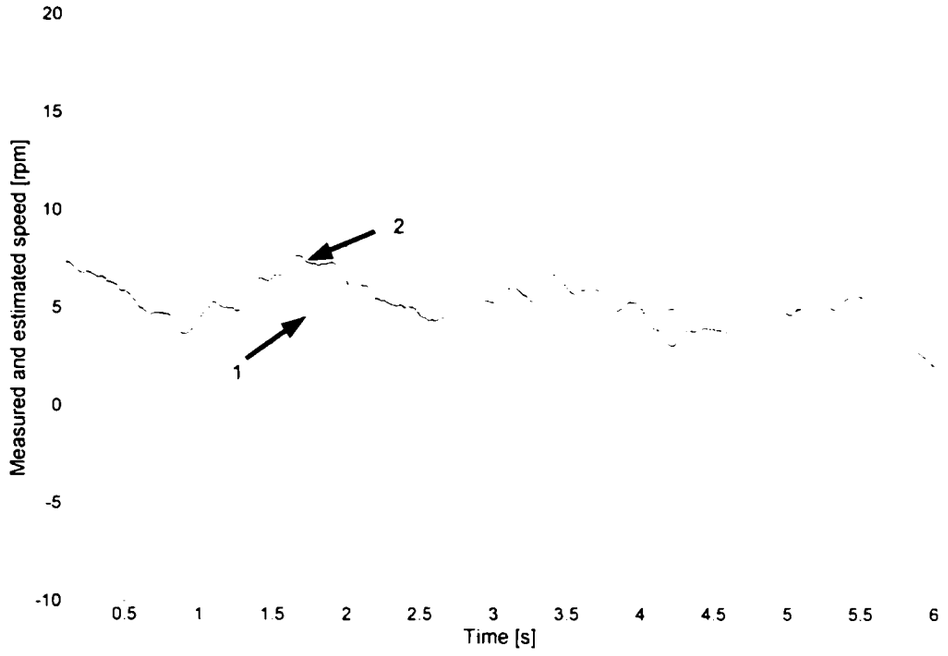

Figure 4.14 1) Estimated speed, and 2) measured speed at 5 rpm.

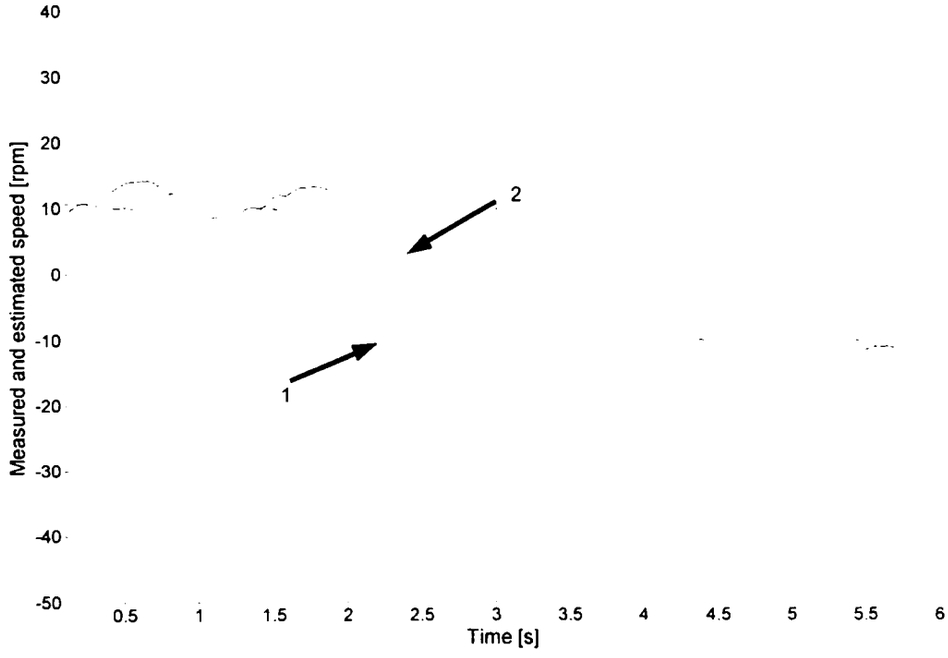

Figure 4.15 1) Estimated speed, and 2) measured speed at step speed from 10 rpm to -10 rpm.

The speed estimator was tested at low and very low speeds. Its behavior is satisfactory up to 5 rpm. In Figure 4.14. the steady state speeds at 5 rpm are shown.

The estimated speed (1) and the measured speed (2) with the encoder are illustrated.

The estimated speed is better than the measured at 5 rpm due to the limited number of the lines of the encoder. which became insufficient at this speed.

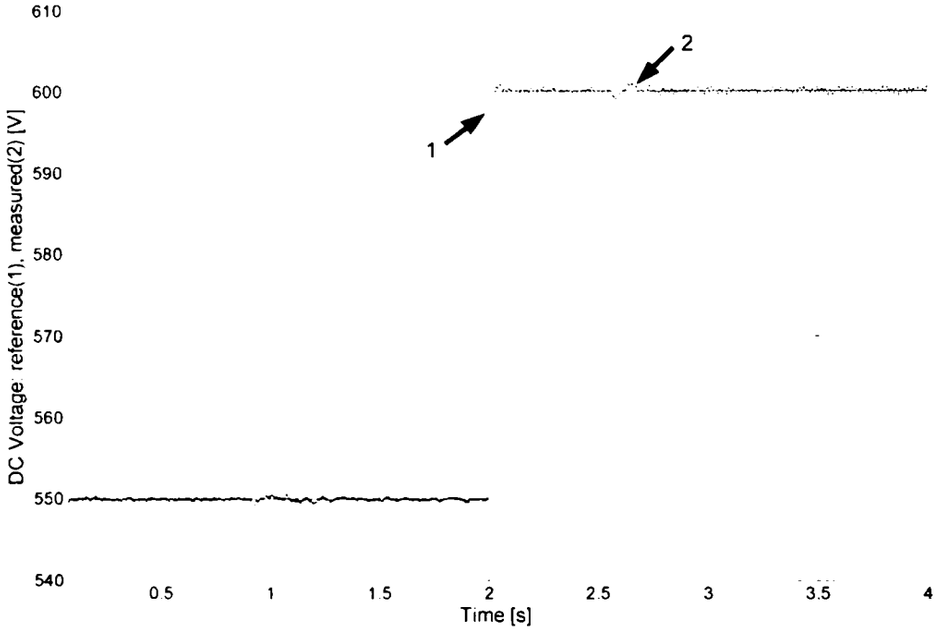

Figure 4.16 1) Reference DC voltage, and 2) measured DC voltage at step DC voltage from 550 V to 600 V.

A transient at low speed is shown in Figure 4.15, from 10 rpm to -10rpm. The estimated rotor speed 1), and measured rotor speed 2) with the encoder are presented. The behavior of the estimator is also very good, still better than the encoder.

For testing the control of the grid-side converter, some experiments have been made. In Figure 4.17, a step in reference of DC voltage from 550 to 600 V is shown. The reference DC voltage 1), and the measured DC voltage 2) are illustrated. Very fast and accurate response in DC voltage is proved.

Conclusion

The motion-sensorless DFIM driving control from rotor with short-circuited stator, with two back-to-back inverters connected in the rotor circuit of the machine, was presented in this chapter. Both inverters are vector controlled; the machine-side converter controls the speed and the reactive rotor current, the grid-side converter controls the DC voltage, regardless of the level and the direction of the rotor power, and the reactive current drawn from the grid. The results of the tests were illustrated and discussed. Rather fast responses of the drive during fast reference speed transients were shown. The drive has higher braking capabilities due to the grid-side inverter and its control. That is, fast injecting the power back to the grid during braking periods is obtained.

Two stator flux observers were developed and compared. Both are based on the voltage and on the current models, but one is using them in parallel and one in series. The topologies and the results are also illustrated and discussed.

A motion sensorless control method, with speed estimation based on a MRAS algorithm from flux stator was implemented, tested and described in the present chapter. The results are also shown. Also, at fast transients the speed estimation is fast and precise. The behavior of the position and speed estimator is satisfactory down to 5 rpm.

References

[1] I. Boldea, S.A. Nasar, "Electric Drives," Chapter 14: "Large power drives, 14.8 Sub and hypersynchronous IM cascade drives," CRC Press, Florida, 1999.

[2] R. Datta, V.T. Ranganathan, "Direct power control of grid-connected wound rotor induction machine without rotor position sensors," *IEEE Transactions on Power Electronics*, vol. 16, no. 3, May 2001, pp. 390-399.

[3] L. Morel, H. Godfroid, A. Mirzaian, J.M. Kauffmann, "Double-fed induction machine: converter optimization and field oriented control without position sensor," *IEE Proc. on Electric Power Applications*, vol. 145, no. 4, July 1998, pp. 360-368.

[4] Morten Lindholm, "Doubly-Fed Drives for Variable Speed Wind Turbines," *Ph.D. Thesis*, Technical University of Denmark,

[5] S.-J. Lee, J.-K. Kang, S.-K. Sul, "A new phase detecting method for power conversion systems considering distorted conditions in power system," *1999 IEEE-IAS Annual Meeting Conf. Record*, vol. 4, pp. 2167-2172, 1999.

[6] V. Kaura, V. Blasko, "Operation of a phase locked loop system under distorted utility conditions," *IEEE Transactions on Industry Applications*, vol. 33, no.1, Jan./Feb. 1997, pp. 58-63.

[7] I. Serban, F. Blaabjerg, I. Boldea, Z. Chen, "A study of the doubly-fed wind power generator under power grid faults," *Proc. of EPE 2003*, Toulouse, France, 2003.

[8] U. Radel, D. Navarro, G. Berger, S. Berg, "Sensorless field-oriented control of a slipring induction generator for a 2.5 MW wind power plant from Nordex Energy GmbH," *Proc. of EPE 2001*, Graz, 2001.

[9] S. Muller, M. Deicke, R.W. De Doncker, "Adjustable speed generators for wind turbines based on double-fed induction machines and 4-quadrant IGBT converters linked to the rotor," *2000 IEEE-IAS Annual Meeting Conf. Record*, vol. 4, pp. 2249-2254, Oct. 2000.

[10] T. Senjyu, N. Sueyoshi, K. Uezato, H. Fujita, "Stability analysis of wind power generating system," *Proc. of Power Conversion Conf. PCC 2002*, Osaka, vol. 3, pp. 1441-1446, April 2002.

[11] R. Datta, V.T. Ranganathan, "A simple position-sensorless algorithm for rotor-side field-oriented control of wound-rotor induction machine," *IEEE Transactions on Industrial Electronics*, vol. 48, no. 4, Aug. 2001, pp. 786-793.

[12] G.D. Andreescu, "Position and speed sensorless control of PMSM drives based on adaptive observer," *Proc. of EPE'99*, Lausanne, Switzerland, Aug. 1999.

Chapter 5

New state observers and sensorless behavior of DFIG at power grid with experimental characterization

Abstract

In this chapter the complete experimental characterization of the DFIG system is performed. The system includes the DFIG itself, the back-to-back inverters connected to the rotor circuit sharing the same DC link, the line filter and the acquisition and control system dSpace DS1103 with its interface.

Two different stator flux observer topologies were investigated and compared, one with the voltage model in parallel with the current model and the other one with both models connected in series. A speed estimation strategy, which also works also during the synchronization procedure, was implemented and tested. It is based on model reference adaptive system (MRAS) principles.

All control strategies, the flux observers and the MRAS, were developed in Matlab-Simulink® and implemented using a dSpace® DS1103 single-board control and acquisition interface. Different tests were performed, and sample results are presented and discussed in this chapter. The schemes used are illustrated in the chapter, and the experimental results are shown and analyzed.

5.1 Introduction

All what it follows is based on a 3kW DFIG setup, which was developed and implemented by the author, as the main central work at the present thesis.

First the main aspects of the wind power and control are discussed. The whole 3kW setup is described in Section 5.3, and the totally new issues (state observers and rotor position-speed estimators) are detailed in Section 5.4. Being entirely an

experimental work, a lot of experimental results are presented and discussed in Section 5.5.

5.2 Wind power and control principle

The mechanical power produced by the wind turbine, P_M, is given by [1]:

$$P_M = \frac{1}{2} \cdot \rho_{air} \cdot C_p(\lambda, \beta) \cdot \pi \cdot R^2 \cdot V^3 \tag{5.1}$$

where C_p – power efficiency coefficient of blade: V – wind velocity; β - pitch angle; R – blade radius; ρ_{air} – air density (1.225 kg/m^3)

Applying the tip speed ratio λ:

$$\lambda = \frac{\omega_m \cdot R}{V} \tag{5.2}$$

where ω_m is the turbine mechanical speed, equation (5.1) becomes the optimal mechanical power:

$$P_M^{opt} = \frac{1}{2} \cdot \rho_{air} \cdot \pi \cdot R^5 \cdot \frac{C_p^{opt}}{\lambda_{opt}^3} \cdot \omega_m^3 = K_w \cdot \omega_m^3 \tag{5.3}$$

where K_w is the wind turbine dependent coefficient.

Commercial wind turbines are designed to extract the maximum power at a given wind speed, as given by equation (5.3). Figure 5.1 shows the normalized electrical power versus normalized rotor speed at various wind velocities.

When the turbine reaches the nominal power, the pitch control system starts to turn the blades slightly out of the wind, and thus the power is limited. Conversely, the blades are turned back into the wind when the power output drops [2].

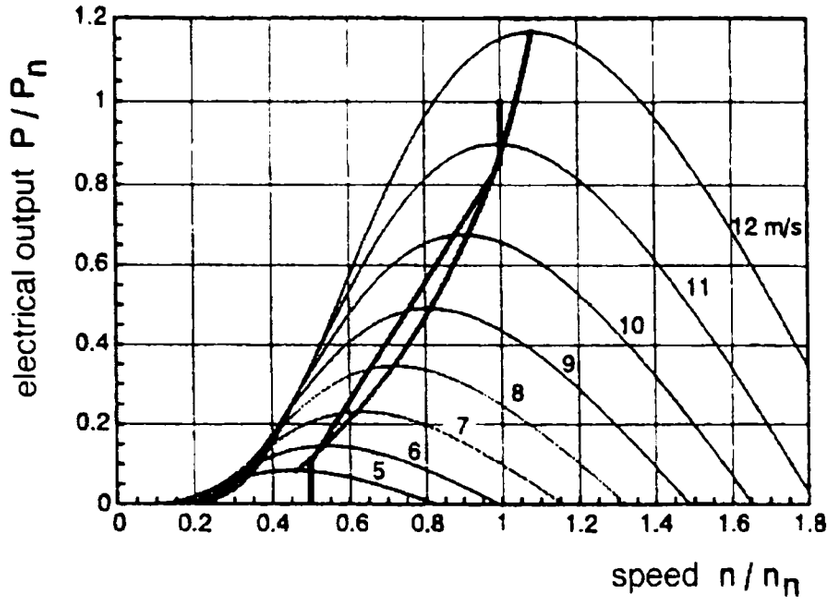

Figure 5.1 Electrical power versus rotor speed at different wind speeds.

5.3 DFIG experimental system and its control

The main components models in the DFIG system are described in what follows. Electrical block-diagram of the whole system is shown in Figure 5.2.

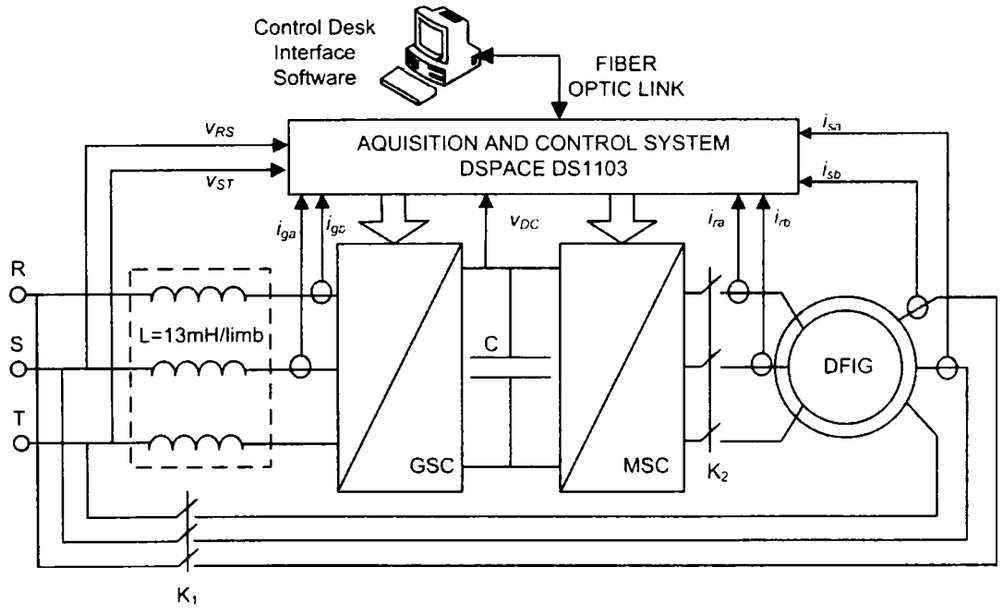

Figure 5.2 The DFIG system and its control.

For the DC link capacitors pre-charging, a resistor was used (not illustrated here) between the grid and the line filter; the resistors were short-circuited after the voltage in the DC link reached approx. 500 V. Also in the rotor circuit, in parallel with the K_2 switch, three lamps were inserted, as a visual indicator for the synchronization condition. In this way, K_2 could be switched on when the lamps are off. The DFIG-to-grid synchronization procedure is described in Paragraph 5.5.

For driving the DFIG, a 3 kW/ 1475 rpm induction motor is used. The motor was supplied with a 4.3 kVA Danfoss VLT5004 commercial voltage source inverter with the original interface for constant speed control mode. In this way, the variable wind speed could be easily simulated.

5.3.1 The generator

DFIG mathematical model in the arbitrary reference frame rotating at speed ω_k are

$$\underline{v}_s = R_s \underline{i}_s + \frac{d\underline{\psi}_s}{dt} + j\omega_k \underline{\psi}_s \tag{5.4}$$

$$\underline{v}_r = R_r \underline{i}_r + \frac{d\underline{\psi}_r}{dt} + j(\omega_k - \omega_r)\underline{\psi}_r \tag{5.5}$$

where $\underline{v}_s$, $\underline{i}_s$, $\underline{\Psi}_s$ are the stator voltage, stator current and stator flux space vectors, $\underline{v}_r$, $\underline{i}_r$, $\underline{\Psi}_r$ are the rotor voltage, rotor current and rotor flux space vectors, R_s and R_r are the stator and rotor resistances, ω_k is the chosen coordinate system speed and ω_r is the rotor electrical speed.

Stator and rotor flux vectors, $\underline{\psi}_s$ and $\underline{\psi}_r$, expressed in terms of stator and rotor currents, $\underline{i}_s$ and $\underline{i}_r$, are:

$$\underline{\psi}_s = L_s \underline{i}_s + L_m \underline{i}_r \tag{5.6}$$

$$\underline{\psi}_r = L_r \underline{i}_r + L_m \underline{i}_s \tag{5.7}$$

The electromagnetic torque T_e is:

$$T_e = 1.5p\left(\psi_{sd} i_{sq} - \psi_{sq} i_{sd}\right) \tag{5.8}$$

The generator name-plate data and parameters are given in Chapter 6.

As the original machine had a nominal rotor voltage of 78 V and a nominal current of 23 A, a re-wounding of the rotor has been performed, in order to fit with the converter ratings, without inserting a transformer in the rotor circuit.

The number of turns per coil was increased five times and the cross section of the conductor was decreased five times. Thus a nominal stator voltage of 380 V, and a five times lower nominal rotor current were obtained.

5.3.2 The grid-side converter (GSC)

The grid-side converter is used to control the DC link voltage and the input power factor regardless of the level and the direction of the rotor power (Figure 5.3). A vector control strategy in stator voltage reference [3] frame is employed for this purpose. The converter is current regulated with the direct axis current used to control the DC-link voltage, meanwhile the transverse axis current is used to regulate the displacement between the voltage and the current, and thus the input power factor [4], [5].

The angle of the grid voltage is:

$$\theta_e = \tan^{-1} \frac{v_{s\beta}}{v_{s\alpha}}$$

Between the grid converter and the grid itself, a line filter was introduced to reduce the higher harmonic content in the line current, produced by the switching [6]. This is a simple L – filter. The value for the inductance per phase is 13 mH [7,8], and it will be dependent of the grid and power level of the wind turbine.

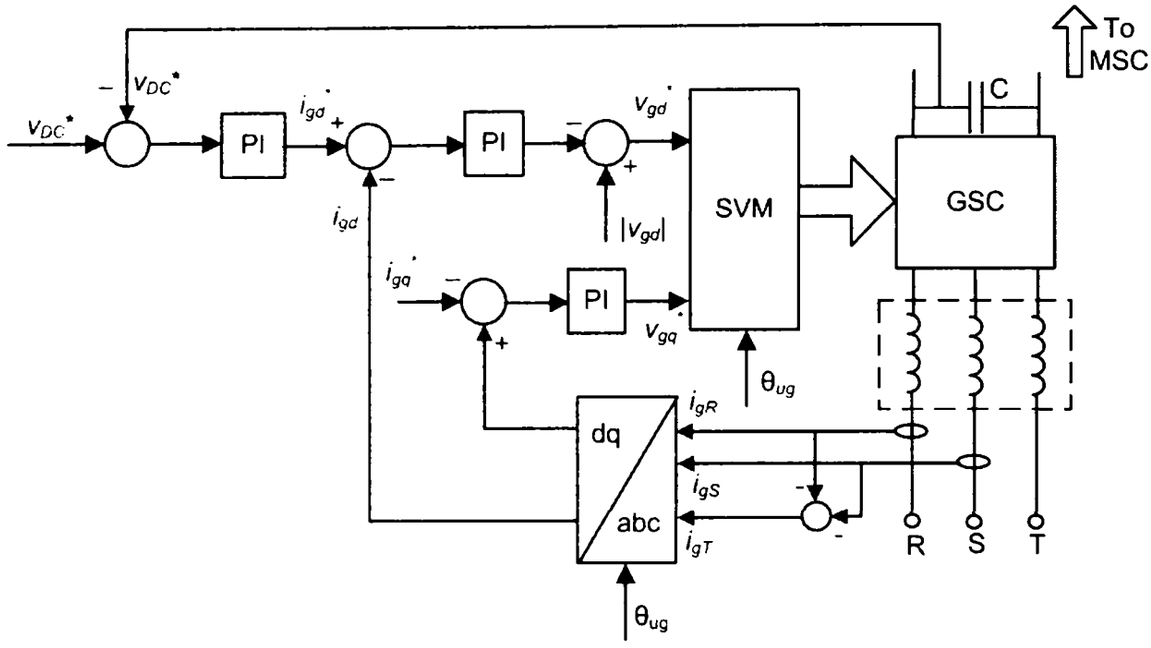

Figure 5.3 The grid-side converter control (GSC).

The design of the PI current controllers [9] follows from the transfer function of the plant (in this case the line filter itself). The controllers produce the reference grid voltage vector $v_g^* = v_{gd}^* + jv_{gq}^*$:

$$v_{gd}^* = -\left(K_{Pig} + \frac{K_{Iig}}{s}\right)e_{igd} + |v_{gd}| \tag{5.9}$$

$$v_{gq}^* = -\left(K_{Pig} + \frac{K_{Iig}}{s}\right)e_{igq} \tag{5.10}$$

where K_{Pig} and K_{Iig} are the PI controllers gains and e_{igd} and e_{igq} are the errors of the grid currents i_{gd} and i_{gq} respectively.

Applying as design constraints a damping ratio of 0.7 and a closed-loop natural frequency of 125 Hz, the gains of the controllers results: $K_{Pig} = 30$ and $K_{Iig} = 1000$.

The design for the DC-link voltage controller [10] may be carried out assuming the inner current loop is ideal and knowing the value of the DC link

capacitor (in our case 470 μF). The controller produces the reference d-axis grid current i_{gd}^*:

$$i_{gd}^* = \left(K_{PVDC} + \frac{K_{IVDC}}{s} \right) e_{VDC} \tag{5.11}$$

where K_{PVDC} and K_{IVDC} are the PI controller gains and e_{VDC} is the error of the DC voltage v_{DC}.

Thus the controller gains yields: $K_{PVDC} = 0.1$ and $K_{IVDC} = 0.3$. This is 10 times slower than the inner current loop.

5.3.3 The machine-side converter (MSC)

The generator is controlled in synchronous reference frame, with the *d*-axis aligned with the stator-flux vector, which ensures decoupled control between the electromagnetic torque and the rotor excitation contribution [12] (Figure 5.4). The control strategy block diagram is shown in Figure 5.5. As it can be seen, two rotor currents and two stator currents are measured and the third current in each case is calculated taking into account that the sum of the currents is always zero.

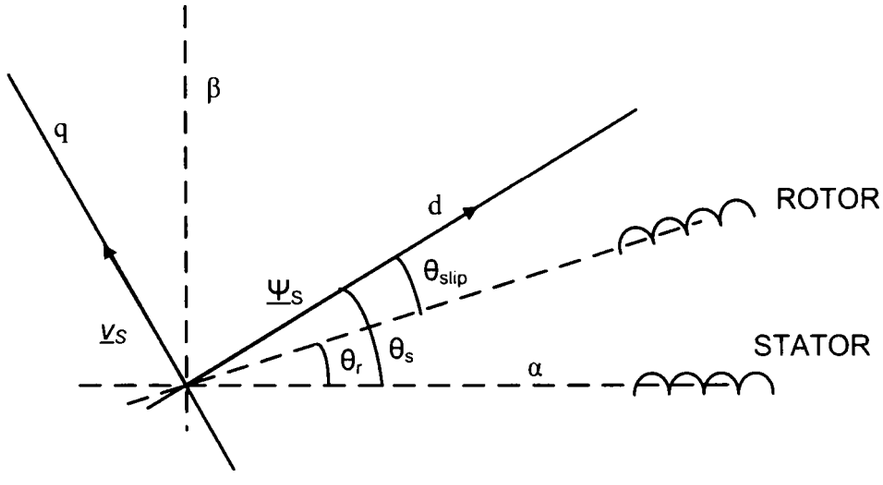

Figure 5.4 Location of stator voltage and flux vectors in stationary frame.

The rotor currents are measured in their natural frame (rotor coordinates) and transformed into synchronous frame using the slip angle:

$$\hat{\theta}_{slip} = \hat{\theta}_s - \hat{\theta}_r \tag{5.12}$$

where $\hat{\theta}_s$ is the stator flux angle, and $\hat{\theta}_r$ the rotor position.

Reference voltages generated by the current control loops are transformed back to the rotor reference frame, using the same angle $\hat{\theta}_{slip}$. Standard space vector modulation is employed to generate the pulses for the inverter.

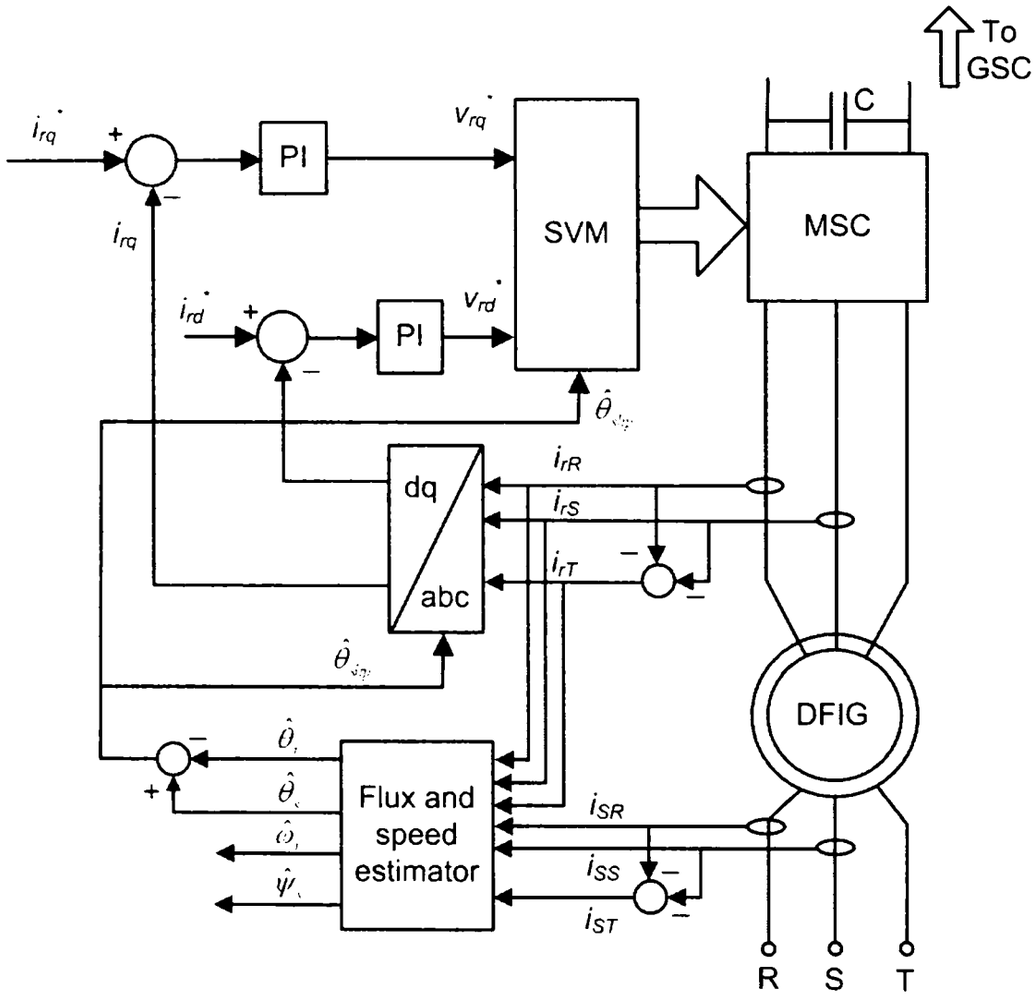

Figure 5.5 The machine side converter control (MSC).

The current controllers are designed using the same strategy as in the case of the current controllers for the grid-side inverter. The controllers produce the reference rotor voltage vector $v_r^* = v_{rd}^* + jv_{rq}^*$:

$$v_{rd}^* = \left(K_{Pir} + \frac{K_{Iir}}{s} \right) e_{ird} \tag{5.13}$$

$$v_{rq}^* = \left(K_{Pir} + \frac{K_{Iir}}{s} \right) e_{irq} \tag{5.14}$$

where K_{Pir} and K_{Iir} are the PI controllers gains and e_{ird} and e_{irq} are the errors of the rotor currents i_{rd} and i_{rq} respectively.

The gains of the rotor current controllers thus results: K_{Pir} = 40 and K_{Iir} = 1500.

5.4 Flux and rotor-speed position estimation

5.4.1 The flux-estimation

Two stator flux estimators were developed and used during the tests. Both of them are based on the voltage and the current stator flux models. The estimator using the voltage and current models connected in parallel is illustrated in Figure 5.6. The voltage model is given by (5.4). Estimated stator flux, as produced by the voltage model, is:

$$\hat{\psi}_{s\alpha\beta} = \int (v_{s\alpha\beta} - R_s i_{s\alpha\beta} + v_{comp\alpha\beta}) dt \tag{5.15}$$

The stator resistance errors due to temperature changes are neglected, and thus this model is supposed to be inaccurate, as any error in R_s is causing error in the estimated stator flux.

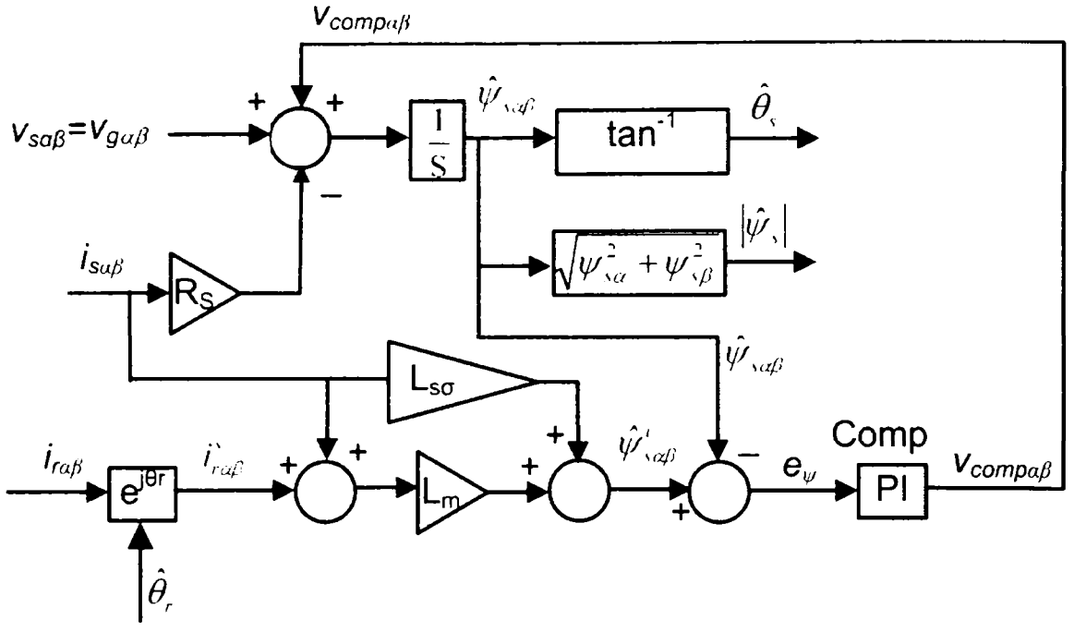

Figure 5.6 Stator flux estimator with voltage and current models in parallel.

The current model is based on (5.6):

$$\hat{\psi}'_{s\alpha\beta} = L_{s\sigma} i_{s\alpha\beta} + L_m (i_{s\alpha\beta} + i'_{r\alpha\beta}) \tag{5.16}$$

The rotor current is measured, but a transformation to stator coordinates is needed, using the estimated rotor position $\hat{\theta}_r$.

The flux error between the voltage model (5.15) and the current model (5.16) is passed through a PI controller, with K_{pcomp} = 10 and K_{icomp} = 10, which outputs a correction signal used to compensate the voltage model (see Figure 5.6):

$$v_{comp\alpha\beta} = \left(K_{Pcomp} + \frac{K_{Icomp}}{s} \right) e_\psi \tag{5.17}$$

where:

$$e_\psi = \hat{\psi}'_{s\alpha\beta} - \hat{\psi}_{s\alpha\beta} \tag{5.18}$$

This way the dc-offset drift of the ideal integrator (5.15) is eliminated. The PI compensator selects the current model at low speeds, while the voltage model prevails at medium and high speeds. Thus, the corrected stator flux vector is $\hat{\psi}_{s\alpha\beta}$ as given by (5.15). For comparison purposes only the stator flux obtained only from the current model, $\hat{\psi}'_{s\alpha\beta}$, was also considered. The stator flux position $\hat{\theta}_s$ is obtained from the resultant stator flux components:

$$\hat{\theta}_s = \tan^{-1}\frac{\hat{\psi}_{s\beta}}{\hat{\psi}_{s\alpha}}.$$

Differences were noticed between the stator flux $\hat{\psi}_{s\alpha\beta}$ obtained from the compensated voltage model (5.15) and the stator flux $\hat{\psi}'_{s\alpha\beta}$ obtained from the current model only (5.16). This was mainly due to parameter mismatch between the model and the real machine.

To have one more view of this problem, another flux estimator was developed. This is an estimator that employs the voltage and the current models connected in series, as shown in Figure 5.7. For the tests, however, the stator flux estimator with voltage and current models in parallel is used.

It is basically relying on the same equations, but the current model is written such that the stator flux obtained from the voltage model is now used to estimate the rotor current in stator coordinates:

$$\hat{i}^{ss}_{r\alpha\beta} = \frac{1}{L_m}\left(\hat{\psi}^{s}_{s\alpha\beta} - L_s i_{s\alpha\beta}\right) \tag{5.19}$$

where estimated stator flux is now:

$$\hat{\psi}^{s}_{s\alpha\beta} = \int\left(v_{s\alpha\beta} - R_s i_{s\alpha\beta} + v^{s}_{comp\alpha\beta}\right) \tag{5.20}$$

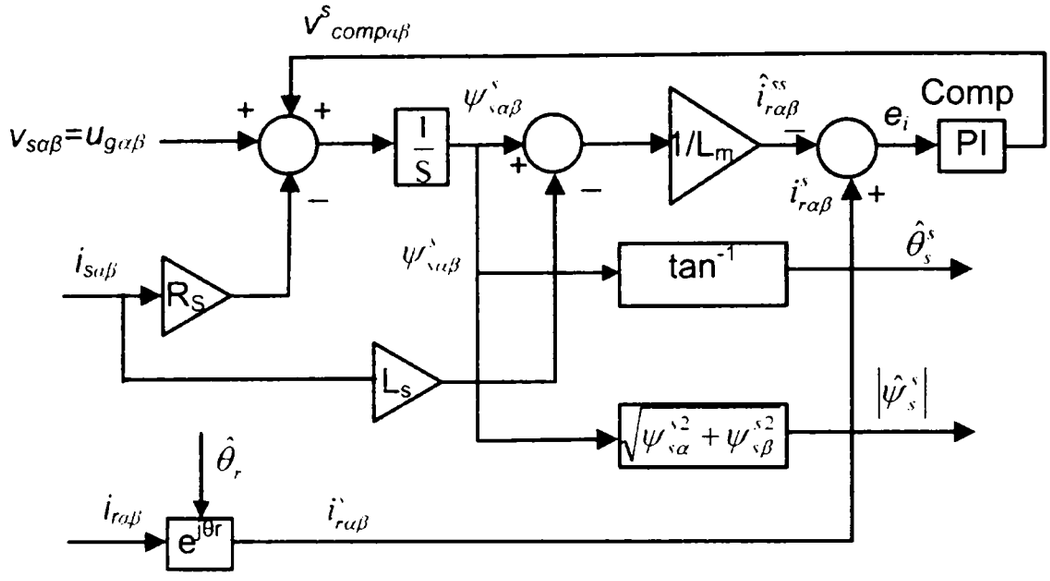

Figure 5.7 Stator flux estimator with voltage and current models in series.

The rotor current is measured and transformed into stator coordinates using the estimated rotor position θ_r. The rotor-current error between the measured and estimated (5.19) rotor current is passed through a PI controller, with the same parameters as for the one in Figure 5.6, and its output is used to compensate the voltage model: (Figure 5.7)

$$v^s_{comp\alpha\beta} = \left(K_{Pcomp} + \frac{K_{Icomp}}{s} \right) e_i \tag{5.21}$$

where:

$$e_i = i^s_{r\alpha\beta} - \hat{i}^{ss}_{r\alpha\beta} \tag{5.22}$$

5.4.2 The rotor speed-position estimation

A speed-position estimator based on model reference adaptive system (MRAS) principles is used for this purpose, due to its relative simplicity and proven efficiency over an extended speed range [13].

The rotor current in stator coordinates is calculated similar with (5.19) but **using the stator flux calculated by the parallel estimator**:

$$\hat{i}_{r\alpha\beta}^{s} = \frac{1}{L_m}\left(\hat{\psi}_{s\alpha\beta} - L_s i_{s\alpha\beta}\right) \tag{5.23}$$

and then transformed into rotor coordinates using the estimated rotor position angle $\hat{\theta}_r$ coming through feed-back:

$$\hat{i}_{r\alpha\beta}^{e} = \hat{i}_{r\alpha\beta}^{s} e^{-j\hat{\theta}_r} \tag{5.24}$$

The MRAS error ε is calculated as the phase difference of the estimated rotor current $\hat{i}_{r\alpha\beta}^{e}$ and the measured rotor current $i_{r\alpha\beta}$ (5.25). The real system is the reference model, while the current model is the adaptive model, with the rotor position θ_r as adaptive parameter.

$$\varepsilon = -i_{r\alpha}\hat{i}_{r\beta}^{e} + \hat{i}_{r\alpha}^{e} i_{r\beta} \tag{5.25}$$

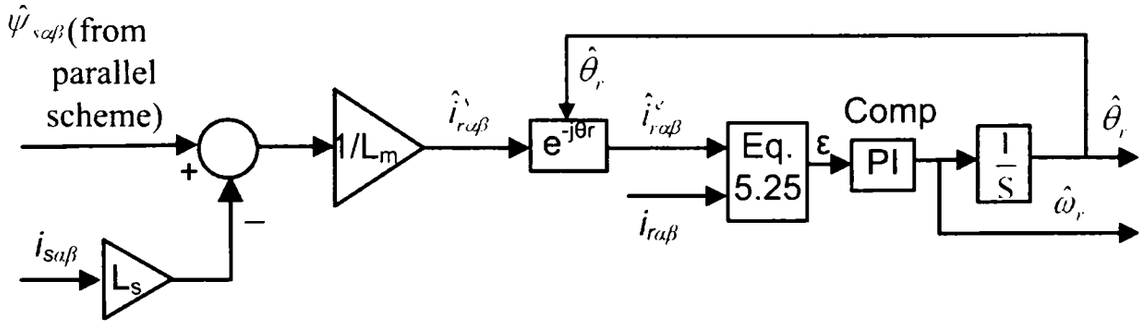

Figure 5.8 The rotor speed and position estimation MRAS.

This error is used to extract the rotor speed and position using a phase-locked loop (PLL) technique (Figure 5.8). The output of the PI compensator gives the

estimated rotor speed ω_r. and after the integration, the estimated rotor position θ_r is obtained:

$$\hat{\omega}_r = \left(K'_{Pcomp} + \frac{K'_{Icomp}}{s} \right) \varepsilon \; ; \; \hat{\theta}_r = \int \hat{\omega}_r dt \tag{5.26}$$

Optimum parameters of the PI compensator were searched as a compromise between the speed of the PLL. especially during transients, and the level of oscillations in speed estimation. especially at low speeds.

The best parameters. seem to be: $K'_{Pcomp} = 100$, and $T_I = 5$ms (time constant of the compensator, $T_I = K'_{Pcomp} / K'_{Icomp}$). Overall. this scheme has shown good accuracy over the whole speed range and also during the start-up procedure.

5.5. Test rig and experimental results

5.5.1 Synchronization procedure

The synchronization procedure at start-up consists on the following steps:the generator is driven with the motor which simulates the wind turbine close to the synchronous speed, and in the same direction of rotation as that of the network; the DC link is charged from the network through the line filter and the pre-charging resistors.

The resistors are disconnected afterwards; K_1 is switched on, and the control algorithms are started with the reference current for the machine side converters (MSC) set to zero;when the stator voltage becomes almost equal to the grid voltage (lamps in parallel with K_2 are off), K_2 is switched on;the reference currents for the machine side converter (in fact the reference for the stator active and reactive power) are then set at desired values.

5.5.2 Experimental results

1. DC Link Control.

First, as the grid side converter (Figure 5.3) was analyzed, a step-up in the DC voltage reference was applied, and the response is shown in Figure 5.9.

As can be noticed, fast and well-damped dynamic response was obtained. The grid side converter is able to accurately control the DC voltage, and the power may bidirectionally flow through the rotor.

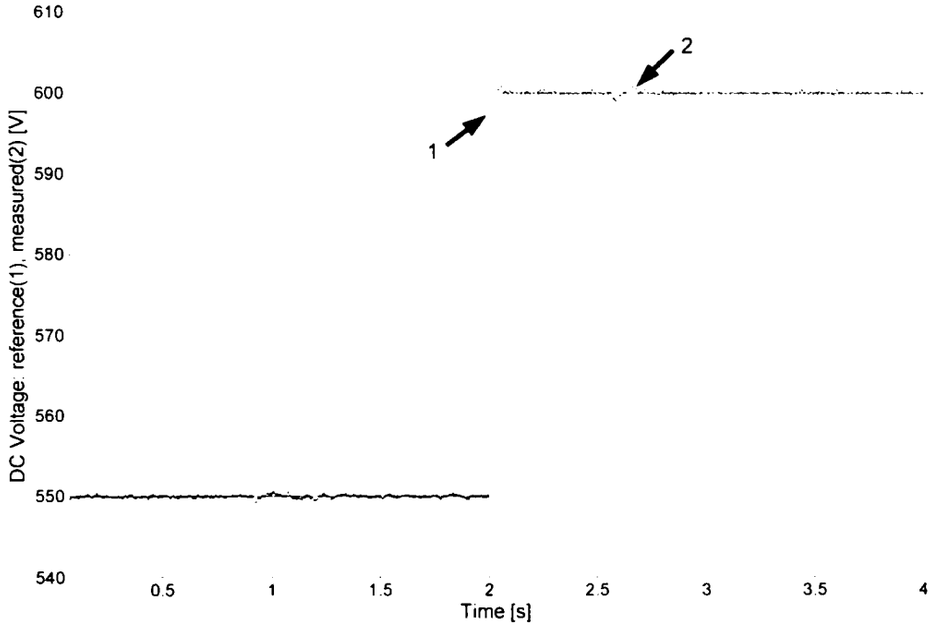

Figure 5.9 DC link voltage dynamic response at step reference from 550 V to 600 V at t=2 s.

2. Subsynchronous operation.

The stator reactive and active power are direct proportional with i_{rd} and i_{rq}. It means that by controlling the rotor currents i_{rd} and i_{rq} a fast decoupled response in terms of stator reactive power Q_s and stator active power P_s is obtained.

The following tests will deal with control of i_{rd} and i_{rq}. Please note that a negative d or q rotor current means a negative reactive or active power (generating), a positive d or q rotor current means a positive reactive or active power (absorbing).

For zero reactive power current i_{rd}^* reference (see Figure 5.5), with the generator in subsynchronous operation (rotor speed below 1000 rpm), a step reference of active power current i_{rq}^* from 0 to –5 A (generating) was applied at t = 2 s.

The dynamic response of rotor currents i_{rd} and i_{rq} is illustrated in Figure 5.10, and the measured and estimated rotor speed response is shown in Figure 5.11.

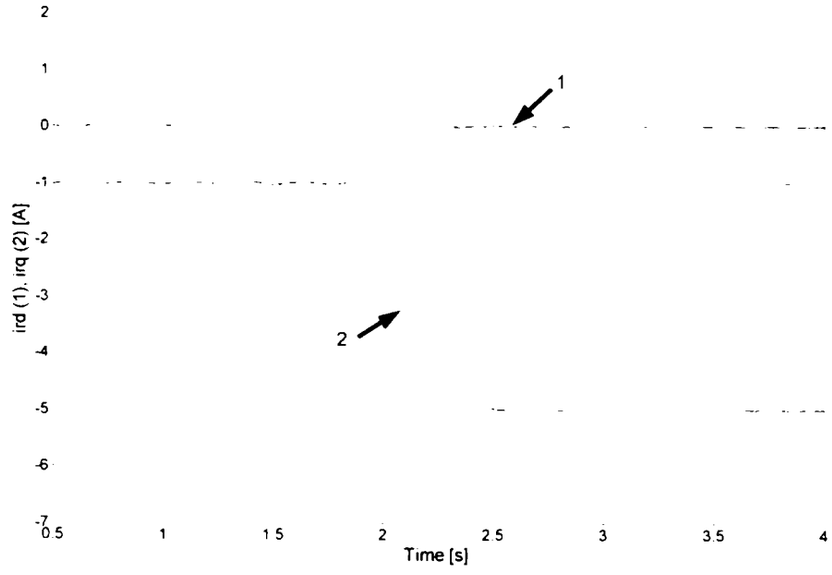

Figure 5.10 Measured rotor currents i_{rd} (1) and i_{rq} (2) for a step reference of i_{rq}^* from 0 to –5 A, and $i_{rd}^* = 0$, at t=2 s in generating subsynchronous operation

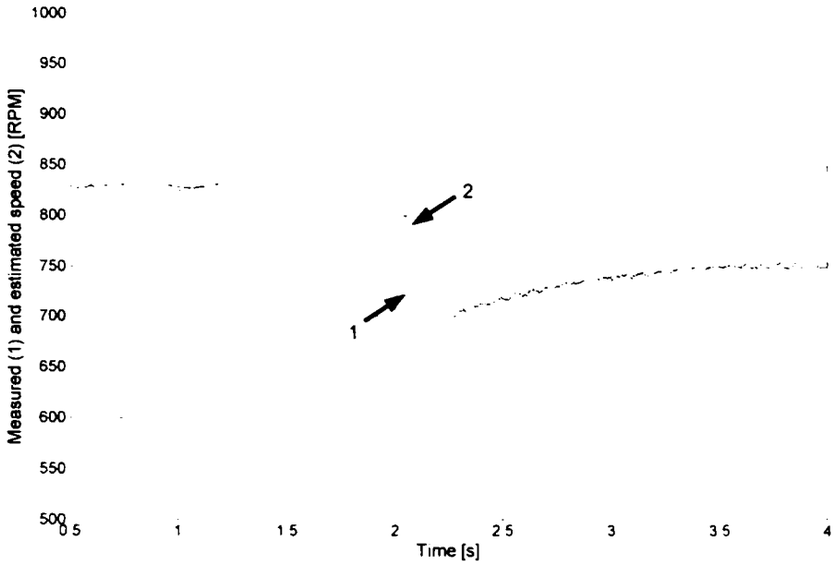

Figure 5.11 Measured (1) and estimated (2) rotor speed for a step reference of i_{rq}^* from 0 to –5 A, and i_{rd}^* = 0, at t=2 s in generating subsynchronous operation

For the same experiment the stator currents are shown in Figure 5.12, and the rotor currents in Figure 5.13.

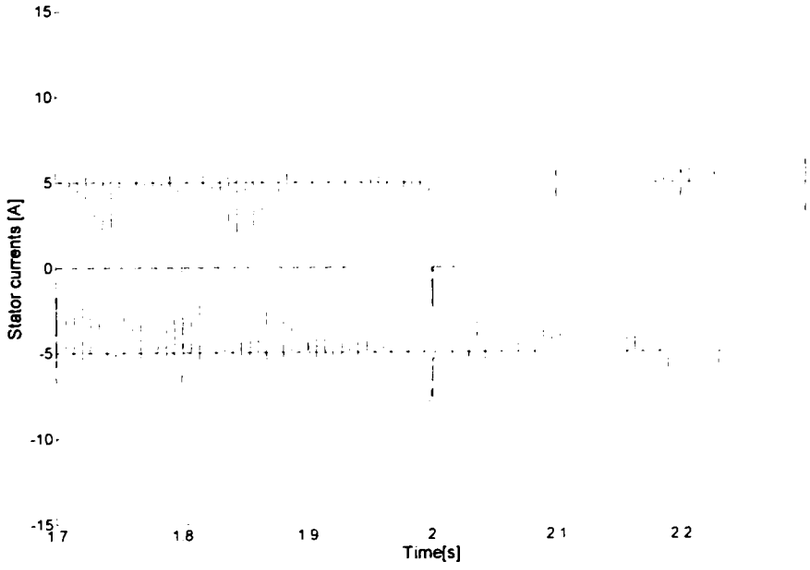

Figure 5.12 Stator currents during step in i_{rq}^* from 0 to –5 A, and i_{rd}^* = 0

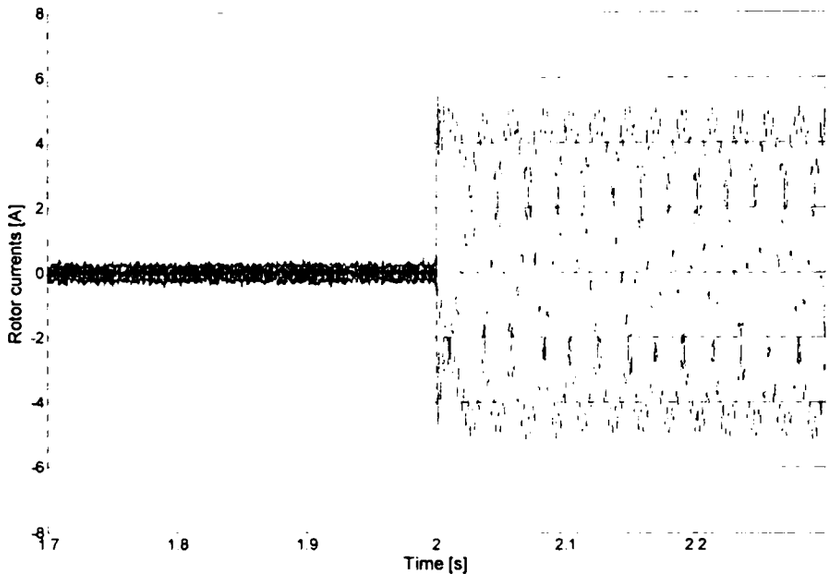

Figure 5.13 Rotor currents during step in I_{rq} from 0 to -5A, $I_{rd}^{*} = 0$.

Also in subsynchronous operation, for constant zero reference of i_{rq}^{*} current, a step-up in i_{rd}^{*} current from –3 A (generating) to +3 A (absorbing) was applied. The dynamic response of rotor currents i_{rd} and i_{rq} is shown in Figure 5.14, and the measured stator currents for the same experiment are shown in Figure 5.15.

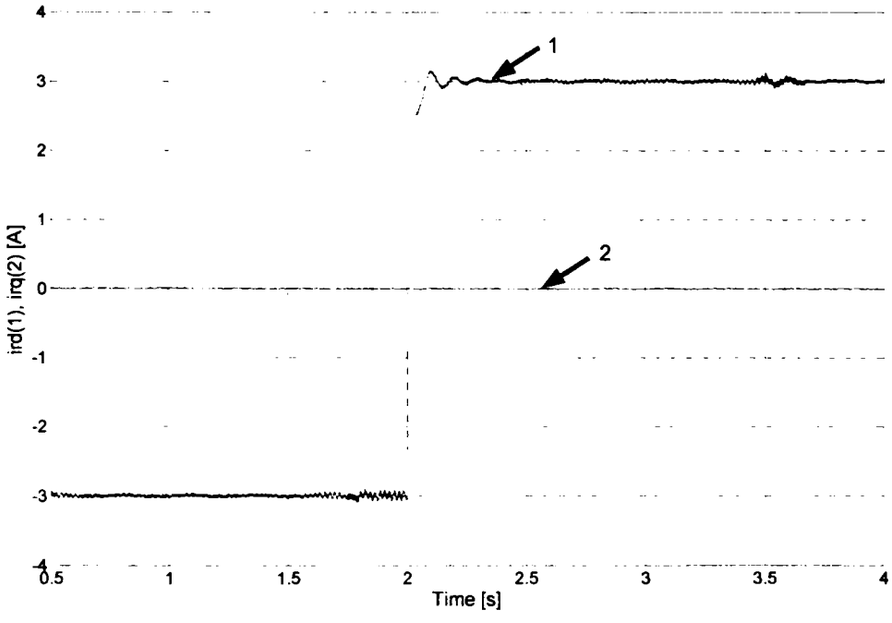

Figure 5.14 Rotor currents i_{rd} (1) and i_{rq} (2) for a step reference of i_{rd}^{*} from -3 A to 3 A, $i_{rq}^{*} = 0$, at t = 2 s in subsynchronous operation

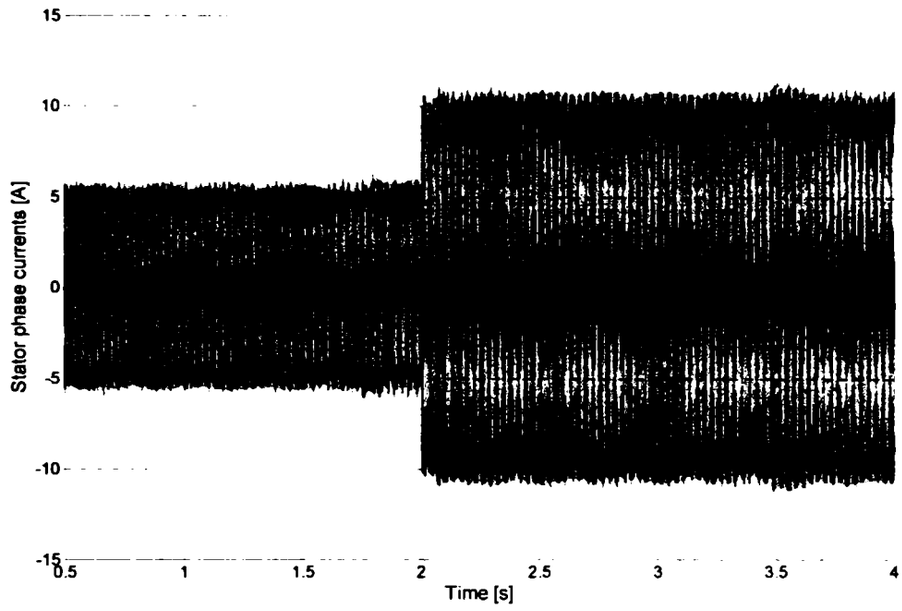

Figure 5.15 Measured stator phase currents for a step reference of i_{rd}^* from -3 A to 3 A, $i_{rq}^* = 0$, at t = 2 s in subsynchronous operation.

The measured and estimated speed are illustrated for this experiment in Figure 5.16, and the measured rotor phase currents in Figure 5.17.

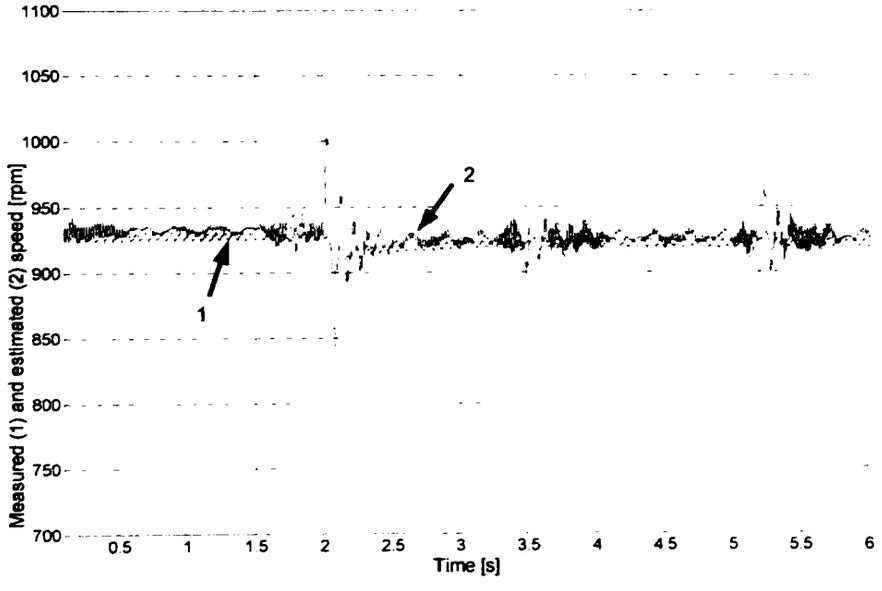

Figure 5.16 Measured (1) and estimated (2) rotor speed for a step in reference of I_{rd} from -3A to 3A, $I_{rq}^* = 0$.

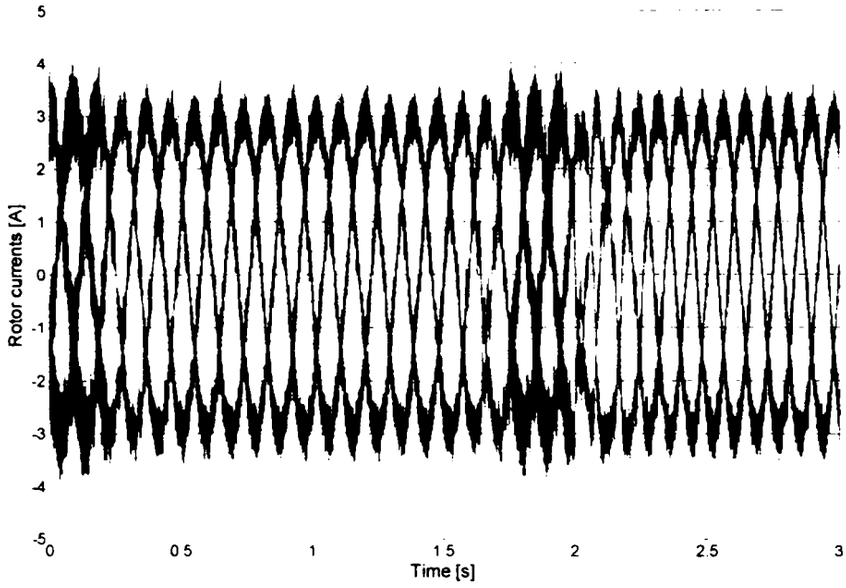

Figure 5.17 Measured rotor phase currents for a step in reference of I_{rd} from -3A to 3A, $I_{rq}^{*} = 0$.

3. Oversynchronous operation.

The previous subsection dealt with the experimental results for under-synchronous operation of the DFIG. The behavior in oversynchronous operation was also investigated. With the generator running at about 1200 rpm, and with the reference current i_{rd}^{*} set at –3 A, a step reference of i_{rq}^{*} from –1 A to –5 A was applied. The rotor current dynamic response is shown in Figure 5.18, and the measured and estimated rotor speeds are shown in Figure 5.19.

In this case, negative direct current i_{rd} means magnetization from the stator. The limited power of the prime mover IM drive makes the speed to vary with DFIG loading.

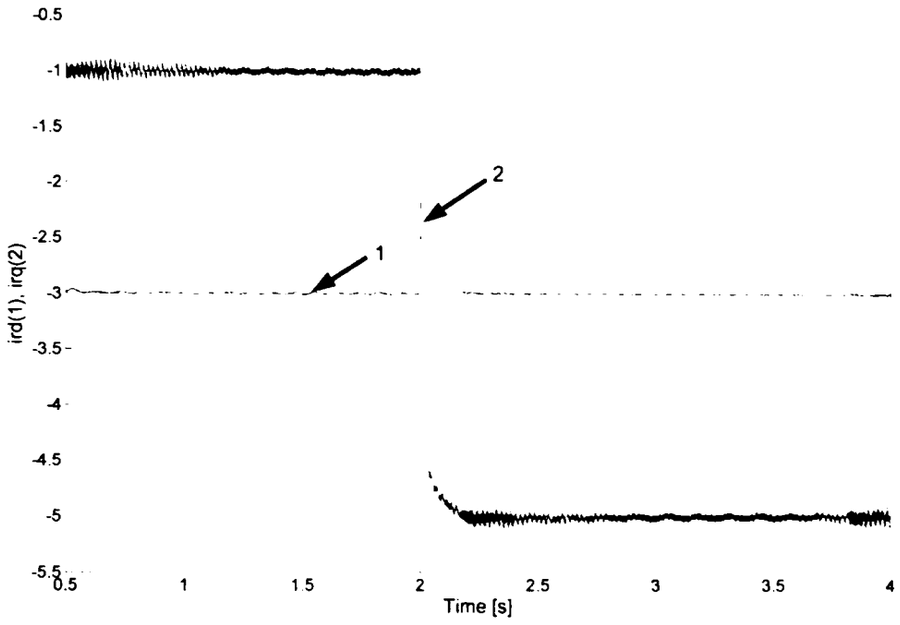

Figure 5.18 Rotor currents for a step reference of i_{rq}^* from –1 A to –5 A, i_{rd}^* = -3 A, at t = 2 s in generating oversynchronous operation

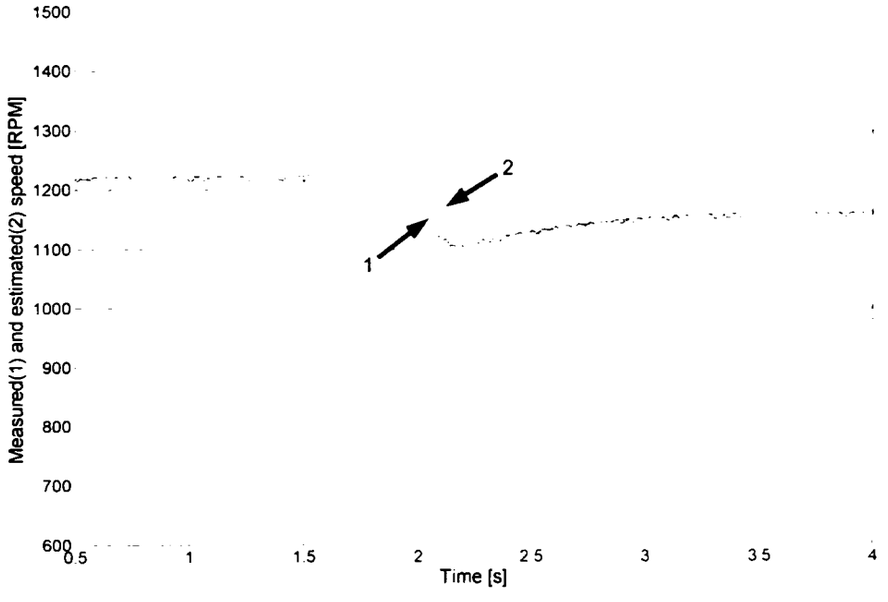

Figure 5.19 Measured (1) and estimated (2) rotor speed for a step in reference of i_{rq}^* from –1 A to –5 A, i_{rd}^* = -3 A, at t = 2 s in oversynchronous operation.

For the same step in i_{rq}^* from –1 A to –5 A (with the reference current i_{rd}^* set at –3 A) the measured rotor currents are shown in Figure 5.20, while the measured stator currents are shown in Figure 5.21.

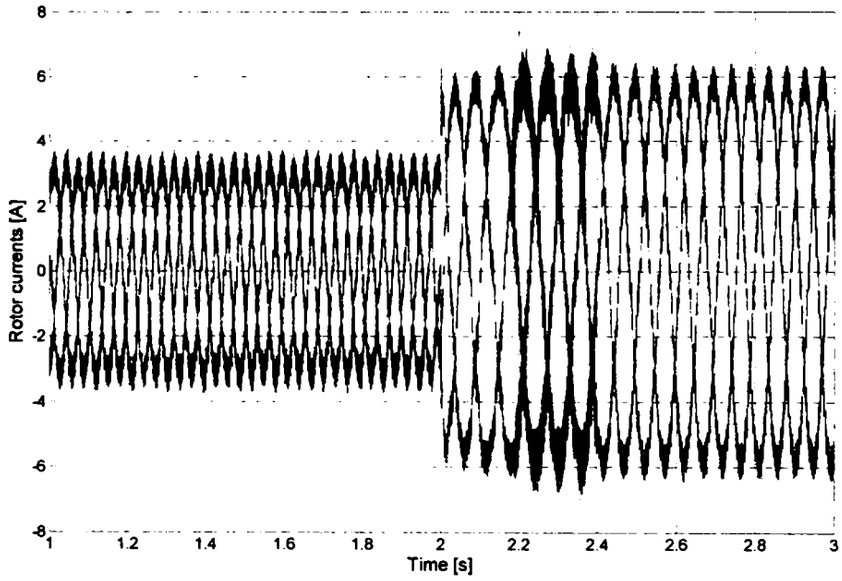

Figure 5.20 Measured rotor currents for a step in reference of I_{rq} from -1A to -5A, I_{rd}^* = -3A.

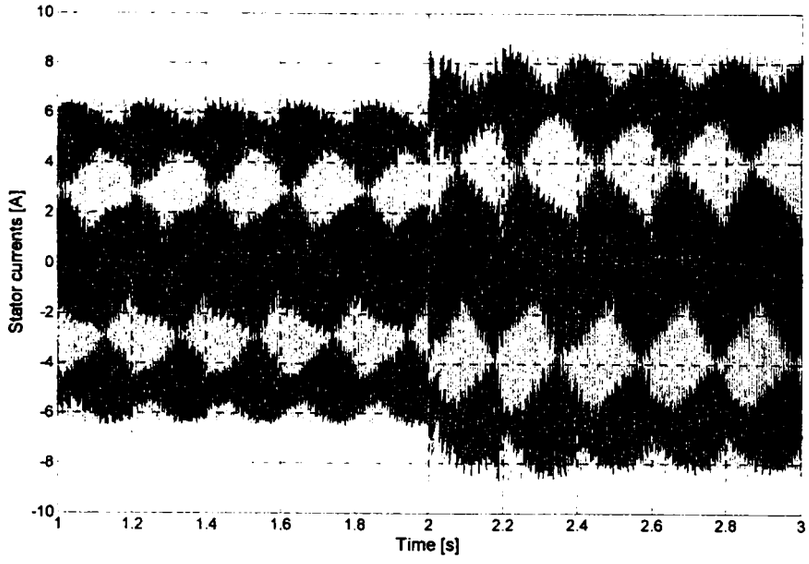

Figure 5.21 Measured stator currents for a step in reference of I_{rq} from -1A to -5A, I_{rd}^* = -3A.

4. Passing through Synchronism.

One of the most interesting features of the doubly-fed induction generator with two back-to-back converters in the rotor circuit is passing through the synchronism and even synchronous operation.

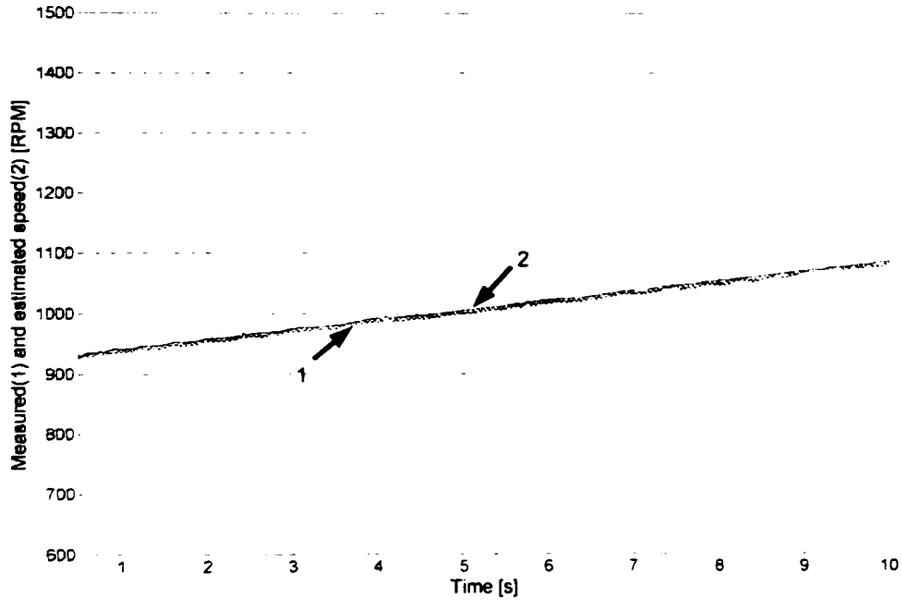

Figure 5.22 Measured (1) and estimated (2) speed at passing through synchronism.

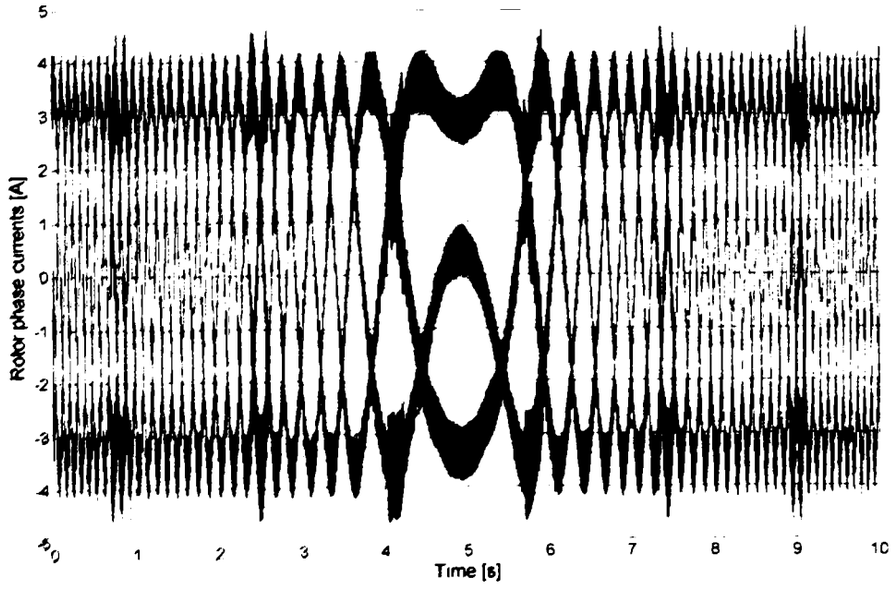

Figure 5.23 Measured rotor currents at passing through synchronism.

Speed and current transients from 930 to 1160 rpm during passing through synchronism are presented in what it follows. The measured and estimated speeds are shown in Figure 5.22, and the measured rotor currents are shown in Figure 5.23. The passing through synchronism occurs at t = 5 s.

Also to compare the three estimators an example is illustrated in Figure 5.24.

The stator flux from parallel estimator, from parallel estimator current model only and from the series estimator are shown.

As it could be seen, the differences between the flux estimated by the parallel estimator and the one estimated by the current model only from the parallel estimator are negligible.

The series estimator in this situation has an enormous error, and it cannot be considered in the experiments. Please note that for all the experiments, the estimated stator flux (and its angle) used, was the one estimated by the parallel estimator.

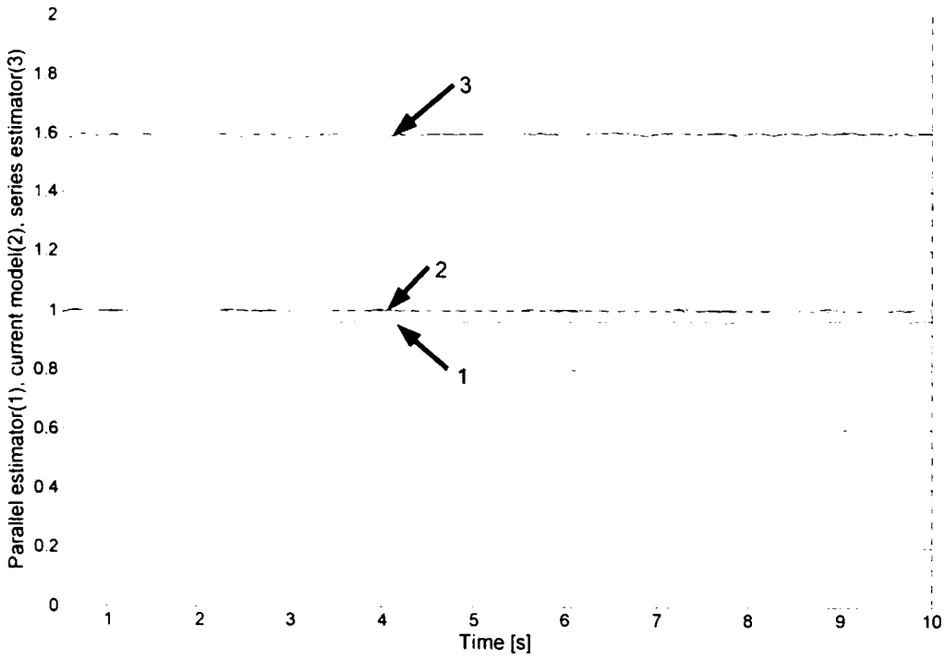

Figure 5.24 Stator flux during passing through synchronism estimated by: parallel estimator $\hat{\psi}_s$ (1), parallel estimator current model only $\hat{\psi}_s^I$ (2), series estimator $\hat{\psi}_s^S$ (3)

5. Synchronous operation.

The DFIG is able of stationary synchronous operation, as a native synchronous generator. In this case, the rotor currents are DC and the generator becomes an electrically excited synchronous generator. In Figure 5.25, the measured rotor phase currents are shown for the generator driven at synchronous speed of 1000 rpm.

This is an important advantage of this generator and its control, i.e. the possibility to impose and maintain the synchronous speed and to generate more reactive power when needed, similarly to the overexcited synchronous generator. This could be realized by setting a negative i_{rd}^* current reference and fixing the rotor speed at its standard synchronous value ($n_r = f_s/p$).

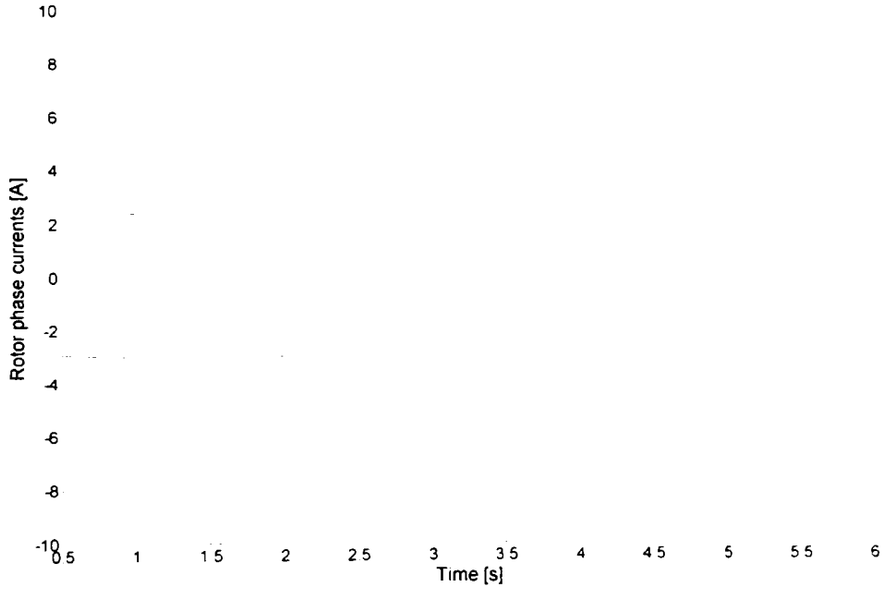

Figure 5.25 Measured rotor currents during stationary synchronous operation.

Conclusion

A complete system with a doubly-fed induction generator was presented and analyzed in this chapter. The main target-application for this system is the wind power generation. Other possible applications are hydropower generation, or other turbines using unconventional power sources like tides or marine currents. The wound-rotor

induction generator uses two back-to-back connected converters in the rotor circuit, both of them vector controlled.

The machine-side converter controls the active and reactive rotor currents (in fact the stator active and reactive powers), while the grid-side converter controls the DC voltage regardless of the magnitude and the direction of the rotor power, and the reactive current drawn or injected from/in the grid. Both control strategies are presented and discussed. A new start-up procedure with a synchronization sequence is presented.

Two stator flux estimators were developed and compared. Both are based on combining of the voltage and current models, One is using them in parallel and the other one in series. A rotor speed and position estimator was developed, based on MRAS principles. The speed and position estimation is accurate over the whole speed range and it has the advantage that is efficient also during the start-up procedure.

Different operational tests were performed, and the results are shown and discussed. Rather fast response in terms of stator active and reactive power is proven. The same holds in terms of DC voltage and reactive current on the power grid side.

The passing through synchronism and stationary synchronous operation were presented. An interesting feature and, in fact, an advantage of this generator and its control is synchronous operation like as a native synchronous generator. The level of the generating (or absorbing) reactive power could be easily set through the rotor flux current reference.

References

[1] I. Serban, F. Blaabjerg, I. Boldea, "Sensorless doubly-fed induction generator control under power system transients and faults: the influence of magnetic saturation", *Proc. of OPTIM 2004*, Brasov, Romania, vol. 2, pp. 311-318, May 2004.

[2] M.P. Kazmierkowski, R. Krishnan, F. Blaabjerg (Eds.), *Control in Power Electronics: Selected Problems*," Chapter 13: L. Helle, F. Blaabjerg, "Wind turbine systems", Academic Press, 2002.

[3] I. Boldea, S.A. Nasar, *Electric Drives*, Chapter 14: "Large power drives, 14.8 Sub and Hypersynchronous IM cascade drives," CRC Press, Florida, 1999.

[4] R. Datta, V.T. Ranganathan, "Direct power control of grid-connected wound rotor induction machine without rotor position sensors," *IEEE Transactions on Power Electronics*, vol. 16, no. 3, May 2001, pp. 390-399.

[5] L. Morel, H. Godfroid, A. Mirzaian, J.M. Kauffmann, "Double-fed induction machine: converter optimization and field oriented control without position sensor," *IEE Proc. on Electric Power Applications*, vol. 145, no. 4, July 1998, pp. 360-368.

[6] Sae-Joon Lee, Jun-Koo Kang, Seung-Ki Sul, "A new phase detecting method for power conversion systems considering distorted conditions in power system," *1999 IEEE-IAS Annual Meeting Conf. Record*, vol. 4, pp. 2167-2172, 1999.

[7] V. Kaura, V. Blasko, "Operation of a phase locked loop system under distorted utility conditions," *IEEE Transactions on Industry Applications*, vol. 33, no.1, Jan./Feb. 1997, pp. 58-63.

[8] Morten Lindholm, "Doubly-Fed Drives for Variable Speed Wind Turbines," *Ph.D. Thesis*, Technical University of Denmark,

[9] I. Serban, F. Blaabjerg, I. Boldea, Z. Chen, "A study of the doubly-fed wind power generator under power grid faults," *Proc. of EPE 2003*, Toulouse, France, 2003.

[10] U. Rädel, D. Navarro, G. Berger, S. Berg, "Sensorless field-oriented control of a slipring induction generator for a 2.5 MW wind power plant from Nordex Energy GmbH," *Proc. of EPE 2001*, Graz, 2001.

[11] S. Müller, M. Deicke, R.W. De Doncker, "Adjustable speed generators for wind turbines based on double-fed induction machines and 4-quadrant IGBT converters linked to the rotor," *2000 IEEE-IAS Annual Meeting Conf. Record*, vol. 4, pp. 2249-2254, Oct. 2000.

[12] R. Datta, V.T. Ranganathan, "A simple position-sensorless algorithm for rotor-side field-oriented control of wound-rotor induction machine," *IEEE Transactions on Industrial Electronics*, vol. 48, no. 4, Aug. 2001, pp. 786-793.

[13] G.D. Andreescu, "Position and speed sensorless control of PMSM drives based on adaptive observer," *Proc. of EPE'99*, Lausanne, Switzerland, Aug. 1999.

Chapter 6

The experimental test platform

Abstract

This chapter deals with the extended description of the laboratory setup used for all the tests presented in Chapters 4 and 5.

It was realized in the Intelligent Motion Control Lab. Faculty of Electrical Engineering Timisoara, with the intended purpose to prove and gain new information about the control of the doubly-fed induction machine with two back-to-back connected inverters in the rotor circuit, as the main part of the thesis.

6.1 Introduction

The setup consists of a 3kW doubly-fed induction generator mechanically connected with a driving squirrel-cage induction motor supplied from an usual frequency converter for speed control operation.

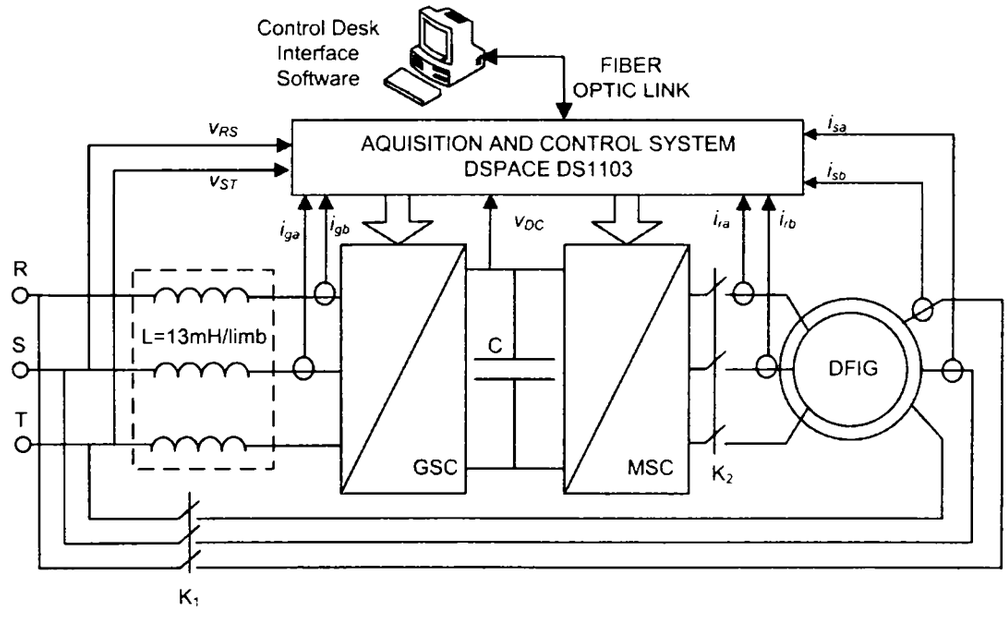

Figure 6.1 The DFIG system.

The DFIG is connected to the power grid directly with the stator, and through the two back-to-back inverters with the rotor.

Besides those main components, there are measuring circuits, the control system, the line filter etc. Figure 6.1 shows the principle schematic of the setup.

6.2 Hardware specifications

6.2.1 The rotating machinery

The main component in the setup is the 3kW doubly-fed induction generator manufactured by IME SA Bucharest Romania. It is a 6-pole machine, star connected stator and rotor. As the original machine had the nominal stator voltage V_{SN} = 380 V and the nominal rotor voltage V_{RN} = 78 V a re-wounded was necessary to fit with the converters requirements without inserting a transformer in the rotor circuit. Thus, a new rotor winding was designed in IMC Lab. and executed in Electromotor SA Timisoara. Hence, the rotor voltage (at slip S = 1) was increased to V'_{RN} = 380 V and the rotor nominal current was decreased from 23 A to 4.6 A.

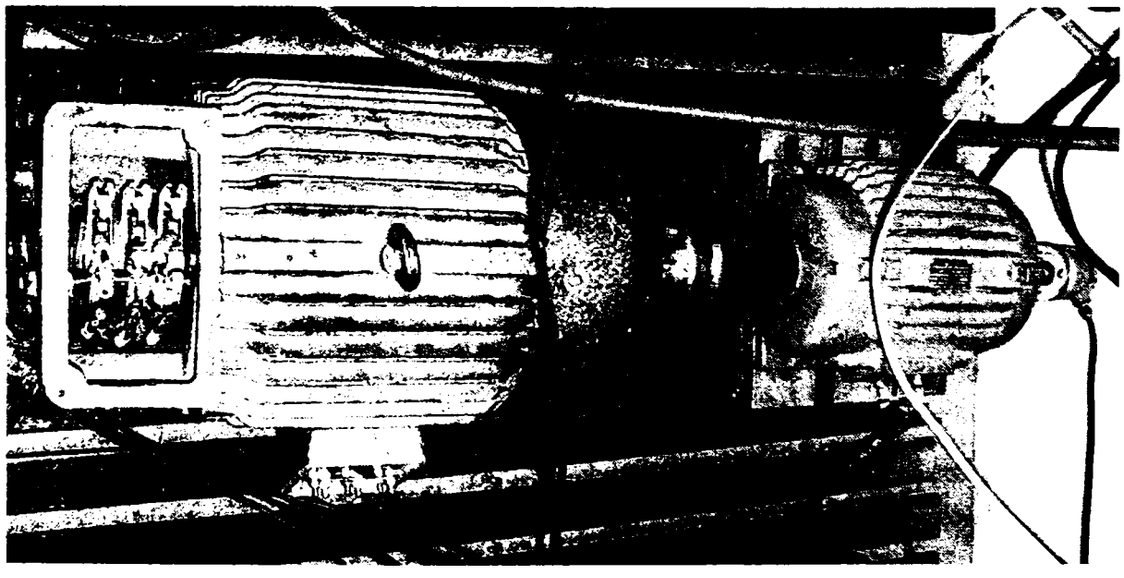

Figure 6.2 The DFIG (left) and its driving motor (right).

The name-plate data of the doubly-fed induction machine:

Type - asynchronous motor with slip rings

Manufacturer: IME SA Bucharest, Romania

Nominal power: $P_N = 3$ kW

Stator nominal voltage $V_{SN} = 380$ V

Rotor nominal voltage $V_{RN} = 380$ V (after re-wounding; the original rotor voltage was 78 V)

$n_N = 940$ rpm.

Parameters of the doubly-fed induction machine:

Stator resistance: $R_s = 1.6\ \Omega$

Rotor resistance: $R_r = 1.6\ \Omega$

Leakage stator inductance: $L_{s\sigma} = 17.51$ mH

Leakage rotor inductance: $L_{r\sigma} = 17.51$ mH

Magnetizing inductance: $L_m = 96.13$ mH.

Number of pole pairs: $p = 3$

The DFIG is mechanically connected with a 3kW, 4-pole squirrel-cage induction motor (not represented in Figure 6.1) manufactured by Electromotor SA Timisoara and with an encoder (see Figure 6.2 for a photo of the machines).

The induction motor (acting as wind turbine) is supplied from a Danfoss VLT 5004/3 kW commercial inverter with the original interface for the speed control mode.

6.2.2 The power inverters and their interface and protection

The power inverters are commercial VLT 5004, 4.2 kVA manufactured by Danfoss Drives, Denmark (see Figure 6.3 for a photo of the inverters). The main data for them are given in Table 6.1.

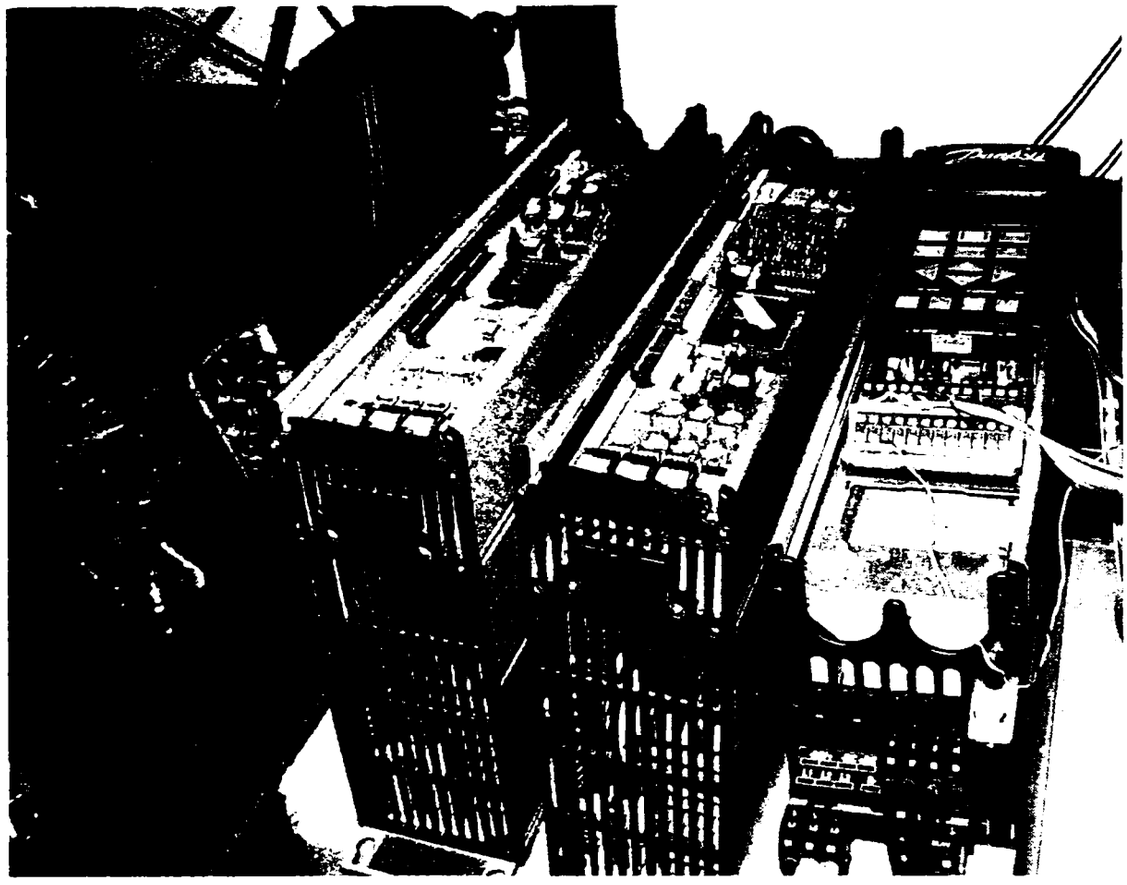

Figure 6.3 The Danfoss power inverters equipped with interface and protection cards (IPC) left – GSC, middle – MSC. In the right side is the inverter for the driving motor with the original interface for speed control mode.

Table 6.1 Power inverters specifications

Rated Power	4.2 kVA
Nominal Voltage	380 V
Nominal Current	6.5 A
Maximum DC Link Voltage	1200 VDC
Switching Frequency	10 kHz

The inverters have the DC links accessible through the DC sharing connectors. By realizing an electrical connection between them, the inverters can be easily connected back-to-back. But for the DC link capacitors pre-charging, a resistor was

used (not illustrated in Figure 6.1) between the grid and the line filter; the resistors were short-circuited after the voltage in the DC link reached approx. 500 V

Their original interface cards and control panels were replaced with interface and protection cards (IPC – see Figure 6.4), produced by IET, Aalborg University.

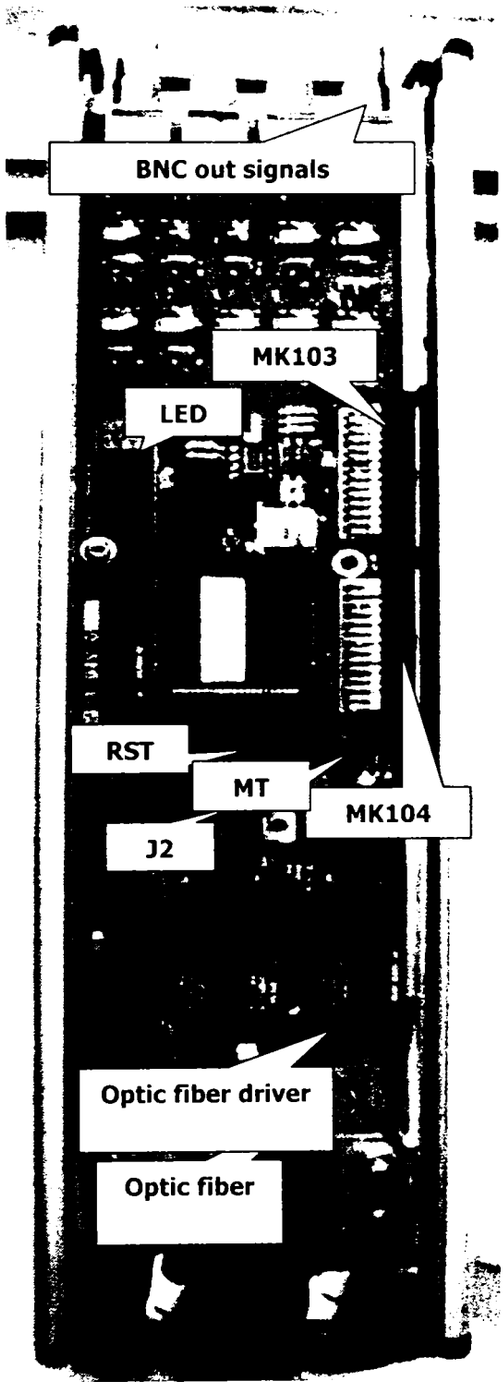

Figure 6.4 Physical layout of the Interface and Protection Card for the power inverters

The IPC is a PCB card with the same dimensions and mounting layout as the original VLT5004 control card. It has two flat cables connected to VLT power-card MK103 and MK104 sockets and four BNC sockets for output currents **IU-VLT, IV-VLT, IW-VLT** and DC-voltage **UD-VLT** signals (not used in our case).

The gate signals can be brought-in via optic fiber using the eight receivers on-board or directly in TTL format, using the J2-socket. Besides the seven IGBT gate signals (**UP, UN, VP, VN, WP, WN** and **BR**), there is an enable signal (**EN**) that inhibits the gate drivers if it is kept low (coasting).

The interface board is featured with two push-buttons: RESET (**RST**) and MANUAL TRIP (**MT**) as they are labeled on the card. Any fault that might occur need to be cleared out by pressing **RST** in order to release the gate signals. **MT** forces a trip when pressed. All faults can be read out the LED digit display, as shown in Table 6.2.

Table 6.2 VLT fault description.

‾	**Over Temp. (OT)**
_	**Manual Trip (MT)**
_	**Shoot Through (ST)**
ı	**DC Over Voltage (OV)**
ı	**Over Current (SC)**
ı	**VLOG out of range**
ı	**Coast (EN)**

IGBT gate signals. The VLT5004 gate drivers require the gate signals to be modulated with 4 MHz. All seven gate signals (**UP, UN, VP, VN, WP, WN** and **BR**) are brought to a CPLD where 4 MHz modulation with edge synchronisation is carried out. Because the optic fiber receivers are inverting devices, gate signals are inverted at the input of the CPLD logic block.

An asynchronous clear is performed by the active high **INHIBIT** signal, which is obtained by NAND-ing **ENABLE** (no trip condition) with the latched **ST** (shoot-through) detection signal. **ST** is generated by AND-ing the upper and lower gate

signals signals, OR-ing them for all three phases and negating for turning it in an active high signal.

Note – In this design a 2 μs dead-time was implemented in the CPLD. Hence, each inverter is controlled through 3 signals (UP, VP, WP) – for the upper IGBTs – and an enable signal (EN) – see Figure 6.5. The ST protection is useful when all gate signals are high as a result of DS1103 reset or a computer crash (DS1103 goes into reset state every time new code is downloaded). ST action inhibits the gate pulses fast (within a few ns.)

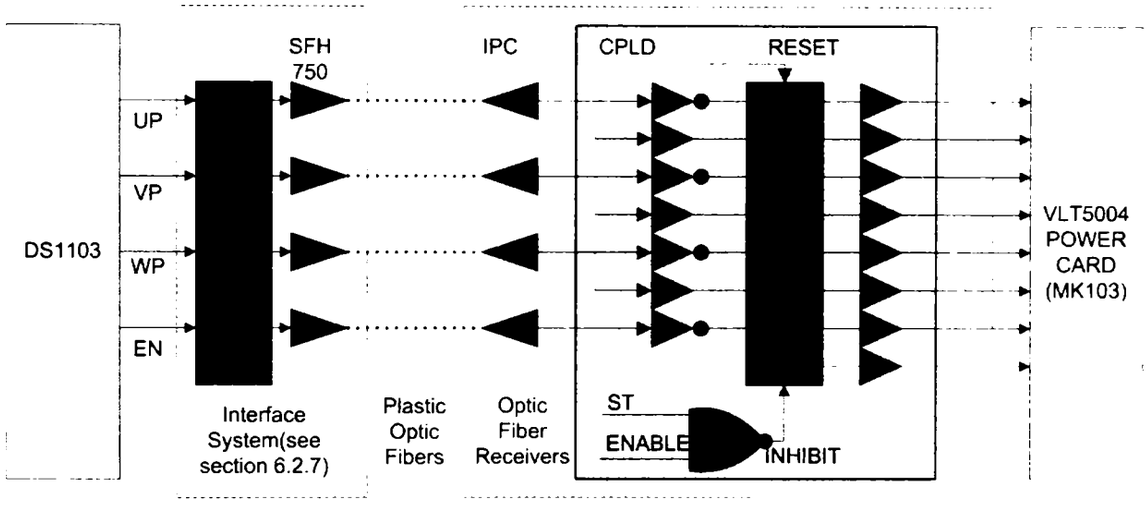

Figure 6.5 Interface and protection card (for one inverter – for the other is identical)

Shortcircuit protection. All three phase currents signals (**IU-VLT**, **IV-VLT** and **IW-VLT**) are compared (see Figure 6.6) against the maximum positive output current (+Isc) and the maximum negative output current (–Isc) levels (Isc threshold= 2.5*Inom(1.6V)*sqrt(2)= ±4.0 V for the whole VLT 5000 series due to the current scaling). 6 fast comparators (AD790 with 45 ns response time) are used. So **IUPSC, IUNSC, IVPSC, IVNSC, IWPSC** and **IWNSC** active high signals are generated. These logical signals are brought to the CPLD for latching, AND-ing with the other faults signals for tripping and LED signaling.

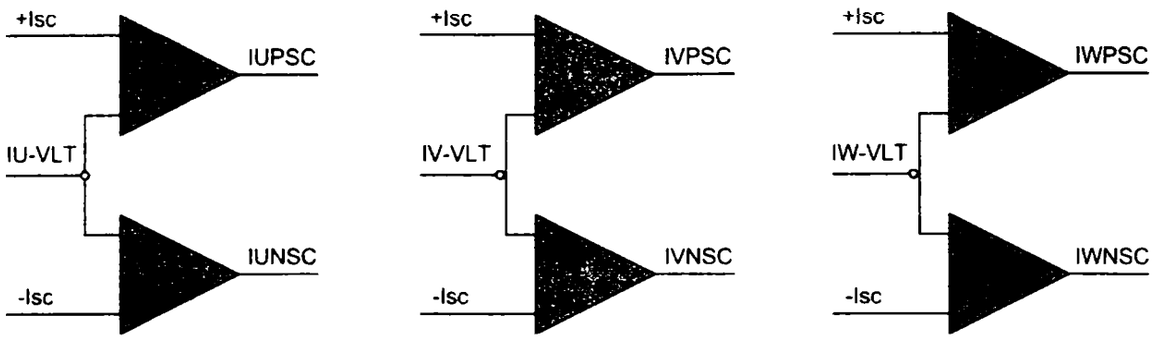

Figure 6.6 The shortcircuit protection implemented on the IPC

DC overvoltage protection. DC voltage signal **UD-VLT** is compared against a threshold that equals 130% of the rated DC-voltage using the same type of fast comparators (see Figure 6.7). The active high **UDOV** produced signal is then brought to CPLD for latching, AND-ing with the other faults signals for tripping and LED signaling.

Additionally, the UD-VLT signal is compared against 75% of the rated dc voltage value in order to generate the **/INRUSH** signal that releases the INRUSH relay from the VLT power board when it is active low.

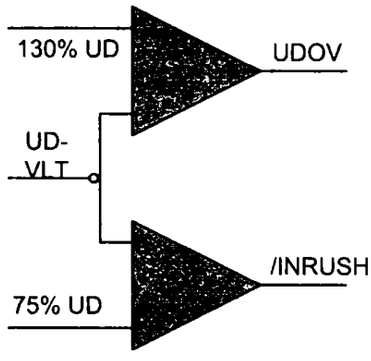

Figure 6.7 The DC overvoltage protection implemented on the IPC

Overtemperature protection. The temperature signal **TEMP** produced on the VLT power board using a 10 kΩ@25° NTC and has a nonlinear scaling. This signal is double compared against 40 °C with ± 5 °C hysteresis and against 90 °C (1.44V) for generating active low **/FANO** and **/OT**, respectively (see Figure 6.8). The **/FANO**

signal is connected directly to MK104-16 for controlling the fan while **/OT** is brought to the CPLD for latching, AND-ing with the other faults signals for tripping and LED signaling. A double comparator (MAX932) with adjustable built-in hysteresis and internal reference is used.

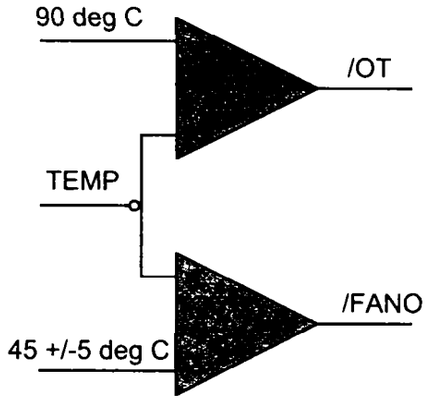

Figure 6.8 The overtemperature protection implemented on the IPC

SMPS check. VLOG signal is compared against 4.75V and 5.25V window generating **VLOV** (high if VLOG > 5.25V) and **VLUV** (high if VLOG < 4.75V) – see Figure 6.9.

The two comparators are supplied from VPOS and it works only if for some reasons, VLOG is out of range, but VPOS is still alive. A tripping out of range signal VLOR (active high) is generated by OR-ing VLUV and VLOV which is brought also to the CPLD for latching, AND-ing with the other faults signals for tripping and LED signaling.

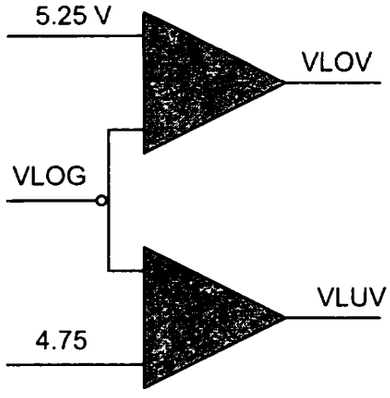

Figure 6.9 The SMPS check implemented on the IPC

All tripping signals are AND-ed in a general **TRIP** signal, and then AND-ed with active low **COAST**, active low manual trip (**MT**) signals to generate an active high **ENABLE** signal for gate signals conditioning.

6.2.3 Line filter

Between grid converter and the grid itself a line filter was introduced to protect the inverter and to reduce the higher harmonic content in the line current, produced by the switching. This is in fact a simple *L*-filter. An *LC* or an *LCL* filter could be used, but the *L*-filter was chosen for simplicity. The frequency response of the *LCL* filter has a resonance peak, so the latter has to be designed such that the resonance peak not to interfere with the frequency response of the inverter output voltage; alternatively, a series resistor must be inserted to damp the resonance peak.

The value for the inductance per limb was chosen 13 mH, and is depending by the grid and the power rating of the turbine. A rather good design value for the inductance in the filter is [2]:

$$L = \max\left(\frac{v_\vartheta}{\vartheta\omega_1 i_\vartheta}\right)$$

where ϑ is the order of the harmonic and v_ϑ the phase RMS value of the output phase voltage harmonic.

6.2.4 Voltage and current sensors

As can be seen in Figure 6.1, 6 currents and 3 voltages were acquired to fulfill the control system requirements. These are:

- 2 rotor currents (the third is calculated in the software taking into account that the sum of them is zero)

- 2 stator currents (the third is calculated in the software taking into account that the sum of them is zero)
- 2 grid currents on the grid-side converter side (the third is calculated in the software taking into account that the sum of them is zero)
- DC voltage
- 2 grid voltages line-to-line which are in fact also the stator voltages (the phase voltages are calculated later in the software from the line voltages)

Thus the acquisition system was designed. It includes:

- 3 small boards with 2 current sensors each - type LEM LA 55-P with adequate signal conditioning such that at 10A measured current the sensor output will be 10V, required for the control system's A/D channels.
- a voltage measurement box with 3 voltage transducers type LEM LV 25-P with appropriate signal conditioning such at 500 V measured voltage the output of the sensor is 10 V, required for the control system's A/D channels.

6.2.5 Position sensor

To prove the sensorless position estimation techniques, a position estimator had to be included in the system. The chosen device was an Telemecanique encoder type XCC which provides a resolution of 5000 lines per revolution. The output is a usual A QUAD B (A+, A-, B+, B-, N+, N-) which can be directly connected to the control system as it provides encoder interfaces.

6.2.6 Control Hardware

The **DS1103 PPC** is a very flexible and powerful system featuring both high computational capability and comprenhensive I/O periphery (see Figure 6.10). Additionally, it features a software SIMULINK interface that allows all applications to be developed in the Matlab/Simulink friendly environment. All compiling and downloading processes are carried out automatically in the background.

An experimenting software called Control Desk. allows real-time management of the running process by providing a virtual control panel with instruments and scopes.

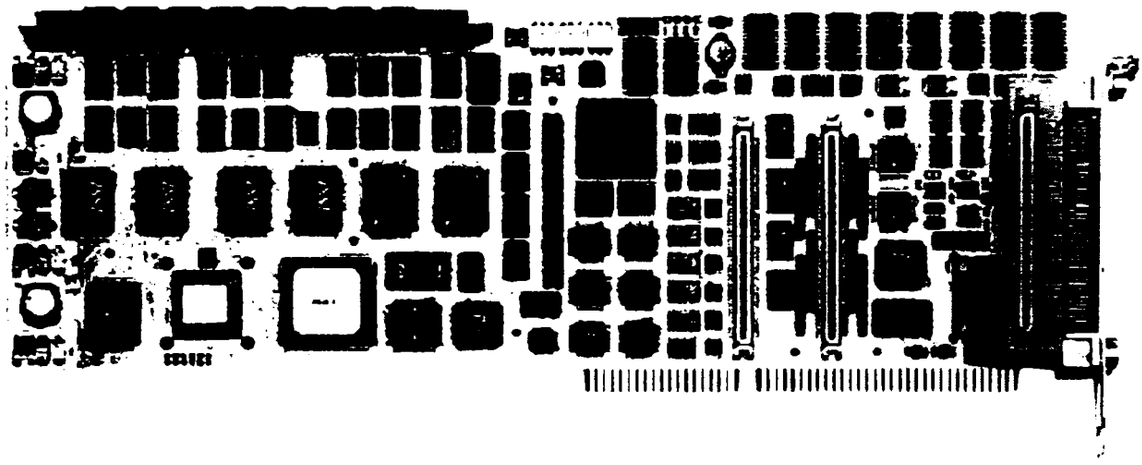

Figure 6.10 The single board control system dSpace DS 1103

The DS1103 is a single board system based on the **Motorola PowerPC 604e/333MHz** processor (PPC), which forms the main processing unit.

Figure 6.11 gives an overview of the functional units of the DS1103.

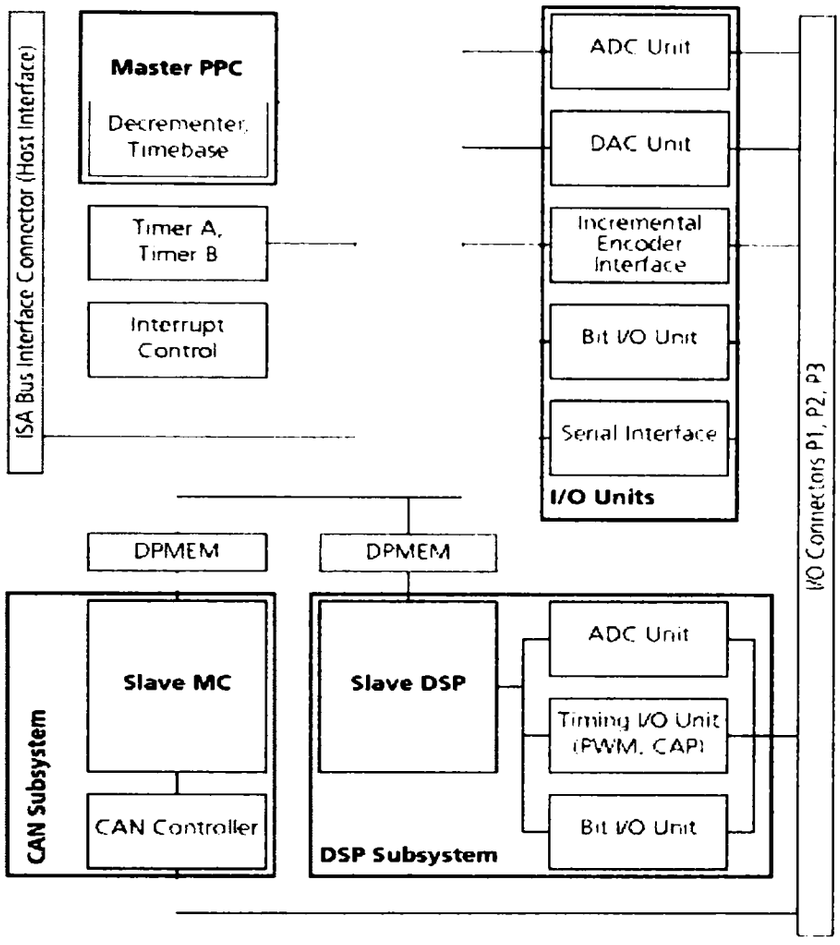

Legend:

ADC	Analog/Digital Converters
MC	CAN Microcontroller 80C164
CAP	Capture
DAC	Digital/Analog Converters
DPMEM	Dual-Port Memory
DSP	Digital Signal Processor TMS320F240
PPC	Power PC 604e Processor
PWM	Pulse Width Modulation

Figure 6.11 DS1103 internal functional block diagram

I/O Units

A set of on-board peripherals frequently used in digital control systems has been added to the PPC. They include: analog-digital and digital-analog converters, digital I/O ports (Bit I/O), and a serial interface. The PPC can also control up to six incremental encoders, which allow the development of advanced controllers for robots.

DSP Subsystem

The DSP subsystem, based on the Texas Instruments TMS320F240 DSP fixed-point processor, is especially designed for the control of electric drives. Among other I/O capabilities, the DSP provides 3-phase **PWM generation** making the subsystem useful for **drive applications**.

CAN Subsystem

A further subsystem, based on Siemens 80C164 micro-controller (MC), is used for connection to a CAN bus.

Master PPC Slave DSP Slave MC

The PPC has access to both the DSP and the CAN subsystems. Spoken in terms of inter-processor communica-tion, the PPC is the master, whereas the DSP and the CAN MC are slaves.

The DS1103 PPC Controller Board provides the following features summarized in alphabetical order:

- **A/D Conversion**

ADC Unit providing:

- 4 parallel A/D-converters, multiplexed to 4 channels each, 16-bit resolution, 4 μs sampling time, ± 10V input voltage range

- 4 parallel A/D-converters with 1 channel each, 12-bit resolution, 800 ns sampling time ± 10V input voltage range

Slave DSP ADC Unit providing:

- 2 parallel A/D converters, multiplexed to 8 channels each, 10-bit resolution, 6 µs sampling time ± 10V input voltage range

- **Digital I/O**

Bit I/O Unit providing:

- 32-bit input/output, configuration byte-wise

Slave DSP Bit I/O-Unit providing:

- 19-bit input/output, configuration bit-wise

- **CAN Support**

Slave MC fulfilling CAN Specifications 2.0 A and 2.0 B, and ISO/DIS 11898.

- **D/A Conversion**

DAC Unit providing:

- 2 D/A converters with 4 channels each, 14-bit resolution ±10 V voltage range

- **Incremental Encoder Interface**

Incremental Encoder Interface comprising:

- 1 analog channel with 22/38-bit counter range,
- 1 digital channel with 16/24/32-bit counter range, and
- 5 digital channels with 24-bit counter range.

- **Interrupt Control** - Interrupt Handling.
- **Serial I/O**

Serial Interface providing:

- standard UART interface, alternatively RS-232 or RS-422 mode.

- **Timer Services**

Timer Services comprising:

- 32-bit downcounter with interrupt function (Timer A),
- 32-bit upcounter with pre-scaler and interrupt function
- 32-bit downcounter with interrupt function (PPC built-in Decrementer), and
- 32/64-bit timebase register (PPC built-in Timebase Counter).

- **Timing I/O**

Slave DSP Timing I/O Unit comprising:

- 4 PWM outputs accessible for standard Slave DSP PWM Generation,
- 3 x 2 PWM outputs accessible for Slave DSP PWM3 Generation and Slave DSP PWM-SV Generation,
- 4 parallel channels accessible for Slave DSP Frequency Generation, and
- 4 parallel channels accessible for Slave DSP Frequency Measurement (F2D) and Slave DSP PWM Analysis (PWM2D).

6.2.7 Interface system

An interface board was designed in order to use the PWM outputs of the slave DSP unit for controlling the IGBT drivers of the both inverters.

It contains 8 pcs. SFH 750 fiber optic emitters (3 SPWM+ 1 ENABLE for each inverter) and a SN74HCT541 non-inverting octal buffer to increase the DS1103 PWM signals current capability according to SFH750 optic fiber driver requirements (see Figure 6.5). Additionally, series connected LED mounted on the front panel display the logic state of the optic fiber signals.

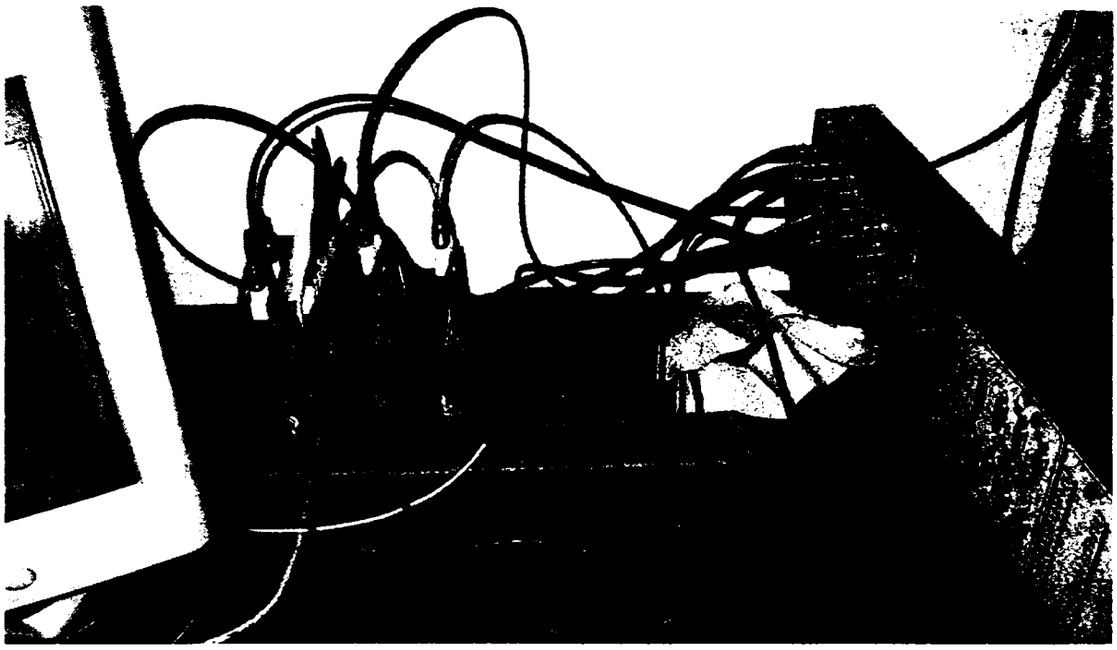

Figure 6.12 The interface system (the boards with current sensors and with fiber optic emmiters are visible. In the right side the terminal of the dSpace

6.3 Software

All the software was developed under Simulink environment, compiled automatically using Microtec C compiler for Motorola Power PC and Texas Instruments C compiler and built/downloaded automatically using the dSpace system specialized MLIB/MTRACE mechanism.

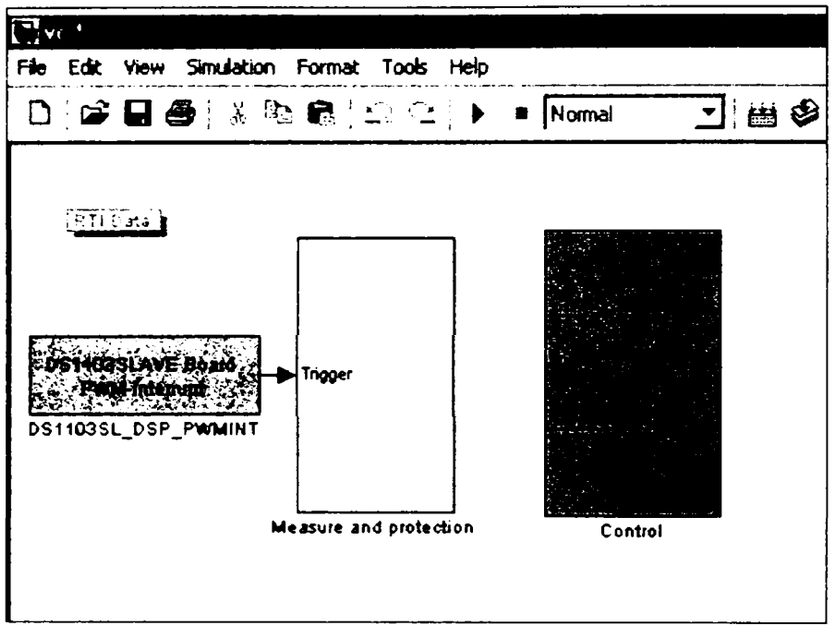

Figure 6.13 The Simulink software (measure and protection + control)

The software is divided in two major parts (see Figure 8):

- measure and protection where acquisition, software signal conditioning and software protection are made

- vector control and estimation algorithms. This part is also divided in two major parts: grid-side converter (GSC) control and machine-side converter (MSC) control.

6.3.1 Measure and protection software

The measure and protection is the first main part of the developed software and has three main parts:

- acquisition software
- scaling and digital filtering of the acquired signals
- encoder interface
- protection

In the acquisition software the ADC channels are settled for acquiring the above discussed 6 currents and 3 voltages. The grid and rotor currents are acquired on the 4 nonmultiplexed A/D channels with 12-bit resolution, 800 ns sampling time. The rest

of the currents and voltages are acquired on the multiplexed channels with 16-bit resolution, 4 μs sampling time. The acquisition process is triggered with the help of the slave-DSP timer interrupt with the same frequency as the switching (10 kHz) and at the 10% of the PWM pulse period (see Figure 6.13).

Afterwards the measured quantities are scaled taking into account the scaling factors of the sensors and filtered with a low-pass filter with a time constant of 10 ms. Also here the third current in each case is calculated from the other two measured.
In the encoder interface the position of the rotor and its speed are calculated. This could be done counting the pulses coming on the dedicated hardware interface and knowing the resolution of the encoder (number the pulses for one revolution) and the sampling time the encoder is "readed" with.

In the software protection part all the desired protection for the inverter/generator are designed.

In the present case 6 protections were implemented: overcurrent in the rotor; overcurrent in the grid; overcurrent in the stator; overvoltage in DC link; undervoltage in DC link: overspeed. The implementation is done as follows: the measured quantities are compared with the threshold values and the negated output of the comparators passed through an OR gate together with the ENABLE signal. Thus the output is inhibited with any of the measured values exceeds its threshold value.

6.3.2 The grid-side converter control software

The grid-side converter is used to control the DC link voltage and the input power factor regardless of the level and the direction of the rotor power (Figure 6.14). A vector control strategy in stator voltage reference [3] frame is employed for this purpose. The converter is current regulated with the direct axis current used to control the DC-link voltage, meanwhile the transverse axis current is used to regulate the displacement between the voltage and the current, and thus the input power factor [4], [5].

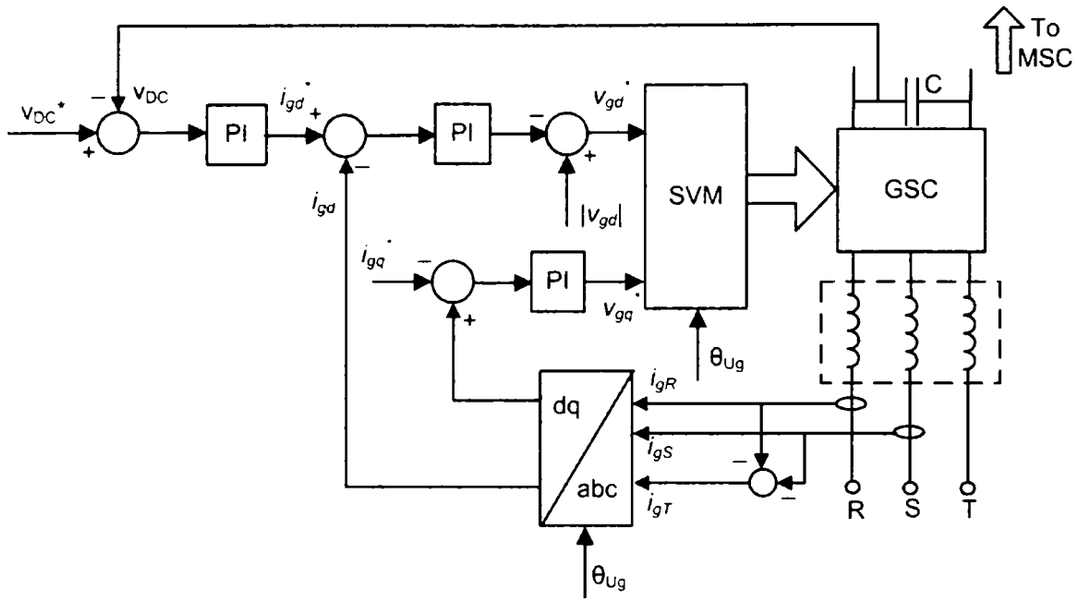

Figure 6.14 The grid-side converter control (GSC)

The phase voltages are calculated from the line voltages (see Figure 6.15) and the $\alpha\beta$ components of the grid voltage are calculated from the phase voltages. Finally, the angle of the grid voltage is extracted [6]:

$$\theta_c = \tan^{-1} \frac{v_{s\beta}}{v_{s\alpha}}$$

This can also be done with more complex structures like filters, PLL, controllers.

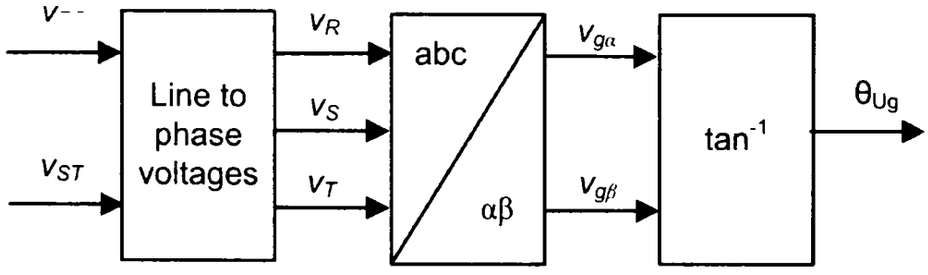

Figure 6.15 The computation of the grid voltage angle used for the coordinate transformations and for the SVM on the grid side converter control.

There are three parts in which the software for controlling the grid-side converter is divided (see Figure 6.16 a): computation of grid voltage angle $\hat{\theta}_c$, see above; vector control and coordinate transformation for calculation of i_{gd} and i_{gq}

(Figure 6.14); space vector modulation and dead-time compensation for calculation of the duty-cycles required for the slave-DSP PWM generation. Those are implemented in a C S-Function. The inputs are the DC voltage, the components α and β of the reference voltage vector and the measured phase currents for dead-time compensation purposes. The outputs of the function are the duty-cycles "ordered" to the slave-DSP which generates the PWM signals for the inverter with the specified switching frequency.

The GSC control software implementation using Simulink is illustrated in Figure 6.16 a. A real-time interface was implemented in the dedicated Control Desk environment for the control and the management of the control software for GSC. A screenshot is presented in Figure 6.16 b.

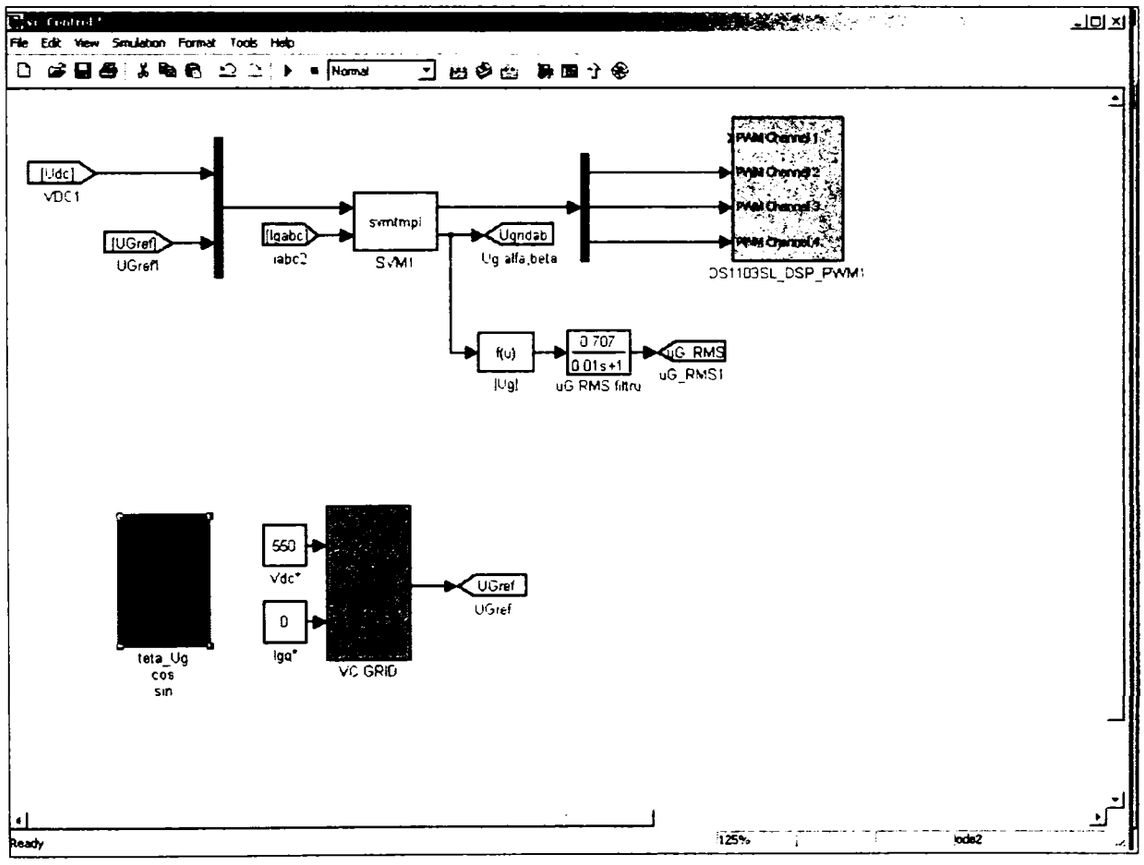

a)

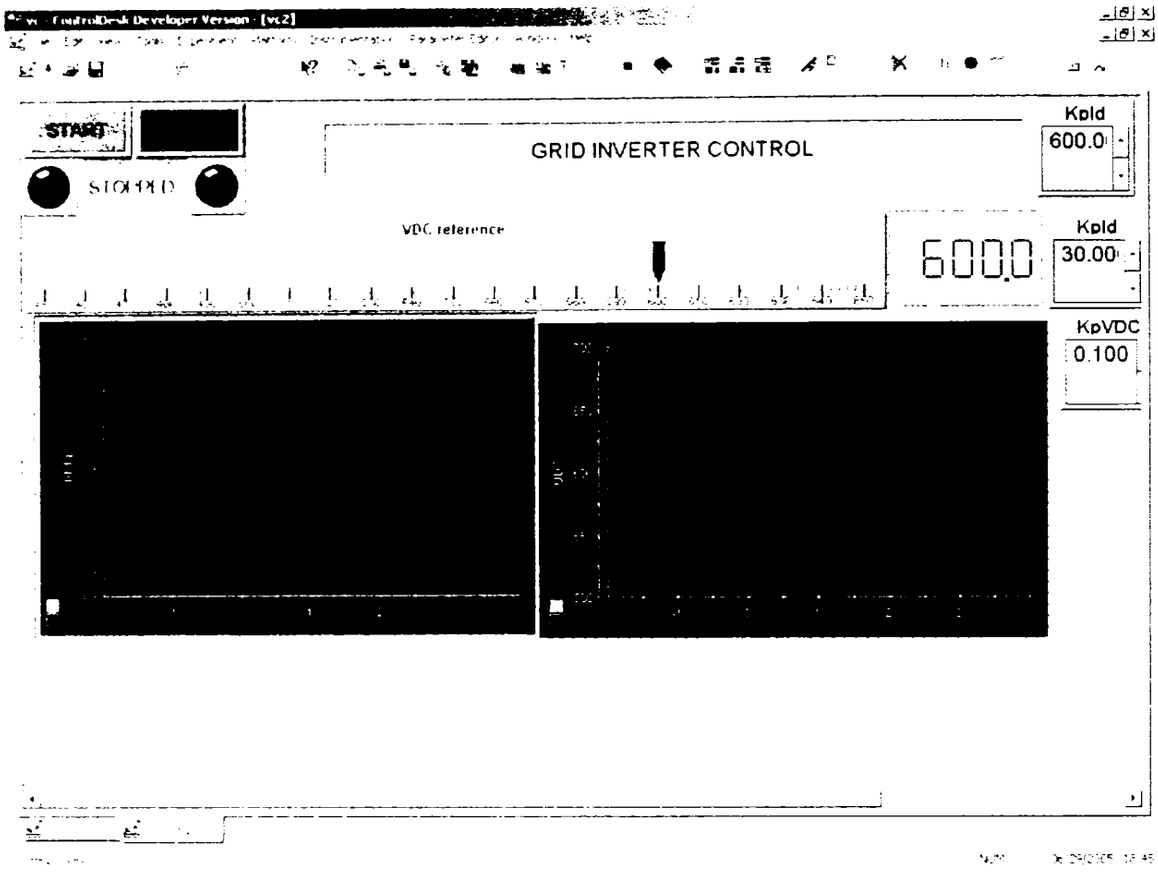

b)

Figure 6.16 The Simulink GSC control software a), and real-time interface b)

6.3.3 The machine-side converter control software

The generator is controlled in synchronous reference frame, with the *d*-axis aligned with the stator-flux vector, which ensures decoupled control between the electromagnetic torque and the rotor excitation contribution [7]. The control strategy block diagram is shown in Figure 6.17.

In fact controlling the rotor currents i_{rd} and i_{rq} the fast decoupled control of the stator reactive and active power is obtained [8,9]. The rotor currents are measured in their natural frame (rotor coordinates) and transformed into synchronous frame using the slip angle $\hat{\theta}_{slip}$. Reference voltages generated by the current control loops are

transformed back to the rotor reference frame, using the same angle $\hat{\theta}_{slip}$ [10]. Standard space vector modulation is employed to generate the pulses for the inverter.

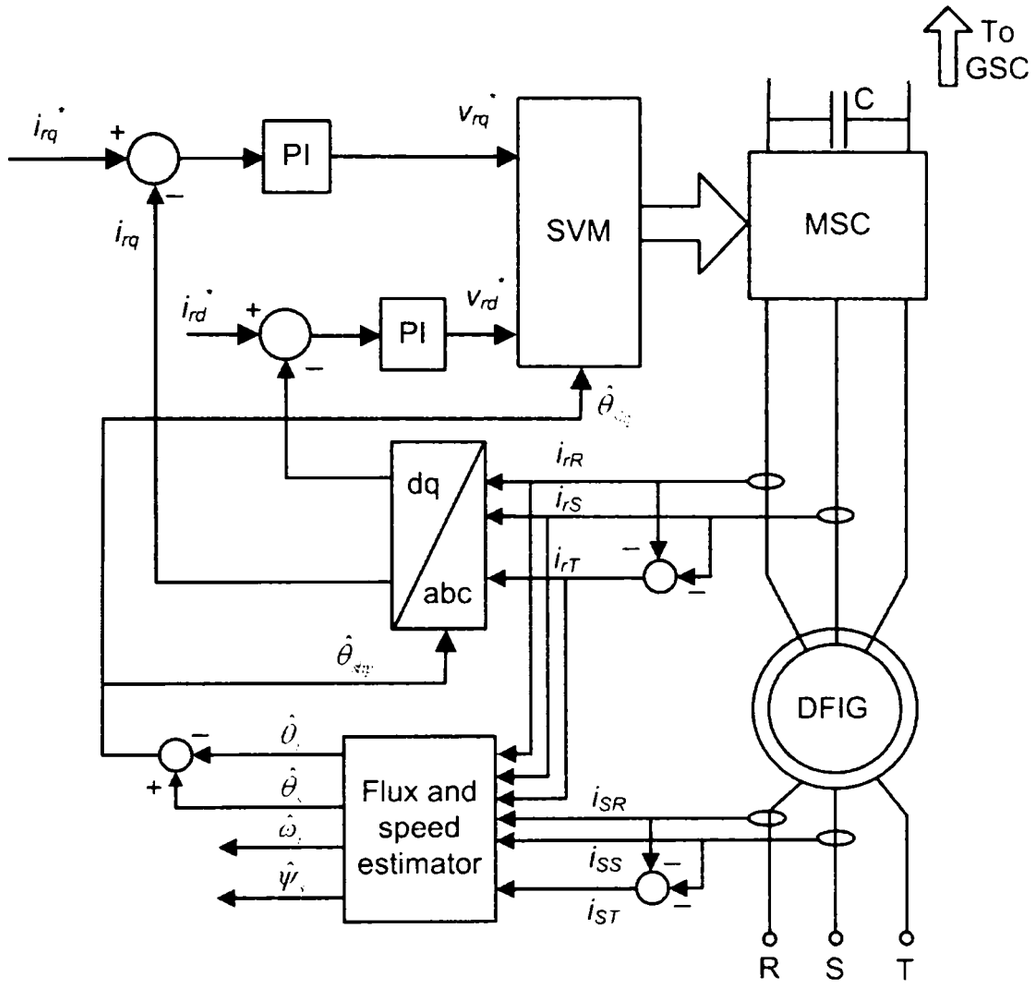

Figure 6.17 The machine-side converter control (MSC)

There are six parts in which the software for controlling the machine-side converter is divided (see Figure 6.18 a):computation of the angle $\hat{\theta}_{slip}$: stator flux estimator with the voltage and current models connected in parallel; stator flux estimator with the voltage and current models connected in series; MRAS algorithm for rotor position and speed observation; vector control and coordinates transformation for calculation of the i_{rd} and i_{rq} ; space vector modulation and dead-time compensation for calculation of the duty-cycles required for the slave-DSP PWM generation. This is identical with the procedure described at the GSC converter software – see the final of previous paragraph.

The implemented Simulink software for control of the MSC is illustrated in Figure 6.18 a) and the Control Desk real-time management interface for the control software is shown in Figure 6.18 b)

The detailed discussions with "in extenso" experimental results about the both vector controls, flux estimators and MRAS used during this project are given in [11].

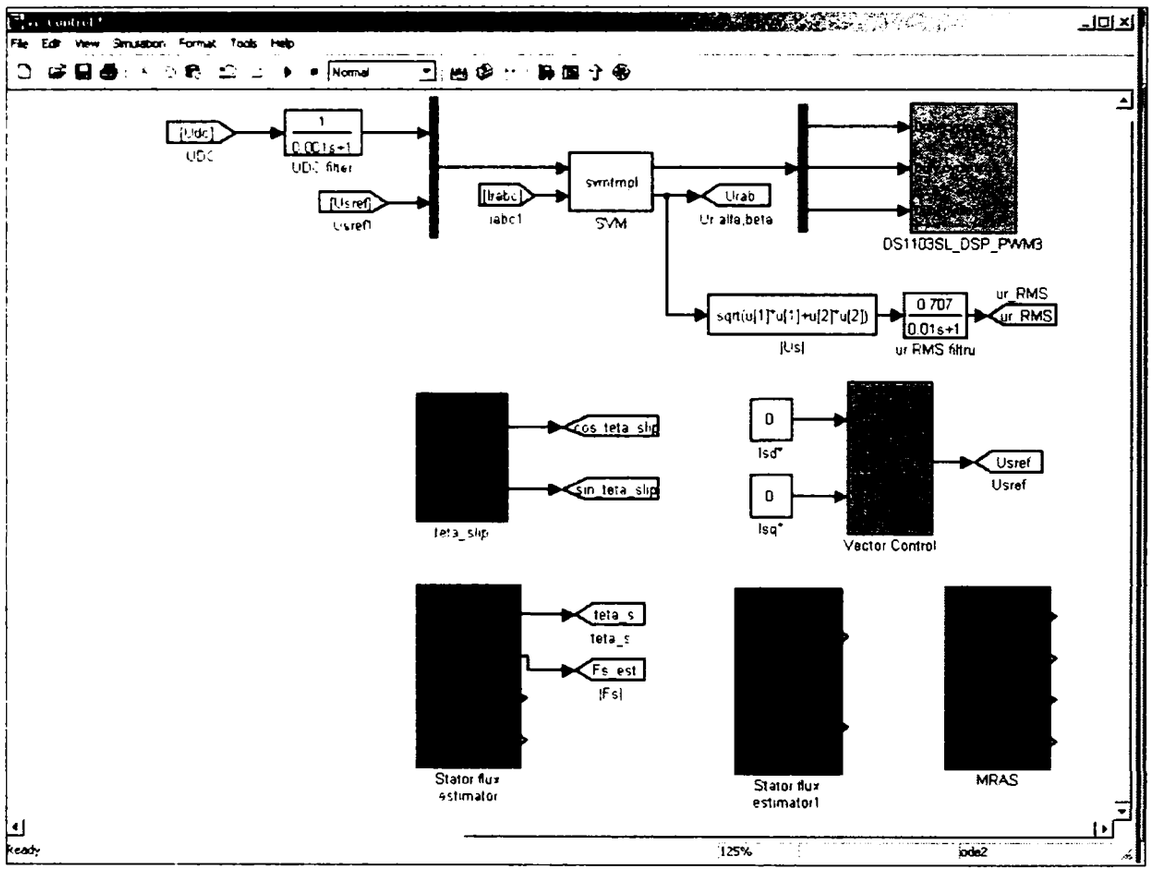

a)

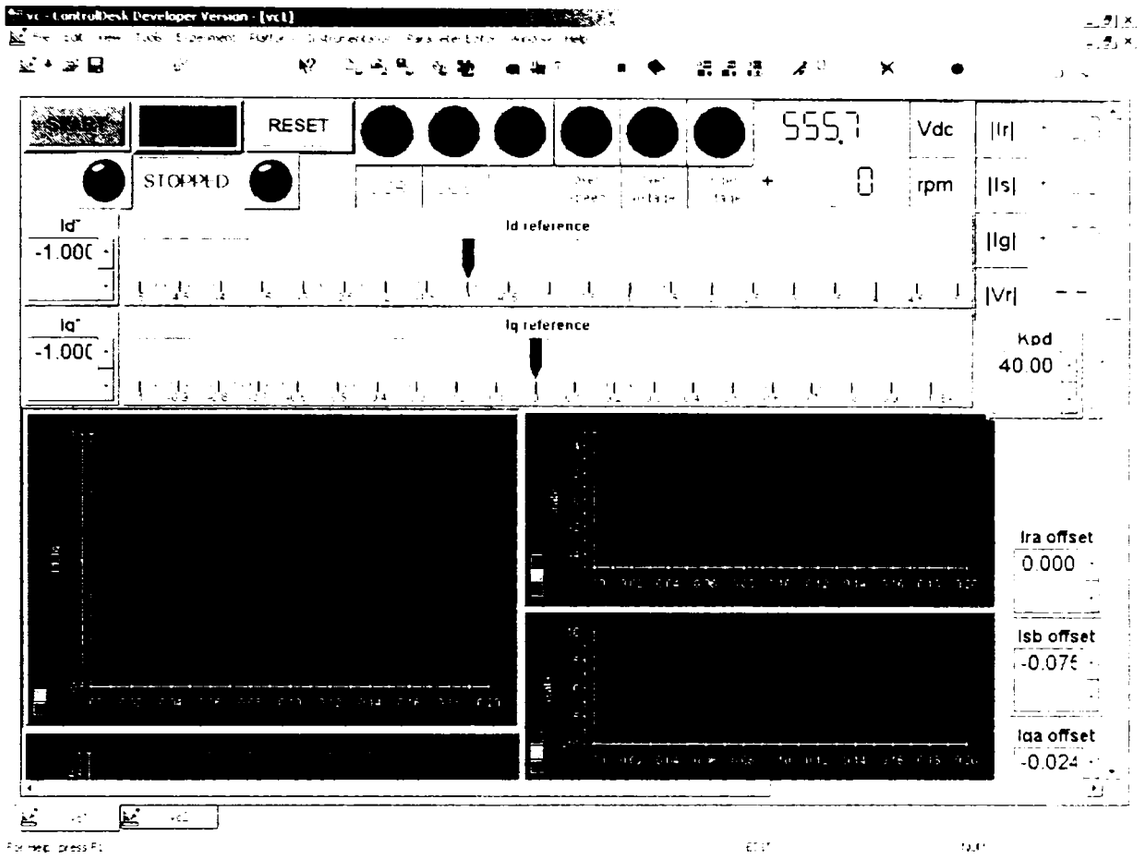

b)

Figure 6.18 MSC control software a) and real-time Control Desk Interface b)

Conclusion

The experimental test platform used during the tests of state observers and sensorless control of a variable speed doubly-fed induction generator system was presented in this chapter.

The main application for this system is wind power, but the platform is also suitable to investigate the motion-sensorless control of pump-storage hydro-turbine doubly-fed induction generator/motor, from selfstarting and synchronization freely within the design speed range to sub- and over-synchronous motoring (pumping) and generating.

The platform is also suitable to characterized the motion-sensorless doubly-fed induction motor limited speed range 4-quadrant large drives.

All the hardware components of the system were presented, discussed and analyzed. The software used for measurements and protections, signal conditioning, vector control for both inverters, flux estimators and MRAS position-speed observation is explained.

References

[1] R. Teodorescu, "Getting Started with dSpace system," *Flexible Drives System Laboratory (FDSL) Reference Manual*, Version 1.0, Institute of Energy Technology, Aalborg University, Denmark

[2] M. Lindholm, "Doubly-Fed Drives for Variable Speed Wind Turbines," *Ph.D. Thesis*, Technical University of Denmark,

[3] I. Serban, F. Blaabjerg, I. Boldea, "Sensorless doubly-fed induction generator control under power system transients and faults: the influence of magnetic saturation", *Proc. of OPTIM 2004*, Brasov, Romania, vol. 2, pp. 311-318, May 2004.

[4] R. Datta, V.T. Ranganathan, "Direct power control of grid-connected wound rotor induction machine without rotor position sensors," *IEEE Transactions on Power Electronics*, vol. 16, no. 3, May 2001, pp. 390-399.

[5] L. Morel, H. Godfroid, A. Mirzaian, J.M. Kauffmann, "Double-fed induction machine: converter optimization and field oriented control without position sensor," *IEE Proc. on Electric Power Applications*, vol. 145, no. 4, July 1998, pp. 360-368.

[6] I. Serban, F. Blaabjerg, I. Boldea, Z. Chen, "A study of the doubly-fed wind power generator under power grid faults," *Proc. of EPE 2003*, Toulouse, France, 2003.

[7] U. Rädel, D. Navarro, G. Berger, S. Berg, "Sensorless field-oriented control of a slipring induction generator for a 2.5 MW wind power plant from Nordex Energy GmbH," *Proc. of EPE 2001*, Graz, 2001.

[8] S. Müller, M. Deicke, R.W. De Doncker, "Adjustable speed generators for wind turbines based on double-fed induction machines and 4-quadrant IGBT converters linked to the rotor," *2000 IEEE-IAS Annual Meeting Conf. Record*, vol. 4, pp. 2249-2254, Oct. 2000.

[9] R. Datta, V.T. Ranganathan, "A simple position-sensorless algorithm for rotor-side field-oriented control of wound-rotor induction machine," *IEEE Transactions on Industrial Electronics*, vol. 48, no. 4, Aug. 2001, pp. 786-793.

[10] G.D. Andreescu, "Position and speed sensorless control of PMSM drives based on adaptive observer," *Proc. of EPE '99*, Lausanne, Switzerland, Aug. 1999.

[11] Ioan Serban, Gheorghe-Daniel Andreescu, Lucian Tutelea, Cristian Lascu, Frede Blaabjerg, Ion Boldea, "State Observers and Sensorless Control of Wound Rotor Induction Generator (WRIG) at Power Grid with Experimental Characterization," *will be published*, 2005

Chapter 7

Conclusion and contributions

7.1 Conclusion

The present work was dedicated to the advanced control of the variable speed generators.

The main application for this system is wind power, but the platform is also suitable to investigate the motion-sensorless control of pump-storage hydro-turbine doubly-fed induction generator/motor, from selfstarting and synchronization freely within the design speed range to sub- and over-synchronous motoring (pumping) and generating.

The platform is also suitable to characterized the motion-sensorless doubly-fed induction motor limited speed range 4-quadrant large drives.

The thesis focused on several major topics like:

- variable speed concept of electric generators;
- hydro power applications;
- wind power applications;
- doubly-fed induction generator system (with cycloconverter or back-to-back inverter in the rotor circuit) as the main candidate for the hydro power generation applications;
- doubly-fed induction generator system (with back-to-back inverter in the rotor circuit) as the main candidate for the wind power generation applications;
- behavior of the DFIG system during power grid faults (shortcircuits);
- improvement of the performance of the DFIG system during power grid faults;
- sensorless robust vector control of the DFIG system including during power grid faults;

- experimental sensorless motoring control of the system with the machine having the stator short-circuited;
- experimental new state observers and sensorless control of the DFIG system.

The experimental new state observers and sensorless control of the DFIG system is also the central main topic of the present work.

In relationship with these topics the main conclusion are as follows:

- the variable speed concept was introduced by the wind energy, but is extremely useful also for hydropower generators, for adding more flexibility to the generator (synchronous generators used mainly in hydropower applications are totally inflexible due to the constant speed they should work at);
- constant attention is paid nowadays for introducing flexibility into the power systems. Flexible AC transmission systems (FACTS) were introduced and developed , but the generators should also become flexible, and the constant speed electric generators are not the proper solution for this;
- from the hydro turbine point of view a 10% increase of efficiency could be obtained by using the variable speed electric generators. This was proved in the hydropower applications in Japan with pump storage (including the biggest generator in the world: 400MW with doubly-fed induction generator/motor with cycloconverter in the rotor circuit) and in two similar applications in Germany at Goldisthal on the river Schwarza in the south Thüringen;
- the wind energy technology is the fast growing technology in the world during the last century. From 1995 on, the worldwide installed capacity doubled every three years and according to estimations it will grow annually with 25%.
- in the wind power applications the doubly-fed induction generator with two back-to-back inverters in the rotor circuit is a proved, robust and widely considered solution having in the present 47% of the world market share of wind turbine concepts and the market is growing. The present thesis is dedicated especially to the control of the doubly-fed induction generator;
- due to the higher and higher penetration of the wind power into the power system, according to the latest regulations, the high power wind turbines

should remain on during faults (shortcircuits) in the power grid. This is called "ride through fault" capability. This is necessary for re-establish rapidly the voltage in the power system immediately after the fault is cleared, in order to avoid voltage drops and oscillations. Thus, special measures should be taken in order to protect the power electronics and the generator from damaging;

- under power grid faults, another serious problem appears in the case of sensorless control. The algorithm for calculation of the rotor position should take into account the variation of the parameters of the machine, especially of the magnetizing inductance (L_m). If the magnetic saturation is not taken into account in the sensorless algorithm, during the power grid shortcircuit a huge error appears in the estimation of the rotor position, the vector control is lost and, finally, the generator should be disconnected from the power grid. That's why special attention should be paid to the sensorless algorithm and especially, magnetic saturation should be taken into account in order to be sure the algorithm is accurate during all the faulty situations could appear;
- the doubly-fed induction motor setup (with the same back-to-back inverters connected in the rotor circuit but with shortcircuited stator) has fast responses during fast references speed references, and high braking capabilities due to the grid-side inverter and its control, which injects fast the power back to the grid during braking periods. Also with the state observers and the sensorless algorithm developed during this investigation (see Chapter 4), the estimation of the rotor position is satisfactory down to 5 rpm;
- the experimental DFIG setup shown fast and accurate active and reactive power control. The state observers and the sensorless algorithm should be accurate on all speed range, including at synchronism, and during the start-up and synchronization procedure;
- The platform, beyond the sensorless wind power applications and motoring/generating pump-storage hydro power application, is suitable also for motion-sensorless doubly-fed induction motor limited speed range 4-quadrant large drives.

7.2 Original contributions

The present thesis includes, from the author, point of view, the following original contributions:

- overview of the systems with variable speed generators and their applications in renewable energy: wind, hydro, tides and marine currents;
- simulation under Simulink® environment of the whole 2 MW DFIG system, as one of the most preferred solution for wind power applications. The simulation includes the models of the wind turbine, DFIG itself and the both inverters each of them with its vector control;
- simulation and analysis of the 2 MW DFIG system behavior under power grid shortcircuit;
- development of a possible method for improving the performance of the DFIG system, under power grid shortcircuit, without disconnecting the generator from the power network;
- development and analysis of a sensorless algorithm for DFIG system, with fast and accurate rotor position estimation including under power grid shortcircuit (taking into account the magnetic saturation, mandatory under such faulty conditions);
- implementation of the 3kW DFIM setup (with 2 back-to-back inverters in the rotor circuit & shortcircuited stator), with advanced experimental characterization: fast dynamic responses with regenerative braking control of the grid-side inverter, accurate state observers and rotor position estimation down to 5 rpm;
- implementation of the 3kW DFIG setup with "in extenso" experimental analysis & results: fast rotor current control (and, in fact, the control of active and reactive power in the stator), state observers fast and accurate over the entire speed range and on all possible working regimes including start-up and network synchronization.

Summary in Romanian

Sumar

Teza de fata este dedicata controlului de inalta performanta al generatoarelor cu turatie variabila pentru aplicatii avand ca sursa primara energii regenerative in general si pentru aplicatii cu turbine de vant in special. Astfel, teza ofera cateva solutii moderne pentru controlul generatorului de inductie dublu-alimentat cu invertor bidirectional conectat in circuitul rotoric, ca si solutie principala pentru acest tip de aplicatii.

La sfarsitul anilor 90 energia vantului a devenit cea mai importanta resursa de energie inepuizabila. In ultima decada a secolului 20, in intreaga lume capacitatea instalata a turbinelor eoliene s-a dublat la aproximativ fiecare 3 ani iar costul electricitatii provenite de la energia vantului a scazut la aproximativ 1/6 din costul avut la inceputul anilor 80. Iar in zilele noastre, capacitatea cumulata este in crestere pe plan mondial cu aproximativ 25% in fiecare an. Actualmente, 5 tari – Germania, SUA, Danemarca, India si Spania detin impreuna mai mult de 83% din capacitatea instalata in lume, dar utilizarea energiei vantului se extinde rapid si in celelate zone, iar tehnologia aferenta a devenit extrem de complexa. Ea implica discipline tehnice precum aerodinamica, dinamica structurilor, mecanica, masinile electrice, electronica de putere, electronica de semnal, teoria sistemelor si controlul automat.

Obiectivul principal al tezei este de e oferi noi solutii performante in domeniul controlului generatorului de inductie dublu alimentat cu invertor bidirectional in circuitul rotoric, solutie care detine la ora actuala mai mult de jumatate din cota de piata mondiala a generatoarelor electrice utilizate de turbinele eoliene si tendinta este in continuare in plina crestere.

Un subiect amplu dezvoltat in teza este controlul fara senzori de miscare (sensorless) al generatorului dublu-alimentat in conditii de avarie a retelei pe care acesta este conectat. Acesta este un subiect extrem de actual, deoarece datorita cresterii masive a prezentei turbinelor de vant in sistemul energetic, ultimele reglementari prevad ca generatoarele de vant sa ramana conectate in timpul

scurtcircuitelor pe reteaua de alimentare, pentru ca dupa eliminarea scurtcircuitului sa se poata restabili rapid si fara perturbatii tensiunea in nodul energetic aferent. Aceasta insa implica luarea unui set de masuri suplimentare pentru prevenirea avariei electronicii de putere sau a generatorului. Astfel o parte importanta a tezei a ocupat-o dezvoltarea de modele complexe de simulare a intregului sistem, analiza comportamentului sistemului in diferite conditii de avarie ale retelei si gasirea de solutii posibile pentru protectia echipamentului cu electronica de putere. Aceste activitati au fost efectuate in perioada de cercetare desfasurata de autor in cadrul "Institute of Energy Technology", Universitatea din Aalborg, Danemarca.

Partea experimentala in intregime a fost desfasurata in cadrul Laboratorului de Reglaj Inteligent al Miscarii, Facultatea de Electrotehnica, Universitatea "Politehnica" Timisoara, Romania.

2. Obiectivele tezei

Obiectivele urmarite in cadrul tezei au fost urmatoarele:

- oferirea unei imagini de ansamblu asupra solutiilor existente sau posibile in domeniul generatoarelor de vant pentru aplicatii care utilizeaza energii regenerative, incluzand masina primara, transmisia, generatorul electric, electronica de putere si reglajul automat;
- dezvoltarea de modele complexe si precise pentru generatorul de inductie dublu-alimentat si sistemele aferente;
- analiza specificatiilor din partea retelei electrice pe care sistemul este conectat, tot mai restrictive din cauza patrunderii masive a generatoarelor de vant in sistemele energetice;
- analiza comportarii sistemului cu generator de inductie dublu-alimentat la avarii ale retelei electrice, in special scurtcircuite si gasirea de solutii posibile pentru controlul si protectia convertorului cu electronica de putere;
- cresterea calitativa a controlului puterii active si reactive in toate circumstantele posibile;

- gasirea unei strategii de control fara senzori de miscare (sensorless), robusta si precisa in toate situatiile de functionare: conectarea la retea, functionare sub-sincrona, functionare la sincronism si supra-sincronism;
- investigarea posibilitatilor de auto-pornire ca motor si functionare in regim de motor, obligatorii in cazul micro-hidrocentralelor cu pompaj sau in cazul actionarilor in 4 cadrane cu domeniu de viteza limitat.

Organizarea tezei

Teza este organizata in 7 capitole, urmarind obiectivele mentionate anterior.

In *primul capitol* o privire de ansamblu asupra generatoarelor cu turatie variabila si a controlului lor este prezentata. Sunt prezentate detaliat atat solutii existente cat si posibile.

In *capitolul doi* modelele de simulare dezvoltate pentru analiza sistemului cu generator de inductie dublu-alimentat si invertor bidirectional in circuitul rotoric sunt descrise si discutate. Simularea comportarii sistemului in conditii de scurtcircuit a retelei electrice este prezentata. Este, de asemenea, introdusa o posibila solutie de control si protectie a convertorului static fara deconectarea sistemului de la reteaua electrica, conditie necesara conform reglementarilor actuale in sistemele energetice.

In *capitolul trei*, controlul sensorless de putere activa si reactiva al sistemului este ilustrat in detaliu. Scurtcircuitul retelei electrice este din nou simulat si analizat. Este in acest capitol dovedit ca in regimuri tranzitorii ale retelei de alimentare este imperios necesara luarea in considerare a saturatiei magnetice in algoritmul de calcul al pozitiei rotorului.

In *capitolul patru*, experimental, controlul sistemului in regim de motor este prezentat. O strategie sensorless este introdusa si discutata cu rezultate satisfactoare pana la 5 rpm. Standul fiind recuperativ, regimuri dinamice foarte bune sunt dovedite.

In *capitolul cinci*, experimental, controlul sistemului in regim de generare este prezentat. Doua observatoare de flux si un algoritm sensorless bazat pe un model de referinta adaptive (MRAS) au fost dezvoltate si testate. Rezultatele sunt ilustrate si discutate. Estimarea precisa a pozitiei si vitezei rotorului este dovedita in toate situatiile si pe toata gama de turatie.

Capitolul sase este dedicate standului experimental utilizat pentru toate testele iar in *capitolul sapte* o sinteza a tezei este prezentata iar contributiile si concluziile tezei sunt subliniate.

Contributii originale

Dupa parerea autorului, teza contine urmatoarele contributii originale:

- oferirea unei priviri de ansamblu asupra sistemelor cu generatoare cu turatie variabila, inclusive electronica de putere aferenta si controlul acestora. Descrierea este facuta in contextual aplicatiilor la care aceste sisteme se preteaza: turbine de vant, turbine hidraulice, sau chiar aplicatii mai putin conventionale: turbine care utilizeaza energia valurilor sau turbine submersibile pentru curenti marini sau oceanici.
- simularea sub mediul Simulink® a intregului sistem cu generator de inductie dublu alimentat avand puterea nominala de 2MW. Simularea include modelele turbinei de vant, generatorul propriu-zis si ambele invertoare conectate spate in spate in circuitul rotoric, fiecare avand propriul control vectorial.
- simularea si analiza comportarii sistemului de 2MW cu generator de inductie dublu-alimentat in conditii de scurtcircuit ale retelei
- dezvoltarea unei metode de imbunatatire a comportamentului sistemului DFIG, in conditii de scurtcircuit ale retelei, fara deconectarea sistemului de la reteaua energetica
- dezvoltarea si analiza unei metode de control fara senzori de miscare (sensorless) pentru sistemul DFIG, cu estimarea precisa a pozitiei rotorului inclusive in conditii de scurtcircuit ale retelei energetice (cu luarea in considerare in algoritmul de estimare a saturatiei magnetice, conditie obligatory, in cazul functionarii sistemului in conditii de scurtcircuit sau alte posibile avarii ale retelei)

- implementarea unui stand cu motorul de inductie dublu-alimentat avand puterea de 3 kW (aceeasi topologie cu generatorul de inductie dublu alimentat cu invertor bidirectional in circuitul rotoric, cu singura deosebire ca in acest caz statorul este scurtcircuitat). Este efectuata analiza experimentala amanuntita in special in ceea ce priveste regimurile dinamice rapide cu recuperare de energie, posibile in acest caz datorita controlul invertorului de pe retea, care pe perioadele de franare, scoate energia din circuitul intermediar de current continuu si o injecteaza in retea. De asemenea sunt dezvoltate noi observatoare de stare si un algoritm de control fara senzori de miscare, rapid si precis in estimarea pozitiei rotorului pana la turatii foarte mici (5 rpm)
- implementarea unui stand cu generatorul de inductie dublu-alimentat avand puterea de 3 kW si analiza experimentala amanuntita. Este obtinut controlul rapid si precis al curentilor rotorici (si de fapt prin acesti curenti, al puterii active si reactive din stator). Sunt dezvoltate noi observatoare de stare si un algoritm de control fara senzori de miscare, rapid si precis in estimarea pozitiei rotorului pe toata plaja de turatii si pe durata tuturor regimurilor de functionare, inclsuiv al pornirii si sincronizarii cu reteaua.

Curriculum vitae

Ioan Serban

Office

ebm-papst St. Georgen GmbH & Co KG
78112 St. Georgen
Germany
Phone: +49 7724 81 1834
Email: Ioan.Serban@de.ebmpapst.com

Home

Schönblickstr. 34
78112 St. Georgen
Germany
Phone: +49 7724 85 40 333
Email: Ioan.Serban@gmx.de

Education

2000	M.Sc degree in Power electronics and electric drives
1999	Dipl. degree in Electrical Engineering
1994-1999	University „Politehnica" of Timisoara, Timisoara, Romania Department of Electrical Engineering
1990-1994	Industrial Metallurgic High School in Hunedoara, Romania

Professional Experience

From 04.2005	ebm-papst St. Georgen GmbH / R&D Laboratory for Electric Drives (formerly PAPST-Motoren GmbH)

Personal Information

Born: March 10th, 1976
Family: Unmarried

Author's papers related to the Ph. D. thesis

Following papers related to this thesis were published or will be published very soon:

- I. Boldea, L. Tutelea, I. Serban, "Variable Speed Generators and Their Control", Proceedings of CNAE 2002, Galati, Romania.

- I. Serban, "Direct Power Control of Doubly-Fed Induction Generators", Proceedings of Summer Seminar of Nordic Network for Multi Disciplinary Optimised Electric Drives (NorMUD), 15-17 June 2002, Taipalsaari, Finland, pp. 64 – 68.

- I. Serban, I. Boldea, F. Blaabjerg, Z. Chen, "A study of the Doubly-Fed Wind Power Generator Under Power Grid Faults", Proceedings of EPE 2003, Toulouse, France

- I. Serban, I. Boldea, F. Blaabjerg, "Sensorless doubly-fed induction control under power system transients and faults: the influence of magnetic saturation", Proceedings of OPTIM 2004, Poiana Brasov, Romania

- I. Serban, G.D. Andreescu, C. Lascu, F. Blaabjerg, I. Boldea "Sensorless wound-rotor induction machine (WRIM): dual-converter motoring control with short-circuited stator", will be published soon.

- I. Serban, G.D. Andreescu, L. Tutelea, C. Lascu, F. Blaabjerg, I. Boldea, "New State Observers and Sensorless Control of Wound Rotor Induction Generator (WRIG) at Power Grid with Experimental Characterization", will be published soon

- I.Serban, D. Iles-Klumpner, I. Boldea, "Sensorless control of wound rotor induction generator (WRIG) for wind power applications: the experimental test platform", will be published soon.

VARIABLE SPEED ELECTRIC GENERATORS AND THEIR CONTROL: AN EMERGING TECHNOLOGY

Prof. Ion BOLDEA **Assist. Prof. Lucian TUTELEA**
Department of Electrical Machines and Drives, University Politehnica of Timisoara, V.Parvan 2, RO - 1900 Timisoara, Romania, Tel.+40-56-204402, E-mail: boldea@lselinux.utt.ro, lucian@lselinux.utt.ro

Ph.D. Student Ioan SERBAN
Department of Electrical Machines and Drives, University Politehnica of Timisoara, V.Parvan 2, RO - 1900 Timisoara, Romania, Tel.+40-56-204402, E-mail: serban@lselinux.utt.ro

Abstract: *The present paper presents recent progress on variable speed electric generators for applications ranging from: pump-storage hydroplants, windpower, Diesel gensets (mobile, UPS for trains or ships) to home electric power generation by linear generators driven by Stirling engines running on natural gas.*

Variable speed provides flexibility, more stability and better energy conversion ratio, so much needed in the flexible distributed power systems of the future or in standalone applications.

1. Introduction

Until not long ago the norm in electric generators was to use synchronous machines at constant speed to obtain constant frequency with regulated voltage output. Environmental and safety constraints and more demanding control requirements have led to variable speed generators electronically controlled for constant frequency and voltage. Wind power took the lead in this respect and there are now a few companies which manufacture doubly-fed induction wind generators at variable speed for higher wind energy extraction and better stability when the wind speed varies ±20% around a base (design) value [1].

Also, this time for power fast control in power systems with nuclear power plants, variable speed doubly fed induction generator-motors up to 330MW per unit have been put rather percently to service in pump-storage hydroelectric power plants [2].

It is only natural to assume that hydropower plants – existing or new, large or small – will take advantage of this technology in the future, to produce peak power in a fast-controlled manner for higher efficiency and with notable environmental benefits.

For distributed industrial power generation high speed combined cycle gas turbines should also use doubly-fed induction generators to cope with stability and control aspects while producing energy with minimum fuel consumption.

Power systems are today strained to the limit by transients and flexible ac transmission systems (FACTS) are proposed to bring more flexibility by parallel/and (or) series power electronics converters with or without storage or by intermediary full power dc power lines. The variable speed generators, in any power plant, even within ±5% speed range – with the power electronics designed at 5-10% rated power, as it feeds the rotor windings – should produce more flexibility to the power system at less costs, with lower harmonics pollution.

It is perhaps thinkable that not only the new generators for power systems will be variable speed, but, when retrofitting existing generators, the existing stator may be maintained and only the rotor core, windings and control will be changed.

All the above tasks should bring extraordinary opportunities for the research, development communities and for industries related to power system electric generators and their control.

Diesel electric trains and vessels are already using in some proportion, synchronous generators and d.c. comutator or a.c. (induction or synchronous) motors for propulsion.

The existing power electronics converters that control them are to be upgraded substantially based on the recent large power IGBT and MCT technologies.

Stand alone Diesel-engine or gas turbine gensets on the markets are still using synchronous generators with constant speed for constant frequency and controlled voltage. Doubly-fed induction generators with rotor-side power electronics at 20-30% rating or, more recently , PM synchronous generator with full power rating converters [4] are being proposed for tens and hundreds of kW. They may run at variable speed but at constant (or controlled, for the PM generator system) frequency and voltage. Faster power control and better efficiency characterize such new systems [4].

Traditionally avionics uses thermal engine – synchronous generators at high speed and 400Hz for auxiliary power. Constant speed control is implicit.

The gradual introduction of inverter fed driven electric actuators may impose a d.c. power bus, on board of aircraft. In this case a simple half-controlled rectifier at the terminals of a PM generator of high efficiency and small size, might become a strong new solution, to give only one example.

Electric generators on road and off road vehicles are required to deliver more and more electric power (actuators for comfort and better performance) to such an extent that the 42V d.c. power bus is by now recognized as the near future standard in automobiles.

If the power increases as generator, the question arises if it wasn't better to eliminate the electric starter andcombine both functions in an integrated starter generator [5]. Thus a "mild" hybrid vehicle working directly on 42V d.c. power bus is obtained. Besides, in "strong"hybrid or electric vehicles a larger motor-generator with 150-600V battery supply (or back up) is required.

The very wide generator constant power speed range (typical from 1000 to 6000rpm for M/G coupled directly to the crankshaft) and high starting (assist) torque required at tightly constraint motor volume, low costs and system low losses, make the design of such motor-generator systems and their control a formidable challenge for Academia and ..... y.

The mild or strong hybrid or electric vehicles are the way of the future. The first commercial hybrids of Toyota and Honda are a great success.

The induction machine used so far for the -cop- [5] i- -der se-ere s-ti-- -- th- lo--- a-- too high.

As the residential areas extend well outside the big cities or in villages with natural gas as the fuel for home heat production, it seems only natural to attempt to produce also electric energy in the home.

Free linear piston Stirling engines, stabilized recently , have been demonstrated to drive reliably (for more than 50000 hours on a prototype) a linear PM generator [6], of 350W at an efficiency above 85%, connected to the commercial power grid.

The low noise and low pollution level (natural gas is burned) of Stirling engine though with an efficiency of 15%, makes it a favourite candidate as a prime mover. For an 1 kW of electric power 7kW of heat power is produced, which corresponds to the order of magnitudes required for home heating systems. Either used as standalone systems or only to cover peak power needs such decentralized systems might gain popularity soon, because of overall larger energy efficiency, reliability, fast energy control and low total costs (energy distribution and delivery costs are eliminated). Now that we presented a panoramic view of variable speed generators let us introduce some sample competitive configurations and their performance, related directly to their application fields.

2. Variable speed wind-generator systems

The total of wind power generators existing in the world by the end of 1999 was 13,932 MW [7], with 3920 installed only in 1999.

Most commercial wind-turbine-generators up to 2 MW per unit, in general, consist of cage-rotor induction generators at power grid (or standalone) with active stall or pitch control of the turbine blade angles for power limitation and protection when wind speed gets too high, above 15 m/s. A soft-starter is used to connect the generator to the power grid with limited transients. Power factor compensation by step-switched capacitors at generator terminals is also common, Fig. 1 [8]. Still notable starting transient power pulsations remain due to wind gusts.

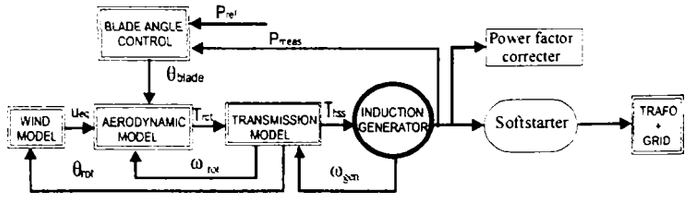

Fig. 1. Wind turbine induction generator system with blade angle control and soft-starter

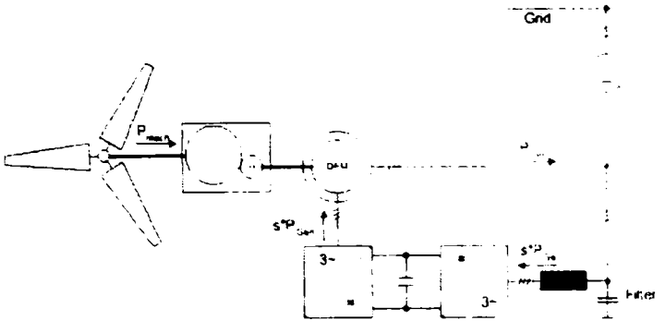

Fig. 2. Doubly-fed IG (DFIG) wind turbine system

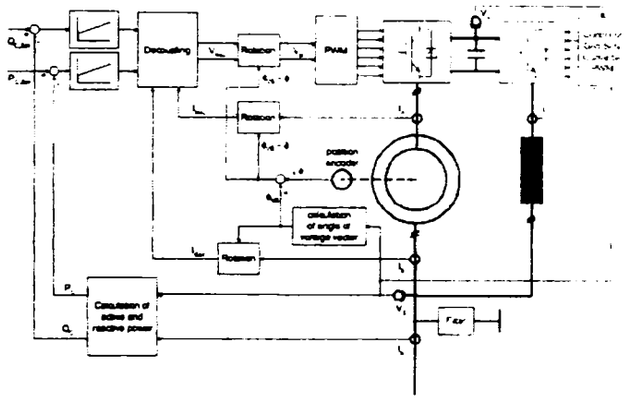

a)

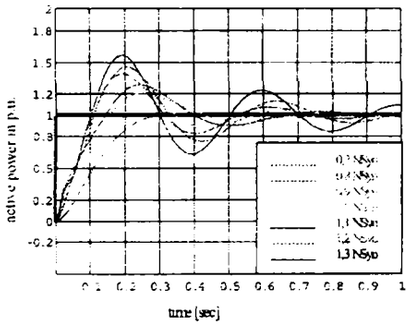

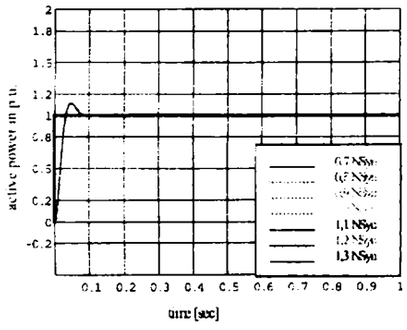

b)

Fig. 3. Vector control of DFIG a), and step active power response b), without and with decoupled control [1]

The introduction of the doubly-fed induction generator with 4 quadrant converter in he o o (F ـ. 2) [1] provides for variable speed operation at constant voltage and frequency and unity power factor.

Position sensorless schemes have been developed recently [11] that are capable of very good starting and loading performance.

Starting is performed from the rotor with the stator n shortcircuit (mode I). Then the stator is opened and the stator voltage, frequency and phase. are quickly "driven" to the power grid voltage vector reference through adequate machine-side rotor converter contro (mo e II). Mo e II s s ort- ve and thus the inertia holds the speed (Fig. 4) and then the machine is accelerated to the desired speed ,according to wind speed and load requirements.

The voltage adaptation transformer reduces the converter rating in relation to maximum speed.

The availability of rotor current feedback makes the flux and rotor position (and speed) observers more robust and simple than in usual sensorless drives. Still, the influence of IG magnetization inductance error has to be corrected to avoid unacceptable errors in rotor position estimation [11]. This only shows that there is more work to do, in this field.

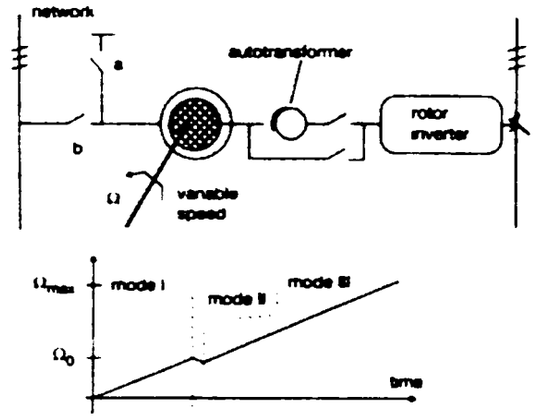

Fig. 4. Sensorless DFIG with operating modes I, II, III

Also system design optimisation approaches a far from a widel accepted methodology. The bidirectional power converter is still somewhat expensive and thus other , less expensive, configurations (even matrix converter) should be explored, especially as the power goes up. The literature abounds in DFIG theory, performance and

control [see Ref. 12 for a recent update]. For directly driven (at 16 rpm – 30 rpm) 2.0MW or more off shore units PM-rotor, high voltage stator (wind-formers from ABB) with diode rectifiers are proposed to transport the energy in d.c. form on shore, where a full power converter will deliver constant frequency and voltage output.

It may well be feasible above 1.5MW, even at such low speeds, to try using the DFIG with a large number of poles, as long as the pole pitch to airgap ratio τ/g >50, to keep the magnetization (reactive) power within reasonable limits.

3. Variable speed hydrogenerator systems

Pump storage necessities prompted by nuclear power usage led to the design and application of two rather large (310MW) power DFIGs; one with a cycloconverter and the other with a GTO inverter-converter in the rotor circuit (Table 1 [2]).

Though the total system costs seem to be 70-80% more than for constant speed pumping-generating system with d.c. rotor excitation control, DFIG brings quite a few advantages [13]

- optimum efficiency in pumping (above "synchronous" speed) and turbining (below "synchronous" speed)
- wider static and dynamic stability limits in motoring and generating at variable speed
- better selfsynchronisation and starting (with shortcircuited stator) performance
- the ±5% speed control interval leads to low relative power rating of the converter (especially with the GTO inverter-converter)
- the machine may be controlled to act also as synchronous generator (motor) with zero frequency excitation control in the rotor, that is, as a synchronous condenser as well
- decoupled fast active and reactive power control

Table 1. Ratings of the main components for Yagisawa (unit 2)

Component	Characteristic	Rating
Pump-turbine	Max. output (MW)	87.4
	Head (m)	53 to 111
	Pump input (MW)	53 to 82
	Pumping head (m)	63 to 112.5
Generator-motor	Rated output (MVA)	85
	Rated voltage (kV)	13.8
	Rotating speed (rpm)	130 to 156
Frequency-converter	Type	Cycloconverter
	Rated output (MVA)	25.8
	Rated voltage (kV)	4.8
	Rated current (kA)	3.1
	Output frequency (Hz)	0.25 to 4.6

The solution, with still to be implemented sensorless vector (DTC) control, can be generalized for all power levels, especially downwards.

Micro-hydro-power-plants are to be targets for DFIG, with or without pumping facilities. The availability of motoring and generating below and above "synchronous" speed with smooth transition through it, makes DFIG ideal for fast and robust active and reactive power or speed control. Cogeneration with Diesel or gas-turbine or steam generators may be included here and dedicated DFIGs can suit them either at the commercial power grid or standalone.

4. Standalone variable speed generators

Emergency generators sets for public buildings (hospitals, banks) require fast starting (intervention) and power delivery to fill in for voltage short or longer sags and for power failure.

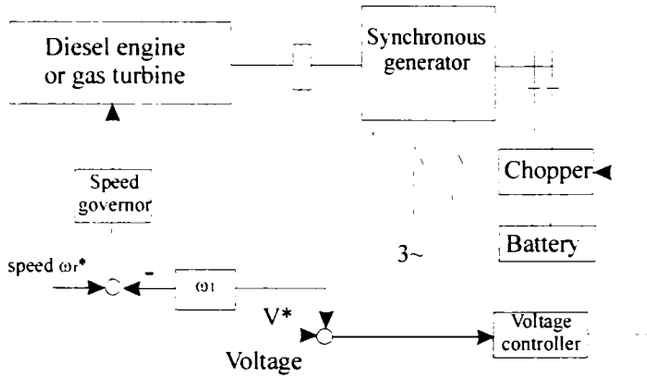

Fig. 5. Stand-alone typical gensets

Typically a Diesel-engine or more recently a gas-turbine drives a synchronous generator with speed (frequency) and voltage control (Fig. 5)

The main advantage to gain from variable speed would be to run the primary mover at max. efficiency (that is at variable speed at variable load).

The time required to start the thermal engine is not trivial and it may be too long for a computerized banking system in case of power failure.

So, a battery acts through a full power generator or converter first, until the thermal engine accelerates, when we may commutate the converter to the generator. In this case a PM a.c. generator with diode rectifier may be more adequate as it has higher efficiency, works at variable speed and is more compact (Fig. 6)

A more sophisticated such system without the short-term back up battery and with 50, 60, or 400 Hz output and a 28 Vd.c. power source has been recently proposed for a mobile genset, Fig. 7 [4].

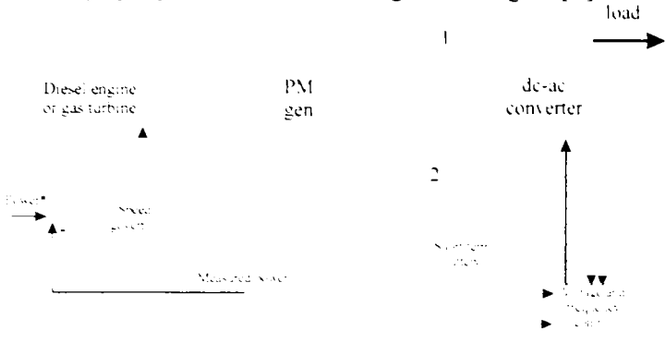

Fig. 6. Standalone MG generator – converter with battery quick back up

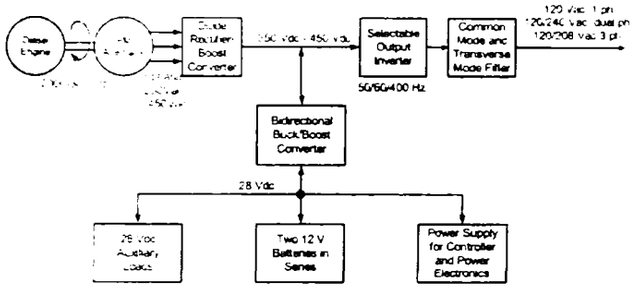

Fig. 7 PM generator advanced mobile genset (AMGS)

The energy saving (in fuel consumption) with variable speed is evident in Fig. 8 [4]

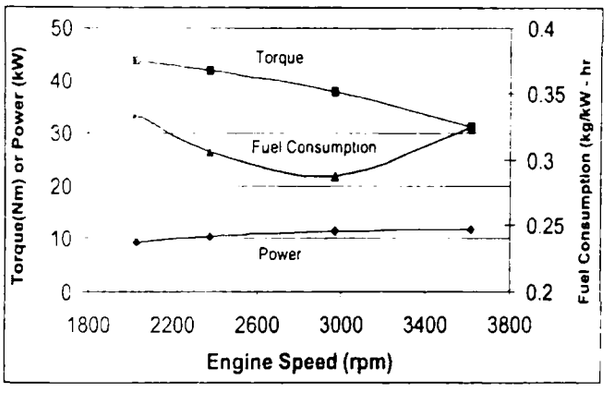

Fig. 8. Peak torque, power and fuel consumption (AMGS)

The whole hardware is shown in Fig. 9 [4]

It is a multipurpose system and produces a 50% reduction in size and notable improvement in fuel consumption.

For less demanding applications cage-rotor induction generators-single phase and three phase with parallel terminal capacitors and an auxiliary stator winding fed through a power PWM converter fed from a battery or a capacitor with a paralleled resistor and switch have been recently proposed (Fig. 10) [14,15]

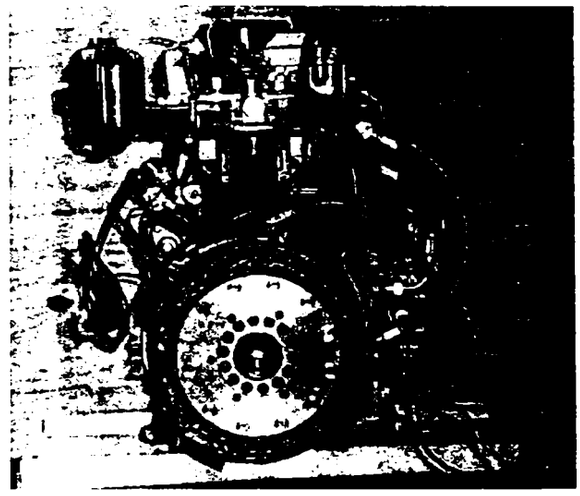

Figure 9. PM alternator genset with Diesel engine [4]

The converter, with fractional power rating, provides constant voltage and frequency at the main stator winding terminals for all loads. Only slight speed variation is allowed, but the costs and volume of the system seem lower than for synchronous generator sets.

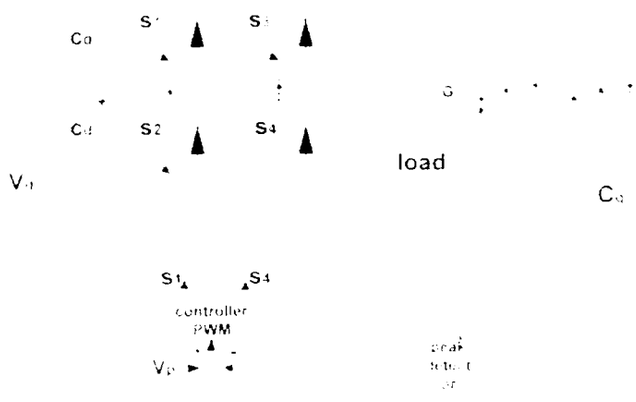

Fig. 10. Dual stator winding IG with reduced count inverter – battery system [15]

5. Automotive starter (torque-assist)/alternator systems

The 42 V d.c. power bus on the near future automobiles facilitates the extension of power electronics use on board, as the conduction power-switch losses are, in relative terms, much lower than for 14 V d.c..

The integration of starter and alternator functions into one system becomes now feasible. The electric machine starts the engine and assists it at low speeds and then turns to generator function to produce electric energy for various loads. This is the "mild hybrid" car (vehicle) which allows for automatic engine turn-off during traffic jams and at traffic lights as it is capable of quick (within 100 ms) repetitive starting. Quite a few electric machines such as PM-assisted reluctance (or IPM) synchronous [16-18] transverse flux PM-rotor [19-21] or SRM [22] schemes with adequate dc-ac converters and controls have been proposed. Only the induction machine [5, 23] has reached the markets already in the heavy (high voltage battery) hybrid cars of Toyota and Honda.

So there is the low voltage (42 V d.c.) starter-alternator and the high voltage (150-400 V d.c.) motor-generator for mild and heavy hybrids electric vehicles.

Typical peak torque and voltage versus speed for a PM-RSM mild hybrid starting and, respectively, torque-assist mode are shown in Fig. 11 [18], with corresponding efficiency in Fig. 11b.

140Nm of peak torque may be provided up to 500rpm (about 4kW) and the peak power of 4kW may be maintained up to 6000 rpm.

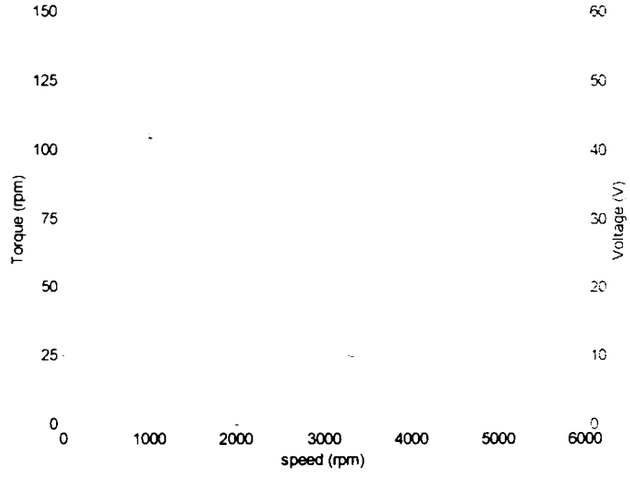

a)

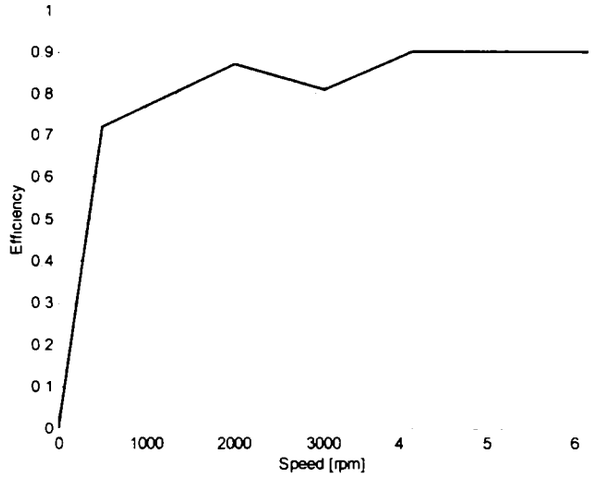

b)

Fig. 11. Peak torque, voltage a) and corresponding machine efficiency versus speed b) [18]

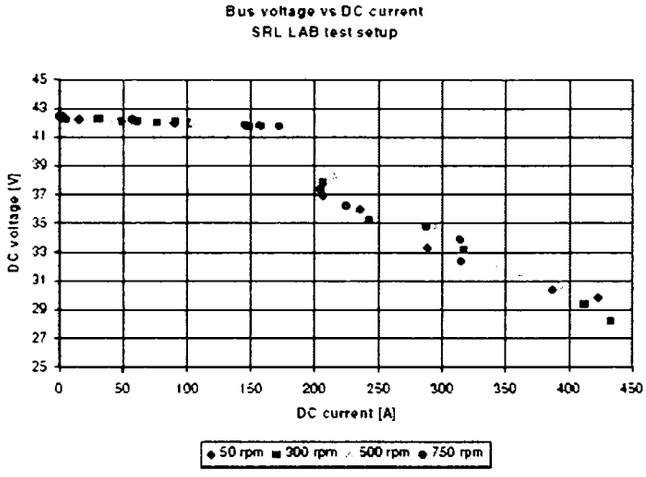

Figure 12. 42V battery voltage versus d.c. current load [24]

Unfortunately the peak phase RMS current would be 270A in this case [18]. However above 150A, the battery voltage falls rapidly below 30V (Fig. 12) [24]

Thus a winding switch or a boost converter (Fig. 13) is required to cover the 500rpm to 6000rpm constant 4kW power range below 150A of d.c. battery current, which is safe for the battery in the long run and secures high system efficiency. Only three existing 14V d.c. car batteries in series are required in a mild hybrid car. This is why the solution is so attractive.

The winding switch (Fig. 13a) operates while the inverter is disengaged so it should be low

(thermal) rating (and cost) and fast closing at zero current.

Fig. 13b illustrates a boost-buck-boost intermediate converter that allows for a higher voltage PWM dc-ac converter and may eliminate the winding switch. While the wide constant power range is secured the slightly higher costs of both converters is apparently offsetted by better overall sys.e... e.fic.e..cv [..], a.. .o e.. .ha.. 150.. d.c. f.r the 42V d.c. ba"ery.

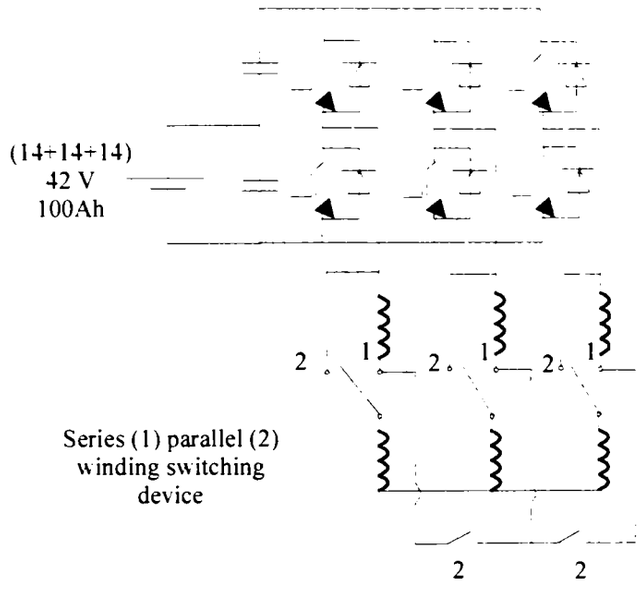

a)

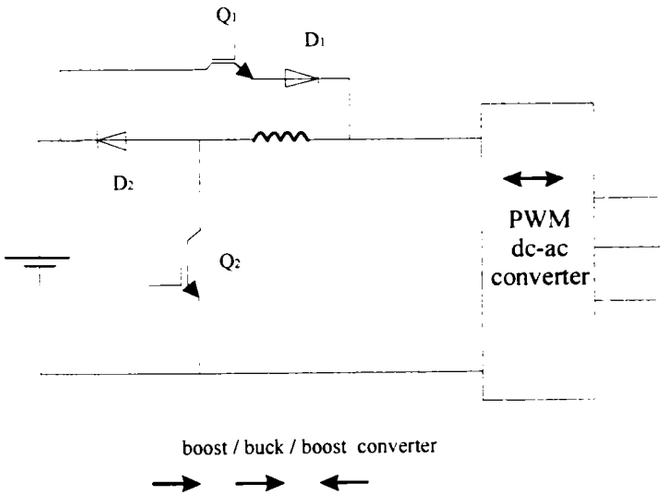

b)

Fig. 13 Potential 42V d.c. automotive starter/alternator system with winding switch (a.c. machines) and passive (capacitor) voltage

6. Home and space electric generator systems

A free piston Stirling thermal engine [27] linear electric generator system (Fig. 14) [28] has been proven capable to produce heat and electricity in the ratio of 7/1 so typical for home purposes.

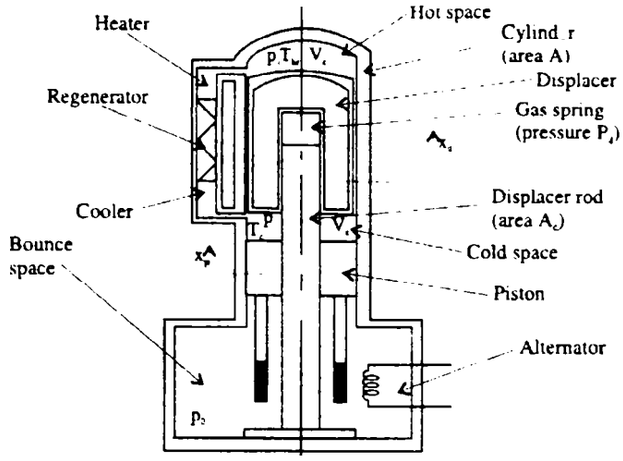

Fig. 14. Stirling engine linear PM generator

350W electric with 1.8kW thermal power have been provided for 45000 hours of continuous and quiet operation at the power grid.

The connection to the power grid is controlled from the Sterling engine side, basically. There are quite a few PM linear generator configurations capable of more than 85% of efficiency above 150W [28] (Fig. 15)

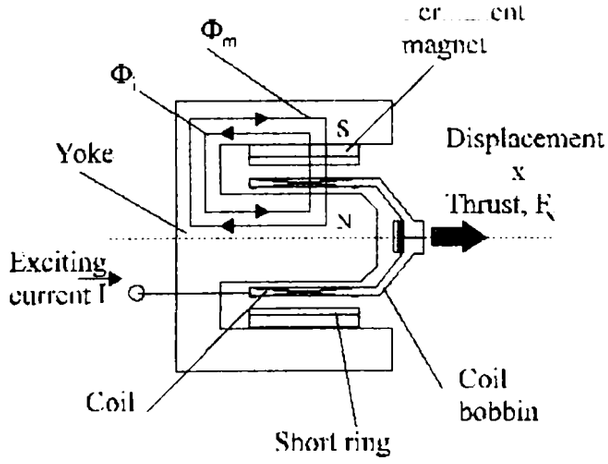

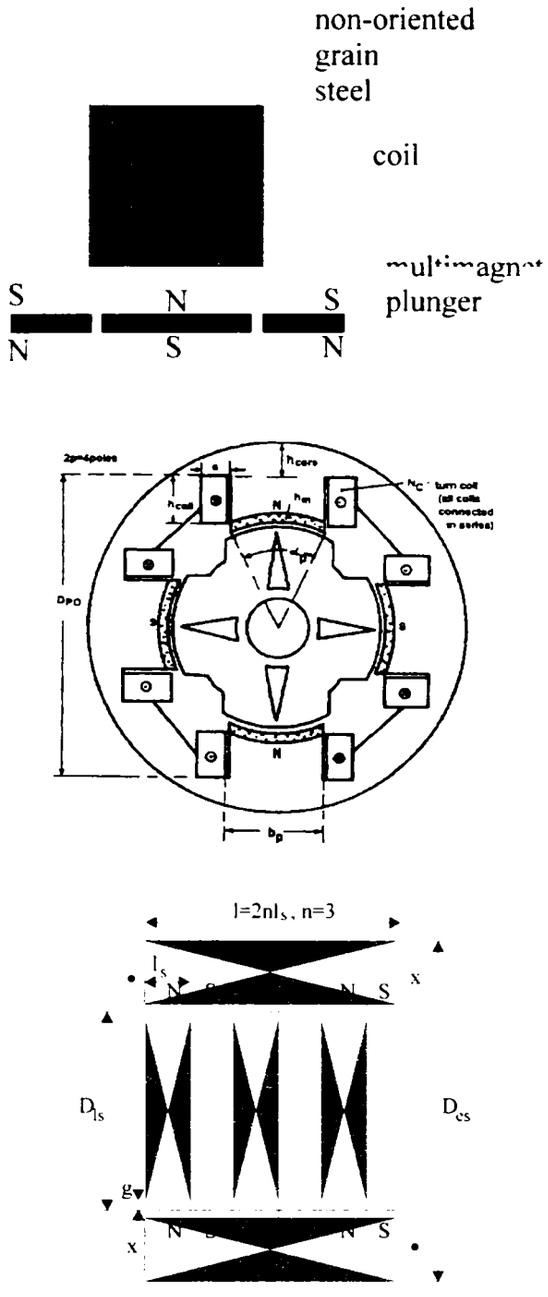

Fig. 15. Various PM linear alternators [28, 29]

They differ mainly in power per volume and manufacturability. The PM-stator linear alternator with conventional SRM-like core and mechanical flexures acting as both linear bearings and energy storage (springs) elements at excursion end, working at resonance conditions, seems very adequate for the scope [29]. It is basically a single phase PM synchronous machines with low voltage regulation. With a series capacitor, higher output for given machine and grid voltage is obtained. Full compensation of machine inductance by the series capacitor produces only RI voltage regulation as in d.c. machines.

For reduced output power, the linear motion amplitude – at rated frequency – is reduced. The efficiency stays high as if the speed was reduced through pole pitch variation in an a.c. machine.

Lower weight (down to less than 12kg per kW of linear power) while maintaining the efficiency above 85% is required to make the Stirling engine – linear alternator system competitive for home applications in terms of $/kW (electric plus thermal). Similar configurations have already been used for space applications with radioactive – isotope – heat source.

7. Conclusion

The present paper leads to conclusions such as:

- variable-speed generator technologies for power systems are already available up to 330MW with doubly-fed induction generator motors. They bring more flexibility to power production and transportation for distributed/power systems wind and hydro electric generators are prime candidates for variable speed
- better system design optimisation and sensorless control methodologies are still desired
- automotive starter-alternator system for mild (42V d.c.) and heavy (150-600V d.c.) hybrid vehicles have been proposed in various configurations. The IM solution has been brought to markets by Toyota and Honda. Up to 35% fuel consumption reduction in town driving has been reported for Toyota Prius but the additional electrical equipment has been rated at 3000 USD. PM-RSM or transverse flux PM rotor configurations are currently proposed as they are credited with slightly less initial system costs for low total torque. No paper expected in this area in the near future as all main vehicle manufacturers are close to market with their hybrid or electric prototypes.
- PM or induction generators with full (respectively fractionary) power electronics rating are proposed for dedicated stand alone or mobile gensets in the tens or hundreds of kW. Faster availability, lower volume and better energy conversion ratio with faster response for load transients are expected for such solutions.
- Home combined electricity and heat production through burning natural gas has been demonstrated with quiet, free piston Stirling engines and linear PM generators for efficiency above 85%, and at the power electric grid for tens of thousands of hours in

the kW range. More compact configurations with still high efficiency and lower initial costs are required to make home electricity generation truly practical with all implicit advantages.

References

1. S. Müller, M. Deicke, R. W. De Doncker, "Adjustable speed generators for wind turbines based on double-fed induction machines and 4-quadrant IGBT converters linked to the rotor," *IEEE-IAS Annual Meeting*, 2000.
2. K. Kudo, "Japanese experience with a converter fed variable speed pump-storage system," *Hydropower and Dams*, no.3, 1994, pp. 67-71.
3. A. Hingorani and L. Gyugyi, "Understanding Facts" – book, IEEE Press 2000.
4. L. M. Tolbert et all, "Electric power conversion system for an advanced mobile generator set," *IEEE Trans*, vol. IA – 38, 2002.
5. F. Leonardi, M. Degner, "Integrated starter-generator based HEVs: a comparison between low and high voltage systems," Record of *IEEE-IEMDC-2001*, MIT, Boston, USA.
6. I. Boldea, S. A. Nasar, "Linear motion electromagnetic devices," – book – Chapter 7, Taylor&Francis, 2001.
7. International Wind Energy Development – *World Market Update*, 1999, BTM Consults Aps, Ringkobing, Denmark 2000, ISBN 87-987788-0-3.
8. L. Mihet-Popa, I. Boldea, F. Blaabjerg, "Simulation of wind generator systems for the power grid," Proceedings of *OPTIM-2002*, vol.2, Poiana Brasov, Romania.
9. L.H. Hansen, F. Blaabjerg, H. C. Christensen, U. Lindhart, P.H. Madsen "Generator and Power Electronics Technology for Wind Turbines," Proceedings of IECON 2001, pp. 2000-2005
10. R. Pena, J. C. Clare, G. M. Asher, "A doubly fed induction generator using back to back PWM converters supplying an isolated load from variable speed wind turbine.
11. L. Morel, H. Godfroid, A. Mirzaian, J. M. Kauffmann, "Double fed induction machine: converter optimization and field oriented control without position sensor," Proc. IEE, vol. PA-145, no.4, 1998, pp.360-367.
12. I. Boldea, S. A. Nasar "Induction machine handbook" – Chapter 19, CRC Press, Boca Raton, Florida, 2001
13. S. Furuya, F. Wada, K. Hachiya, K. Kudo, "Large capacity GTO inverter-converter for double-fed adjustable speed system," CIGRE Symposium in Tokyo, 1995, paper 530-4
14. O. Ojo, O. Omozusi, A. A. Jimoh, "Expanding the operating range of a single-phase induction generator with a PWM inverter," Record of *IEEE-IAS*-1998 Annual Meeting.
15. O. Ojo et al, "A dual stator winding induction generator with a four switch DC/AC inverter," Record of *IEEE-IAS-2000* Annual Meeting.
16. A. Vagati at al, "Comparison of a.c. motor based drives for electric vehicle operation" Record *PCIM – Intelligent Motion*, June, 1999, pp.173-181.
17. E. C. Lovelace, T. M. Jahus, I. L. Kirtley, J. M. Lang, "An interior PM alternator for automotive applications," Record of *ICEM – 1998*, Istambul, Turkey, vol. 3, pp. 1801-1808.
18. I. Boldea, L. Tutelea, C. I. Pitic, "PM-assisted reluctance synchronous motor/generator (PM-RSM) for mild hybrid vehicles," Record of *OPTIM 2002*, Poiana Brasov, Romania
19. M. Bark, G. Henneberger, "New transverse flux concept for an electric vehicle drive system," Proc. of *ICEM 1996*
20. R. Müller, "Voith elvo electric drive for a city bus" *Nachverkehrspraxis*, no.1, 1997 (in german).
21. A. Lange, W. R Canders, F. Laube, M. Mosebach "Comparison of different drive systems for a 75kW electrical vehicle drive," Record of ICEM-2000, pp. 1308-1312.
22. H. Bausch, A. Graaf, A. B. A. Nickel " A switched reluctance and an induction machine in a drive train for an electrical vehicle under conditions of car applications" Record of *ICEM-2000*, Espoo, Finland, vol. 3, pp. 1313-1316.
23. L. Tutelea, E. Ritchie, I. Boldea, "Comparative performance of induction and synchronous permanent magnet machine electric vehicle drives," Record of *OPTIM-2002*, Poiana Brasov, Romania.
24. S. K. Sul, "Sensorless control of a.c. motors," Record of *International workshop for control motors*, Ministry of Commerce, Industry & Energy, Korea, 2001
25. G. Alenbernd, H. Schaffer, L. Wahner, "Vector controlled crankshaft starter-generator for motor vehicle," Record of *ICEM-2000*, Espoo, Finland, vol. 3, pp. 1549-1553.

26. I. Boldea and S. A. Nasar, "Electric Drives," book, CRC Press, 1998.
27. G. Walker, O. R. Fauvel, G. Reader, E.R. Bingham, "The Stirling alternative: Power Systems, Refrigerants and Heat Pumps," book, Gordon & Breach Science Publishers, 1994
28. I. Boldea, S.A. Nasar, "Linear electric actuators and generators," book, Cambridge University Press 1997.
29. I. Boldea, S.A. Nasar, "Linear electrodynamic machine and a way to build it" – US Patent 5564596/1996.

Direct Power Control of Doubly Fed Induction Generators

Ioan Serban, M.Sc.E.E
Ph. D. Student
University Politehnica of Timisoara
Department of Electrical Machines and Drives,
V.Parvan 2, RO - 1900 Timisoara, Romania
Email: serban@lselinux.utt.ro

Guest Researcher
Aalborg University
Institute of Energy Technology
Pontoppidanstraede 101
DK-9220 Aalborg East, Denmark

ABSTRACT

This paper represents a literature study made by the author for one of his reports. It is based on the concept of direct active and reactive power control of a grid connected wound rotor induction machine fed by back-to-back connected voltage source inverters on the rotor side. This solution is suitable for both wind and hydro power generation, provides good dynamic performance and there is no need for rotor position sensing.

Keywords: power control, sensorless control, variable speed constant frequency applications, power generation

1 INTRODUCTION [1]

Until not long ago the norm in electric generators was to use synchronous machines at constant speed to obtain constant frequency with regulated voltage output. Environmental and safety constraints and more demanding control requirements have led to variable speed generators electronically controlled for constant frequency and voltage. Wind power took the lead in this respect and there are now a few companies which manufacture doubly-fed induction wind generators at variable speed for higher wind energy extraction and better stability when the wind speed varies ±20% around a base (design) value [2].
Also, this time for power fast control in power systems, with nuclear power plants, variable speed doubly fed induction generator-motors up to 330MW per unit have been put rather percently to service in pump-storage hydroelectric power plants [3].
It is only natural to assume that, hydropower plants – existing or new, large or small – will take advantage of this technology in the future to produce peak power in a fast-controlled manner for higher efficiency and with notable environmental benefits.
For distributed industrial power generation high speed combined cycle gas turbines should also use doubly-fed in uction generators to cope wi h s a' ili y an ' con rol aspec s while producing energy with minimum fuel consumption.
Powe systems are loa strain to t.e limit ov transients an flexible ac transmission systems (FACTS) are proposed to bring more flexibility by parallel/and (or) series power electronics converters with or without storage or by intermediary full power dc power lines. The variable speed generators, in any power plant, even within ±5% - with the power electronics designed at 5 – 10% rated power, as it feeds the rotor windings – should produce more flexibility to the power system at less costs, with lower harmonics pollution.
It is thinkable that not only the new generators for power systems will be variable speed, but, when retrofitting existing generators, the existing stator may be maintained and only the rotor core, windings and control will be changed.
All the above tasks should bring extraordinary opportunities for the research, development communities and for industries related to power system electric generators and their control.

2 THE SYSTEM [4]

As mentioned above there has been an increased attention toward wind power generation. Conventionally, grid-connected cage rotor induction machines are used as wind generators at medium power level. When connected to the constant frequency network, the induction generator runs at near synchronous speed drawing the magnetizing current from the mains, thereby resulting in constant speed constant frequency (CSCF) operation. However, the power capture due to fluctuating wind speed can be substantially improved if there is flexibility in varying the shaft speed.
In such variable speed constant frequency (VSCF) application rotor side control of grid-connected wound rotor induction machine is an attractive solution. In the system under consideration, the stator is directly connected to the three phase grid and the rotor is supplied by two back-to-back PWM converters (Fig. 1).

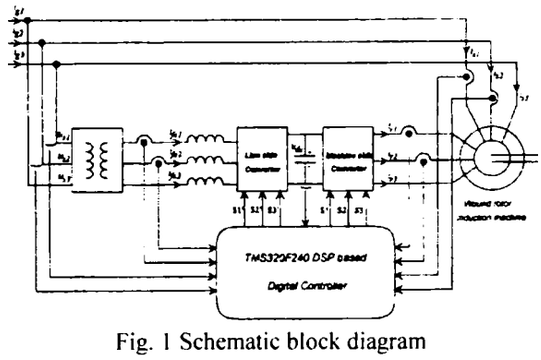

Fig. 1 Schematic block diagram

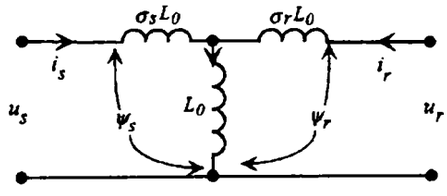

Fig. 2 Approximate equivalent circuit

Such an arrangement provides flexibility of operation in subsynchronous and supersynchronous speeds both in the generating and motoring modes. The rating of the power converters used in the rotor circuit is substantially lower than the machine rating and is decided by the range of operating speed. Of the two converters, the function of the line side converter is to regulate the dc bus voltage and act as unity power factor interface to the grid for either direction of power flow. The machine side converter has to control the torque and flux of the machine or alternatively the active and reactive powers.

The conventional approach for independent control of active and reactive powers handled by the machine is stator flux oriented vector control with rotor position sensors. [5], [6]. The performance of the system in this case depends on the accuracy of computation of the stator flux and the accuracy of the rotor position information derived from the position encoder. Alignment of the position sensor is moreover, difficult in a doubly-fed wound rotor machine. Position sensorless vector control methods have been proposed by several research groups in the recent past. [7] – [8]. In [7], a dynamic torque angle controller is proposed. This method uses integration of the PWM rotor voltage to compute the rotor flux; hence satisfactory performance cannot be achieved at or near synchronous speed. Most of the other methods proposed make use of the measured rotor current and use coordinate transformations for estimating the rotor position.[8] – [10]. Varying degree of dependence on machine parameters is observed in all these strategies.

Alternative approaches to field oriented control such as direct self control (DSC) [11] and direct torque control (DTC) [12], [13] have been proposed for cage rotor induction machines. In these strategies, two hysteresis controllers, namely a torque controller and a flux controller, are used to determine the instantaneous switching state for the inverter. These methods of control are computationally very simple and do not require rotor position information.

Recently an algorithm [14], [15] for independent control of active and reactive powers with high dynamic response in case of a wound rotor induction machine was developed. The instantaneous switching state of the rotor side converter is determined based on the active and reactive powers measured in the stator circuit. Thus, unlike existing DTC techniques, measurements are carried out at one terminal of the machine whereas the switching action is carried out at another terminal. Here the directly-controlled quantities are the stator active and reactive powers; hence, the algorithm is referred to as *direct power control (DPC)*. The proposed algorithm also differs from conventional DTC in that it does not use integration of PWM voltages. Hence, it can work stably even at zero rotor frequency. The method is inherently position sensorless and does not depend on machine parameters like stator/rotor resistance. It can be applied to VSCF applications like wind power generation as well as high power drives. The concept of direct power control was first introduced and details of the strategy [14]. Recently experimental results have been presented to validate the performance of the proposed method.

The basic concept of direct control of active and reactive powers can be appreciated from the phasor diagrams based on the equivalent circuit of the doubly-fed machine as shown in Fig. 2. From the phasor diagram in Fig. 3 it is noted that the component of the stator current i_{sq} has to be controlled to control the stator active power P_s and i_{sd} has to be controlled to control the stator reactive power Q_s.

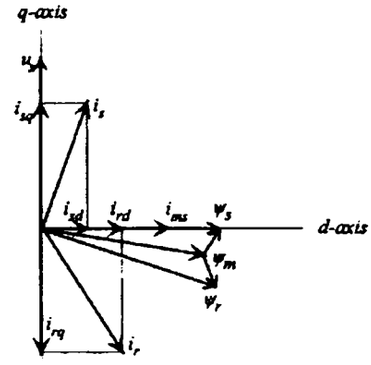

Fig. 3 Phasor diagram

This is achieved in turn by controlling the rotor currents i_{rq} and i_{rd}, respectively, in conventional field oriented control strategy. The effect of injection of these rotor currents on the air-gap and rotor fluxes can be derived by subtracting and adding the respective leakage fluxes. The variation of the rotor flux with variations in the active and reactive power demand is shown in Fig. 4(a) and (b). In Fig. 4(a) $i_{rd} = 0$, i.e., the reactive power is fed completely from the stator side. Under this condition if i_{rq} is varied from 0 to full load, the locus of ψ_r varies along A–B which indicates a predominant change in angle δ between ψ_s and ψ_r, whereas the magnitude of ψ_r does not change appreciably. In other words, a change in the angle δ would definitely result in a change in the active power handled by the stator in a predictable fashion.

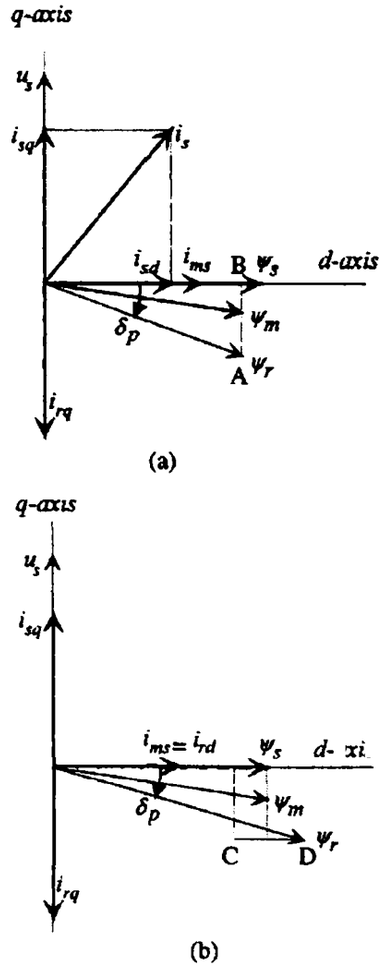

Fig. 4 Phasor diagram showing variations in rotor flux with change in active and reactive power.

In Fig. 4(b) the stator active power demand is maintained constant so that i_{rq} is constant and i_{rd} is varied from 0 to the rated value of i . Here the locus of varies along C–D. resulting in a predominant change in magnitude of Ψ_r, whereas the variation of δ is small. Therefore. the reactive power drawn from the grid by the stator can be reduced by increasing the magnitude of the rotor flux and vice-versa. It may be noted that the phasor diagrams as indicated in Fig. 4(a) and (b) remain the same irrespective of the reference frame: the frequency of the phasors merely changes from one reference frame to the other. It can be concluded ..om the abo . e d.scuss.on that:

The stator active power can be controlled by controlling the angular position of the rotor flux vector.

The stator reactive power can be controlled by controlling the magnitude of the rotor flux vector.

These two basic notions have been used to determine the instantaneous switching state of the rotor side converter to control the active and reactive power as discussed in the following section.

3. CONTROL OF SUPPLY (LINE) – SIDE PWM CONVERTER [6]

The objective of the supply-side converter is to keep the DC-link voltage constant regardless of the magnitude and direction of the rotor power. A vector-control approach is used with a reference frame oriented along the stator voltage vector. enabling independent control of the active and reactive power flowing between the supply and the supply-side converter. The PWM converter is current regulated. with the direct axis current used to regulate the DC-link voltage and the quadrature axis current component used to regulate the reactive power. A standard regular asymmetric sampling PWM scheme [16] is used. Fig. 5 shows the schematic of the supply-side converter. The voltage balance across the inductors is:

$$\begin{bmatrix} v_a \\ v_b \\ v_c \end{bmatrix} = R\begin{bmatrix} i_a \\ i_b \\ i_c \end{bmatrix} + L\frac{d}{dt}\begin{bmatrix} i_a \\ i_b \\ i_c \end{bmatrix} + \begin{bmatrix} v_{al} \\ v_{bl} \\ v_{cl} \end{bmatrix} \qquad (1)$$

where L and R are the line inductance and resistance, respectively. using the transformations eqn. 1 is transformed into a dq reference frame rotating at ω_e:

$$\begin{aligned} v_d &= Ri_d + L\frac{di_d}{dt} - \omega_e L i_q + v_{dl} \\ v_q &= Ri_q + L\frac{di_q}{dt} + \omega_e L i_d + v_{ql} \end{aligned} \qquad (2)$$

With the scaling factors used in the transformations of the Appendix, the active and reactive power flow is:

$$\begin{aligned} P &= 3(v_d i_d + v_q i_q) \\ Q &= 3(v_d i_q + v_q i_d) \end{aligned} \qquad (3)$$

The angular position of the supply voltage is calculated as:

$$\theta_e = \int \omega_e dt = \tan^{-1}\frac{v_\beta}{v_\alpha} \qquad (4)$$

where v_α and v_β are the α, β (stationary 2-axis) stator-voltage components.

Aligning the d-axis of the reference frame along the stator-voltage position given by eqn. 4, v_q is zero, and, since the amplitude of the supply voltage is constant v_d is constant. The active and reactive power will be proportional to i_d and i_q respectively.

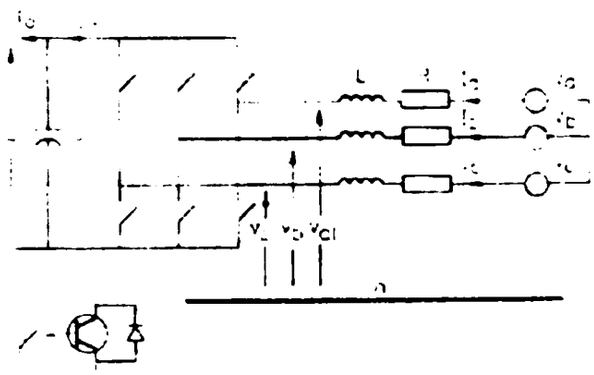

Fig. 5 Supply-side converter arrangement

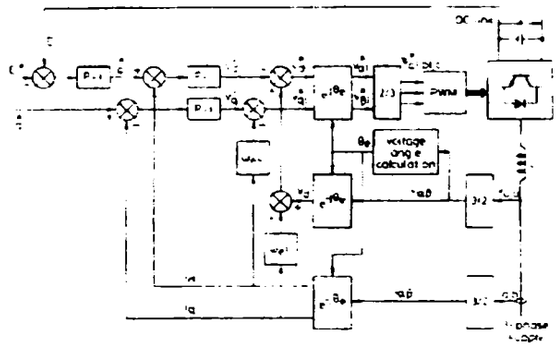

Fig. 6 Vector control structure for supply-side converter

Neglecting harmonics due to switching and the losses in the inductor resistance and converter, we have:

$$\begin{aligned} Ei_{os} &= 3v_d i_d \\ v_d &= \frac{m_1}{2\sqrt{2}}E \\ i_{os} &= \frac{3}{2\sqrt{2}}m_1 i_d \\ C\frac{dE}{dt} &= i_{os} - i_{or} \end{aligned} \qquad (5)$$

From eqn. 5, it is seen that the DC-link voltage can be contolled via i_d. The control scheme thus utilises current control loops for i_d and i_q, with the i_d demand being derived from the DC link voltage error through a standard PI controller. The i_q demand determines the displacement factor on the supply-side of the inductors. The strategy is shown in Fig. 6. From eqn. 2 the plant for the current control loops is given by:

$$F(s) = \frac{i_d(s)}{v_d(s)} = \frac{i_q(s)}{v_q(s)} = \frac{1}{Ls+R} \qquad (6)$$

where

$$\begin{aligned} v_{dl}^* &= -v_d^* + (\omega_e L i_q + v_d) \\ v_{ql}^* &= -v_q^* - (\omega_e L i_d) \end{aligned} \qquad (7)$$

In eqn. 7, v^*_{dl} and v^*_{ql} are the references values for the supply-side converter, and the terms in brackets constitute voltage-compensation terms.

The design of the current controllers follows directly from eqn. (6), which can be written in the z domain as:

$$F(z) = \frac{(1-A)/R}{(z-A)};\ A = e^{-(R/L)Ts} \qquad (8)$$

where T_s is the sample time (0.5ms). The converter may be modelled by a pure delay of two sample periods yielding the control schematic of Fig. 7 for which standard design techniques may be applied. For the inductors used, R=0.1Ω, L = 12mH, a design for a nominal closed-loop natural frequency of 125 Hz and ζ=0.8 can be obtained using the PI controller:

$$G(z) = 4.72(z-0.96)/(z-1)$$

The design of the DC-link voltage controller may carried out in the continous domain, and it is assumed that the inner i_d loop is ideal. From eqn. 5 the effective transfer function of the plant is:

$$\frac{E(s)}{i_d(s)} = \frac{3m_1}{2\sqrt{2}C_s} \qquad (9)$$

and the closed-loop block diagram is shown in Fig. 7, in which i_{dr} is represented as a disturbance. Again, standard classical design is appropriate. Inserting values of $E^* = 550V$, $m_1 = 0.75$ (for $V_s = 250V$), $C = 2.4mF$ and $T_s = 5ms$, a controller of $0.12(z-0.9248)/(z-1)$ can be shown to give a nominal closed-loop natural frequency of $25rads^{-1}$, with $\zeta = 0.7$. This is 50 times slower than th loop sampling frequency, and justifies the continous design.

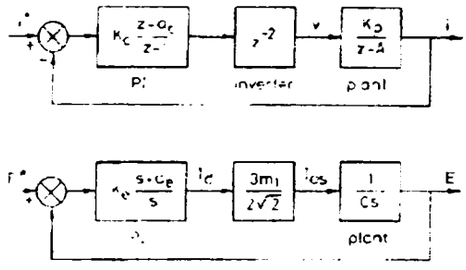

Fig. 7 Supply-side converter current control loop and DC-link voltage control loop.

4. INDUCTION MACHINE CONTROL

The induction machine is controlled in a synchronously rotating dq frame with the d-axis oriented along the stator-flux vector position. In this way, a decoupled controol between the electrical torque and the rotor excitation is obtained. The rotor-side PWM converter provides the actuation, and the control requires the measurement of the stator and rotor currents, stator voltage and the rotor position. There is no need to know the rotor-induced EMF, as is the case for the implementation with naturally commutated converters.

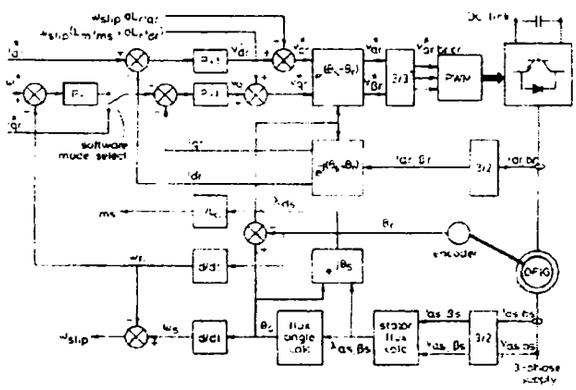

Fig. 8 Vector-control structure for DFIG

Since the stator is connected to the grid, and the influence of the stator resistance is small, the stator magnetizing current i_{ms} can be considered constant. Under stator-flux orientation, the relationship between the torque and the dq axis voltages, currents and fluxes (all scaled to be numerically equal to the AC per-phase values) may be written as:

$$\begin{aligned}
\psi_s &= \psi_{ds} = L_0 i_{ms} = L_s i_{ds} + L_0 i_{dr} \\
\psi_{dr} &= \frac{L_0^2}{L_s} i_{ms} + \sigma L_r i_{dr} \\
\psi_{qr} &= \sigma L_r i_{qr} \\
i_{qs} &= -\frac{L_0}{L_s} i_{qr} \\
v_{dr} &= R_r i_{dr} + \sigma L_r \frac{di_{dr}}{dt} - \omega_{slip}\sigma L_r i_{qr} \\
v_{qr} &= R_r i_{qr} + \sigma L_r \frac{di_{qr}}{dt} + \omega_{slip}(L_m i_{ms} + \sigma L_r i_{dr}) \\
T_e &= -3\frac{P}{2} L_m i_{ms} i_{qr} \\
\omega_{slip} &= \omega_e - \omega_r \\
\sigma &= 1 - \frac{L_0^2}{L_s L_r} \\
L_m &= \frac{L_0^2}{L_s}
\end{aligned} \qquad (10)$$

The stator flux angle is calculated from:

$$\begin{aligned}
\psi_{\alpha s} &= \int (v_{\alpha s} - R_s i_{\alpha s}) dt \\
\psi_{\beta s} &= \int (v_{\beta s} - R_s i_{\beta s}) dt \\
\theta_s &= \tan^{-1} \frac{\lambda_{\beta s}}{\lambda_{\alpha s}}
\end{aligned} \qquad (11)$$

where θ_s is the stator-flux vector position. The integral in eqn. 11 is solved using the digital passband filter, with cutoff frequencies of 0.5 Hz and 1 Hz to eliminate DC offsets. From eqn. 10, the torque is proportional to i_{qr} and can be regulated using v_{qr}. The rotor excitation current i_{dr} is controlled using v_{dr}. Assuming that all reactive power to the machine is supplied by the stator, i^*_{dr} may be set to zero.

Fig. 8 shows a schematic block diagram for the machine control. The reference q axis rotor current can be obtained either from a outer speed-control loop or from a reference torque imposed on the machine. These two options may be termed a speed-control mode or torque-control mode for the generator.

A similar analysis for the control of the dq current can be carried out for the supply-side converter can likewise be done for the control of the dq rotor machine currents. From the rotor voltage equation in eqn. 20 we have:

$$\begin{aligned}
v_{dr} &= R_r i_{dr} + \sigma L_r \frac{di_{dr}}{dt} \\
v_{qr} &= R_r i_{qr} + \sigma L_r \frac{di_{qr}}{dt}
\end{aligned} \qquad (12)$$

The i_{dr} and i_{qr} errors are processed by the PI controller to give v'_{dr} and v'_{qr}, respectively. To ensure good tracking of these constant, compensating terms are added to v'_{dr} and v'_{qr} to obtain the reference voltages v^*_{dr} and v^*_{qr} according to:

$$\begin{aligned}
v^*_{dr} &= v'_{dr} - \omega_{slip}\sigma L_r i_{qr} \\
v^*_{qr} &= v'_{qr} + \omega_{slip}(L_m i_{ms} + \sigma L_r i_{dr})
\end{aligned} \qquad (13)$$

which is analogous to eqn. 7.

The plant for the current-control design is similar to the case of the supply-side converter current controller (see Fig. 7) with the following variable substitutions:

$$i_d,\ i_q \Rightarrow i_{dr},\ i_{qr}$$

$$v`_d,\ v`_q \Rightarrow v`_{dr},\ v`_{qr}$$

$$R \Rightarrow R_r$$

$$L \Rightarrow \sigma L_r \qquad (14)$$

$$K_c \Rightarrow K_i$$

$$a_c \Rightarrow a_i$$

With T_s = 0.5ms and with the motor parameters of the Appendix, a nominal closed-loop natural frequency of 130Hz with $\zeta = 0.8$ is obtained, with the controller 20 (z-0.985)(z-1). A speed controller is needed when the machine operates in the speed controller is carried out in the continous domain, in a similar way to that of the voltage controller for the supply-side converter, assuming also that the current controllers are much faster than the speed loop and are thus considered ideal. The second order system of Fig. 7 is obtained (without the i_{or} disturbance) with the following variable substitutions:

$$E \Rightarrow \omega_r$$

$$i_d \Rightarrow i_{qr}$$

$$\frac{3m_1}{2\sqrt{2}} \Rightarrow \frac{-3p}{2} L_m i_{ms}$$

$$i_{os} \Rightarrow T_e \qquad (15)$$

$$\frac{1}{Cs} \Rightarrow \frac{1}{Js+B}$$

$$K_e \Rightarrow K_\omega$$

$$a_e \Rightarrow a_\omega$$

The rotor speed is obtained from a rotor-position measurement, which provides 720 pulses per revolution. With a sample time of 0.1s a resolution of 0.833rpm is obtained, the magnetizing current can be obtained as $i_{ms} = V_s/\omega_e L_0$. With T_s = 0.1s and with the appropriate parameters , a nominal closed-loop natural frequency of 0.05Hz with ζ = 0.9 is obtained, with the controller 0.49 (z-0.988)/(z-1). Although a faster speed controller can be designed for the speed-control mode, in practice it is found the noise considerations limit the closed-loop natural frequency. This derives from the fact that the speed demand is obtained from a mechanical torque observer, which effectively estimates the shaft acceleration from a limited-resolution speed encoder.[17]

4. CONCLUSION

In this study a method for decoupled control of the active and reactive power of a wound rotor induction generator fed by back to back connected vector controlled voltage source inverters on the rotor side was presented. It offers good dynamic responses and it is also functional with an adequate sensorless algorithm started "on-the-fly" and running stably even at zero rotor frequency.

It is also appropriate for hydro energy applications with or without pumped storage because of the possibility to make use of one starting and synchronisation procedure. But all these together with faults and power quality analysis of this system will be treated in the next papers.

5. REFERENCES

[1] I. Boldea, L. Tutelea, I. Serban, "Variable Speed Electric Generators and Their Control: an emerging technology," *Proceedings of CNAE, Galati, Romania* 2002

[2] S. Müller, M. Deicke, R. W. De Doncker, "Adjustable speed generators for wind turbines based on double-fed induction machines and 4-quadrant IGBT converters linked to the rotor," *IEEE-IAS Annual Meeting*, 2000

[3] K. Kudo, "Japanese experience with a converter fed variable speed pump-storage system," *Hydropower and Dams*, no.3, 1994, pp. 67-71

[4] R. Datta, V.T. Ranganathan, "Direct Power Control of Grid-Connected Wound Rotor Induction Machine Without Rotor Position Sensors," IEEE Transactions On Power Electronics, vol. 16, no. 3, May

[5] W. Leonhard, "Control of Electrical Drives," *New York: Springer-Verlag*, 1985, ch.13

[6] R. Pena, J. C. Clare, G. M. Asher, "Doubly fed induction generator using back-to-back PWM converters and its application to variable-speed wind-energy generation," *Proc. Inst. Elect. Eng.*, pt. B, vol. 143, pp. 231-241, May 1996

[7] L. Xu, W. Cheng, "Torque and reactive power control of a doubly-fed induction machine by position sensorless scheme," *IEEE Trans. Ind. Applicat*, vol. 31, pp. 636-642, May/June 1995

[8] R. Datta, V. T. Ranganathan, "Decoupled control of active and reactive power for a grid-connected doubly-fed wound rotor induction machine without position sensors," *Proc. Conf. Rec. 1999 IEEE IAS Anu.Meeting*, 1999, pp. 2623-2630

[9] L. Morel, H. Godfroid, A. Mirzaian, J. M. Kauffmann, "Double-fed induction machine: converter optimization and field oriented control without position sensor," *Proc. Inst. Elect. Eng.*, pt.B, vol. 145, pp. 360-368, July 1998

[10] E. Bogalecka, "Power control of a double fed induction generator without speed or position sensor," *Proc. Conf. Rec. EPE Brighton*, vol. 8, ch. 50, 1993, pp. 224-228

[11] M. Depenbrock, "Direct self control (DSC) of inverter-fed induction machine," *IEEE Trans. Power Electron*, vol. 3, pp. 420-429, Oct. 1998

[12] I. Takahashi, T. Noguchi, "A new quick response and high efficiency control strategy of an induction motor," *IEEE Trans. Ind. Applicat.*, vol. IA-22, pp. 820-827, Sept. Oct. 1986

[13] R. Datta, V.T. Ranganathan, "Method for direct control of active and reactive power from the rotor side for a grid connected doubly-fed slip-ring induction machine without position encoder," *Indian Patent 797/MAS 99*, June 8, 1999

[14] R. Datta, "Rotor side control of grid-connected wound rotor induction machine and its application to wind power generation," *Ph.D dissertation*, Dept. Elect. Eng. Indian Inst. Sci., Bangalore, India, Feb. 2000

A Study of the Doubly-Fed Wind Power Generator Under Power System Faults

Ioan Serban*, Frede Blaabjerg**, Ion Boldea*, Zhe Chen**

* UNIVERSITY "POLITEHNICA"
Piata Victoriei nr.1,
1900 Timisoara, Romania
Phone/Fax: +40 – 256 204 402
E-mail: serban@lselinux.utt.ro; boldea@lselinux.utt.ro

** INSTITUTE OF ENERGY TECHNOLOGY
Pontoppidanstraede 101,
9200 Aalborg, Denmark
Phone/Fax:
E-mail: fbl@iet.auc.dk; zch@iet.auc.dk

1.Keywords:

Adjustable speed generation systems, Generation of electrical energy, Renewable energy systems, Vector control, Wind Turbines

2. Abstract

The paper presents an investigation made on the doubly-fed-induction generator for wind power applications and on its behavior under a three-phase grid short-circuit. A vector controlled back-to-back power electronics converter is connected in the rotor circuit of the generator.
A rather accurate decoupled active and reactive power control strategy and simulation results are presented in detail.
A three-phase short-circuit on the grid is modeled and analyzed, the effects are discussed and some potential mechanisms to improve the performance during the fault and to reduce the destructive effects of this fault are described. It is concluded that the limitation of the rotor currents references is, accorded to this study, the best method to reduce the dominant stator and rotor current peaks during short-circuit with approximate 50%.

3. Introduction

Wind energy was the fastest growing energy technology in the 1990s in terms of percentage of yearly growth of installed capacity per technology source. The distribution of wind energy around the world can be seen in Table 1. By the end of 2001, around 70% of the worldwide wind energy capacity was installed in Europe, a further 19% in North America and 9% in Asia and the Pacific. [1]
Between the end of 1995 and the end of 2001, around 75% of all new grid-connected wind turbines worldwide have been installed in Europe and in 2002 another 5871 MW were installed in the European Union which reached at the end of the last year a total of 23056 MW installed wind power installed [source: European Wind Energy Association (www.ewea.org)]
So there is an immense interest renewed in the last years, related to "harnessing" power from wind, which has proven to be a renewable source for generation of electricity with a minimum of environmental impact.
Actually wind turbines from a few kilowatts to several megawatts are available and integrated to the grid. They are sited in remote areas (including off-shore sites) and in large concentrations counting up to several hundred megawatts of installed power [2]. They are producing a substantial amount of power, which can supplement the base power generated by thermal, nuclear or hydro power plants.

This opens up new technical opportunities for designing and controlling the wind turbines, but at the same time increases the demands for reliability, supplied power quality and grid impact [3]
Along the past years several wind turbine concepts have been proposed: the Darrieus turbine, the Chalk multiblade turbine, and the horizontal three blade turbine. The last one represents in fact the overall dominating topology.

Table 1. Operational wind power capacity worldwide (source: issues of *Wind Power Monthly*)

Region	Installed Capacity (MW)				
	End 1995	End 1997	End 1999	End 2000	End 2001
Europe	2518	4766	9307	12972	16362
North America	1676	1611	2619	2695	4440
South and Central America	11	38	87	103	103
Asia and Pacific	626	1149	1403	1795	2162
Middle East and Africa	13	24	39	141	203
Total Worldwide	**4844**	**7588**	**13455**	**17706**	**23720**

The majority of the installed wind turbines operate at constant or near constant speed, which implies the speed of the electric generator to be fixed (determined by the frequency of the grid) regardless of the wind speed. For this, different topologies with the induction generator and the wound rotor synchronous generator have been proposed and applied but the majority of the fixed speed wind turbines are based on the induction generator.
The inherent problems with the constant speed wind turbines (poorer energy capture, rather big mechanical stress and modest power quality) became more and more significant as the size of the wind turbines and the penetration of wind energy increase.
So the variable speed concept became more and more attractive and today is in fact almost the main applied concept. The most important candidates in this concept are the wound rotor induction generator with a back-to-back inverter feeding the rotor circuit, and the permanent magnets synchronous generator. By the use of the last one solution the slip rings are avoided but with a rather large additional costs due to the prices of permanent magnets and of the power electronics converter which has to handle in this case the full power of the system.
The doubly fed induction generator with a bi-directional power flow converter in the rotor doubtlessly has some advantages:

- enhanced energy capture from the wind in a wide range of wind velocities
- ability of reactive power control
- fast decoupled control of active and reactive power by independent control of torque and rotor excitation
- reduced size and implicitly costs of the power electronics converter (the converter rating is only around 25% of the total generator power)

A study on this solution is made in the present paper, which is divided in the following sections: the simulation model of the generator and its control, case study – three-phase short-circuit on the power grid, mechanism to improve performance during fault.

When a short-circuit fault occurs in the network, then the voltage dip and the current transients in the generator windings and in the converter occur. Although, due to the lack of power transfer from the generator to the network, the turbine severely accelerates. In this situations, there are two risks:

- damage of the converter due to the over-currents
- mechanical damage of the turbine due to the overspeeding

A lot of attention must be paid in order to avoid these problems. The actions that may be taken are different, and are dependent of the type of the turbine: small on-land or large off-shore.
In the case of small on-land wind turbines farms, no technical specifications are made, and the turbines could be automatically tripped and stopped when the settings of the monitored values are exceeded. The converter could be blocked, the rotor could be opened or short-circuited and a "safety

stop" procedure could be initiated. This can be realized by aerodynamic breaking which means pitching the blades at the maximum reference and locking the shaft at the zero speed. Extended discussion of these methods is made in [4].
The technical requirements for the wind turbines in large off-shore wind farms are defined in standards. Those wind farms are treated as large power supply units and their disconnection will not be accepted as the turbine should contribute with power after the fault.
In those cases, other methods for improving the performance under such conditions, and protection should be taken into account.
In the following paragraphs the extended presentation of the studied system (2 MW/660V, 4 pole generator) and how it was modeled will be made, its control will be discussed and various simulation results (in normal operation and under a power grid short-circuit) will be presented.

4. Simulation model of the generator and its control

A schematic diagram of the overall studied system is shown in Figure 1. Two voltage-fed PWM converters are inserted in the rotor circuit, with the supply-side PWM converter connected to the grid via a RL filter, which limits the high-frequency ripple due to switching harmonics.[5].

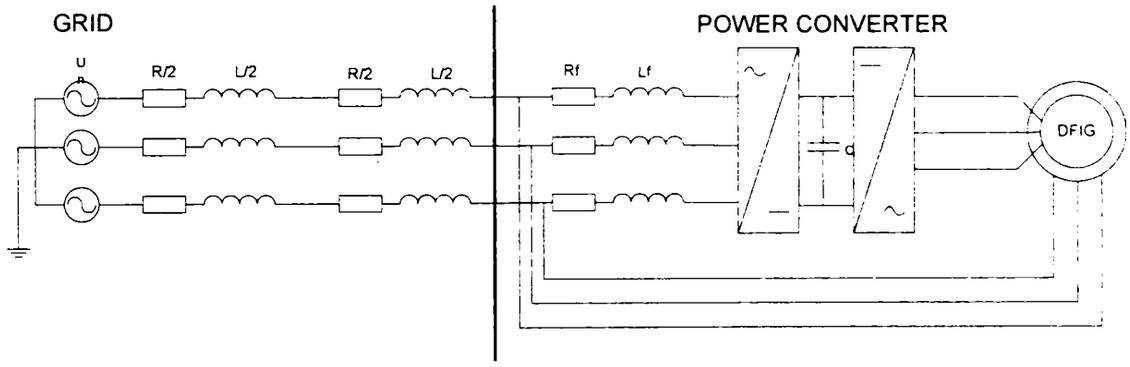

Figure 1. The doubly-fed induction generator connected to the power grid.

The complete simulation model of the system was implemented in Matlab-Simulink, and the parts are explained in what it follows.

4.1. The wind turbine model

The wind turbine is modeled in terms of optimal tracking, to provide maximum energy capture from the wind. The implemented characteristics are presented in Fig. 2

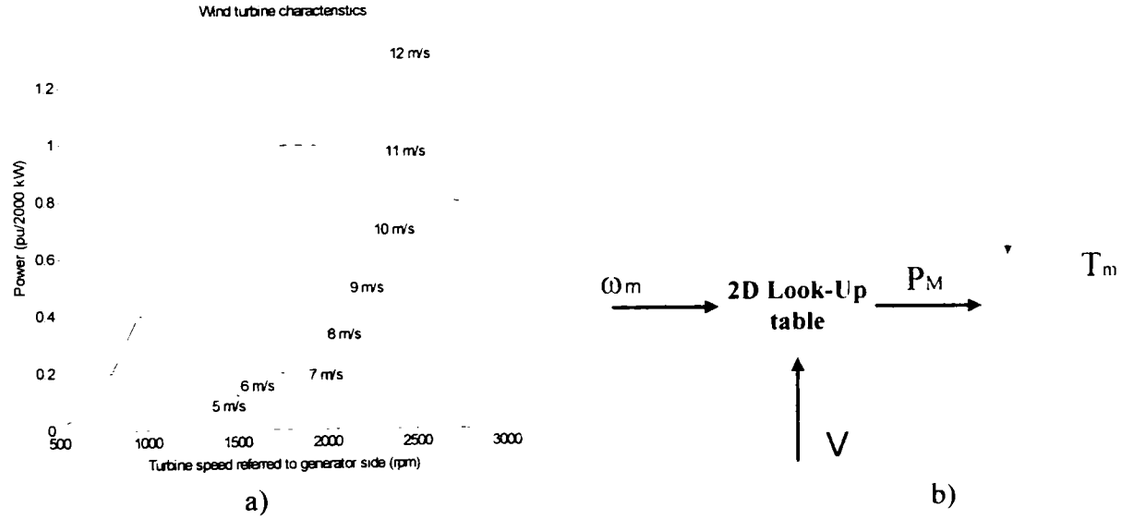

Figure 2. Implemented wind turbine characteristics: a) aerodynamic characteristics, b) the turbine torque model.

These characteristics are based on:

$$P_M = \frac{1}{2} \cdot \rho_{air} \cdot C_p(\lambda,\beta) \cdot \pi \cdot R^2 \cdot V^3 \quad (1)$$

where C_p - power efficiency coefficient; V – wind velocity; β - pitch angle; R – blade radius; P_M – mechanical power produced by the wind turbine; ρ_{air} – air density (usually 1.225 kg/m^3)
Applying the tip speed ratio λ :

$$\lambda = \frac{\omega_m \cdot R}{V} \quad (2)$$

equation (1) may be rewritten as:

$$P_M^{opt} = \frac{1}{2} \cdot \rho_{air} \cdot \pi \cdot R^5 \cdot \frac{C_P^{opt}}{\lambda_{opt}^3} \cdot \omega_m^3 = K_w \cdot \omega_m^3 \quad (3)$$

where K_w is the wind turbine dependent coefficient
Equation (3) holds the key of the optimization of the variable-speed wind turbine by tracking the optimal turbine speed at a given wind speed. The result of the optimization is reaching in fact the optimal power efficiency at the given speed. In the simulation the optimum power is returned by the model through a 2D look-up table with interpolation of the turbine characteristics, with the action of the governor considered as instantaneous.

4.2. The doubly fed induction generator model

Stator and rotor voltages expressed in terms of d and q axes quantities rotating in an arbitrary reference frame with the speed ω_k are given by [6]:

$$U_{sd} = R_s \cdot i_{sd} + \frac{d\psi_{sd}}{dt} - \omega_k \cdot \psi_{sq} \quad (4)$$

$$U_{sq} = R_s \cdot i_{sq} + \frac{d\psi_{sq}}{dt} + \omega_k \cdot \psi_{sd} \quad (5)$$

$$U_{rd} = R_r \cdot i_{rd} + \frac{d\psi_{rd}}{dt} - (\omega_k - \omega_r) \cdot \psi_{rq} \quad (6)$$

$$U_{rq} = R_r \cdot i_{rq} + \frac{d\psi_{rq}}{dt} + (\omega_k - \omega_r) \cdot \psi_{rd} \quad (7)$$

Stator and rotor fluxes are expressed in function of the current by:

$$\psi_{sd} = L_s \cdot i_{sd} + L_m \cdot i_{rd} \quad (8)$$

$$\psi_{sq} = L_s \cdot i_{sq} + L_m \cdot i_{rq} \quad (9)$$

$$\psi_{rd} = L_r \cdot i_{rd} + L_m \cdot i_{sd} \quad (10)$$

$$\psi_{rq} = L_r \cdot i_{rq} + L_m \cdot i_{sq} \quad (11)$$

Also:

$$\Omega = \frac{\omega_m}{p} = \frac{\omega_s - \omega_r}{p} \quad (12)$$

$$T_e = \frac{3}{2} \cdot p \cdot (\psi_{sd} \cdot i_{sq} - \psi_{sq} \cdot i_{sd}) \quad (13)$$

Usually a speed range of ± 25% is chosen around the synchronous speed [7]. To have a lower current at the rotor-side of the machine equivalent with a lower converter sizing, and the same voltage at the rotor-side and the stator-side at the limits of the speed range (the voltage adapting transformer between the converter and the power system is avoided), a transformer ratio K of the generator windings of 4 is chosen:

$$U_{r\max} = K \cdot |s_{\max}| \cdot (U_s)_{rated} \tag{14}$$

4.3. The supply side converter model

The supply side converter is used to control the DC link voltage regardless of the level and the direction of the rotor power (Fig. 3). A vector-control strategy is used, with the reference frame oriented along the stator voltage [8]. The converter is current regulated with the direct axis current used to control the DC-link voltage, meanwhile the transverse axis current is used to regulate the displacement between the voltage and the current (and thus the power factor) [9].

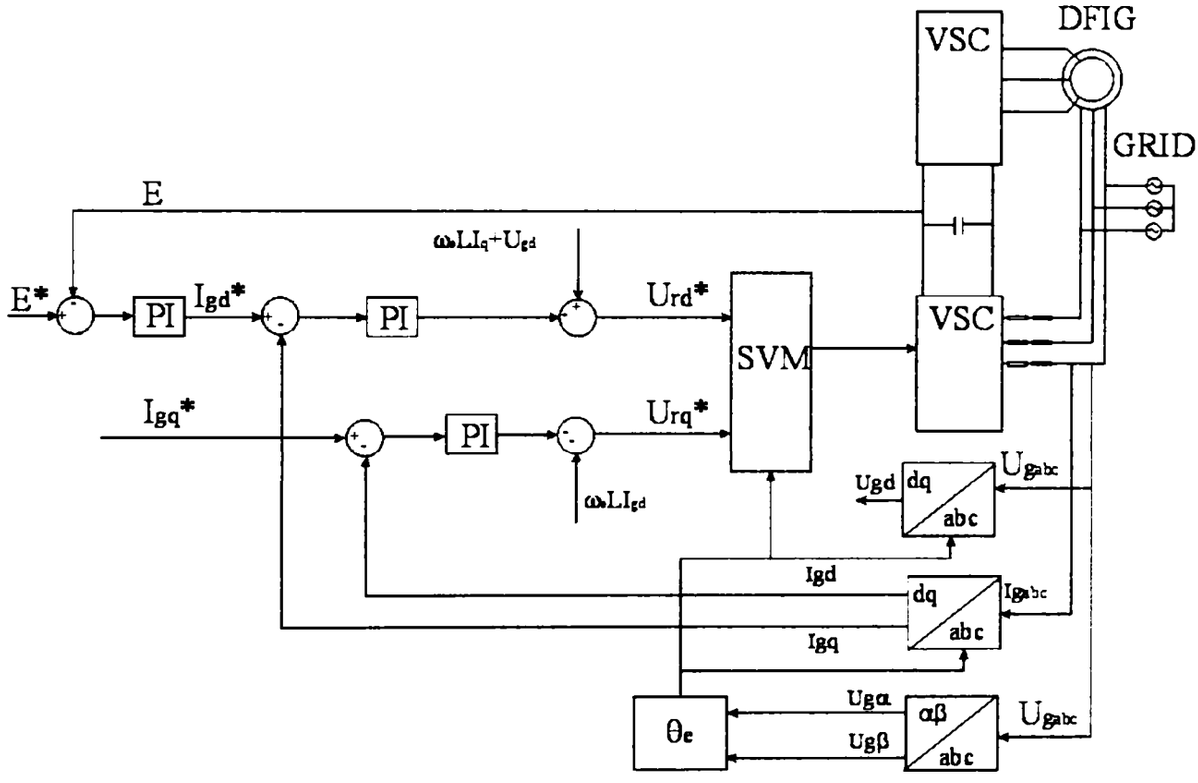

Figure 3. The block diagram of the supply-side converter control.

The angular position of the supply voltage θ_e is calculated as:

$$\theta_e = a\tan\frac{U_{s\beta}}{U_{s\alpha}} \tag{15}$$

where $U_{s\alpha}$ and $U_{s\beta}$ are the stator voltages expressed in terms of α and β axes (stationary).
The design of the current controllers follows from the transfer function of the plant in the z-domain, the sampling time being 0.45 ms. For a nominal closed-loop natural frequency of 125 Hz and a damping factor of 0.8 the transfer function of the PI controller is 18.69(z-1335.4)/(z-1). The current loop is designed much faster than the DC voltage loop and thus considered ideal. The transfer function of the DC voltage controller results in 17.95(z-2640)/(z-1).

4.4 The generator side converter model

The generator is controlled in a synchronously rotating dq-frame, with the d-axis aligned with the stator-flux vector position, which ensures a decoupled control between the electromagnetic torque and the rotor excitation contribution (see Fig. 4). In fact decoupled active and reactive power control [10,11] of the generator is obtained (Fig. 5).

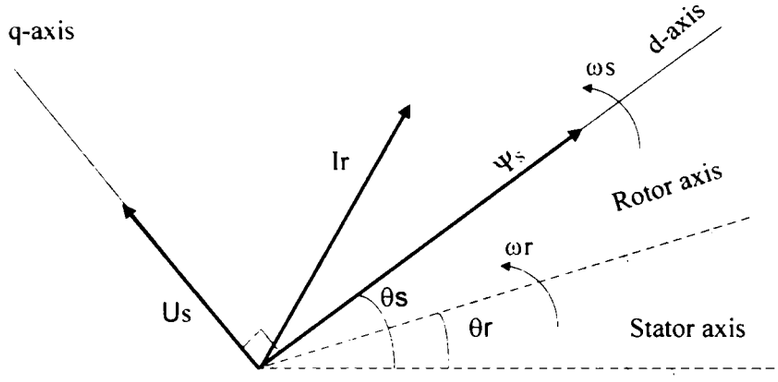

Figure 4. Location of different vectors in stationary coordinates.

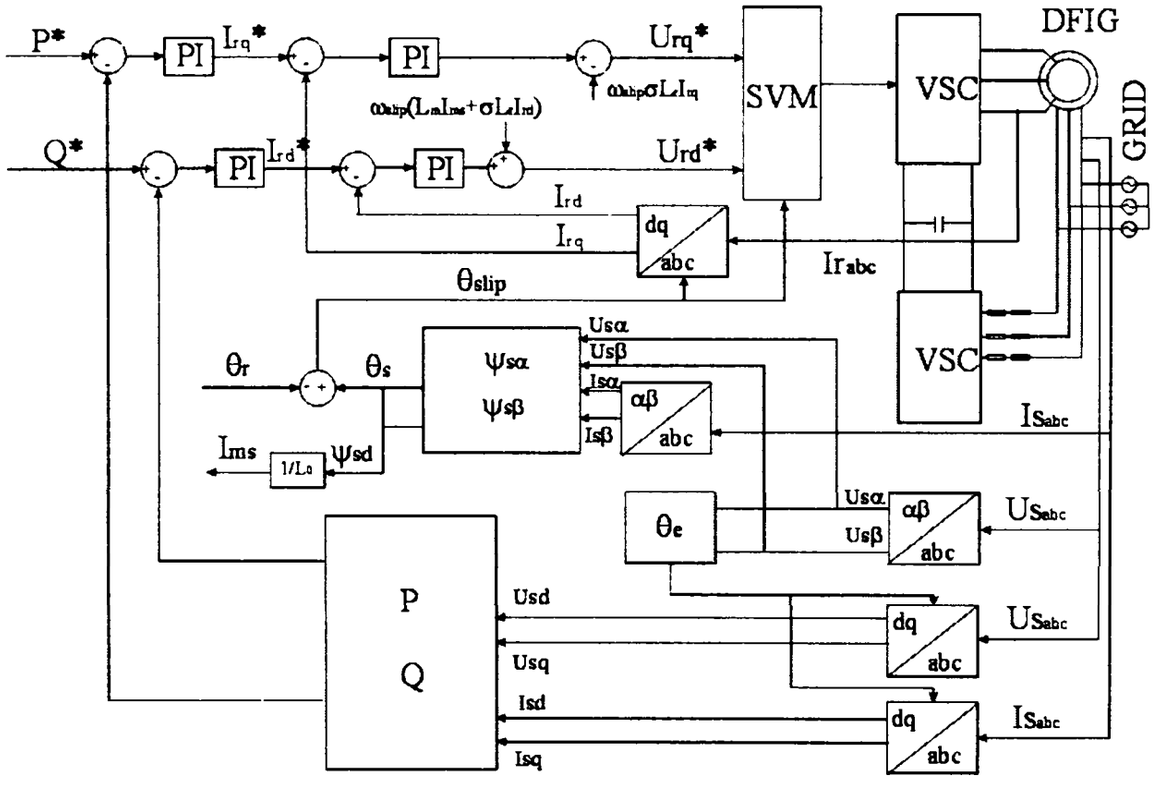

Figure 5. The block diagram of the machine-side converter control in a doubly-fed wind turbine.

Again knowing the transfer function of the plant and imposing the natural closed-loop frequency and the damping factor, the transfer function of the current controllers results in 12 (z-0.995)/(z-1). The power loops are designed much slower than the current loops and the transfer function for the power controllers are thus obtained:0.00009(z-0.9)/(z-1)

The reference voltages generated by the current control loops with back-EMF compensated are transformed back to the rotor reference frame and space vector modulated to generate the pulses for the inverter (VSC).

4.5 Simulation results

Extended simulations were performed on the model thus implemented. At 1.5 sec the wind speed is increased from 7 to 11m/s, then at 6 sec the reference of active power is increased from 1.2 MW at 1.4 MW while the reference of the reactive power is maintained at 300 kVAR

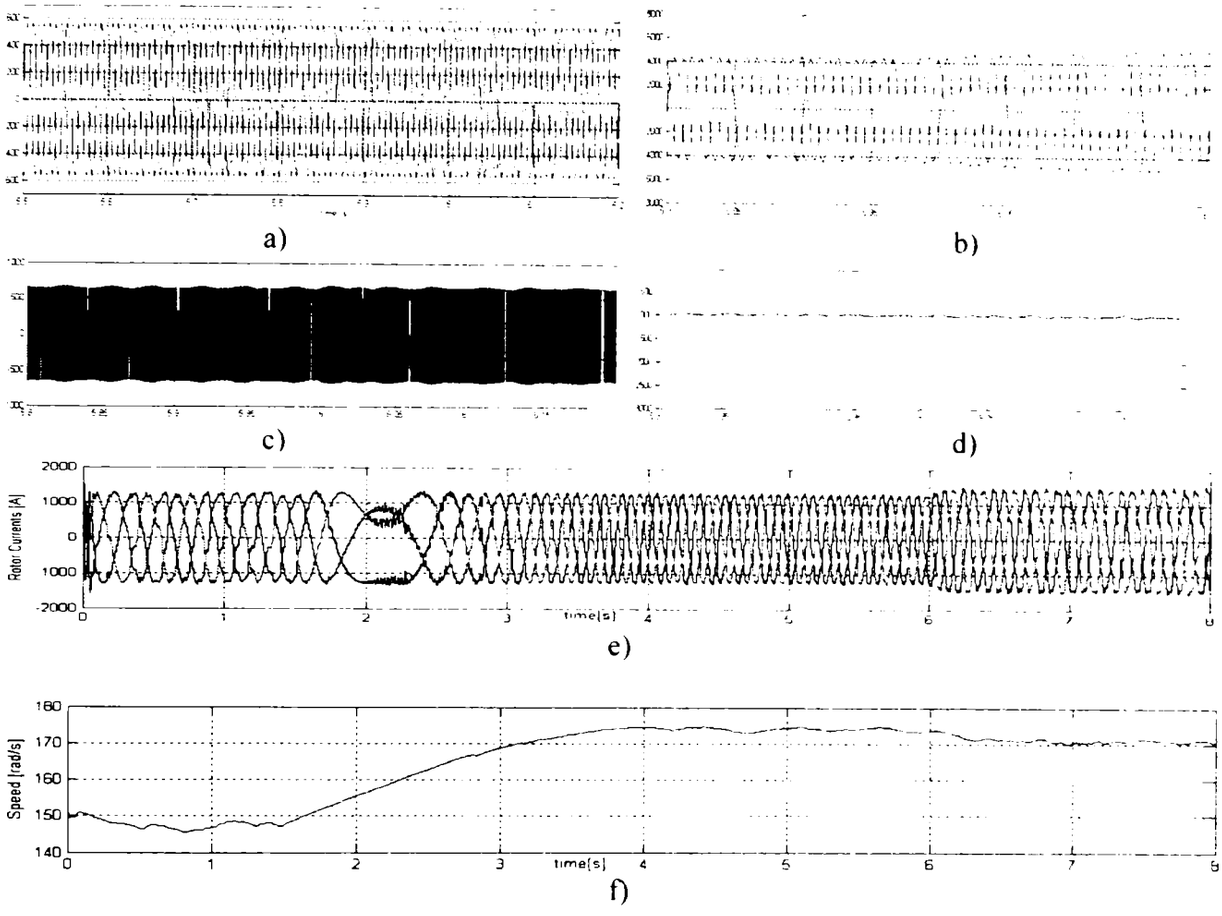

Figure 6. The generator waveforms: a) stator voltages, b) stator currents, c) rotor voltages, d) DC-link voltage, e) rotor currents, f) speed.

The active and reactive power are shown in Figure 7.

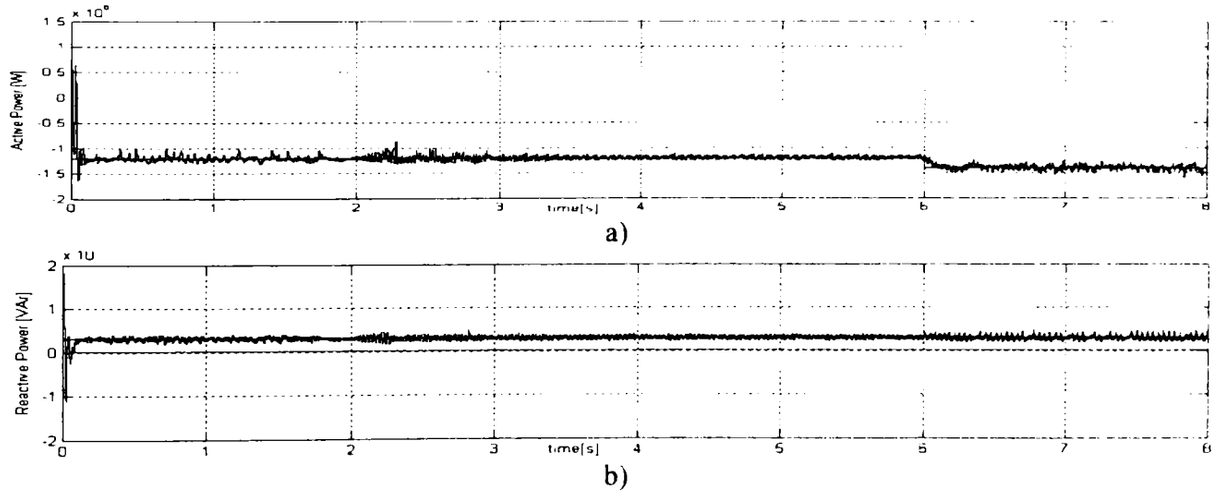

Figure 7. a) The active and b) reactive stator power control.

It can be noticed from here that the system response is stable and rather quick in terms of active power

5. Case Study – three-phase short-circuit on the power grid

In order to study the behavior of the whole system under a three-phase short-circuit on the power grid, without taking any protective measure, the grid is modeled as in Fig.1 and divided in two parts [12]. The short-circuit is applied at the middle of the line (see Figure 1).

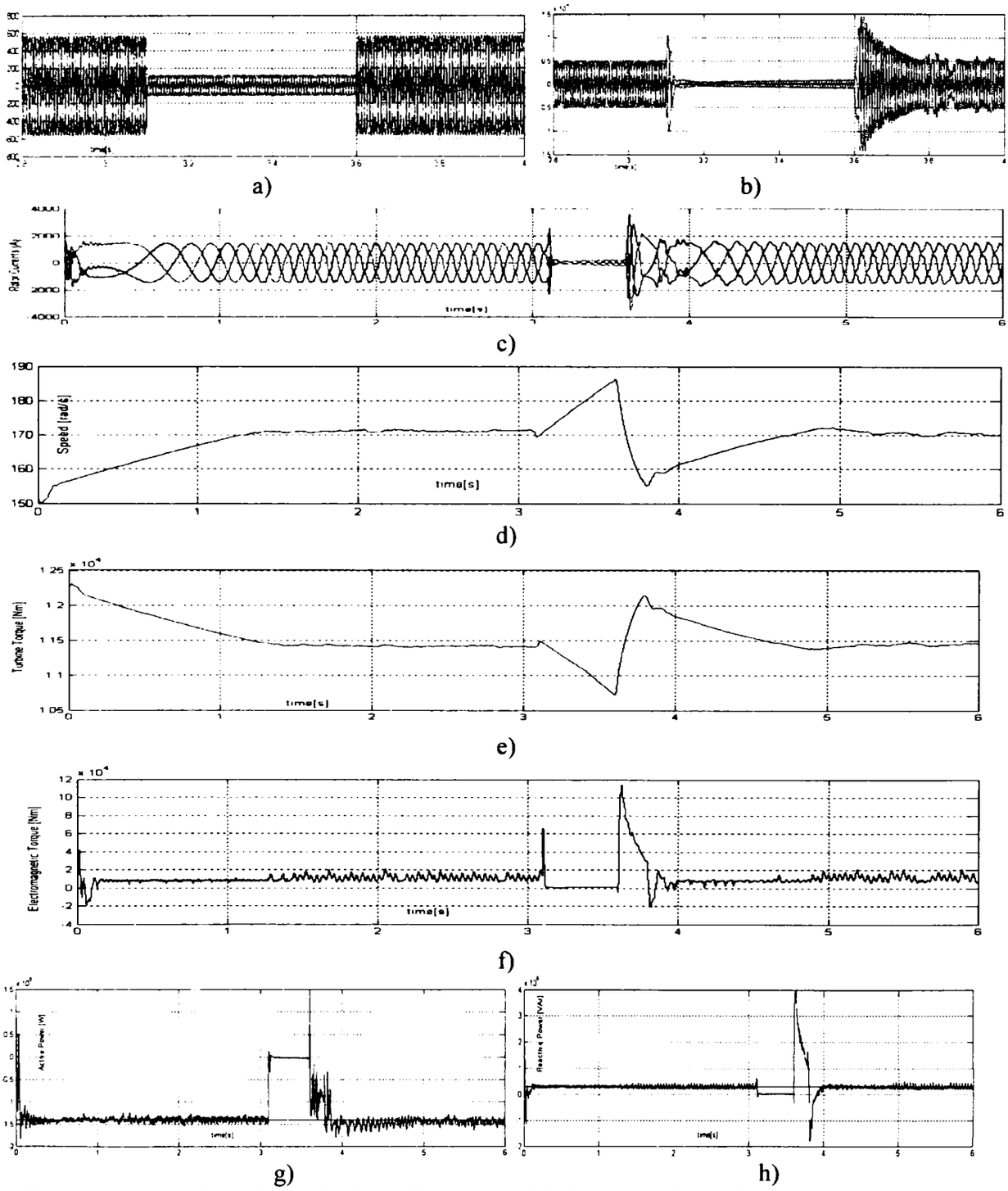

Figure 8. Three-phase short-circuit on the power grid: a) stator voltage, b) stator currents, c) rotor currents, d) speed, e) turbine torque, f) electromagnetic torque, g) active power, h) reactive power.

It can be seen there are two dominant current peaks, one at the start of the short-circuit, and one even more severe when the short-circuit is cleared. Two severe transients in torque also occur, and a

transient in speed, which means that during the fault the electromagnetic torque is very small and thus the generator accelerates. The torque of the turbine is naturally decreased during the fault as the generator speed is increasing and the wind speed remains constant (see the characteristics in Fig.2)

6. Mechanism to improve the performance during fault

To reduce the transients due to short-circuit a few methods were investigated. The first was to reduce the active and reactive power references immediately after the fault occurs. But this did not produce any improvement.

The most efficient method according to this study was to limit the rotor currents. This was done by limiting the reference of the rotor currents, in fact the output of the active and reactive power PI controllers at the $\pm 1.5\ I_m$ in q-axis and at $\pm 0.5\ I_m$ in d-axis. The results are presented in what follows.

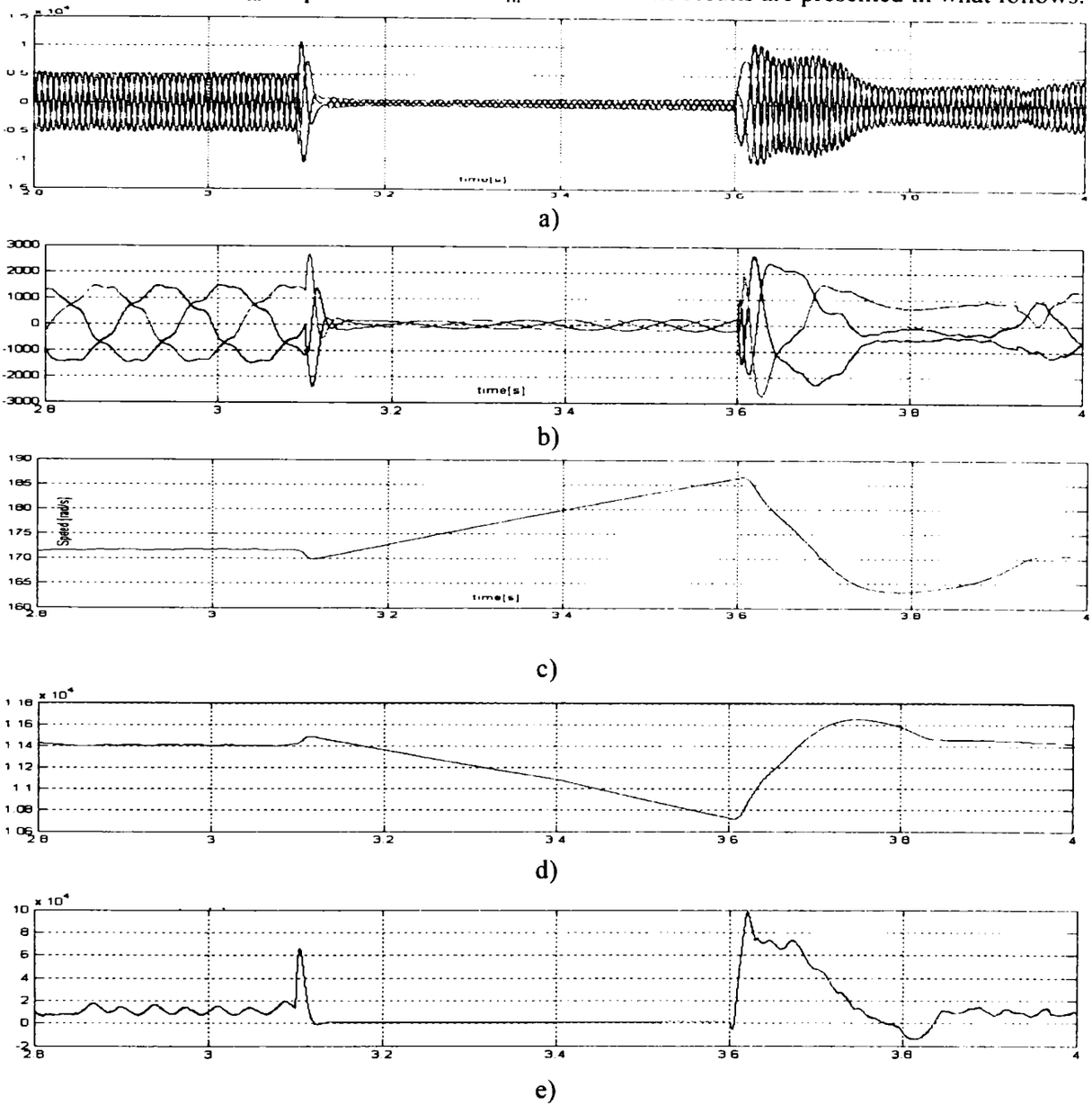

Figure 9. Three phase short-circuit on the power grid, with limited rotor currents in the generator: a) stator currents, b) rotor currents, c) speed, d) turbine torque, e) electromagnetic torque

Notable improvements can be easily noticed. First and the most important is the reduction of the second rotor current peak (when the short-circuit is cleared) with 50%. The stator current second peak is also reduced with the same amount. The acceleration of the generator is not avoided but when the system is restoring the deceleration is not so pronounced and the speed of the generator is stabilizing

earlier (practically the system is recovering with 1 sec more quickly than in the case with no limitations in the rotor currents)

7. Conclusion

For large power wind farms continuous operation during short-circuit faults is required. This mode becomes more and more important as the wind turbine should be able to contribute with power just after a short circuit. A detailed investigation on the control and behavior on the doubly-fed induction generator under power grid short-circuit was done. The good dynamic performances and accuracy of the active and reactive power control were demonstrated. Also the waveforms of the generator in a three-phase short-circuit are presented. For better continuous operation during short-circuit faults different methods were investigated. The modification of the power references during the fault in order to prevent the rotor overcurrents and generator overspeeding was performed but it did not produce the expected results. The best situation was obtained with the limitation of the rotor currents references through the output limitation of the active and reactive power controllers. This study will be continued and other methods will be investigated.

8. References

[1] T. Ackermann, L. Söder, "An overview of wind energy: status 2002," Renewable and Sustainable Energy Reviews, pp. 67 – 128, June 2002.

[2] Horns Rev Website: http://www.hornsrev.dk

[3] Marian P. Kazmierkowski (Editor), Ramu Krishnan (Editor), Frede Blaabjerg (Editor), "Control in Power Electronics: Selected Problems" Chapter 13: Lars Helle, Frede Blaabjerg, "Wind Turbine Systems", Publisher: Academic Press ISBN: 0124027725, 1st edition (August 2002).

[4] V. Akhmatov, "Modelling of variable speed wind turbines with doubly-fed induction generators in short term stability investigations," *3rd Int. Workshop on Transmission Networks for Offshore Wind Farms*, April 11-12, 2002, Stockholm, Sweden.

[5] R. Pena, J. C. Clare, G. M. Asher, "Doubly-fed induction generator using back-to-back PWM converters and its application to variable-speed wind-energy generation," *Proc. Inst. Elect. Eng.*, pt. B, vol. 143, pp. 231-241, May 1996.

[6] Ion Boldea, "Electric Drives", Chapter 14: Large Power Drives, 14.8 Sub and Hypersynchronous IM cascade drives, CRC Press Florida, ISBN: 0849325218, 1998.

[7] U. Rädel, D. Navarro, G. Berger, S. Berg, "Sensorless Field-Oriented Control of a Slipring Induction Generator for a 2.5 MW Wind Power Plant from Nordex Energy GmbH", EPE 2001 Conference Proceedings, Graz.

[8] R. Datta, V.T. Ranganathan, "Direct Power Control of Grid-Connected Wound Rotor Induction Machine Without Rotor Position Sensors," IEEE Transactions On Power Electronics, vol. 16, no. 3, May 2001, pp. 390-399.

[9] L. Morel, H. Godfroid, A. Mirzaian, J. M. Kauffmann, "Double-fed induction machine: converter optimization and field oriented control without position sensor," *Proc. Inst. Elect. Eng.*, pt.B, vol. 145, pp. 360-368, July 1998.

[10] S. Müller, M. Deicke, R. W. De Doncker, "Adjustable speed generators for wind turbines based on double-fed induction machines and 4-quadrant IGBT converters linked to the rotor," *IEEE-IAS Annual Meeting*, 2000

[11] T. Senjyu, N. Sueyoshi, K. Uezato, H. Fujita, "Stability analysis of wind power generating system" Power Conversion Conference, 2002. PCC Osaka 2002 Proceedings, vol. 3: 2002 pp. 1441 –1446.

[12] P. Ledesma, J. Usaola, "Minimum Voltage Protections in Variable Speed Wind Farms", 2001 Porto Power Tech Conference, 10th – 13th September, Porto, Portugal

Sensorless doubly-fed induction generator control under power system transients and faults: the influence of magnetic saturation

Ioan Serban[1], Ion Boldea[1], Frede Blaabjerg[2]

[1]University Politehnica Timisoara, Faculty of Electrical Engineering,
Bd. Parvan nr.2, Lab D108
300223 Timisoara, ROMANIA
Phone/Fax: +40-256-204402
Email: serban@lselinux.utt.ro , boldea@lselinux.utt.ro

[2] Institute of Energy Technology, Aalborg University
Pontoppidanstraede 101
9220 Aalborg, DENMARK
Phone/Fax: + 45 9635 9254
E-mail: fbl@iet.auc.dk

Abstract **– The present paper investigates the influence of magnetic saturation on the rotor position and speed estimators and the machine behavior during transients and shortcircuit faults for a doubly-fed induction generator (DFIG) connected to the power grid.**

The DFIG is considered driven by a wind turbine whose torque vs. generator speed at different wind speeds is optimized. The DFIG is connected to the grid, at a certain initial speed, simultaneously in the stator and in the rotor for given values of active and reactive stator power references. Subsequently a sudden three-phase shortcircuit at the middle of a typical local power grid is investigated. A computer program in Matlab-Simulink package for the whole system has been developed and applied to simulate transients as described above with and without considering the magnetic saturation in the machine. It is shown by digital simulations that during shortcircuit the sensorless control fails without considering the magnetic saturation and even during the sudden connection to the grid the errors in position and speed estimation and in the transients description are notable.

Index Terms **– wind turbines, doubly-fed induction generator, back-to-back inverter, vector control, sensorless techniques, magnetic saturation.**

I. Introduction

Harnessing energy from renewable sources became a global phenomenon and the world's fastest growing technology. The impetus behind this expansion has come increasingly from the urgent need to combat global climate changes whereas the electrical energy demand is more and more increased [1]. Most countries now accept that greenhouse gas emissions must be cut in order to avoid environmental catastrophe.

In this challenge, the worldwide installed hydro and, recently, tidal and marine currents turbine power [2] has increased dramatically but the wind energy technology is the real "silver bullet". Table 1 shows the wind capacity in June 2003 and its trend for some EU countries

TABLE I
INSTALLED WIND POWER IN SOME EU COUNTRIES [3]

Country	Total of the end of 2002	Installed summer 2003	Total 2003
Germany	12001	835	12836
Spain	4830	230	5060
Denmark	2881	36	2916
Netherlands	678	125	803
Italy	788	12	800
UK	552	34	586
Sweden	328	36	364
Greece	297	57	354
France	148	72	220
Austria	139	80	219
Portugal	196	21	217
Ireland	137	0	137
European Union	**23076**	**1550**	**24626**
Other European Countries	**237**	**41**	**278**

Among these, the European Commission has scheduled 12% penetration of renewable energy by the year 2010 and the objective for United States is 10 000 MW by the same year [4].

These high ambitions along with fast progress in generator concepts, power electronics and control have founded a strong basis for the development of large and cost-competitive wind turbines.

The average rating of the installed wind turbines has increased from 0.2MW in 1990 at 1.6 MW in this and the

price of the wind energy has decreased with 80% in the last 20 years. This opens up new technical opportunities for designing and controlling the wind turbines, but at the same time increases the demands for reliability, supplied power quality and grid impact.

The majority of the installed wind turbines operate at constant or near constant speed, which implies the speed of the electric generator to be fixed (determined by the frequency of the grid) regardless of the wind speed. For this, different topologies with the induction generator and the wound rotor synchronous generator have been proposed and applied but the majority of the fixed speed wind turbines are based on the induction generator.

The inherent problems with the constant speed wind turbines (poorer energy capture, rather big mechanical stress and modest power quality) became more and more significant as the size of the wind turbines and the penetration of wind energy increase.

So the variable speed concept became more and more attractive and today is in fact almost the main applied concept. The most important candidates in this concept are the wound rotor induction generator with a back-to-back inverter feeding the rotor circuit, and the permanent magnets synchronous generator. By the use of the PM generators the slip rings are avoided but with a rather large additional costs due to the prices of permanent magnets and of the power electronics converter which has to handle in this case the full power of the system.

The doubly fed induction generator with a bi-directional power flow converter in the rotor doubtlessly has some advantages:

- enhanced energy capture from the wind in a wide range of wind velocities
- ability of reactive power control
- fast decoupled control of active and reactive power by independent control of torque and rotor excitation
- reduced size and implicitly costs of the power electronics converter (the converter rating is only around 25% of the total generator power)

In this paper a study based on this solution is done. Both inverters are vector controlled and the strategy will be described.

One sensorless algorithm is presented and discussed "in extenso". The influence of saturation in the position observer is taken into account and discussed. For this objective, a severe three-phase shortcircuit on the power grid is modeled and the behavior of the observer is studied.

The importance of the behavior of the whole system under power grid faults and transients is crucial as by standards the large off-shore wind turbines should not be disconnected during grid shortcircuits, for example, because the turbine has to contribute at the power recovery immediately after the fault. One method to improve the performance of the DFIG under a three-phase shortcircuit without disconnection is presented in [5].

The following sections are related to: DFIG control, sensorless algorithm with results for position and speed estimator with and without taking into account the saturation of the machine under a sudden three-phase shortcircuit of the power grid.

II. The DFIG System and its Control

All the models in the DFIG system used are described in what it follows. The electrical schematic of the whole system is shown in Figure 1.

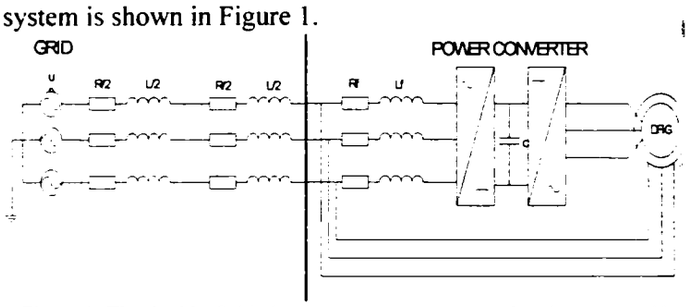

Figure 1. The doubly-fed induction generator connected to the power grid

The grid is modeled as divided in two equal parts in order to apply the shortcircuit at the middle.

A. The wind turbine model

The wind turbine is modeled in terms of optimal tracking, to provide maximum energy capture from the wind. The implemented characteristics are presented in Fig. 2

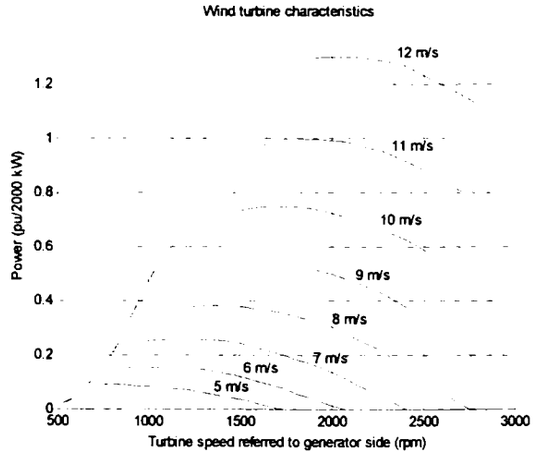

Figure 2. Implemented wind turbine characteristics: a) aerodynamic characteristics, b) the turbine torque model.

These characteristics are based on:

$$P_M = \frac{1}{2} \cdot \rho_{air} \cdot C_p(\lambda,\beta) \cdot \pi \cdot R^2 \cdot V^3 \quad (1)$$

where C_p - power efficiency coefficient; V – wind velocity; β - pitch angle; R – blade radius; P_M – mechanical power produced by the wind turbine; ρ_{air} – air density (usually 1.225 kg/m^3)

Applying the tip speed ratio λ :

$$\lambda = \frac{\omega_m \cdot R}{V} \quad (2)$$

equation (1) may be rewritten as:

$$P_M^{opt} = \frac{1}{2} \cdot \rho_{air} \cdot \pi \cdot R^5 \cdot \frac{C_P^{opt}}{\lambda_{opt}^3} \cdot \omega_m^3 = K_w \cdot \omega_m^3 \quad (3)$$

where K_w is the wind turbine dependent coefficient

Equation (3) holds the key of the optimization of the variable-speed wind turbine by tracking the optimal turbine speed at a given wind speed. The result of the optimization is reaching in fact the optimal power efficiency at the given speed. In the simulation the optimum power is returned by the model through a 2D look-up table with interpolation of the turbine characteristics, with the action of the governor considered as instantaneous.

B. The doubly fed induction generator model

Stator and rotor voltages expressed in terms of d and q axes quantities rotating in an arbitrary reference frame with the speed ω_k are given by [6]:

$$U_{sd} = R_s \cdot i_{sd} + \frac{d\psi_{sd}}{dt} - \omega_k \cdot \psi_{sq} \quad (4)$$

$$U_{sq} = R_s \cdot i_{sq} + \frac{d\psi_{sq}}{dt} + \omega_k \cdot \psi_{sd} \quad (5)$$

$$U_{rd} = R_r \cdot i_{rd} + \frac{d\psi_{rd}}{dt} - (\omega_k - \omega_r) \cdot \psi_{rq} \quad (6)$$

$$U_{rq} = R_r \cdot i_{rq} + \frac{d\psi_{rq}}{dt} + (\omega_k - \omega_r) \cdot \psi_{rd} \quad (7)$$

Stator and rotor fluxes are expressed in function of the current by:

$$\psi_{sd} = L_s \cdot i_{sd} + L_m \cdot i_{rd} \quad (8)$$

$$\psi_{sq} = L_s \cdot i_{sq} + L_m \cdot i_{rq} \quad (9)$$

$$\psi_{rd} = L_r \cdot i_{rd} + L_m \cdot i_{sd} \quad (10)$$

$$\psi_{rq} = L_r \cdot i_{rq} + L_m \cdot i_{sq} \quad (11)$$

where variation of Lm is implemented as in Figure 3.

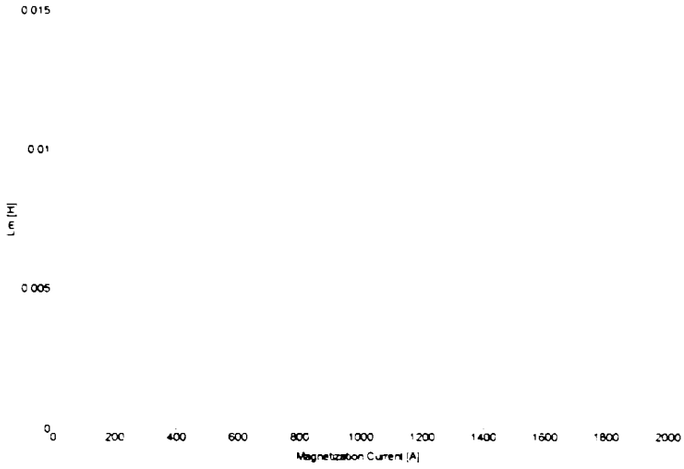

Figure 3. The magnetic saturation: variation of L_m versus magnetization current

Also:

$$\Omega = \frac{\omega_m}{p} = \frac{\omega_s - \omega_r}{p} \quad (12)$$

$$T_e = \frac{3}{2} \cdot p \cdot (\psi_{sd} \cdot i_{sq} - \psi_{sq} \cdot i_{sd}) \quad (13)$$

Usually a speed range of ± 25% is chosen around the synchronous speed [7]. To have a lower current at the rotor-side of the machine, equivalent with a lower converter sizing, and the same voltage at the rotor-side and the stator-side at the limits of the speed range (the voltage adapting transformer between the converter and the power system is avoided), a turn ratio K of the generator windings of 4 is chosen:

$$U_{r\,max} = K \cdot |s_{max}| \cdot (U_s)_{rated} \quad (14)$$

C. The supply side converter model

The supply side converter is used to control the DC link voltage regardless of the level and the direction of the rotor power (Fig. 4). A vector-control strategy is used, with the reference frame oriented along the stator voltage [8]. The converter is current regulated with the direct axis current used to control the DC-link voltage, meanwhile the transverse axis current is used to regulate the displacement between the voltage and the current (and thus the power factor) [9].

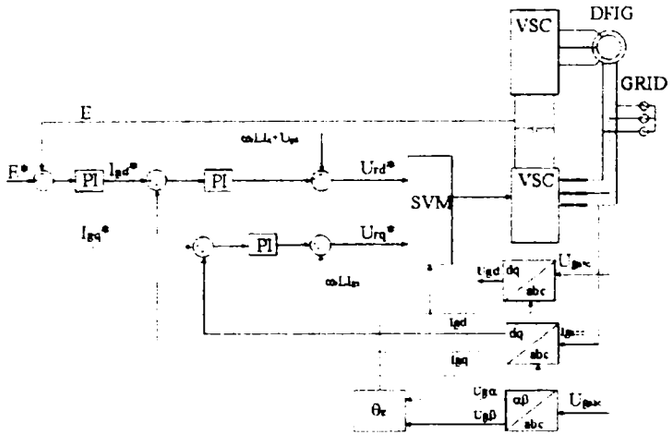

Figure 4. The block diagram of the supply-side converter control.

The angular position of the supply voltage θ_e is calculated as:

$$\theta_e = a\tan\frac{U_{s\beta}}{U_{s\alpha}} \qquad (15)$$

where $U_{s\alpha}$ and $U_{s\beta}$ are the stator voltages expressed in terms of α and β axes (stationary).

The design of the current controllers follows from the transfer function of the plant in the z-domain, the sampling time being 0.45 ms. For a nominal closed-loop natural frequency of 125 Hz and a damping factor of 0.8 the transfer function of the PI controller is 18.69(z-1335.4)/(z-1). The current loop is designed much faster than the DC voltage loop and thus considered ideal. The transfer function of the DC voltage controller results in 17.95(z-2640)/(z-1).

D. The generator side converter model

The generator is controlled in a synchronously rotating dq-frame, with the d-axis aligned with the stator-flux vector position, which ensures a decoupled control between the electromagnetic torque and the rotor excitation contribution (see Fig. 5). In fact decoupled active and reactive power control [10,11] of the generator is obtained (Fig. 6).

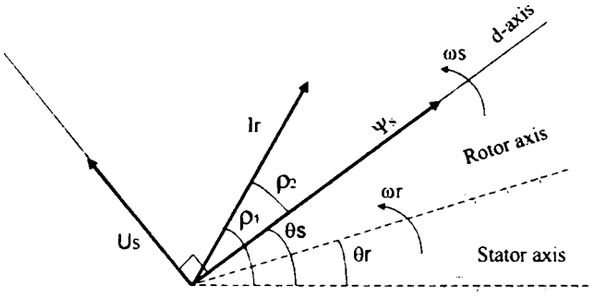

Figure 5. Location of different vectors in stationary coordinates.

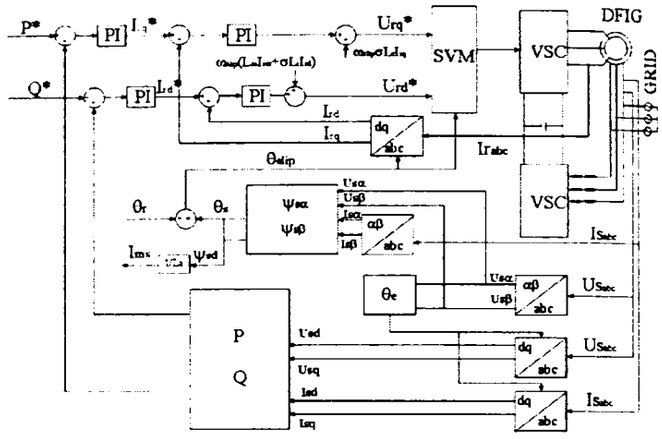

Figure 6. The block diagram of the machine-side converter control in a doubly-fed wind turbine.

Again knowing the transfer function of the plant and imposing the natural closed-loop frequency and the damping factor, the transfer function of the current controllers results in 12 (z-0.995)/(z-1). The power loops are designed much slower than the current loops and the transfer function for the power controllers are thus obtained: 0.00009(z-0.9)/(z-1)

The reference voltages generated by the current control loops with back-EMF compensation are transformed back to the rotor reference frame and space vector modulated to generate the pulses for the inverter (VSC).

III. Position and Speed Estimation with and without Saturation Considered

In order to avoid using an encoder the position should be estimated for the vector control. Also speed information for the back-EMF compensation is needed.

The sensorless algorithm is based on the vector diagram in Figure 5 and is adapted from [12]. The rotor current (which can be measured in rotor coordinates) makes an angle ρ_1 with the stator axis and an angle ρ_2 with the rotor axis. The difference between ρ_1 and ρ_2 is the rotor position θ_r which must be determined. In Figure 7 the block diagram of the sensorless algorithm is presented and in what it follows it will be explained in detail.

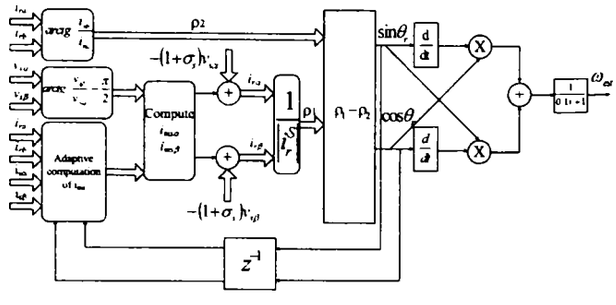

Figure 7. Block diagram of the position/speed sensorless algorithm

The position of the stator flux magnetizing current is calculated assuming the stator resistance is very small and, hence, the stator flux is in quadrature with the stator voltage.

The magnitude of the stator magnetizing current is:

$$I_{ms} = \frac{U_s}{\omega_s L_m} \tag{16}$$

This is used as an initializing value in the algorithm, if the saturation is considered, and the value is continuously recalculated as we will show later. If the saturation is neglected this value can be considered along the entire algorithm.

The I_{ms} components in stator coordinates can be calculated as:

$$I_{ms\alpha} = I_{ms} \cdot \sin\theta_e \tag{17}$$

$$I_{ms\beta} = -I_{ms} \cdot \cos\theta_e \tag{18}$$

The rotor currents in stator coordinates are:

$$I_{r\alpha} = I_{ms\alpha} - (1+\sigma_s) I_{s\alpha} \tag{19}$$

$$I_{r\beta} = I_{ms\beta} - (1+\sigma_s) I_{s\beta} \tag{20}$$

where: $\sigma_s = \frac{L_{sl}}{L_m}$, L_{sl} – stator leakage inductance

Hence, the angle ρ_2 results:

$$\rho_1 = \frac{I_{r\beta}}{I_{r\alpha}} \tag{21}$$

As the rotor currents are directly measured in the rotor circuit, the angle ρ_1 can be immediately computed as:

$$\rho_2 = \frac{I_{rb}}{I_{ra}} \tag{22}$$

With angles ρ_1 and ρ_2 thus calculated, the rotor position can be now easily calculated:

$$\theta_r = \rho_1 - \rho_2 \tag{23}$$

The speed is estimated with the following equation:

$$\omega_{est} = -\sin\theta_r \frac{d}{dt} \cdot \cos\theta_r + \cos\theta_r \cdot \frac{d}{dt} \cdot \sin\theta_r \tag{24}$$

The differential terms introduces some noise which has to be eliminated using a first order low-pass filter with a transfer function: $\frac{1}{0.1 \cdot s + 1}$.

The accuracy of computation of the rotor position depends on the value of I_{ms}. To estimate the magnetization current the magnetizing inductance L_m is required. If there is a serious variation in the grid voltage or in the supply frequency L_m will most likely saturate. In this condition the estimation of the rotor position is seriously affected.

However, any change in the magnitude of the stator flux can be correctly estimated using the following adaptive algorithm [12].

First, the algorithm is started with the value of I_{ms} in equation 16. After that, I_{ms} is computed by transforming the present rotor current sample to the stator coordinates using the unit vectors computed in the previous interval.

This is based on the following equations:

$$I'_{r\alpha}[k] = I_{ra}[k] \cdot \cos\theta_r[k-1] - I_{rb}[k] \cdot \sin\theta_r[k-1] \tag{25}$$

$$I'_{r\beta}[k] = I_{rb}[k] \cdot \cos\theta_r[k-1] + I_{ra}[k] \cdot \sin\theta_r[k-1] \tag{26}$$

$$I'_{ms\alpha}[k] = (1+\sigma_s) \cdot I_{s\alpha}[k] + I'_{r\alpha}[k] \tag{27}$$

$$I'_{ms\beta}[k] = (1+\sigma_s) \cdot I_{s\beta}[k] + I'_{r\beta}[k] \tag{28}$$

$$I'_{ms} = \sqrt{\left(I'^2_{ms\alpha} + I'^2_{ms\beta}\right)} \tag{29}$$

The algorithm is implemented and the results are presented in what it follows.

In figure 8a the comparison between the measured and the estimated rotor position is presented and in 8b the comparison between the estimated and the measured speed is shown.

The results are satisfactory even during (3.1-3.6s) and after the shortcircuit (after 3.6s). The active power reference is maintained at 1.4MW. The reactive power reference is set at 0.4MVAR. The control in terms of active and reactive power and also in rotor currents is rather accurate as it is shown in Figure 9 and 10 respectively.

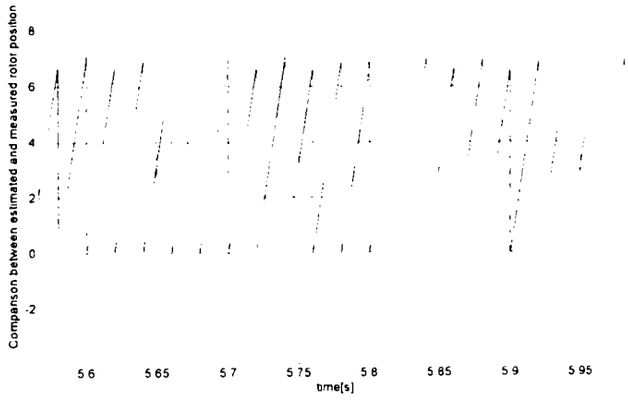

a)

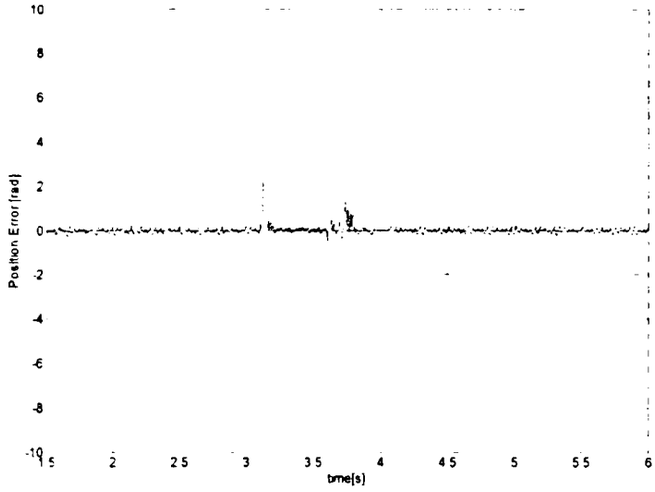

b)

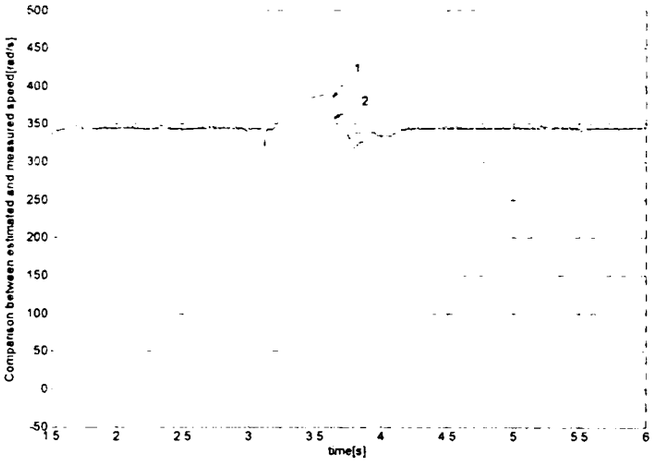

c)

Figure 8. The estimated and measured rotor position (a), the error in position estimation (b) and the estimated (1) and measured (2) speed (c)

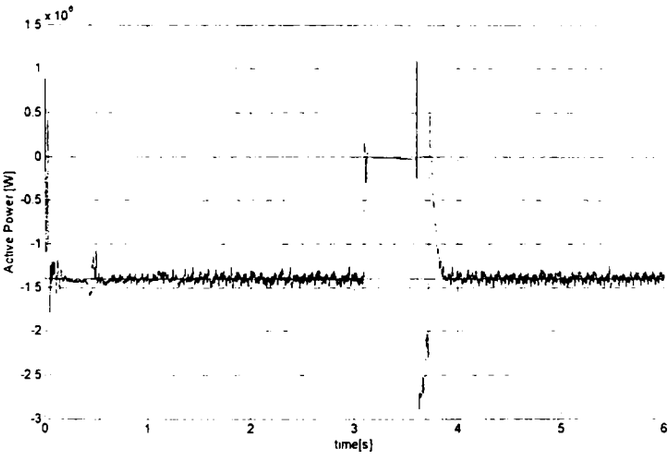

a)

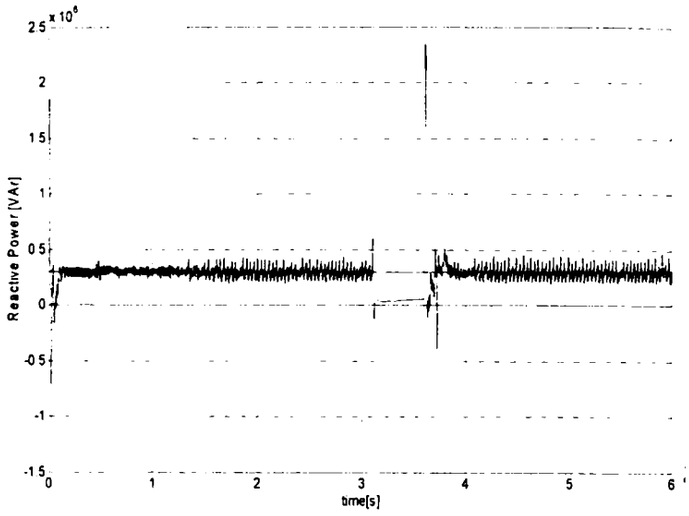

b)

Figure 9. The active (a) and reactive (b) power

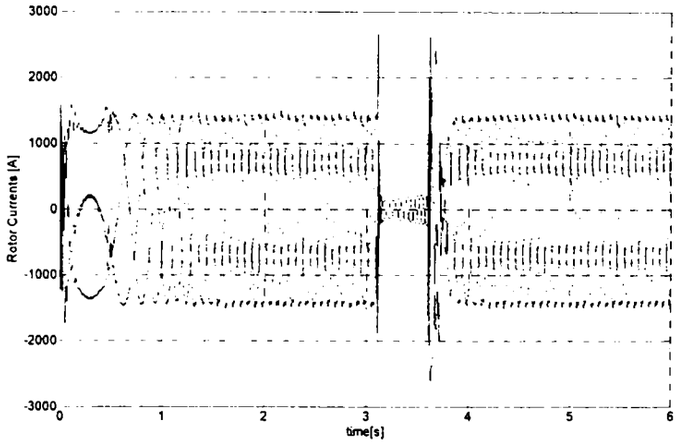

Figure 10. The rotor currents

In order to study the influence of taking into account the magnetic saturation in the estimator, the adaptive algorithm for calculation of I_{ms} is neglected, and the value of I_{ms} is considered constant along the simulation. In this new circumstance Figure 11 shows the comparison between the measured and estimated angle and between the estimated and measured speed.

It could be easily observed that immediately after the shortcircuit occurs the estimation is totally compromised due to imprecision in calculations with constant L_m. but the system works with the motion observer with variable L_m as it was discussed above.

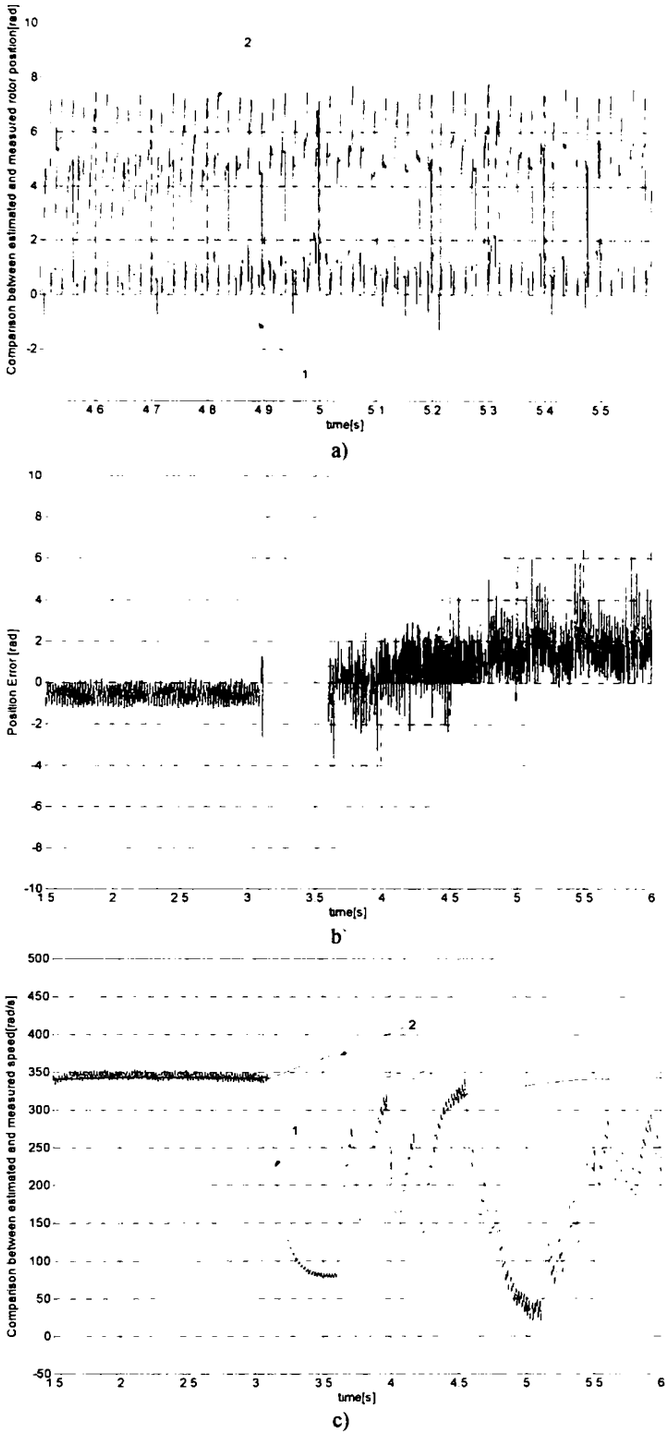

Figure 11. The estimated (1) and measured (2) rotor position (a), the error in rotor position estimation (b) and the estimated (1) and measured (2) speed (c) without considering the saturation in the estimators

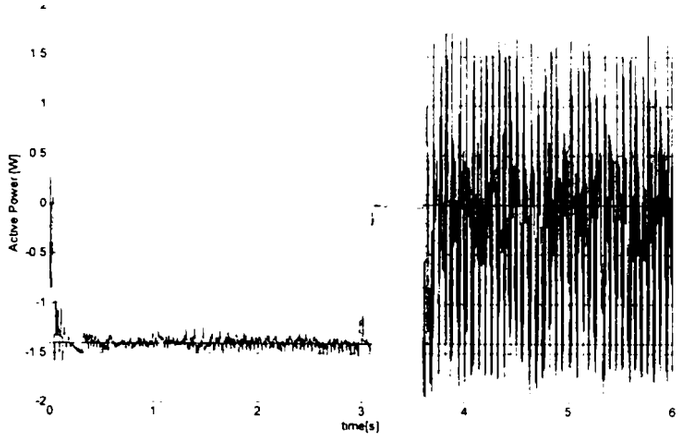

Figure 12. The active power without considering the saturation in the estimators

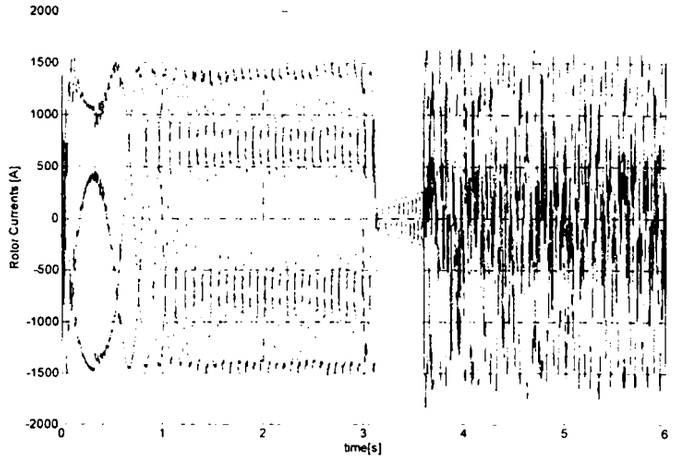

Figure 13 The rotor currents without considering the saturation in the estimators.

Also the control is irreversibly lost. For the same transient the control failure in power and rotor current (with constant L_m) is further illustrated in Figures 12 and 13.

We believe this a conclusive evidence that magnetic saturation is a must in the motion observer for successful robust control even during grid faults.

IV. Conclusion

Position sensorless control is a very desirable feature for the DFIG for wind or hydro-power applications.

A motion state estimator was implemented, and the taking into account of the magnetic saturation is shown mandatory both in connecting to the grid and shortcircuits faults by system digital simulations.

V. REFERENCES

[1] Wind Energy, "Clean power for generations," *Documents of European Renewable Energy Council*, www.erec-renewables.org

[2] C. Lang, "Harnessing tidal energy takes new turn," *IEEE Spectrum, vol. Sept. 2003*

[3] EWEA website: www.ewea.org

[4] M. P. Kazmierkowski (Editor), R. Krishnan (Editor), F. Blaabjerg (Editor), "Control in power electronics: selected problems," Chapter 13: L. Helle, F. Blaabjerg, "Wind turbine systems", *Publisher: Academic Press ISBN: 0124027725, 1st edition (August 2002).*

[5] I. Serban, F. Blaabjerg, I. Boldea, Z. Chen, "A study of the doubly-fed wind power generator under power grid faults," *Proc. of EPE Conference 2003, Toulouse, FRANCE*

[6] I. Boldea, "Electric drives," Chapter 14: "Large power drives, 14.8 Sub and Hypersynchronous IM cascade drives," *CRC Press Florida, ISBN: 0849325218, 1998.*

[7] U. Rädel, D. Navarro, G. Berger, S. Berg, "Sensorless field-oriented control of a slipring induction generator for a 2.5 MW wind power plant from Nordex Energy GmbH," *EPE 2001 Conference Proceedings, Graz.*

[8] R. Datta, V.T. Ranganathan, "Direct Power Control of Grid-Connected Wound Rotor Induction Machine Without Rotor Position Sensors," *IEEE Transactions On Power Electronics, vol. 16, no. 3, May 2001, pp. 390-399.*

[9] L. Morel, H. Godfroid, A. Mirzaian, J. M. Kauffmann, "Double-fed induction machine: converter optimization and field oriented control without position sensor," *Proc. Inst. Elect. Eng., pt.B, vol. 145, pp. 360-368, July 1998.*

[10] S. Müller, M. Deicke, R. W. De Doncker, "Adjustable speed generators for wind turbines based on double-fed induction machines and 4-quadrant IGBT converters linked to the rotor," *IEEE-IAS Annual Meeting, 2000*

[11] T. Senjyu, N. Sueyoshi, K. Uezato, H. Fujita, "Stability analysis of wind power generating system," *Power Conversion Conference, 2002. PCC Osaka 2002 Proceedings, vol. 3: 2002 pp. 1441 –1446.*

[12] R. Datta, V.T. Ranganathan, "A simple position-sensorless algorithm for rotor-side field-oriented control of wound-rotor induction machine," *IEEE Transactions on Industrial Electronics, vol. 48, no.4, August 2001.*

Sensorless wound-rotor induction machine (WRIM): dual-converter motoring control with short-circuited stator

Ioan Serban[1], Gheorghe-Daniel Andreescu[2], Cristian Lascu[3], Frede Blaabjerg[4], Ion Boldea[3]

[1]ebmpapst St. Georgen GmbH & Co. KG, Research and Development Laboratory for Electric Drives
Hermann-Papst-Str. 1, D-78112 St. Georgen/Schwarzwald, GERMANY, Phone: +49-7724-811834, Fax: +49-7724-8151834, Email: Ioan.Serban@de.ebmpapst.com

[2]University Politehnica of Timisoara, Faculty of Automation and Computers, Bd. V. Parvan nr.2, 300223 Timisoara, ROMANIA, Phone/Fax: +40-256-403245 / +40-256-403214, Email: dandre@aut.utt.ro

[3]University Politehnica of Timisoara, Faculty of Electrical Engineering,
Bd. V. Parvan nr.2, 300223 Timisoara, ROMANIA, Phone/Fax: +40-256-403463 +40-256-403452
Email: luci@lselinux.utt.ro, cristi@et.utt.ro, boldea@lselinux.utt.ro

[4] Aalborg University, Institute of Energy Technology, Pontoppidanstraede 101, 9220 Aalborg East, DENMARK
Phone/Fax: + 45-9635-9254, Email: fbl@iet.auc.dk

***Abstract* – The present paper deals with a wound rotor induction machine (WRIM) drive. The machine is fed in the rotor by 2 inverters connected back to back, both of them vector controlled. This is similar with the recent doubly-fed induction wind generators setups, but with the difference that in the present case the stator is short-circuited instead of being connected to the power grid. This operation mode is required for self or assist starting in pump storage and wind generator applications.**

The inverters used are commercial. They share the same DC bus and one is connected with the output on the power grid (through an inductance), and the other with the output on the rotor of the WRIM.

Different kinds of tests were performed. Two combined flux observers were investigated and compared, one with the voltage model in parallel with the current model and one with both models connected in series.

A sensorless strategy based on a MRAS (model reference adaptive system) was implemented and tested at low speeds.

The control strategies, the flux observers and the MRAS were developed in Matlab-Simulink® and implemented using a dSpace® DS1103 single-board control and acquisition interface. The schemes used are illustrated in the paper, and the experimental results are shown and discussed.

***Index Terms* – electric drives, power electronics, back-to-back inverter, wound-rotor induction machine, vector control, sensorless strategies, model reference adaptive system (MRAS).**

I. Introduction

The wound rotor induction machine (WRIM) aka doubly-fed induction machine (DFIM) lives nowadays its "second life" due to the enormous interest paid to find the most efficient variable speed wind generator solution. And it seems that this rather old machine, but now rejuvenated with the help from power electronics and advanced control, has been rediscovered and now it is one of the most important candidates in the concept of high efficiency, variable speed, electric power generating, especially when renewable primary sources are harnessed: wind, hydro, tides and more recently marine currents [1].

The generator is connected with the stator on the power grid and on this side is producing constant voltage of constant frequency independently by the driving speed. However, to ensure this, it is necessary to feed the machine in the rotor from a bidirectional power flow converter with variable speed and frequency corresponding with the generator slip (±20% to size the rotor converter at only 20% from the generator power, and implicitly reducing the costs of power electronics). These solutions are presented in extenso in the recent technical literature and they are fall beyond our scope here [2].

A similar setup will be presented in what follows. The machine will be most of the time in motoring regime, and the stator is short-circuited. The rotor side is kept the same as in the wind generator cases. This way, a dual inverter regenerative drive is in discussion. Its usage for self or assist starting in pump-storage or wind generators is of main interest here.

II. The WRIM drive system and its control

The main components models in the DFIG system are described in what it follows. The electrical schematic of the whole system is shown in Figure 1.

For pre-charging the DC link capacitors, a 3×100Ω resistor was used (not illustrated here) between the grid and

the L filter; the resistors were short-circuited after the voltage in the DC link did reach approx 500V.

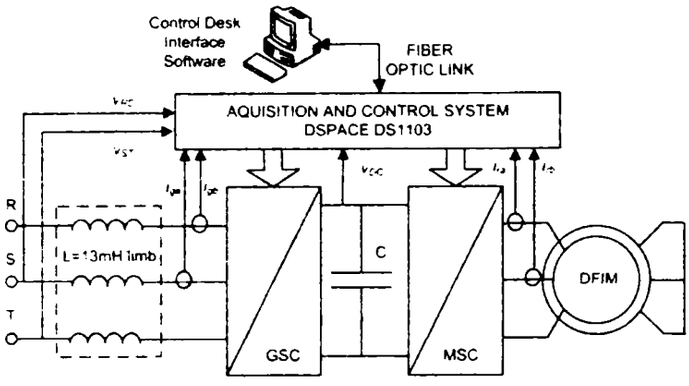

Figure 1. The WRIM drive system.

A. The machine (DFIM)

Stator and rotor voltage equations in dq axes quantities rotating in an arbitrary reference frame with the speed ω_k are given by [3]:

$$\underline{v}_s = R_s \underline{i}_s + \frac{d\underline{\psi}_s}{dt} + j\omega_k \underline{\psi}_s \tag{1}$$

$$\underline{v}_r = R_r \underline{i}_r + \frac{d\underline{\psi}_r}{dt} + j(\omega_k - \omega_r)\underline{\psi}_r \tag{2}$$

where $\underline{v}_s$, $\underline{i}_s$, $\underline{\Psi}_s$ are the stator voltage, stator current and stator flux space vectors, $\underline{v}_r$, $\underline{i}_r$, $\underline{\Psi}_r$ are the rotor voltage, rotor current and rotor flux space vectors. R_s and R_r are the stator and rotor resistances, ω_k is the chosen coordinate system speed and ω_r is the rotor electrical speed.

Stator and rotor flux vectors, $\underline{\psi}_s$ and $\underline{\psi}_r$, expressed in terms of stator and rotor currents, $\underline{i}_s$ and $\underline{i}_r$, are:

$$\underline{\psi}_s = L_s \underline{i}_s + L_m \underline{i}_r \tag{3}$$

$$\underline{\psi}_r = L_r \underline{i}_r + L_m \underline{i}_s \tag{4}$$

The electromagnetic torque T_e is:

$$T_e = 1.5p\left(\psi_{sd} i_{sq} - \psi_{sq} i_{sd}\right) \tag{5}$$

The parameters for the motor are given in the Appendix.

As the original motor had a rated rotor voltage of 78V and a rated current of 23 A, a re-wounding of the rotor was made, in order to fit the converters ratings without inserting a transformer in the rotor circuit. The number of turns per coil was increased 5 times and the cross section of the conductor was decreased 5 times. Thus a rated stator voltage of 380 V was obtained together with a 5 times lower rated rotor current.

B. The grid-side converter (GSC)

The grid-side converter is used to control the DC link voltage and the power factor (Figure 2). A vector-control strategy is used, with the reference frame oriented along the stator voltage [4]. The converter is current regulated with the direct axis current used to control the DC-link voltage; meanwhile the transverse axis current is used to regulate the displacement between the voltage and the current (and thus the power factor) [5].

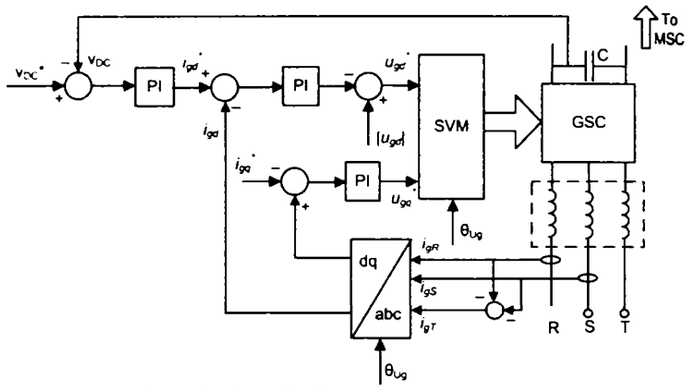

Figure 2. The grid-side converter control (GSC).

One of the most important tasks when connecting a power converter to the electrical grid is to make a fast and accurate measurement of the grid voltage phase angle in order to be able to control properly the power flow in or out of the power converter [6]. There are some methods well described in the literature. One of the simplest is zero crossing detection and in most cases this is sufficient, but will cause problems due to the switching noise and it is not precise when the grid is unbalanced [7]. Another method is to use a synchronous *dq*-reference PLL [8], synchronized with the input voltage frequency, but it still has problems when the grid is distorted. The angle produced will have harmonics, in that case. Filtering of the high-order harmonics is possible, but the low-order harmonics cannot be filtered, otherwise the bandwidth of the PLL will be too low. Finally one of the best methods is to split the three-phase system into positive, negative and zero sequence and to use only the positive sequence part of the signal for PLL [7]. But these methods will not be covered here. In the present case, a simplest method to get information on the grid voltage phase angle is used, due to its simplicity and due to the grid, which was without disturbances. This is briefly described in what follows.

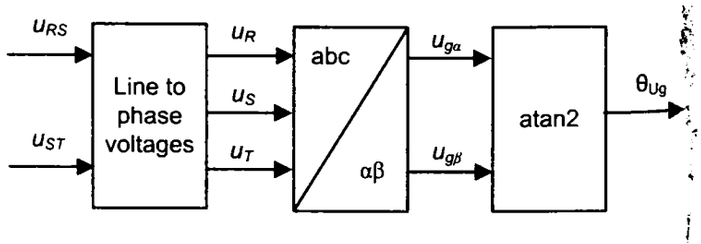

Figure 3. The computation of the grid voltage angle used for the coordinate transformations and for the SVM on the grid side converter control.

The line voltages are measured using two LEM LV 25-P voltage transducers with appropriate signal condition, thus at 500 V the output is 10 V, required for the A/D channels. The phase voltages are calculated from the line voltages (see Figure 3) and the $\alpha\beta$ components of the grid voltage are calculated from the phase voltages. Finally, the angle of the grid voltage is extracted [9]:

$$\theta_e = \tan^{-1}\frac{v_{s\beta}}{v_{s\alpha}} \tag{6}$$

A third LEM LV 25-P is used to measure the DC voltage with the same signal-conditioning interface. The grid currents are measured using two LA 55-P current transducers interfaced such that at 10A output will be 10V. The third grid current is calculated from the two measured, taking into account that the sum of all three currents is always zero.

Between grid converter and the grid itself a line filter was introduced to protect the inverter and to reduce the higher harmonic content in the line current, produced by the switching. This is in fact a simple *L*-filter. An *LC* or an *LCL* filter could be used, but the *L*-filter was chosen for simplicity. The frequency response of the *LCL* filter has a resonance peak, so the latter has to be designed such that the resonance peak not to interfere with the frequency response of the inverter output voltage; alternatively, a series resistor must be inserted to damp the resonance peak.

The value for the inductance per limb was chosen 13 mH, but a rather good design value for the inductance in the filter is [6]:

$$L = \max\left(\frac{V_\vartheta}{\vartheta\omega_1 I_\vartheta}\right) \tag{7}$$

where ϑ is the order of the harmonic and V_ϑ the phase RMS value of the output phase voltage harmonic.

The design of the PI current controller starts from the transfer function of the plant (in this case the line filter itself). The controllers produce the reference grid voltage vector $u_g^* = u_{gd}^* + ju_{gq}^*$:

$$u_{gd}^* = -\left(K_{Pig} + \frac{K_{Iig}}{s}\right)e_{igd} + |u_{gd}| \tag{8}$$

$$u_{gq}^* = -\left(K_{Pig} + \frac{K_{Iig}}{s}\right)e_{igq} \tag{9}$$

where K_{Pig} and K_{Iig} are the PI controllers gains and e_{igd} and e_{igq} are the errors of the grid currents i_{gd} and i_{gq} respectively.

Applying as design constraints a damping ratio of 0.7 and a closed-loop natural frequency of 125 Hz, the gains of the controllers results: $K_{Pig} = 30$ and $K_{Iig} = 1000$. The design for the DC-link voltage controller may be carried out assuming the inner current loop is ideal and knowing the value of the DC link capacitor (in our case 470 μF). The controller produces the reference d-axis grid current i_{gd}^*:

$$i_{gd}^* = \left(K_{PVDC} + \frac{K_{IVDC}}{s}\right)e_{VDC} \tag{10}$$

where K_{PVDC} and K_{IVDC} are the PI controller gains and e_{VDC} is the error of the DC voltage v_{DC}. Thus the controller gains yields: $K_{PVDC} = 0.1$ and $K_{IVDC} = 0.3$. This is 10 times slower than the inner current loop.

C. The machine-side converter (MSC)

The generator is controlled in a synchronously rotating *dq*-frame, with the d-axis aligned with the stator-flux vector position, which ensures a decoupled control between the electromagnetic torque and the rotor excitation contribution [10] (see Figure 4).

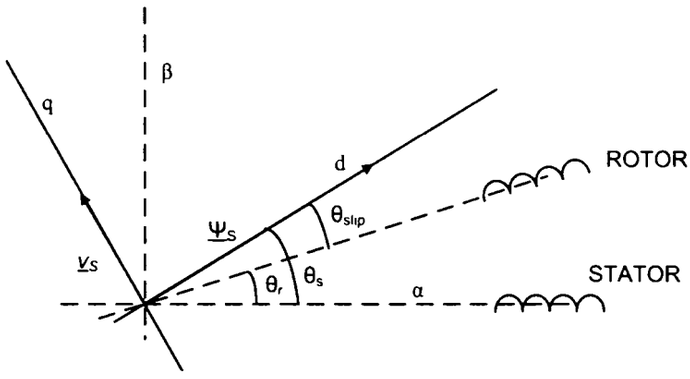

Figure 4. Location of vectors in stationary coordinates.

The control strategy is shown in Figure 5.

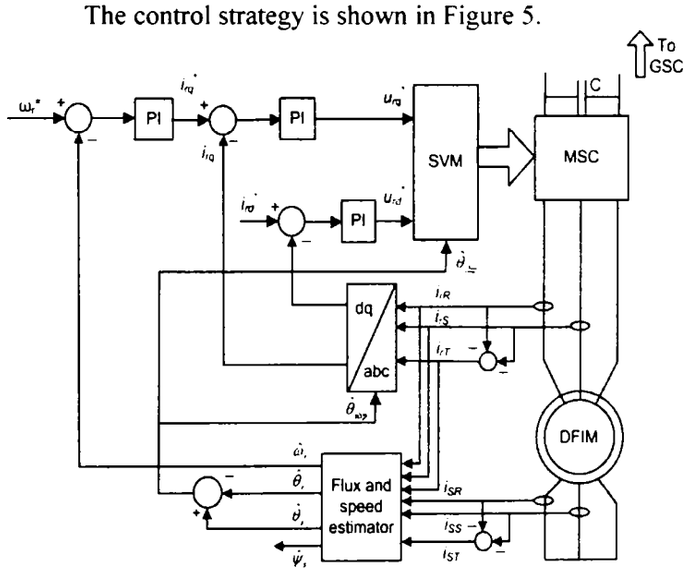

Figure 5. The machine-side converter control (MSC).

As it can be seen, two rotor currents and two stator currents are measured, and the third current in each case is calculated taking into account that always the sum of the currents is zero. The sensors are also type LEM LA 55-P.

The rotor currents are measured in their coordinates (rotor coordinates) and transformed into synchronous coordinates using the angle:

$$\hat{\theta}_{slip} = \hat{\theta}_s - \hat{\theta}_r \tag{11}$$

where $\hat{\theta}_s$ is the stator flux angle, and $\hat{\theta}_r$ the rotor position [11, 12]. About how these two angles are calculated we will discuss in the following section.

Reference voltages generated by the current control loops are transformed back to the rotor reference frame, using the same angle $\hat{\theta}_{slip}$. Standard space vector modulation is employed to generate the pulses for the inverter.

The current controllers are designing the same strategy as in the case of the current controllers for the grid-side inverter. The controllers produce the reference rotor voltage vector $u_r^* = u_{rd}^* + ju_{rq}^*$:

$$u_{rd}^* = \left(K_{Pir} + \frac{K_{Iir}}{s}\right) e_{ird} \tag{12}$$

$$u_{rq}^* = \left(K_{Pir} + \frac{K_{Iir}}{s}\right) e_{irq} \tag{13}$$

where K_{Pir} and K_{Iir} are the PI controllers gains and e_{ird} and e_{irq} are the errors of the rotor currents i_{rd} and i_{rq} respectively. The gains of the rotor current controllers thus results: $K_{Pir} = 40$ and $K_{Iir} = 1500$.

The design for the speed controller may be carried out assuming again that the inner current loop is ideal. The controller produces the reference q-axis grid current i_{gd}^*:

$$i_{rq}^* = \left(K_{P\omega} + \frac{K_{I\omega}}{s}\right) e_\omega \tag{14}$$

where $K_{P\omega}$ and $K_{I\omega}$ are the PI controller gains and e_ω is the error of therotor speed. Thus the controller gains yields: $K_{P\omega} = 0.1$ and $K_{I\omega} = 0.3$. This is almost 30 times slower than the inner current loop.

III. Flux, and Rotor Speed-Position Estimation

A. The flux estimation

As it was already stated two flux estimators were developed and used during the tests. Both of them are based on the voltage and the current stator flux models. The estimator using the voltage and current models connected in parallel is illustrated in Figure 6. Estimated stator flux, as produced by the voltage model, is:

$$\hat{\psi}_{s\alpha\beta} = \int (v_{s\alpha\beta} - R_s i_{s\alpha\beta} + v_{comp\alpha\beta})dt \tag{15}$$

where $v_{s\alpha\beta} = 0$ in this case (the stator is short-circuited). Thus this model is supposed to be inaccurate, as any error in R_s is causing errors in the estimated stator flux.

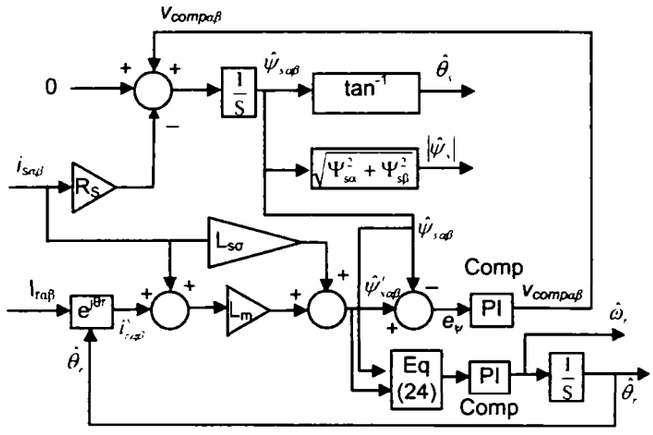

Figure 6. The flux estimator with parallel voltage and current models, and the rotor speed-position estimator MRAS.

The current model is based on (3):

$$\hat{\psi}'_{s\alpha\beta} = L_{s\sigma} i_{s\alpha\beta} + L_m (i_{s\alpha\beta} + i^s_{r\alpha\beta}) \tag{16}$$

The rotor current is measured, but a transformation to stator coordinates is needed, using the estimated rotor position $\hat{\theta}_r$.

The flux error between the voltage model (15) and the current model (16) is passed through a PI controller, with $K_{pcomp} = 10$ and $K_{icomp} = 10$, which outputs a correction signal used to compensate the voltage model (see Figure 6):

$$v_{comp\alpha\beta} = \left(K_{Pcomp} + \frac{K_{Icomp}}{s}\right) e_\psi \tag{17}$$

where:

$$e_\psi = \hat{\psi}'_{s\alpha\beta} - \hat{\psi}_{s\alpha\beta} \tag{18}$$

This way the dc-offset drift of the ideal integrator (15) is eliminated. The PI compensator selects the current model at low speeds, while the voltage model prevails at medium and high speeds. Thus, the corrected stator flux vector is $\hat{\psi}_{s\alpha\beta}$ as given by (15). For comparison purposes only the stator flux obtained only from the current model, $\hat{\psi}'_{s\alpha\beta}$, was also considered.

The angle θ_s is obtained from the resultant stator flux components [13]:

$$\hat{\theta}_s = \tan^{-1} \frac{\hat{\psi}_{s\beta}}{\hat{\psi}_{s\alpha}} \tag{19}$$

Differences were noticed between the stator flux $\hat{\psi}_{s\alpha\beta}$ obtained from the compensated voltage model (15) and the

stator flux $\hat{\psi}'_{s\alpha\beta}$ obtained from the current model only (16). This was mainly due to parameter mismatch between the model and the real machine. To have one more view of this problem, another flux estimator was developed. This is an estimator that employs the voltage and the current models connected in series, as shown in Fig. 7.

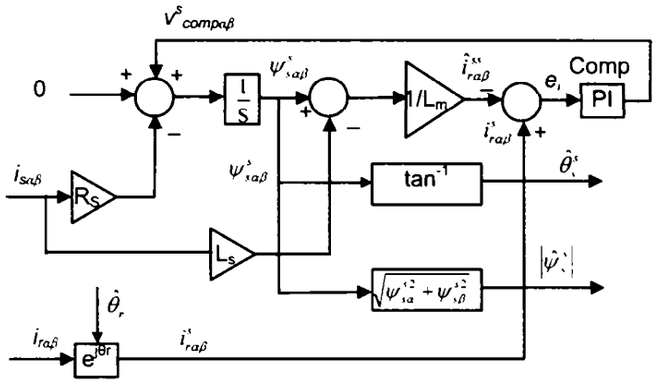

Figure 7. The alternative flux estimator with the voltage and current models connected in series.

It is basically relying on the same equations, but the current model is written such that the stator flux obtained from the voltage model is now used to estimate the rotor current in stator coordinates:

$$\hat{i}^{ss}_{r\alpha\beta} = \frac{1}{L_m}\left(\hat{\psi}^{s}_{s\alpha\beta} - L_s i_{s\alpha\beta}\right) \tag{20}$$

where estimated stator flux is now:

$$\hat{\psi}^{s}_{s\alpha\beta} = \int\left(v_{s\alpha\beta} - R_s i_{s\alpha\beta} + v^{s}_{compa\beta}\right) \tag{21}$$

The rotor current is measured and transformed into stator coordinates using the estimated rotor position θ_r. The rotor-current error between the measured and estimated (20) rotor current is passed through a PI controller, with the same parameters as for the one in Fig. 6, and its output is used to compensate the voltage model: (Fig. 7)

$$v^{s}_{compa\beta} = \left(K_{Pcomp} + \frac{K_{Icomp}}{s}\right)e_i \tag{22}$$

where:

$$e_i = i^{s}_{r\alpha\beta} - \hat{i}^{ss}_{r\alpha\beta} \tag{23}$$

B. The rotor speed-position estimation

A speed-position estimator is developed based on MRAS (model reference adaptive system) algorithm. It is chosen for this purpose, due to its relative simplicity and proven efficiency over an extended speed range. There is quite simple to develop such a method because the flux estimator with parallel voltage and current models (Fig. 6) offer $\alpha\beta$ components of the flux vectors obtained from both models [14].

The MRAS flux position error ε was calculated from the phases of the two flux estimations (24). The voltage model $\hat{\psi}_{s\alpha\beta}$ is the reference model, while the current model $\hat{\psi}'_{s\alpha\beta}$ is the adaptive model with the rotor position $\hat{\theta}_r$ as adaptive para te .

$$\varepsilon = -\psi_{s\alpha}\psi'_{s\beta} + \psi'_{s\alpha}\psi_{s\beta} \tag{24}$$

This error is used to extract the rotor speed and position using a phase-locked loop (PLL) technique (Figure 6). The output of the PI compensator gives the estimated rotor speed ω_r, and after the integration, the estimated rotor position θ_r is obtained:

$$\hat{\omega}_r = \left(K'_{Pcomp} + \frac{K'_{Icomp}}{s}\right)\varepsilon \; ; \; \hat{\theta}_r = \int\hat{\omega}_r dt \tag{25}$$

Optimum parameters of the PI compensator were searched as a compromise between the speed of the PLL, especially during transients, and the level of oscillations in speed estimation, especially at low speeds. The best parameters, seem to be: $K'_{Pcomp} = 100$, and $T_I = 5$ms (time constant of the compensator, $T_I = K'_{Pcomp} / K'_{Icomp}$). Overall, this scheme has shown good accuracy over the whole speed range.

IV. The Test Rig and Experimental Results

First, a speed response is shown at a step in reference speed from 15 to 1000 rpm. In Figure 8, the estimated speed 1), and the measured speed 2) are illustrated. The speed was measured for comparison using a Telemecanique - 5000 pulse encoder.

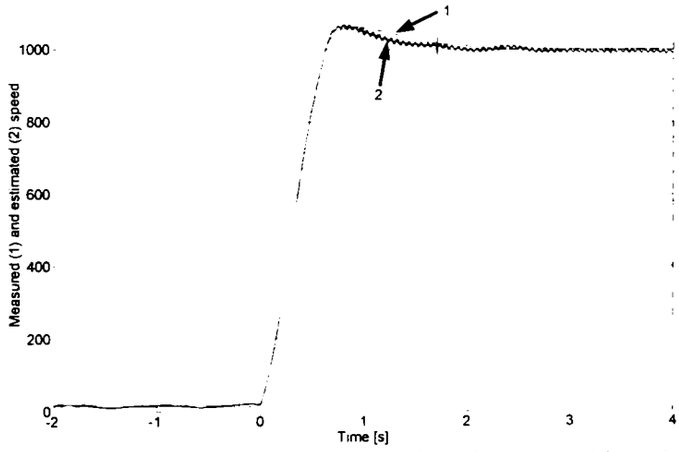

Figure 8. 1) Estimated speed, and 2) measured speed at step speed from 15 rpm to 1000 rpm.

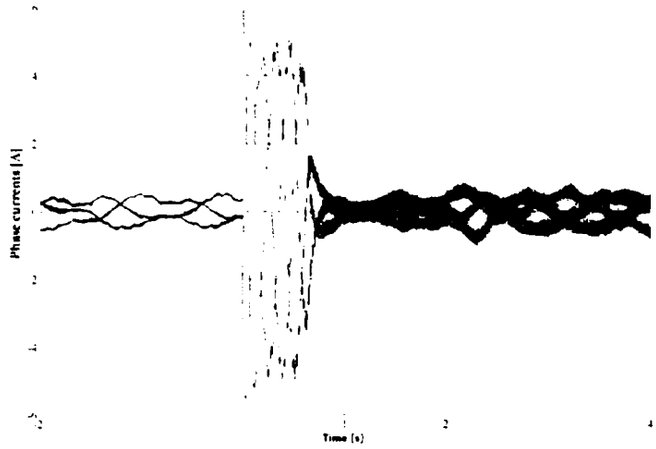

Figure 9 Phase stator currents at step speed from 15 rpm to 1000 rpm.

For the same experiment, the stator phase currents are shown in Figure 9, and the rotor phase currents are shown in Figure 10.

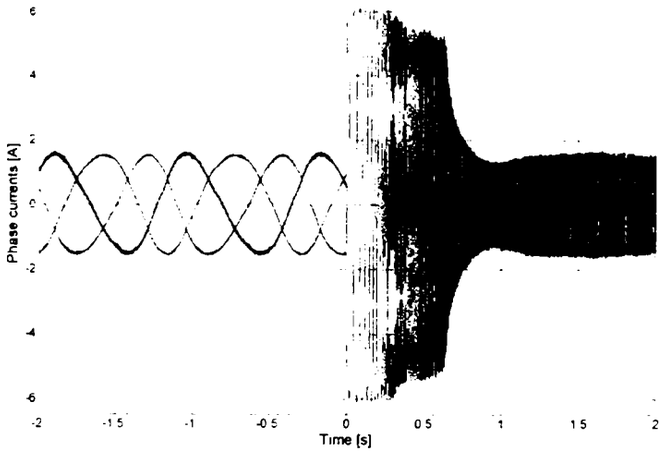

Figure 10. Phase rotor currents at step speed from 15 rpm to 1000 rpm.

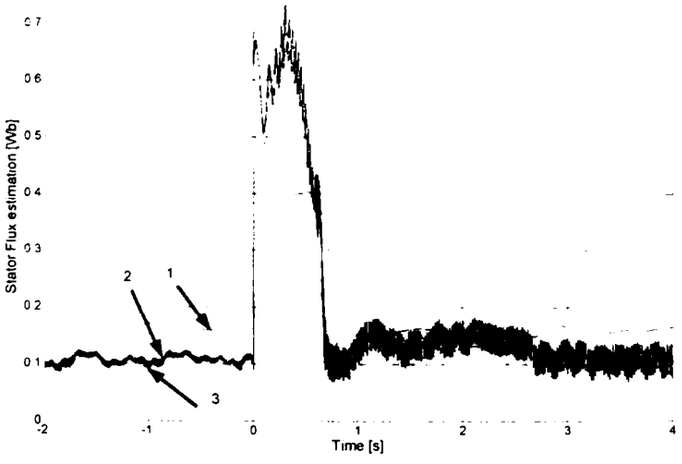

Figure 11. Stator flux estimation at step speed from 15 rpm to 1000 rpm: 1) parallel estimator, 2) series estimator, 3) parallel estimator, current model.

The estimated stator flux is illustrated in Figure 11 for the same step in reference speed from 15 to 1000 rpm.

Both estimations from the parallel estimator are shown: voltage compensated model 1), and current model 3); also, the estimation from the series estimator 2). It seems that the current model from the parallel estimator is quite the same with the series model, but the parallel estimator (voltage compensated model) has unrecoverable errors.

In Figure 12, also speed transients are shown, but from 500 to -500 rpm (reversal). The estimated rotor speed 1), and measured rotor speed 2) with the encoder are illustrated.

In Figure 13, the reference DC link voltage 1), and the measured DC link voltage 2) at the step reversal from 500 to -500 rpm are shown.

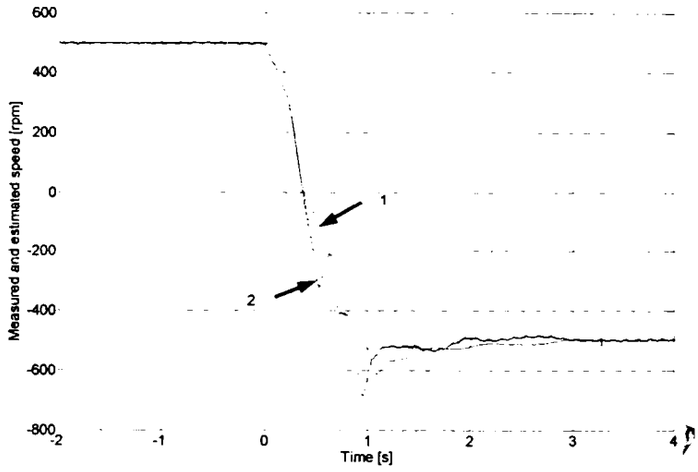

Figure 12. 1) Estimated speed, and 2) measured speed at step speed from 500 rpm to -500 rpm.

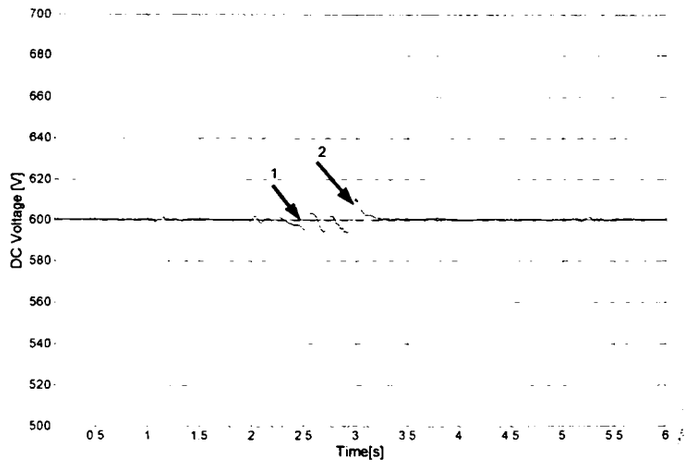

Figure 13. 1) Reference DC voltage, and 2) measured DC voltage at step speed from 500 rpm to -500 rpm.

The speed estimator was tested at low and very low speeds. Its behavior is satisfactory up to 5 rpm. In Figure 14, the steady state speeds at 5 rpm are shown. The estimated speed 1), and the measured speed 2) with the encoder are illustrated. The estimated speed is better than the measured at

5 rpm due to the limited number of the lines of the encoder, which became insufficient at this speed.

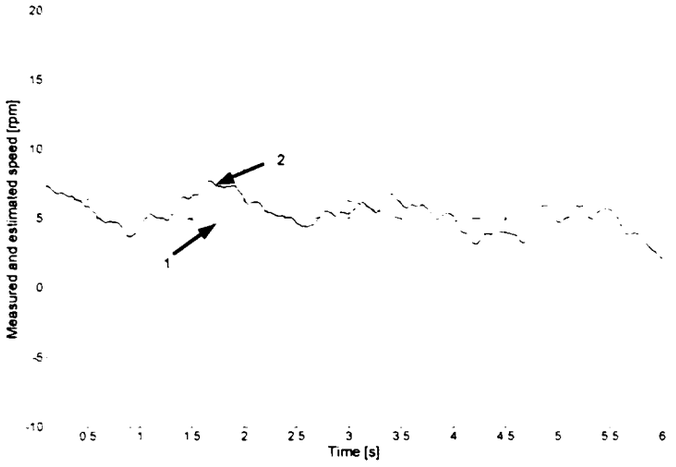

Figure 14. 1) Estimated speed, and 2) measured speed at 5 rpm.

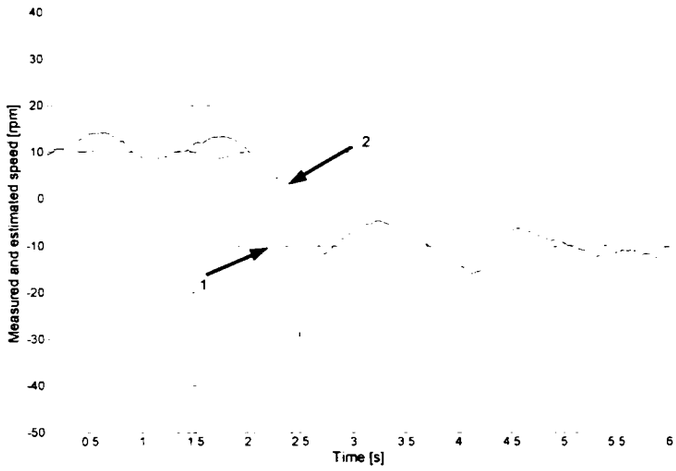

Figure 15. 1) Estimated speed, and 2) measured speed at step speed from 10 rpm to -10 rpm.

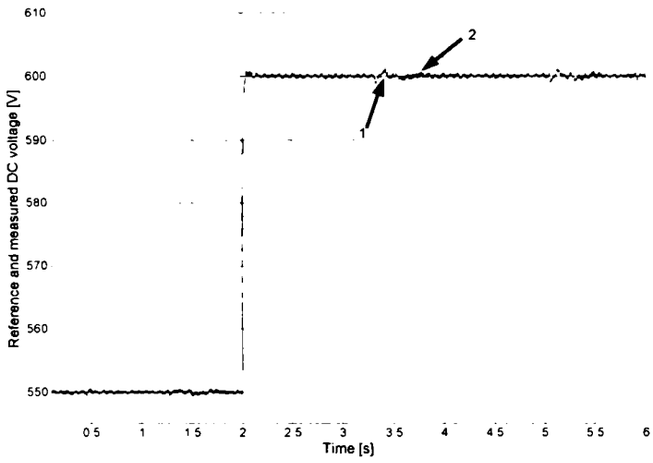

Figure 16. 1) Reference DC voltage, and 2) measured DC voltage at step DC voltage from 550 V to 600 V.

A transient at low speed is shown in Figure 15, from 10 rpm to -10rpm. The estimated rotor speed 1), and measured rotor speed 2) with the encoder are presented. The behavior of the estimator is also very good, still better than the encoder.

For testing the control of the grid-side converter, some experiments have been made. In Figure 17, a step in reference of DC voltage from 550 to 600 V is shown. The reference DC voltage 1), and the measured DC voltage 2) are illustrated. Very fast and accurate response in DC voltage is proved.

V. Conclusion

The motion-sensorless WRIM driving control from rotor with short-circuited stator, with two back-to-back inverters connected in the rotor circuit of the machine, was presented. Both inverters are vector controlled; the machine-side converter controls the speed and the reactive rotor current, the grid-side converter controls the DC voltage, regardless of the level and the direction of the rotor power, and the reactive current drawn from the grid. The results of the tests were illustrated and discussed. Rather fast responses of the drive during fast reference speed transients were shown. The drive has higher braking capabilities due to the grid-side inverter and its control. That is, fast injecting the power back to the grid during braking periods is obtained.

Two stator flux observers were developed and compared. Both are based on the voltage and on the current models, but one is using them in parallel and one in series. The topologies and the results are also illustrated and discussed.

A motion sensorless control method, with speed estimation based on a MRAS algorithm from flux stator was implemented, tested and described in the present paper. The results are also shown. Also, at fast transients the speed estimation is fast and precise. The behavior of the position and speed estimator is satisfactory down to 5 rpm.

Appendix

The Doubly-Fed Machine: Nameplate data: Type - asynchronous motor with slip rings, Manufacturer: IME SA Bucharest, Romania, P_N = 3 kW, stator voltage V_{SN} = 380 V, rotor voltage V_{RN} = 380 V (after re-wounding; the original rotor voltage was 78 V), n_N = 940 rpm.
Parameters: R_s = 1.6 Ω, R_r = 1.6 Ω, $L_{s\sigma} = L_{r\sigma}$ = 17.51 mH, L_m = 96.13 mH, p =3 pole pairs

The Converters: Type: VLT 5004, S_N = 4.2 kVA, Manufacturer: Danfoss Drives, Denmark.

Control and Acquisition Unit: Type: DS 1103, Manufacturer: dSpace GmbH, Germany.

References

[1] I. Serban, F. Blaabjerg, I. Boldea, "Sensorless doubly-fed induction generator control under power system transients and faults: The influence of magnetic saturation", *Proc. of OPTIM 2004*, Brasov, Romania, vol. 2, pp. 311-318, May 2004.

[2] M.P. Kazmierkowski, R. Krishnan, F. Blaabjerg (Eds.), "Control in Power Electronics: Selected Problems," Chapter 13: L. Helle, F. Blaabjerg, "Wind turbine systems", Academic Press, 2002.

[3] I. Boldea, S.A. Nasar, "Electric Drives," Chapter 14: "Large power drives, 14.8 Sub and hypersynchronous IM cascade drives," CRC Press, Florida, 1999.

[4] R. Datta, V.T. Ranganathan, "Direct power control of grid-connected wound rotor induction machine without rotor position sensors," *IEEE Transactions on Power Electronics*, vol. 16, no. 3, May 2001, pp. 390-399.

[5] L. Morel, H. Godfroid, A. Mirzaian, J.M. Kauffmann, "Double-fed induction machine: converter optimization and field oriented control without position sensor," *IEE Proc. on Electric Power Applications*, vol. 145, no. 4, July 1998, pp. 360-368.

[6] Morten Lindholm, "Doubly-Fed Drives for Variable Speed Wind Turbines," *Ph.D. Thesis*, Technical University of Denmark,

[7] S.-J. Lee, J.-K. Kang, S.-K. Sul, "A new phase detecting method for power conversion systems considering distorted conditions in power system," *1999 IEEE-IAS Annual Meeting Conf. Record*, vol. 4, pp. 2167-2172, 1999.

[8] V. Kaura, V. Blasko, "Operation of a phase locked loop system under distorted utility conditions," *IEEE Transactions on Industry Applications,* vol. 33, no.1, Jan./Feb. 1997, pp. 58-63.

[9] I. Serban, F. Blaabjerg, I. Boldea, Z. Chen, "A study of the doubly-fed wind power generator under power grid faults," *Proc. of EPE 2003*, Toulouse, France, 2003.

[10] U. Radel, D. Navarro, G. Berger, S. Berg, "Sensorless field-oriented control of a slipring induction generator for a 2.5 MW wind power plant from Nordex Energy GmbH," *Proc. of EPE 2001*, Graz, 2001.

[11] S. Muller, M. Deicke, R.W. De Doncker, "Adjustable speed generators for wind turbines based on double-fed induction machines and 4-quadrant IGBT converters linked to the rotor," *2000 IEEE-IAS Annual Meeting Conf. Record*, vol. 4, pp. 2249-2254, Oct. 2000.

[12] T. Senjyu, N. Sueyoshi, K. Uezato, H. Fujita, "Stability analysis of wind power generating system," *Proc. of Power Conversion Conf. PCC 2002,* Osaka, vol. 3, pp. 1441-1446, April 2002.

[13] R. Datta, V.T. Ranganathan, "A simple position-sensorless algorithm for rotor-side field-oriented control of wound-rotor induction machine," *IEEE Transactions on Industrial Electronics*, vol. 48, no. 4, Aug. 2001, pp. 786-793.

[14] G.D. Andreescu, "Position and speed sensorless control of PMSM drives based on adaptive observer," *Proc. of EPE'99*, Lausanne, Switzerland, Aug. 1999.

New State Observers and Sensorless Control of Wound Rotor Induction Generator (WRIG) at Power Grid with Experimental Characterization

Ioan Serban[1], Gheorghe-Daniel Andreescu[2], Lucian Tutelea[3], Cristian Lascu[3], Frede Blaabjerg[4], Ion Boldea[3]

[1]ebmpapst St. Georgen GmbH & Co. KG, Research and Development Laboratory for Electric Drives Hermann-Papst-Str. 1, D-78112 St. Georgen/Schwarzwald, GERMANY, Phone: +49-7724-811834, Fax: +49-7724-8151834, Email: Ioan.Serban@de.ebmpapst.com

[2]University Politehnica of Timisoara, Faculty of Automation and Computers, Bd. V. Parvan nr.2, 300223 Timisoara, ROMANIA, Phone/Fax: +40-256-403245 / +40-256-403214, Email: dandre@aut.utt.ro

[3]University Politehnica of Timisoara, Faculty of Electrical Engineering, Bd. V. Parvan nr.2, 300223 Timisoara, ROMANIA, Phone/Fax: +40-256-403463 / +40-256-403452 Email: luci@lselinux.utt.ro, cristi@et.utt.ro, boldea@lselinux.utt.ro

[4] Aalborg University, Institute of Energy Technology, Pontoppidanstraede 101, 9220 Aalborg East, DENMARK Phone/Fax: + 45-9635-9254, Email: fbl@iet.auc.dk

***Abstract* – The paper deals with a wound rotor induction generator (WRIG), also known as the doubly-fed induction generator. A complete experimental set-up is presented and analyzed. It is composed of: WRIG, two power electronics converters connected in the rotor side of WRIG, a line filter, and the data acquisition and control system (dSpace DS 1103). Both converters are commercial units and are vector controlled using appropriate interfaces. They are back-to-back connected, sharing the same DC bus, one supplied through a line filter from the power grid, and the other one with the output on the rotor of the generator. The stator of the generator is directly connected to the power grid.**

Two stator flux observer topologies were investigated and compared, one with the voltage model in parallel with the current model and the other one with both models connected in series. A speed estimation strategy, which works also during the synchronization procedure, was implemented and tested. It is based on model reference adaptive system (MRAS) principles.

All control strategies, the flux observers and the MRAS, were developed in Matlab-Simulink® and implemented using a dSpace® DS1103 single-board control and acquisition interface. Different tests were performed, and sample results are presented and discussed in the paper. The schemes used are illustrated in the paper, and the experimental results are shown and analyzed.

***Index Terms* – wind generators, back-to-back inverter, wound-rotor induction machine, vector control, sensorless control, model reference adaptive system (MRAS).**

I. Introduction

The penetration of wind power generation into the electrical grid has increased tremendously in the last ten to fifteen years, especially in the northern Europe and in the US [1]. Five to ten years ago, the wind turbine was a simple stall controlled turbine. Nowadays, as the penetration of wind power is higher and higher, the wind turbines have to be more controllable, and a way to do this is by variable speed generators. By pitching the rotor blades, a variable speed turbine can control the power output at theoretically any wind speed. To transfer the wind energy from a variable speed turbine to the constant frequency electrical grid, an electrical generator and a power converter are needed [2].

The doubly fed induction generator with a bi-directional power flow converter in the rotor has, doubtlessly, advantages with respect to other solutions:

- enhanced energy capture capability from the wind in a wide range of wind velocities;
- ability of reactive power control on the grid side;
- fast decoupled control of active and reactive power by independent control of torque and rotor excitation;
- reduced size and implicitly costs of the power electronics converter (the converter rating is only around 25% of the total generator power).

II. Wind Power and Control Principle

The mechanical power produced by the wind turbine, P_M, is given by [3]

$$P_M = \frac{1}{2} \cdot \rho_{air} \cdot C_p(\lambda, \beta) \cdot \pi \cdot R^2 \cdot V^3 \qquad (1)$$

where C_p – power efficiency coefficient; V – wind velocity; β - pitch angle; R - blade radius; ρ_{air} – air density (1.225 kg/m^3)

Applying the tip speed ratio λ

$$\lambda = \frac{\omega_m \cdot R}{V} \qquad (2)$$

where ω_m is the turbine mechanical speed, equation (1) becomes the optimal mechanical power (2).

$$P_M^{opt} = \frac{1}{2} \cdot \rho_{air} \cdot \pi \cdot R^5 \cdot \frac{C_P^{opt}}{\lambda_{opt}^3} \cdot \omega_m^3 = K_w \cdot \omega_m^3 \qquad (3)$$

where K_w is the wind turbine dependent coefficient.

Commercial wind turbines are designed to extract the maximum power at a given wind speed, as given by equation (3). Fig. 1 shows the normalized electrical power versus normalized rotor speed at various wind velocities [4].

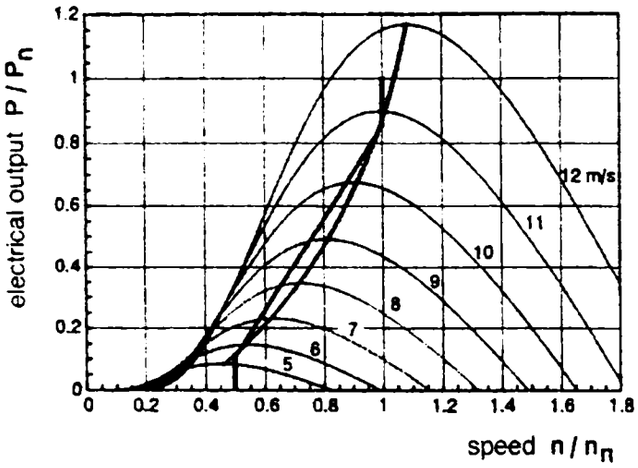

Fig. 1. Electrical power versus rotor speed at different wind speeds.

III. The WRIG System and its Control

The main components models in the WRIG system are described in what follows. Electrical block-diagram of the whole system is shown in Fig. 2.

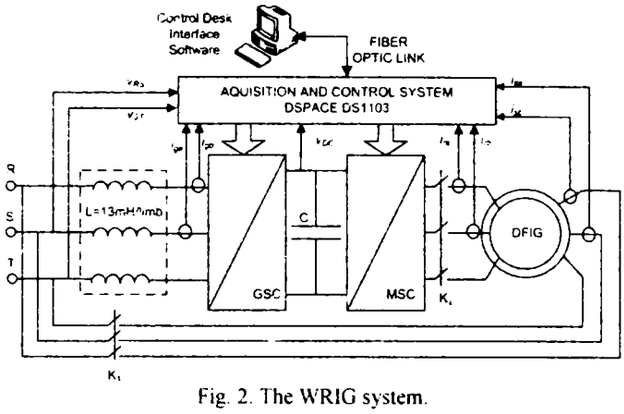

Fig. 2. The WRIG system.

For the DC link capacitors pre-charging, a resistor was used (not illustrated here) between the grid and the line filter; the resistors were short-circuited after the voltage in the DC link reached approx. 500 V. Also in the rotor circuit, in parallel with the K_2 switch, three lamps were inserted, as a visual indicator for the synchronization condition. In this way, K_2 could be switched on when the lamps are off. The WRIG-to-grid synchronization procedure is described in Section IV.

For driving the WRIG, a 3 kW/ 1475 rpm induction motor is used. The motor was supplied with a 4.3 kVA Danfoss VLT5004 commercial voltage source inverter with the original interface for constant speed control mode. In this way, the variable wind speed could be easily simulated.

A. The Generator

WRIG mathematical model in arbitrary reference frame rotating at speed ω_k are

$$\underline{v}_s = R_s \underline{i}_s + \frac{d\underline{\psi}_s}{dt} + j\omega_k \underline{\psi}_s \qquad (4)$$

$$\underline{v}_r = R_r \underline{i}_r + \frac{d\underline{\psi}_r}{dt} + j(\omega_k - \omega_r)\underline{\psi}_r \qquad (5)$$

where $\underline{v}_s$, $\underline{i}_s$, $\underline{\Psi}_s$ are the stator voltage, stator current and stator flux space vectors, $\underline{v}_r$, $\underline{i}_r$, $\underline{\Psi}_r$ are the rotor voltage, rotor current and rotor flux space vectors, R_s and R_r are the stator and rotor resistances, ω_k is the chosen coordinate system speed and ω_r is the rotor electrical speed.

Stator and rotor flux vectors, $\underline{\psi}_s$ and $\underline{\psi}_r$, expressed in terms of stator and rotor currents, $\underline{i}_s$ and $\underline{i}_r$, are:

$$\underline{\psi}_s = L_s \underline{i}_s + L_m \underline{i}_r \qquad (6)$$

$$\underline{\psi}_r = L_r \underline{i}_r + L_m \underline{i}_s \qquad (7)$$

The electromagnetic torque T_e is:

$$T_e = 1.5p\left(\psi_{sd} i_{sq} - \psi_{sq} i_{sd}\right) \qquad (8)$$

The generator nameplate data and parameters are given in the Appendix. As the original machine had a nominal rotor voltage of 78 V and a nominal current of 23 A, a re-winding of the rotor has been performed, in order to fit with the converter ratings, without inserting a transformer in the rotor circuit. The number of turns per coil was increased five times and the cross section of the conductor was decreased five times. Thus a nominal stator voltage of 380 V, and a five times lower nominal rotor current were obtained.

B. The Grid-Side Converter (GSC)

The grid-side converter is used to control the DC link voltage and the input power factor regardless of the level and the direction of the rotor p (F g.). A r control strategy in stator voltage reference [5] frame is employed for this purpose. The converter is current regulated with the direct axis current used to control the DC-link voltage, meanwhile the transverse axis current is used to regulate the displacement between the voltage and the current, and thus the input power factor [6], [7]. The angle of the grid voltage is: $\theta_e = \tan^{-1}\left(u_{s\beta} / u_{s\alpha}\right)$. Between the grid converter and the grid itself, a line filter was introduced to reduce the higher

harmonic content in the line current, produced by the switching [8]. This is a simple L – filter. The value for the inductance per phase is 13 mH [9].

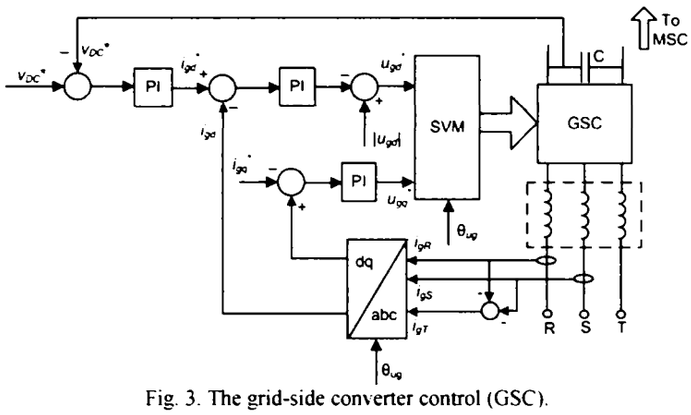

Fig. 3. The grid-side converter control (GSC).

The design of the PI current controllers [10] follows from the transfer function of the plant (in this case the line filter itself). The controllers produce the reference grid voltage vector $u_g^* = u_{gd}^* + ju_{gq}^*$:

$$u_{gd}^* = -\left(K_{Pig} + \frac{K_{Iig}}{s}\right)e_{igd} + |u_{gd}| \qquad (9)$$

$$u_{gq}^* = -\left(K_{Pig} + \frac{K_{Iig}}{s}\right)e_{igq} \qquad (10)$$

where K_{Pig} and K_{Iig} are the PI controllers gains and e_{igd} and e_{igq} are the errors of the grid currents i_{gd} and i_{gq} respectively.

Applying as design constraints a damping ratio of 0.7 and a closed-loop natural frequency of 125 Hz, the gains of t e contro ers resu ts: K_{Pig} = 30 an K_{Iig} = 1000.The design for the DC-link voltage controller [11] may be carried out assuming the inner current loop is ideal and knowing the value of the DC link capacitor (in our case 470 μF). The controller produces the reference d-axis grid current i_{gd}^*:

$$i_{gd}^* = \left(K_{PVDC} + \frac{K_{IVDC}}{s}\right)e_{VDC} \qquad (11)$$

where K_{PVDC} and K_{IVDC} are the PI controller gains and e_{VDC} is the error of the DC voltage v_{DC}. Thus the controller gains yields: K_{PVDC} = 0.1 and K_{IVDC} = 0.3. This is 10 times slower than the inner current loop.

C. The Machine-Side Converter (MSC)

The generator is controlled in synchronous reference frame, with the *d*-axis aligned with the stator-flux vector, which ensures decoupled control between the electromagnetic torque and the rotor excitation contribution [12] (Fig. 4). The control strategy block diagram is shown in Fig. 5. As it can be seen, two rotor currents and two stator currents are measured and the third current in each case is calculated taking into account that the currents' sum is always zero.

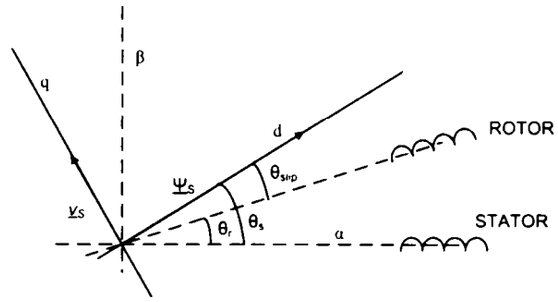

Fig. 4. Location of stator voltage and flux vectors in stationary frame.

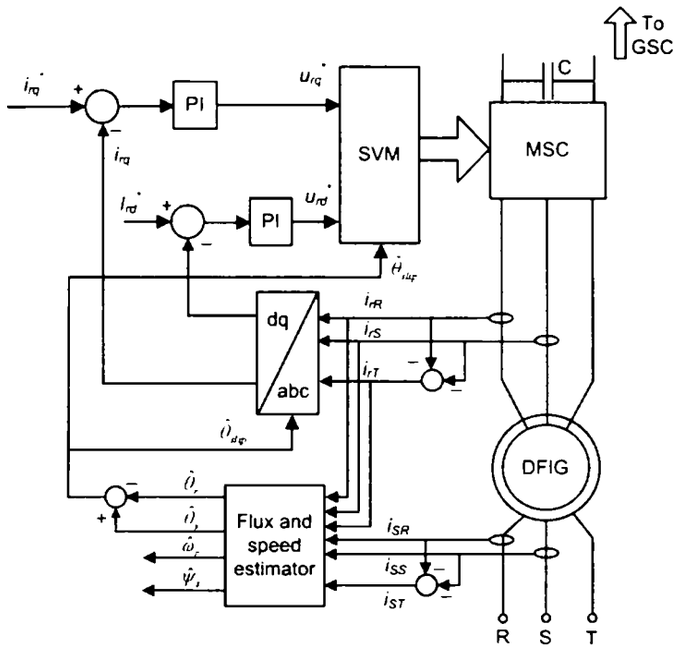

Fig. 5. The machine side converter control (MSC).

The rotor currents are measured in their natural frame (rotor coordinates) and transformed into synchronous frame using the slip angle:

$$\hat{\theta}_{slip} = \hat{\theta}_s - \hat{\theta}_r \qquad (12)$$

where $\hat{\theta}_s$ is the stator flux angle, and $\hat{\theta}_r$ the rotor position. About how these two angles are calculated we will discuss in the following section.

Reference voltages generated by the current control loops are transformed back to the rotor reference frame, using the same angle $\hat{\theta}_{slip}$. Standard space vector modulation is employed to generate the pulses for the inverter.

The current controllers are designed using the same strategy as in the case of the current controllers for the grid-side inverter. The controllers produce the reference rotor voltage vector $u_r^* = u_{rd}^* + ju_{rq}^*$:

$$u^{*}_{rd} = \left(K_{Plr} + \frac{K_{Ilr}}{s} \right) e_{ird} \qquad (13)$$

$$u^{*}_{rq} = \left(K_{Plr} + \frac{K_{Ilr}}{s} \right) e_{irq} \qquad (14)$$

where K_{Plr} and K_{Ilr} are the PI controllers gains and e_{ird} and e_{irq} are the errors of the rotor currents i_{rd} and i_{rq} respectively. The gains of the rotor current controllers thus results: $K_{Plr} = 40$ and $K_{Ilr} = 1500$.

IV. Flux and Rotor Speed – Position Estimation

A. The Flux Estimation

Two stator flux estimators were developed and used during the tests. Both of them are based on the voltage and the current stator flux models. The estimator using the voltage and current models connected in parallel is illustrated in Fig. 6. The voltage model is given by (4). Estimated stator flux, as produced by the voltage model, is

$$\hat{\psi}_{s\alpha\beta} = \int (v_{s\alpha\beta} - R_s i_{s\alpha\beta} + v_{comp\alpha\beta}) dt \qquad (15)$$

The stator resistance errors due to temperature changes are g . l pp , any error in R_s is causing error in the estimated stator flux.

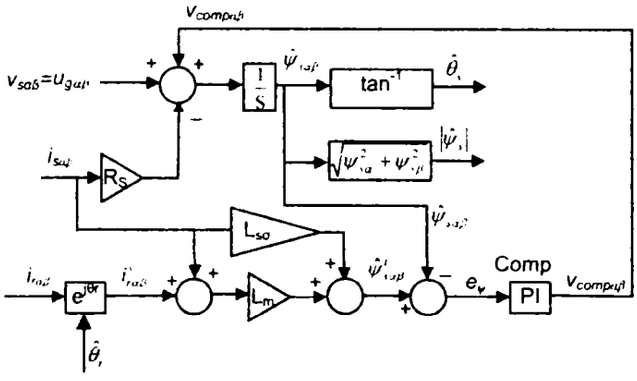

Figure 6. Stator flux estimator with voltage and current models in parallel.

The current model is based on (6):

$$\hat{\psi}'_{s\alpha\beta} = L_{s\sigma} i_{s\alpha\beta} + L_m (i_{s\alpha\beta} + i^{s}_{r\alpha\beta}) \qquad (16)$$

The rotor current is measured, but a transformation to stator coordinates is needed, using the estimated rotor position $\hat{\theta}_r$.

The flux error between the voltage model (15) and the current model (16) is passed through a PI controller, with $K_{pcomp} = 10$ and $K_{Icomp} = 10$, which outputs a correction signal used to compensate the voltage model (see Figure 6):

$$v_{comp\alpha\beta} = \left(K_{Pcomp} + \frac{K_{Icomp}}{s} \right) e_{\psi} \qquad (17)$$

where:

$$e_{\psi} = \hat{\psi}'_{s\alpha\beta} - \hat{\psi}_{s\alpha\beta} \qquad (18)$$

This way the dc-offset drift of the ideal integrator (15) is eliminated. The PI compensator selects the current model at low speeds, while the voltage model prevails at medium and high speeds. Thus, the corrected stator flux vector is $\hat{\psi}_{s\alpha\beta}$ as given by (15). For comparison purposes only the stator flux obtained only from the current model, $\hat{\psi}'_{s\alpha\beta}$, was also considered. The stator flux position $\hat{\theta}_s$ is obtained from the resultant stator flux components: $\hat{\theta}_s = \tan^{-1}\left(\hat{\psi}_{s\beta} / \hat{\psi}_{s\alpha}\right)$.

Differences were noticed between the stator flux $\hat{\psi}_{s\alpha\beta}$ obtained from the compensated voltage model (15) and the stator flux $\hat{\psi}'_{s\alpha\beta}$ obtained from the current model only (16). This was mainly due to parameter mismatch between the model and the real machine. To have one more view of this problem, another flux estimator was developed. This is an estimator that employs the voltage and the current models connected in series, as shown in Fig. 7. For the tests, however, the stator flux estimator with voltage and current models in parallel is used.

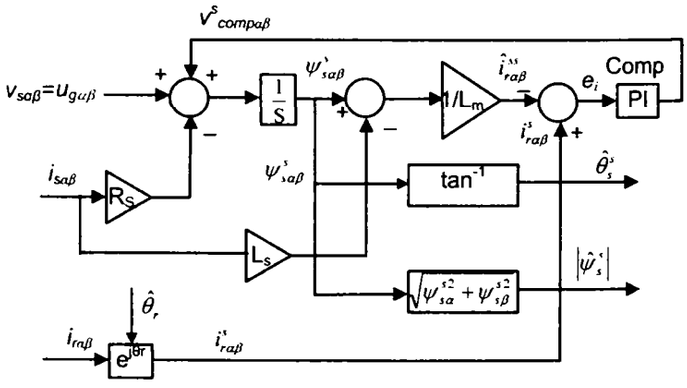

Fig. 7. Stator flux estimator with voltage and current models in series.

It is basically relying on the same equations, but the current model is written such that the stator flux obtained from the voltage model is now used to estimate the rotor current in stator coordinates:

$$\hat{i}^{ss}_{r\alpha\beta} = \frac{1}{L_m} \left(\hat{\psi}^{s}_{s\alpha\beta} - L_s i_{s\alpha\beta} \right) \qquad (19)$$

where estimated stator flux is now:

$$\hat{\psi}^{s}_{s\alpha\beta} = \int \left(v_{s\alpha\beta} - R_s i_{s\alpha\beta} + v^{s}_{comp\alpha\beta} \right) \qquad (20)$$

The rotor current is measured and transformed into stator coordinates using the estimated rotor position θ_r. The rotor-current error between the measured and estimated (19) rotor current is passed through a PI controller, with the same

parameters as for the one in Fig. 6, and its output is used to compensate the voltage model: (Fig. 7)

$$v^{s}_{compr\alpha\beta} = \left(K_{Pcomp} + \frac{K_{Icomp}}{s} \right) e_1 \qquad (21)$$

where:

$$e_1 = i^{s}_{r\alpha\beta} - \hat{i}^{ss}_{r\alpha\beta} \qquad (22)$$

B. The Rotor Speed-Position Estimation

A speed-position estimator based on model reference adaptive system (MRAS) principles is used for this purpose, due to its relative simplicity and proven efficiency over an extended speed range [14].

The rotor current in stator coordinates is calculated similar with (19) but **using the stator flux calculated by the parallel estimator**:

$$\hat{i}^{s}_{r\alpha\beta} = \frac{1}{L_m}\left(\hat{\psi}_{s\alpha\beta} - L_s i_{s\alpha\beta} \right) \qquad (23)$$

and then transformed into rotor coordinates using the estimated rotor position angle $\hat{\theta}_r$ coming through feed-back:

$$\hat{i}^{e}_{r\alpha\beta} = \hat{i}^{s}_{r\alpha\beta} e^{-j\hat{\theta}_r} \qquad (24)$$

The MRAS error ε is calculated as the phase difference of the estimated rotor current $\hat{i}^{e}_{r\alpha\beta}$ and the measured rotor current $i_{r\alpha\beta}$ (25). The real system is the reference model, while the current model is the adaptive model, with the rotor position θ_r as adaptive parameter.

$$\varepsilon = -i_{r\alpha}\hat{i}^{e}_{r\beta} + \hat{i}^{e}_{r\alpha} i_{r\beta} \qquad (25)$$

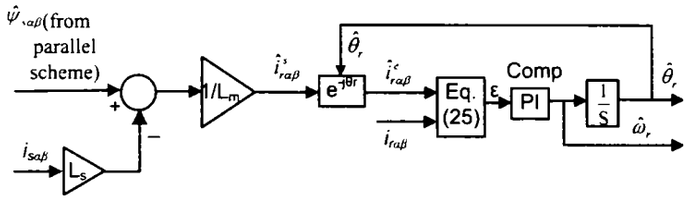

Fig. 8. The rotor speed and position estimation MRAS.

This error is used to extract the rotor speed and position using a phase-locked loop (PLL) technique (Figure 8). The output of the PI compensator gives the estimated rotor speed ω_r, and after the integration, the estimated rotor position θ_r is obtained:

$$\hat{\omega}_r = \left(K'_{Pcomp} + \frac{K'_{Icomp}}{s} \right) \varepsilon \; ; \; \hat{\theta}_r = \int \hat{\omega}_r dt \qquad (26)$$

Optimum parameters of the PI compensator were searched as a compromise between the speed of the PLL, especially during transients, and the level of oscillations in speed estimation, especially at low speeds. The best parameters, seem to be: K'_{Pcomp} = 100, and T_I = 5ms (time constant of the compensator, $T_I = K'_{Pcomp} / K'_{Icomp}$). Overall, this scheme has shown good accuracy over the whole speed range and also during the start-up procedure.

V. Test Rig and Experimental Results

A. Synchronization Procedure

The synchronization procedure at start-up consists on the following steps: the generator is driven with the motor which simulates the wind turbine close to the synchronous speed, and in the same direction of rotation as that of the network; the DC link is charged from the network through the line filter and the pre-charging resistors. The resistors are disconnected afterwards; K_1 is switched on, and the control algorithms are started with the reference current for the machine side converters (MSC) set to zero; when the stator voltage becomes almost equal to the grid voltage (lamps in parallel with K_2 are off), K_2 is switched on;the reference currents for the machine side converter (in fact the reference for the stator active and reactive power) are then set at desired values.

B. Experimental Results

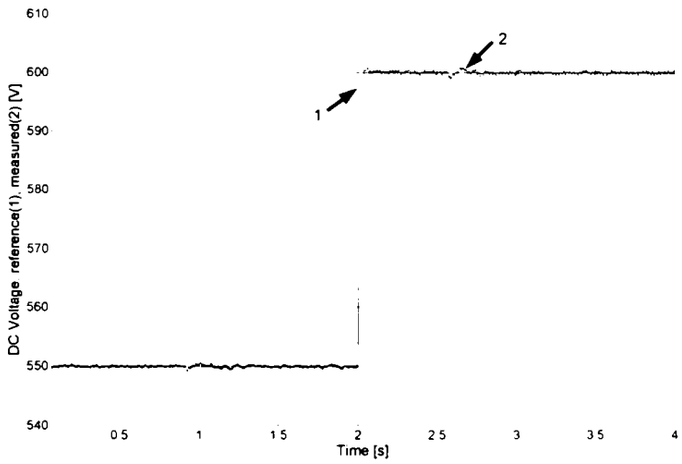

Fig. 9. DC link voltage dynamic response at step reference from 550 V to 600 V at t=2 s.

1) DC Link Control. First, as the grid side converter (Fig. 3) was analyzed, a step-up in the DC voltage reference was applied, and the response is shown in Fig. 9.As can be noticed, fast and well-damped dynamic response was obtained. The grid side converter is able to accurately control the DC voltage, and the power may bidirectionally flow through the rotor.

2) Subsynchronous operation. The stator reactive and active power are direct proportional with i_{rd} and i_{rq}. It means that by controlling the rotor currents i_{rd} and i_{rq} a fast decoupled response in terms of stator reactive power Q_s and

stator active power P_s is obtained. The following tests will deal with control of i_{rd} and i_{rq}. Please note that a negative d or q rotor current means a negative reactive or active power (generating). a positive d or q rotor current means a positive reactive or active power (absorbing). For zero reactive power current i_{rd}^* reference (Fig. 5), with the generator in subsynchronous operation (rotor speed below 1000 rpm), a step reference of active power current i_{rq}^* from 0 to –5 A (generating) was applied at t=2 s. The dynamic response of rotor currents i_{rd} and i_{rq} is illustrated in Fig. 10, and the measured and estimated rotor speed response is shown in Fig. 11.

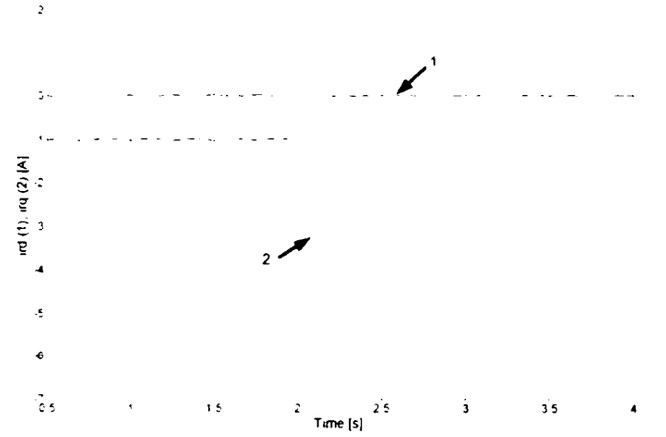

Fig. 10. Measured rotor currents i_{rd} (1) and i_{rq} (2) for a step reference of i_{rq}^* from 0 to –5 A, and i_{rd}^* = 0, at t=2 s in generating subsynchronous operation

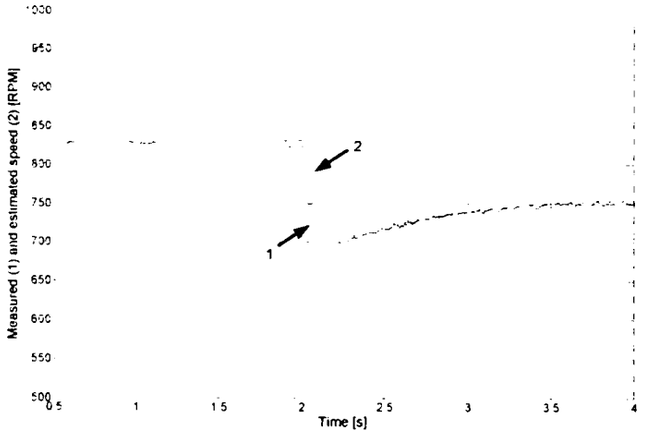

Fig. 11. Measured (1) and estimated (2) rotor speed for a step reference of i_{rq}^* from 0 to –5 A, and i_{rd}^* = 0, at t=2 s in generating subsynchronous operation

Also in subsynchronous operation, for constant zero reference of i_{rq}^* current, a step-up in i_{rd}^* current from –3 A (generating) to +3 A (absorbing) was applied. The dynamic response of rotor currents i_{rd} and i_{rq} is shown in Fig. 12, and the measured stator currents for the same experiment are shown in Fig. 13.

3) Oversynchronous operation. The WRIG behavior in oversynchronous operation was also investigated. With the generator running at about 1200 rpm, and with the reference current i_{rd}^* set at –3 A, a step reference of i_{rq}^* from –1 A to –5 A was applied. The rotor current dynamic response is shown in Fig. 14, and the measured and estimated rotor speed are shown in Fig. 15. In this case, negative direct current i_{rd} means magnetization from the stator. The limited power of the prime mover IM drive makes the speed to vary with WRIG loading.

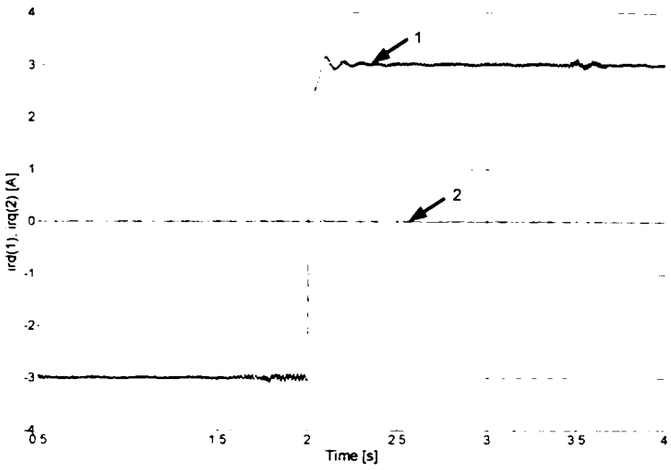

Fig. 12. Rotor currents i_{rd} (1) and i_{rq} (2) for a step reference of i_{rd}^* from -3 A to 3 A, i_{rq}^* = 0, at t = 2 s in subsynchronous operation

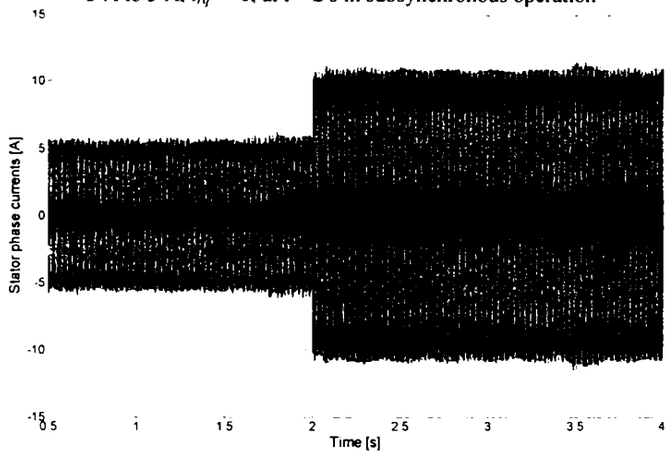

Fig. 13. Measured stator phase currents for a step reference of i_{rd}^* from -3 A to 3 A, i_{rq}^* = 0, at t = 2 s in subsynchronous operation.

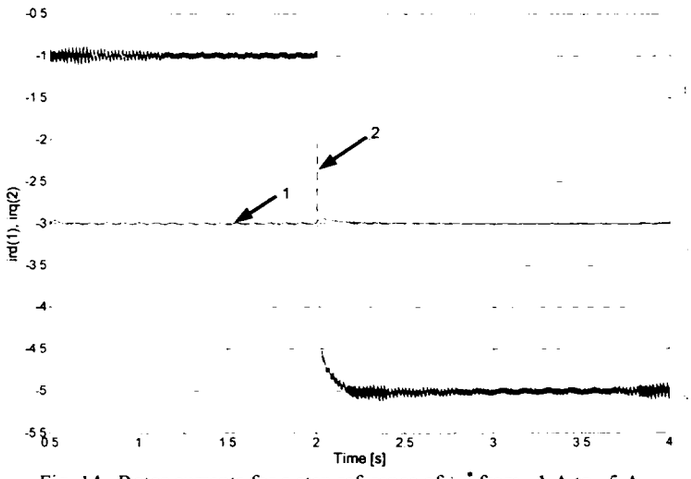

Fig. 14. Rotor currents for a step reference of i_{rq}^* from –1 A to –5 A, i_{rd}^* = -3 A, at t = 2 s in generating oversynchronous operation

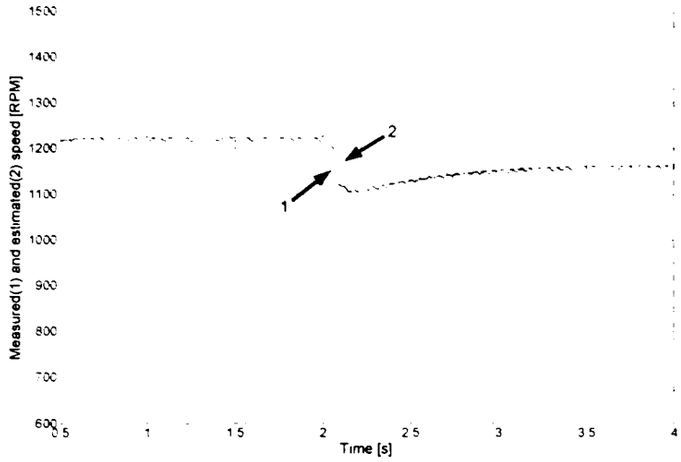

Fig. 15. Measured (1) and estimated (2) rotor speed for a step in reference of i_{rq}^* from –1 A to –5 A, i_{rd}^* = -3 A, at t = 2 s in oversynchronous operation.

4) Passing through Synchronism. One of the most interesting features of the doubly-fed induction generator with two back-to-back converters in the rotor circuit is passing through the synchronism and even synchronous operation.

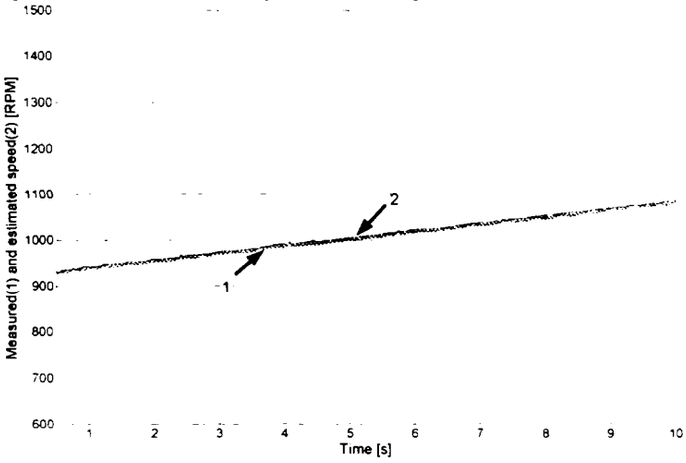

Fig. 16. Measured (1) and estimated (2) speed at passing through synchronism.

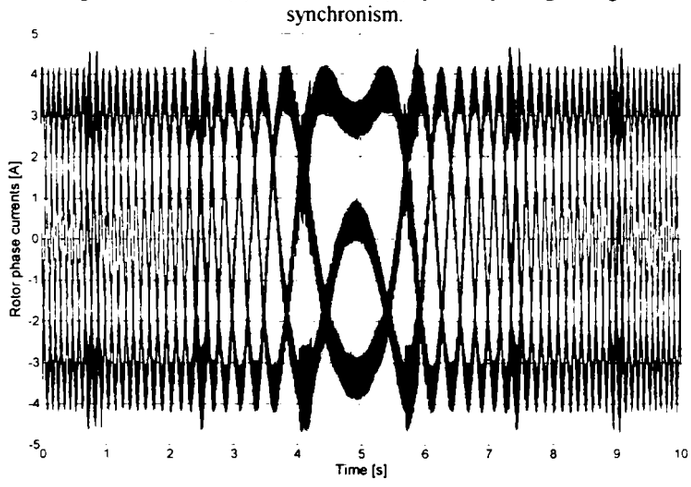

Fig. 17. Measured rotor currents at passing through synchronism.

Speed and current transients from 930 to 1160 rpm during passing through synchronism are illustrated in Figs. 16 and 17. The measured and estimated speeds are shown in Figure 16, and the measured rotor currents are shown in Figure 17. The passing through synchronism occurs at t=5 s.

Also to compare the three estimators an example is illustrated in Figure 18. The stator flux from parallel estimator, from parallel estimator current model only and from the series estimator are shown.

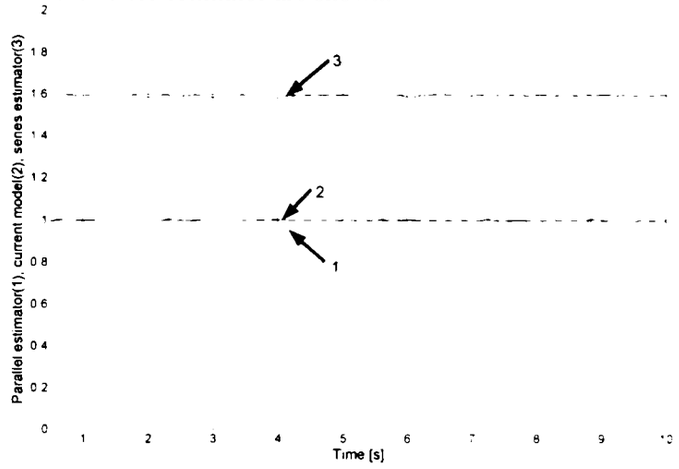

Fig. 18. Stator flux during passing through synchronism estimated by: parallel estimator $\hat{\psi}_s$ (1), parallel estimator current model only $\hat{\psi}_s^I$ (2), series estimator $\hat{\psi}_s^S$ (3)

5) S nchronous operation. The WRIG is able of stationary synchronous operation, as a native synchronous generator. In this case, the rotor currents are d.c. and the generator becomes an electrically excited synchronous generator. In Fig. 19, the measured rotor phase currents are shown for the generator driven at synchronous speed of 1000 rpm.

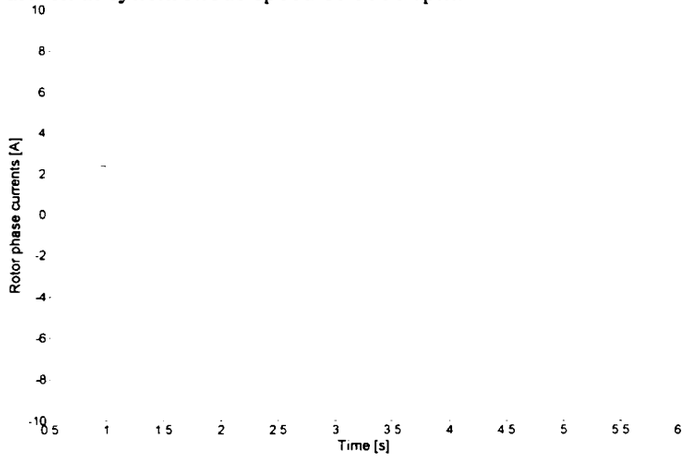

Fig. 19. Measured rotor currents during stationary synchronous operation.

This is an important advantage of this generator and its control, i.e. the possibility to impose and maintain the synchronous speed and to generate more reactive power when needed, similarly to the overexcited synchronous generator. This could be easily be realized by setting a negative i_{rd}^* current reference and fixing the rotor speed at its standard synchronous value ($n_r = f_s/p$).

VI. Conclusion

A complete system with a doubly-fed induction generator was presented and analyzed. The main target-application for this system is the wind power generation. Other possible applications are hydropower generation, or other turbines using unconventional power sources like tides or marine currents. The wound-rotor induction generator uses two back-to-back connected converters in the rotor circuit, both of them vector controlled. The machine-side converter controls the active and reactive rotor currents (in fact the stator active and reactive powers), while the grid-side converter controls the DC voltage regardless of the magnitude and the direction of the rotor power, and the reactive current drawn or injected from/in the grid. Both control strategies are presented and discussed. A new start-up procedure with a synchronization sequence is presented.

Two stator flux estimators were developed and compared. Both are based on combining of the voltage and current models. One is using them in parallel and the other one in series. A rotor speed and position estimator was developed, based on MRAS principles. The speed and position estimation is accurate over the whole speed range and it has the advantage that is efficient also during the start-up procedure.

Different operational tests were performed, and the results are shown and discussed. Rather fast response in terms of stator active and reactive power is proven. The same holds in terms of DC voltage and reactive current on the power grid side. The passing through synchronism and stationary synchronous operation were presented. An interesting feature and, in fact, an advantage of this generator and its control is synchronous operation like as a native synchronous generator. The level of the generating (or absorbing) reactive power could be easily set through the rotor flux current reference.

Appendix

The Doubly-Fed Machine: Nameplate data: Type - asynchronous motor with slip rings, Manufacturer: IME SA Bucharest, Romania, P_N = 3 kW, stator voltage V_{SN} = 380 V, rotor voltage V_{RN} = 380 V (after re-wounding; the original rotor voltage was 78 V), n_N = 940 rpm.

Parameters: R_s = 1.6 Ω, R_r = 1.6 Ω, $L_{s\sigma} = L_{r\sigma}$ = 17.51 mH, L_m = 96.13 mH, p =3 pole pairs

The Converters: Type: VLT 5004, S_N = 4.2 kVA, Manufacturer: Danfoss Drives, Denmark.

Control and Acquisition Unit: Type: DS 1103, Manufacturer: dSpace GmbH, Germany.

References

[1] S. Heier, *Grid Integration of Wind Energy Conversion Systems*, John Wiley and Sons, 1998.

[2] Morten Lindholm, "Doubly-Fed Drives for Variable Speed Wind Turbines," *Ph.D. Thesis*, Technical University of Denmark,

[3] I. Serban, F. Blaabjerg, I. Boldea, "Sensorless doubly-fed induction generator control under power system transients and faults: the influence of magnetic saturation", *Proc. of OPTIM 2004*, Brasov, Romania, vol. 2, pp. 311-318, May 2004.

[4] M.P. Kazmierkowski, R. Krishnan, F. Blaabjerg (Eds.), *Control in Power Electronics: Selected Problems*," Chapter 13: L. Helle, F. Blaabjerg, "Wind turbine systems", Academic Press, 2002.

[5] I. Boldea, S.A. Nasar, *Electric Drives*, Chapter 14: "Large power drives, 14.8 Sub and Hypersynchronous IM cascade drives," CRC Press, Florida, 1999.

[6] R. Datta, V.T. Ranganathan, "Direct power control of grid-connected wound rotor induction machine without rotor position sensors," *IEEE Transactions on Power Electronics*, vol. 16, no. 3, May 2001, pp. 390-399.

[7] L. Morel, H. Godfroid, A. Mirzaian, J.M. Kauffmann, "Double-fed induction machine: converter optimization and field oriented control without position sensor," *IEE Proc. on Electric Power Applications*, vol. 145, no. 4, July 1998, pp. 360-368.

[8] Sae-Joon Lee, Jun-Koo Kang, Seung-Ki Sul, "A new phase detecting method for power conversion systems considering distorted conditions in power system," *1999 IEEE-IAS Annual Meeting Conf. Record*, vol. 4, pp. 2167-2172, 1999.

[9] V. Kaura, V. Blasko, "Operation of a phase locked loop system under distorted utility conditions," *IEEE Transactions on Industry Applications*, vol. 33, no.1, Jan./Feb. 1997, pp. 58-63.

[10] I. Serban, F. Blaabjerg, I. Boldea, Z. Chen, "A study of the doubly-fed wind power generator under power grid faults," *Proc. of EPE 2003*, Toulouse, France, 2003.

[11] U. Rädel, D. Navarro, G. Berger, S. Berg, "Sensorless field-oriented control of a slipring induction generator for a 2.5 MW wind power plant from Nordex Energy GmbH," *Proc. of EPE 2001*, Graz, 2001.

[12] S. Müller, M. Deicke, R.W. De Doncker, "Adjustable speed generators for wind turbines based on double-fed induction machines and 4-quadrant IGBT converters linked to the rotor," *2000 IEEE-IAS Annual Meeting Conf. Record*, vol. 4, pp. 2249-2254, Oct. 2000.

[13] R. Datta, V.T. Ranganathan, "A simple position-sensorless algorithm for rotor-side field-oriented control of wound-rotor induction machine," *IEEE Transactions on Industrial Electronics*, vol. 48, no. 4, Aug. 2001, pp. 786-793.

[14] G.D. Andreescu, "Position and speed sensorless control of PMSM drives based on adaptive observer," *Proc. of EPE'99*, Lausanne, Switzerland, Aug. 1999.

Sensorless control of wound rotor induction generator (WRIG) for wind power applications: the experimental test platform

Ioan Serban[1], Dorin Iles-Klumpner[1], Frede Blaabjerg[2], Ion Boldea[3]

[1]ebm-papst St. Georgen GmbH & Co. KG, Research and Development Laboratory for Electric Drives
Hermann-Papst-Str. 1, D-78112 St. Georgen/Schwarzwald, GERMANY, Phone: +49-7724-811834, Fax: +49-7724-8151834, Email: Ioan.Serban@de.ebmpapst.com, Dorin.Iles-Klumpner@de.ebmpapst.com

[2] Aalborg University, Institute of Energy Technology, Pontoppidanstraede 101, 9220 Aalborg East, DENMARK
Phone/Fax: + 45-9635-9254, Email: fbl@iet.auc.dk

[3]University Politehnica of Timisoara, Faculty of Electrical Engineering,
Bd. V. Parvan nr.2, 300223 Timisoara, ROMANIA, Phone/Fax: +40-256-403463 / +40-256-403452
Email: boldea@lselinux.utt.ro

Abstract **– The present paper presents the experimental platform used during the tests of state observers and sensorless control of a variable speed wound rotor induction generator system. The main application of this system is wind power and it was developed and improved in the latest years as interest in power generation especially using wind as primary energy, has increased tremendously.**

It is basically composed by: WRIG, two power electronics converters connected in the rotor side of WRIG: machine-side inverter (MSC) and grid-side inverter (GSC), a line filter, and the data acquisition and control system (dSpace DS 1103). Both converters are commercial units and are vector controlled using appropriate interfaces. They are back-to-back connected, sharing the same DC bus, one supplied through a line filter from the power grid, and the other one with the output on the rotor of the generator. The stator of the generator is directly connected to the power grid.

All components are extensively described in the paper and their functions are discussed.

The control structures for both inverters and the Matlab-Simulink® software used for implementing them using the control and acquisition system DS1103 and its interface are presented. Some basic measurements are illustrated and discussed.

Index Terms **– wind generators, back-to-back inverter, wound-rotor induction machine, vector control, sensorless control, model reference adaptive system (MRAS).**

I. Introduction

Wind energy was the fastest growing energy technology in the 1990s. During the last decade of the twentieth century, worldwide wind capacity doubled every three years and the cost of electricity from wind power has fallen to about one sixth of the cost in the early 1980s [1]. And the trend seems to continue. The cumulative capacity is growing worldwide by about 25% per year.

By the end of 2003, around 74% was installed in Europe (28706 MW), a further 18% in North America (6677 MW) and 8% in Asia and the Pacific (3034 MW).

The countries with the largest installed wind power capacity in Europe are Germany (14609 MW), Denmark (3110 MW) and Spain (6202 MW), countries which thus have 62% of the total install capacity worldwide.

Wind energy technology itself also moved very fast in new dimensions. At the end of 1989 a 300kW wind turbine with a 30 meters rotor diameter was state of the art. 10 years later, 2 MW turbines with 80 meters rotor diameter were available and now 5MW wind turbines (128 meters rotor diameter) have already been tested and 6-7 MW turbines are planned to be built in the near future.

Thus, the penetration of wind power in the power systems is higher and higher. Hence a lot of energy quality requirements and interconnection rules were required.

In addition, wind energy introduced new technologies such as wound-rotor induction generator with two power electronics converters connected back-to-back in the rotor circuit. Nowadays, this solution has 46.8% from the world market share of wind turbine concepts. The main competitors are the permanent magnet synchronous generator (with 20.3 % from the market share) and the squirrel-cage induction generator (with 27.8 % from the market share) both with full-scale frequency converters in the stator circuit.

The WRIG has several advantages:

- the ability to control reactive power and to decouple active and reactive power control by independently controlling the rotor excitation current
- is not necessary to be magnetized from the power grid, it can magnetized from the rotor circuit, too. It is also capable of generating reactive power that can be delivered to the stator by the grid-side converter. In the case of a weak grid, where the voltage may fluctuate, the WRIG may be ordered to produce or absorb an amount of reactive power to or from the grid, with the purpose of voltage control.

- the size of the converter is not related to the generator total power but to the selected speed range, and thus to the slip power. Hence, a rating of the converter of around 25% from the generator total power is usual, based on the economic optimization of investment costs and on increased efficiency.

II. Hardware Specifications

The laboratory setup was realized in the Intelligent Motion Control Lab, Faculty of Electrical Engineering Timisoara as the main objective of the Ioan Serban's Ph.D Project "Contributions to the control of variable speed generators for renewable energy" with the intended purpose to prove and gain new information about sensorless control of the WRIG with two back-to-back connected inverters in the rotor circuit.

The setup consists of a 3kW wound rotor induction generator mechanically connected with a driving squirrel-cage induction motor supplied from an usual frequency converter for speed control operation. The WRIG is connected to the power grid directly with the stator, and through the two back-to-back inverters with the rotor.

Besides those main components, there are measuring circuits, the control system, the line filter etc. Figure 1 shows the principle schematic of the setup.

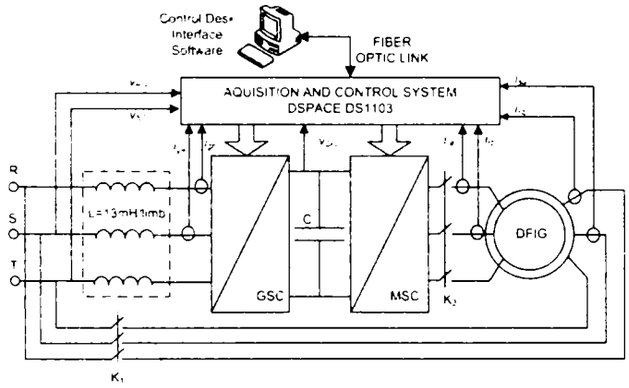

Figure 1. The WRIG system.

A. The Rotating Machinery

The main component in the setup is the 3kW wound rotor induction generator manufactured by IME SA Bucharest Romania. It is a 6-pole machine, star connected stator and rotor. As the original machine had the nominal stator voltage V_{SN} = 380 V and the nominal rotor voltage V_{RN} = 78 V a re-wounded was necessary to fit with the converters requirements without inserting a transformer in the rotor circuit. Thus, a new rotor winding was designed by the authors and executed in Electromotor SA Timisoara.. Hence, the rotor voltage (at slip S = 1) was increased to V'_{RN} = 380 V and the rotor nominal current was decreased from 23 A to 4.6 A.

The WRIG is mechanically connected with a 3kW, 4-poles squirrel-cage induction motor (not represented in Fig.1) manufactured by Electromotor SA Timisoara and with an encoder (see Figure 2 for a photo of the machines).

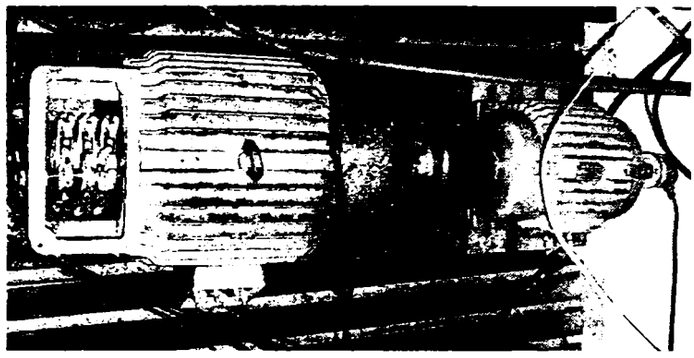

Figure 2. The WRIG (left) and its driving motor (right).

The induction motor is supplied from a Danfoss VLT 5004 3 kW commercial inverter with the original interface for the speed control mode.

B. The Power Inverters

The power inverters are commercial VLT 5004, 4.2 kVA manufactured by Danfoss Drives, Denmark (see Figure 3 for a photo of the inverters). The main data for them are given in Table.1.

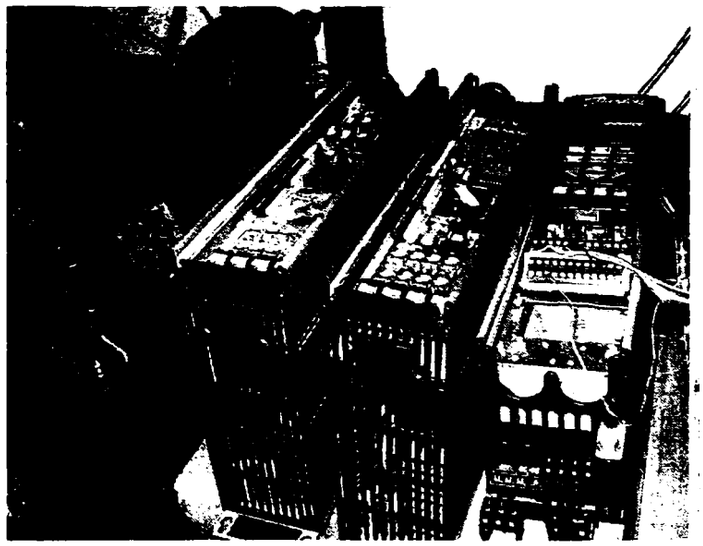

Figure 3. The Danfoss power inverters equipped with interface and protection cards (IPC) left – GSC, middle – MSC. In the right side is the inverter for the driving motor with the original interface for speed control mode.

Table 1. Power inverters specifications

Rated Power	4.2 kVA
Nominal Voltage	380 V
Nominal Current	6.5 A
Maximum DC Link Voltage	1200 VDC
Switching Frequency	10 kHz

Their original interface cards and control panels were replaced with interface and protection cards (IPC), produced by IET, Aalborg University which enables the IGBT drivers to be controlled from an external digital controller via plastic fiber optics (see Figure 4). The IPC provides, besides the fiber optic receivers, also reliable short-circuit, shoot-through, dc-overvoltage and overtemperature protections [2].

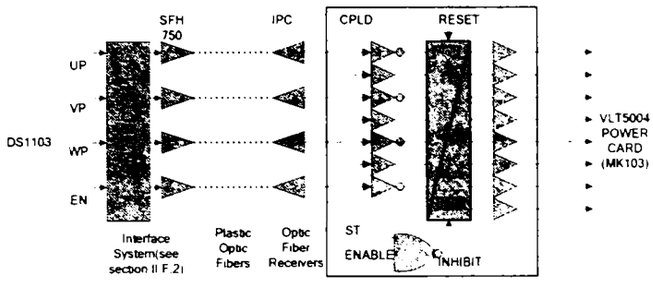

Figure 4. Interface and protection card (for one inverter – for the other is identical)

Each inverter is controlled through 3 signals (UP, VP, WP) – for the upper IGBTs – and an enable signal (EN). The inversed signals for the lower IGBTs and the corresponding deadtime (2 μs) are implemented in the programmable logic device (CPLD).

The inverters have the DC links accessible through the DC sharing connectors. By realizing an electrical connection between them, the inverters can be easily connected back-to-back. But for the DC link capacitors pre-charging, a resistor was used (not illustrated in Figure 1) between the grid and the line filter; the resistors were short-circuited after the voltage in the DC link reached approx. 500 V

C. Line Filter

Between grid converter and the grid itself a line filter was introduced to protect the inverter and to reduce the higher harmonic content in the line current, produced by the switching. This is in fact a simple *L*-filter. An *LC* or an *LCL* filter could be used, but the *L*-filter was chosen for simplicity. The frequency response of the *LCL* filter has a resonance peak, so the latter has to be designed such that the resonance peak not to interfere with the frequency response of the inverter out_ut volta_e; alternativel_, a series resistor must be inserted to damp the resonance peak.

The value for the inductance per limb was chosen 13 mH, but a rather good design value for the inductance in the filter is [3]: $L = \max\left(V_\vartheta / \vartheta\omega_1 I_\vartheta\right)$

where ϑ is the order of the harmonic and V_ϑ the phase RMS value of the output phase voltage harmonic.

D. Voltage and current sensors

As can be seen in Figure 1, 6 currents and 3 voltages were acquired to fulfill the control system requirements. These are:

- 2 rotor currents (the third is calculated in the software taking into account that the sum of them is zero)
- 2 stator currents (the third is calculated in the software taking into account that the sum of them is zero)
- 2 grid currents on the grid-side converter side (the third is calculated in the software taking into account that the sum of them is zero)
- DC voltage
- 2 grid voltages line-to-line which are in fact also the stator voltages (the phase voltages are calculated later in the software from the line voltages)

Thus the acquisition system was designed. It includes:

- 3 small boards with 2 current sensors each - type LEM LA 55-P with adequate signal conditioning such that at 10A measured current the sensor output will be 10V, required for the control system's A/D channels.
- a voltage measurement box with 3 voltage transducers type LEM LV 25-P with appropriate signal conditioning such at 500 V measured voltage the output of the sensor is 10 V, required for the control system's A/D channels.

E. Position sensor

To prove the sensorless position estimation techniques, a position estimator had to be included in the system. The chosen device was an Telemecanique encoder type XCC which provides a resolution of 5000 lines per revolution. The output is a usual A QUAD B (A+, A-, B+, B-, N+, N-) which can be directly connected to the control system as it provides encoder interfaces.

F. Control Hardware

The **DS1103 PPC** is a very flexible and powerful system featuring both high computational capability and comprenhensive I/O periphery. Additionally, it features a software SIMULINK interface that allows all applications to be developed in the Matlab/Simulink friendly environment. All compiling and downloading processes are carried out automatically in the background.
An experimenting software called Control Desk, allows real-time management of the running process by providing a virtual control panel with instruments and scopes.

1. DSP Board

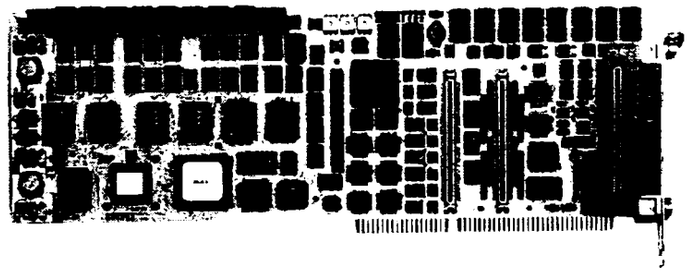

Figure 5. The single board control system dSpace DS 1103

The DS1103 is a single board system based on the **Motorola PowerPC 604e/333MHz** processor (PPC), which forms the main processing unit.

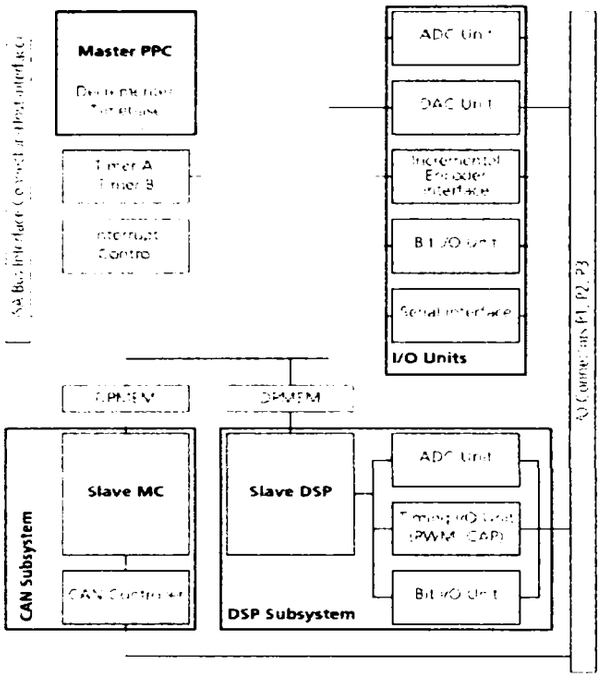

Legend:

ADC	Analog/Digital Converters
MC	CAN Microcontroller 80C164
CAP	Capture
DAC	Digital/Analog Converters
DPMEM	Dual-Port Memory
DSP	Digital Signal Processor TMS320F240
PPC	Power PC 604e Processor
PWM	Pulse Width Modulation

Figure 6. DS1103 internal functional block diagram

- **I/O Units**

A set of on-board peripherals frequently used in digital control systems has been added to the PPC. They include: analog-digital and digital-analog converters, digital I/O ports (Bit I/O), and a serial interface. The PPC can also control up to six incremental encoders, which allow the development of advanced controllers for robots.

- **DSP Subsystem**

The DSP subsystem, based on the Texas Instruments TMS320F240 DSP fixed-point processor, is especially designed for the control of electric drives. Among other I/O capabilities, the DSP provides 3-phase **PWM generation** making the subsystem useful for **drive applications**.

- **CAN Subsystem**

A further subsystem, based on Siemens 80C164 micro-controller (MC), is used for connection to a CAN bus.

- **Master PPC Slave DSP Slave MC**

The PPC has access to both the DSP and the CAN subsystems. Spoken in terms of inter-processor communication, the PPC is the master, whereas the DSP and the CAN MC are slaves.

Figure 6 gives an overview of the functional units of the DS1103.

2. Interface System

An interface board was designed in order to use the PWM outputs of the slave DSP unit for controlling the IGBT drivers of the both inverters.

It contains 8 pcs. SFH 750 fiber optic emitters (3 SPWM+ 1 ENABLE for each inverter) and a SN74HCT541 non-inverting octal buffer to increase the DS1103 PWM signals current capability according to SFH750 optic fiber driver requirements (see Figure 4). Additionally, series connected LED mounted on the front panel display the logic state of the optic fiber signals.

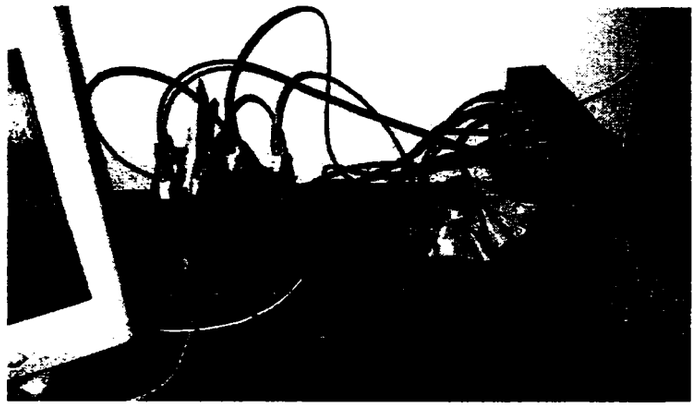

Figure 7. The interface system (the boards with current sensors and with fiber optic emmiters are visible. In the right side the terminal of the dSpace system)

III. SOFTWARE

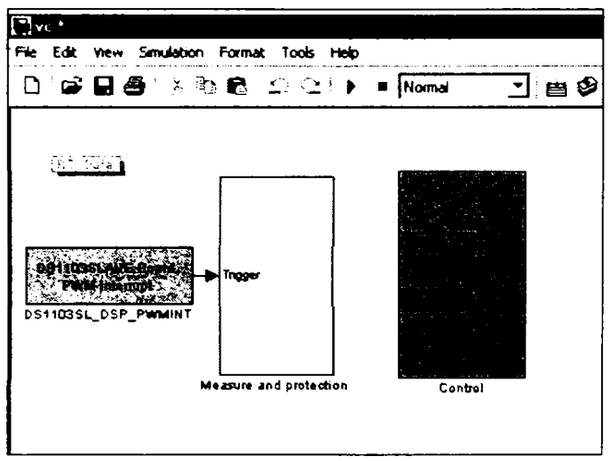

Figure 8. The Simulink software (measure and protection + control)

All the software was developed under Simulink environment, compiled automatically using Microtec C

compiler for Motorola Power PC and Texas Instruments C compiler and built/downloaded automatically using the dSpace system specialized MLIB/MTRACE mechanism.

The software is divided in two major parts (see Figure 8):

- measure and protection where acquisition, software signal conditioning and software protection are made
- vector control and estimation algorithms. This part is also divided in two major parts: grid-side converter (GSC) control and machine-side converter (MSC) control.

A. Measure and protection software

The measure and protection is the first main part of the developed software and has three main parts:

- acquisition software
- scaling and digital filtering of the acquired signals
- encoder interface
- _rotection

In the acquisition software the ADC channels are settled for acquiring the above discussed 6 currents and 3 voltages. The grid and rotor currents are acquired on the 4 nonmultiplexed A/D channels with 12-bit resolution, 800 ns sampling time. The rest of the currents and voltages are acquired on the multiplexed channels with 16-bit resolution, 4 μs sampling time. The acquisition process is triggered with the help of the slave-DSP timer interrupt with the same frequency as the switching (10 kHz) and at the 10% of the PWM pulse period (see Figure 8).

Afterwards the measured quantities are scaled taking into account the scaling factors of the sensors and filtered with a low-pass filter with a time constant of 10 ms. Also here the third current in each case is calculated from the other two measured.

In the encoder interface the position of the rotor and its speed are calculated. This could be done counting the pulses coming on the dedicated hardware interface and knowing the resolution of the encoder (number the pulses for one revolution) and the sampling time the encoder is "readed" with.

In the software protection part all the desired protection for the inverter/generator are designed.

In the present case 6 protections were implemented: overcurrent in the rotor;overcurrent in the grid; overcurrent in the stator; overvoltage in DC link; undervoltage in DC link: overspeed. The implementation is done as follows: the measured quantities are compared with the threshold values and the negated output of the comparators passed through an OR gate together with the ENABLE signal. Thus the output is inhibited with any of the measured values exceeds its threshold value.

B. The GSC Software

The grid-side converter is used to control the DC link voltage and the input power factor regardless of the level and the direction of the rotor power (Figure 9). A vector control strategy in stator voltage reference [4] frame is employed for this purpose. The converter is current regulated with the direct axis current used to control the DC-link voltage, meanwhile the transverse axis current is used to regulate the displacement between the voltage and the current, and thus the input power factor [5], [6].

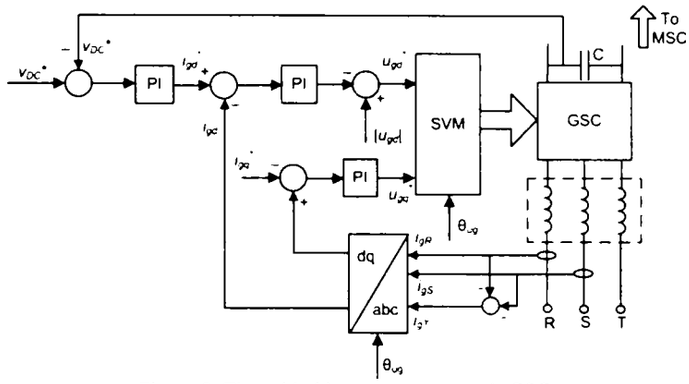

Figure 9. The grid-side converter control (GSC)

The phase voltages are calculated from the line voltages (see Figure 10) and the $\alpha\beta$ components of the grid voltage are calculated from the phase voltages. Finally, the angle of the grid voltage is extracted $\theta_e = \tan^{-1}\left(u_{s\beta} / u_{s\alpha}\right)$ [7]

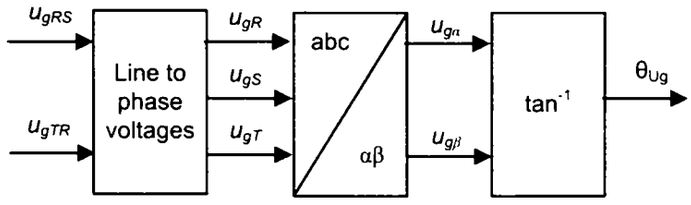

Figure 10. The computation of the grid voltage angle used for the coordinate transformations and for the SVM on the grid side converter control.

There are three parts in which the software for controlling the grid-side converter is divided (see Figure 11a): computation of grid voltage angle $\hat{\theta}_e$, see above; vector control and coordinate transformation for calculation of i_{gd} and i_{gq} (Figure 9); space vector modulation and dead-time compensation for calculation of the duty-cycles required for the slave-DSP PWM generation. Those are implemented in a C S-Function. The inputs are the DC voltage, the components α and β of the reference voltage vector and the measured phase currents for dead-time compensation purposes. The output of the function are the duty-cycles "ordered" to the slave-DSP which generates the PWM signals for the inverter with the specified switching frequency.

The GSC control software implementation using Simulink is illustrated in Figure 11a. A real-time interface was implemented in the dedicated Control Desk environment for the control and the management of the control software for GSC. A screenshot is presented in Figure 11b.

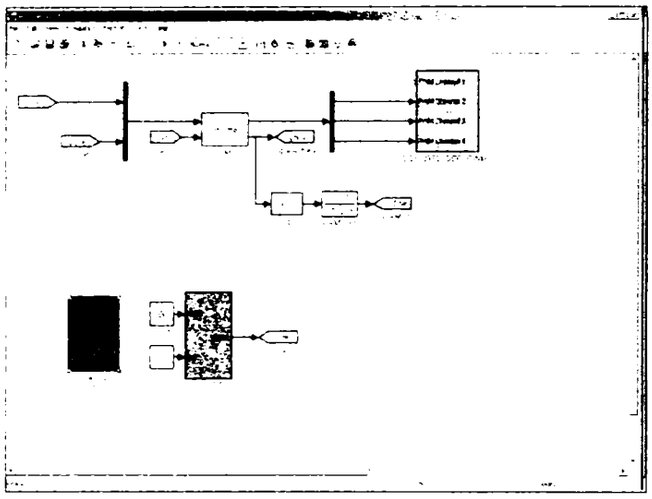

a)

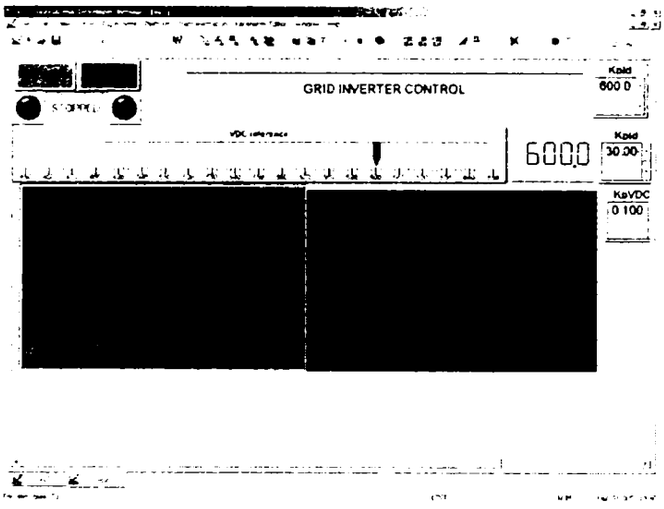

b)

Figure 11. The Simulink GSC control software a). and real-time interface b)

C. The MSC Software

The generator is controlled in synchronous reference frame, with the *d*-axis aligned with the stator-flux vector, which ensures decoupled control between the electromagnetic torque and h i xci a i n c ibu i [8]. T e control strategy block diagram is shown in Figure 12.

In fact controlling the rotor currents i_{rd} and i_{rq} the fast decoupl control of the stator reactive and active power is obtained [9,10]. The rotor currents are measured in their natural frame (rotor coordinates) and transformed into synchronous frame using the slip angle $\hat{\theta}_{slip}$. Reference voltages generated by the current control loops are transformed back to the rotor reference frame, using the same angle $\hat{\theta}_{slip}$ [11]. Standard space vector modulation is employed to generate the pulses for the inverter.

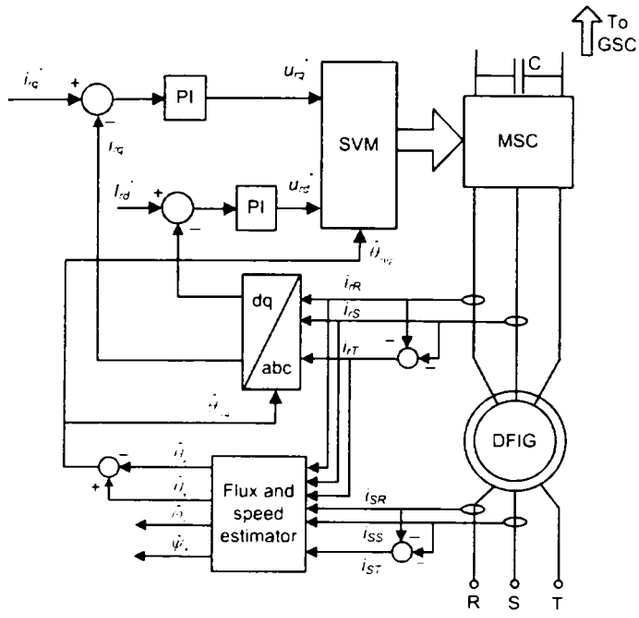

Figure 12. The machine-side converter control (MSC)

There are six parts in which the software for controlling the machine-side converter is divided (see Figure 13a):computation of the angle $\hat{\theta}_{slip}$; stator flux estimator with the voltage and current models connected in parallel; stator flux estimator with the voltage and current models connected in series; MRAS algorithm for rotor position and speed o servat on; vector control and coordinates transformation for calculation of the i_{rd} and i_{rq} ; space vector modulation and dead-time compensation for calculation of the duty-cycles required for the slave-DSP PWM generation. This is identical with the procedure described at the GSC converter software – see the final of previous paragraph.

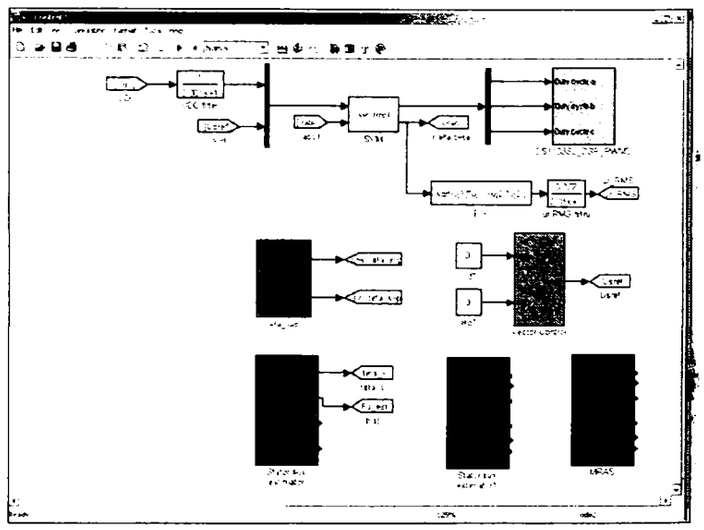

a)

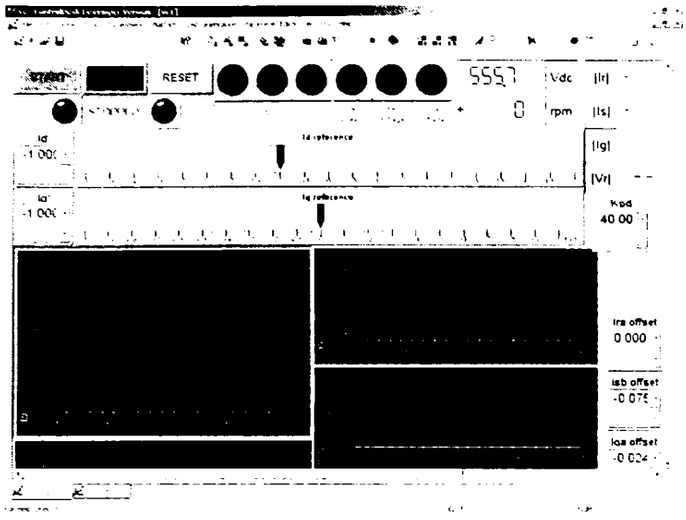

b)

Figure 13. MSC control software a) and real-time Control Desk Interface b)

The implemented Simulink software for control of the MSC is illustrated in Figure 13a and the Control Desk real-time management interface for the control software is shown in Figure 13b.

The detailed discussions with "in extenso" experimental results about the both vector controls, flux estimators and MRAS used during this project are given in [12].

IV. Measurements

Some basic measurements will be presented briefly in what it follows. The DC link is first illustrated in Figure 14. A step in DC voltage reference (in the GSC vector control) is performed. The reference and the response are shown.

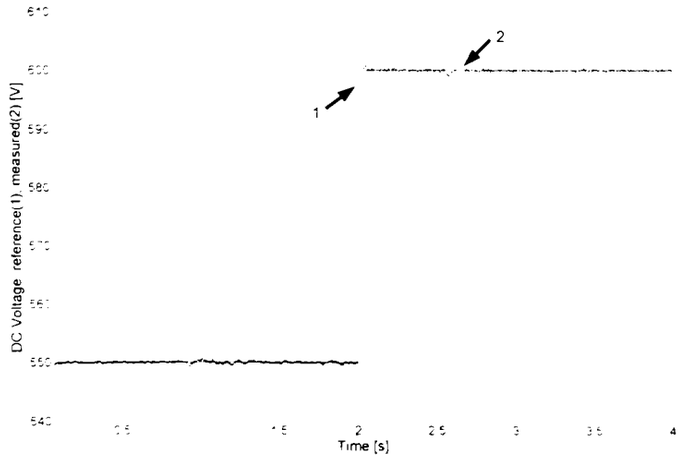

Figure 14. DC link voltage dynamic response at step reference from 550 V to 600 V at t=2 s.

The stator currents at the same experiment are presented in Figure 15 and measured line voltages in Figure 16.

Figure 15. Measured stator currents

One of the most interesting features of the wound-rotor induction generator with two back-to-back converters in the rotor circuit is passing through the synchronism and synchronous operation. In Figure 17 a) the rotor currents at the passing through synchronism are shown.

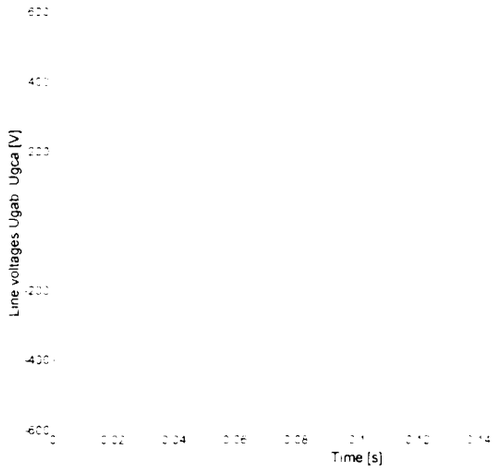

Figure 16. Measured grid/stator line voltages U_{gab}, U_{gca}

The mechanical speed is modified here from 930 to 1070 rpm in 10 sec. The passing through synchronism take place at t = 5 sec. In Figure 17 b) the measured and estimated speed are shown. The rotor speed and position estimator is a model reference adaptive system (MRAS) based on the error between the measured and the estimated rotor current. Thus, the estimation is efficient and accurate over the whole speed range.

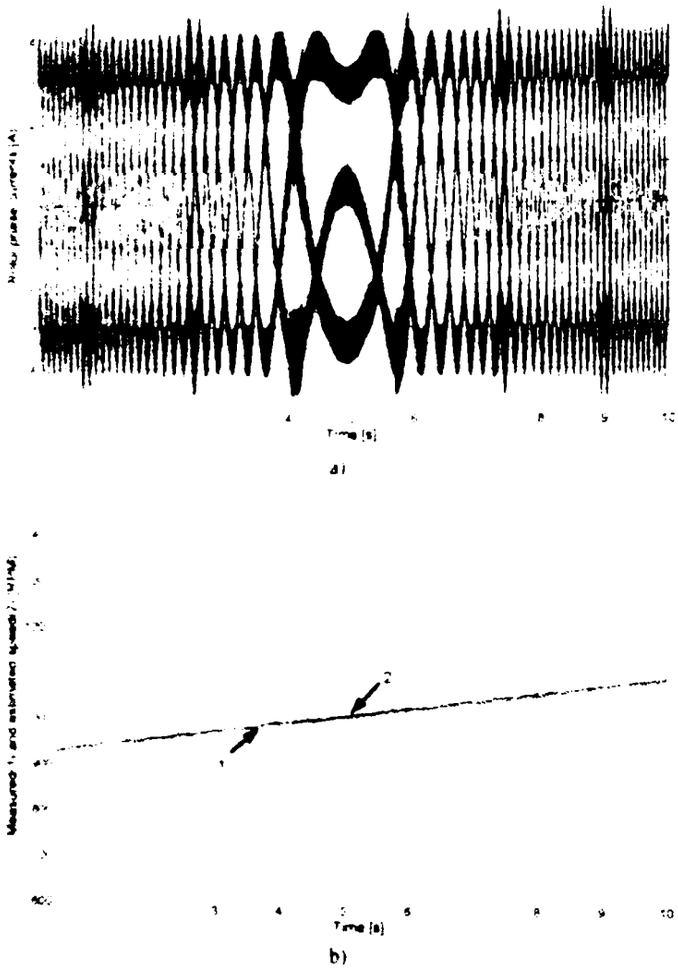

Fig. 17. a) Measured rotor currents at passing through synchronism, b) measured (1) and estimated (2) speed at passing through synchronism

V. Conclusion

The experimental test platform used during the tests of state observers and sensorless control of a variable speed wound rotor induction generator system was presented.

The main application for this system is wind power, but the platform is also suitable to investigate the motion-sensorless control of pump-storage hydro-turbine wound rotor induction generator motor, from selfstarting and synchronization freely within the design speed range to sub- and over-synchronous motoring (pumping) and generating.

The platform is also suitable to characterized the motion-sensorless wound rotor induction motor limited speed range 4-quadrant largedrive.

All the hardware components of the system were presented, discussed and analyzed. The software used for measurements and protections, signal conditioning, vector control for both inverters, flux estimators and MRAS position and speed observation is explained

Some basic measurem_nt_ whi... ...s the ac urac of the acquisition system and of the control are illustrated.

References

[1] T. Ackermann (edito.), "W.... Power in Powe Systems," *book*, John Wiley and Sons, 2005.

[2] R. Teodorescu, "Getting Started with dSpace system, *Flexible Drives System Laborator (FDSL) Refrenc Manual*, Version 1.0, Institute of Energy Technology Aalborg University, Denmark

[3] M. Lindholm, "Doubly-Fed Drives for Variable Spee Wind Turbines," *Ph.D. Thesis*, ...ch .cal U...v...s.ty c Denmark,

[4] I. Serban, F. Blaabjerg, I. Boldea, "Sensorless doubly fed induction generator control under power syster transients and faults: the influence of magneti saturation", *Proc. of OPTIM 2004*, Brasov, Romani vol. 2, pp. 311-318, May 2004.

[5] R. Datta, V.T. Ranganathan, "Direct power control c grid-connected wound rotor induction machine witho rotor position sensors," *IEEE Transactions on Pow Electronics*, vol. 16, no. 3, May 2001, pp. 390-399.

[6] L. Morel, H. Godfroid, A. Mirzaian, J.M. Kauffmann "Double-fed induction machine: converter optimizatio and field oriented control without position sensor," *IE Proc. on Electric Power Applications*, vol. 145, no. July 1998, pp. 360-368.

[7] I. Serban, F. Blaabjerg, I. Boldea, Z. Chen, "A study the doubly-fed wind power generator under power gr faults," *Proc. of EPE 2003*, Toulouse, France, 2003.

[8] U. Rädel, D. Navarro, G. Berger, S. Berg, "Sensorle field-oriented control of a slipring induction generat for a 2.5 MW wind power plant from Nordex Ener GmbH," *Proc. of EPE 2001*, Graz, 2001.

[9] S. Müller, M. Deicke, R.W. De Doncker, "Adjustab speed generators for wind turbines based on double-fe induction machines and 4-quadrant IGBT converte linked to the rotor," *2000 IEEE-IAS Annual Meeti Conf. Record*, vol. 4, pp. 2249-2254, Oct. 2000.

[10] R. Datta, V.T. Ranganathan, "A simple positio sensorless algorithm for rotor-side field-oriented cont of wound-rotor induction machine," *IEEE Transactio on Industrial Electronics*, vol. 48, no. 4, Aug. 2001, p 786-793.

[11] G.D. Andreescu, "Position and speed sensorless cont of PMSM drives based on adaptive observer," *Proc EPE'99*, Lausanne, Switzerland, Aug. 1999.

[12] Ioan Serban, Gheorghe-Daniel Andreescu, Luc Tutelea, Cristian Lascu, Frede Blaabjerg, Ion Bol "State Observers and Sensorless Control of Wo Rotor Induction Generator (WRIG) at Power Grid w Experimental Characterization," *will be published*, 20